Journal of Nucleic Acids

G-Quadruplex Nucleic Acids

Guest Editors: Ramon Eritja, Jean-Louis Mergny, Daniela Montesarchio, Lea Spindler, and Mateus Webba da Silva

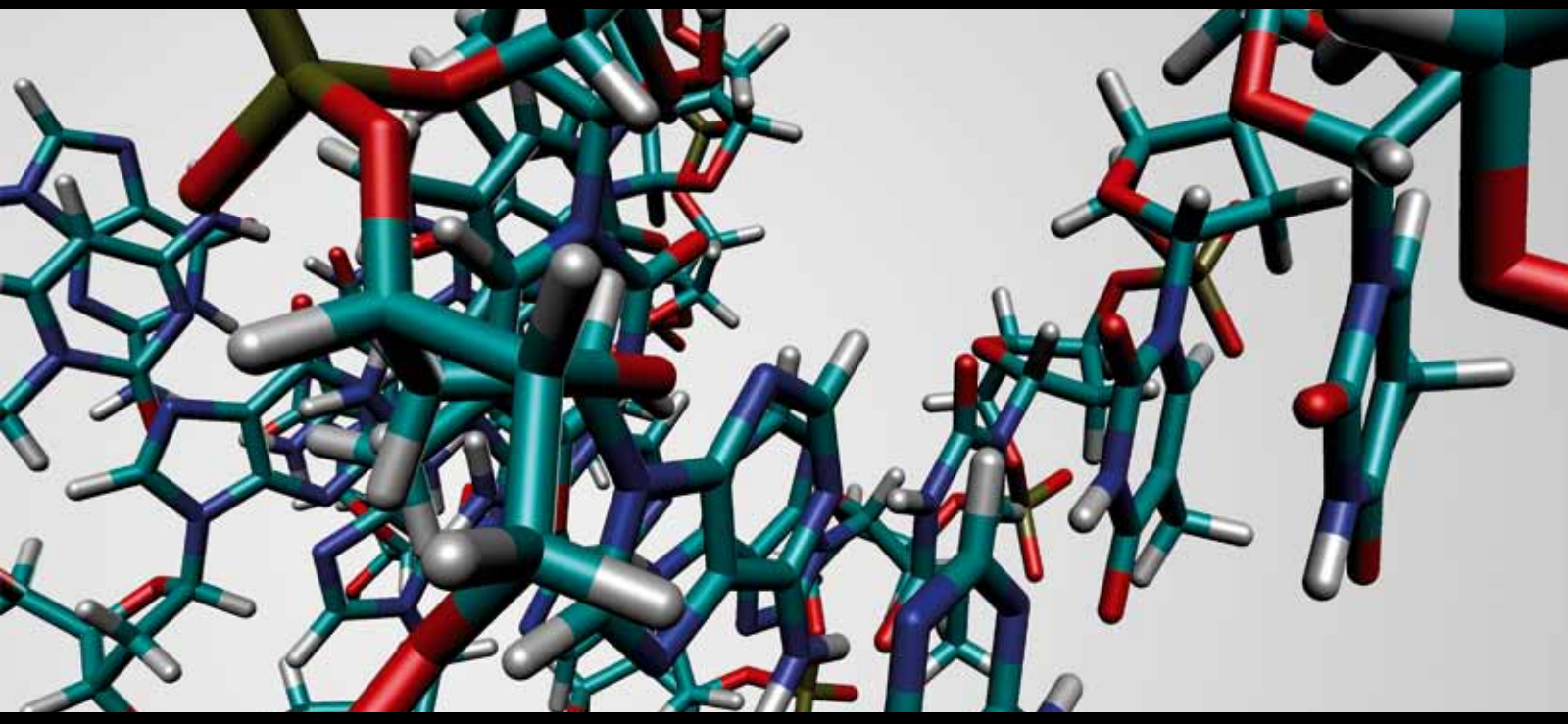

G-Quadruplex Nucleic Acids

Journal of Nucleic Acids

G-Quadruplex Nucleic Acids

Guest Editors: Ramon Eritja, Jean-Louis Mergny, Daniela Montesarchio, Lea Spindler, and Mateus Webba da Silva

Editorial Board

Contents

SAGE-Hindawi Access to Research
Journal of Nucleic Acids
Volume 2010, Article ID 147650, 2 pages
doi:10.4061/2010/147650

Editorial
G-Quadruplex Nucleic Acids

Ramon Eritja,[1] Jean-Louis Mergny,[2] Daniela Montesarchio,[3] Lea Spindler,[4,5] and Mateus Webba da Silva[6]

[1] *IRB Barcelona, IQAC-CSIC, Jordi Girona 16-26, 08034 Barcelona, Spain*
[2] *2 INSERM U869, Laboratoire ARNA, Université de Bordeaux 2, Institut Européen de Chimie-Biologie, 2 rue Robert Escarpit, 33607 Pessac Cedex, France*
[3] *Dipartimento di Chimica Organica e Biochimica, Università degli Studi di Napoli "Federico II", I-80126 Naples, Italy*
[4] *Faculty of Mechanical Engineering, University of Maribor, Smetanova 17, SI-2000 Maribor, Ljubljana, Slovenia*
[5] *Department of Complex Matter, J. Stefan Institute, Jamova 39, SI-1000, Ljubljana, Slovenia*
[6] *Faculty of Life and Health Sciences, University of Ulster, Cromore Road, Coleraine, BT52 1SA, Northern Ireland*

Correspondence should be addressed to Ramon Eritja, recgma@cid.csic.es

Received 9 June 2010; Accepted 9 June 2010

G-quadruplexes are a family of four-stranded structures stabilized by guanine quartets, in which four planar guanines establish a cyclic array of hydrogen bonds. They are of special interest due to the increasing evidence for their formation in vivo and their possible implication in biology, especially at telomeres and as contributors to gene regulation. Moreover, G-quadruplexes are also formed as a result of self-assembling processes of guanosine derivatives, yielding several interesting motifs such as G-ribbons and G-wires which have peculiar electrical conductivity properties that are being explored as molecular wires.

This special issue is initiated with two articles discussing the self-assembling properties of guanosine derivatives which describe the basic principles of G-quadruplex formation. The first article by Neviani et al. analyzes the presence of several levels of organization of guanosine derivatives carrying one or two lipophilic units as observed by light scattering techniques and transmission electron microscopy (TEM) experiments. The second article by Mariani et al. describes a study on quadruplex formation of 2′-deoxyguanosine monophosphate by small-angle X-ray scattering techniques.

The determination of the structural properties of short G-rich oligonucleotides is the aim of the following three articles. First the formation and dimensions of G-wires formed by the assembly of short G-rich sequences have been investigated by dynamic light scattering and electrophoresis. Spindler et al. show that macromolecular aggregates formed by self-assembly of quadruplex (G-wires) up to 11 nm can be observed. Next, the structure of a G-quadruplex formed between two cyclic oligonucleotides determined by nuclear magnetic resonance (NMR) and circular dichroism (CD) is described by Casals et al. Due to steric constraints, the global topology and the stability of the antiparallel G-quadruplex are different from the linear oligonucleotides. The adsorption and the redox behaviour of two intramolecular G-quadruplexes related with the thrombin binding aptamer are studied by atomic force microscopy (AFM) and voltammetry. Quadruplexes have distinct adsorption properties and redox behaviour that are characterized by Diculescu et al. in this article.

The natural occurrence and properties of G-quadruplex sequences including telomeres are the aim of the next three articles. Wong et al. provide useful information on a computational tool currently available at http://www.quadruplex.org/ for predicting the formation of G-quadruplex from sequence data. Next, a comparative study of the impact of G-spot probes on affymetrix GeneChips of mammalia is described by Memon et al. The thermodynamic properties of human telomeric repeats are the aim of the next article by Viglaski et al. demonstrating the importance of the overhanging sequences as a determining factor for the thermal stability and topology of G-quadruplexes.

The last section of this special issue is devoted to the study of the binding of small molecules to G-quadruplexes. An extensive up-to-date review on macrocyclic ligands for G-quadruplex DNA recognition by Monchaud et al. is heading this section. A second manuscript by Granzhan et al. describes the search of cyclophan-type macrocycles with

enhanced selective binding to quadruplex over duplex DNA sequences. The characterization of the binding of distamycin A derivatives to the tetrameric parallel TGGGGT quadruplex by isothermal titration calorimetry (ITC) is the aim of the work of Pagano et al. In a successive study, the binding mode of telomestatin to G-quadruplex DNA has been analyzed by mass spectrometry. The requirement of an extra monovalent cation between telomestatin and G-quadruplex DNA is analyzed by molecular modelling by Gabelica et al. The synthesis and properties of novel ligands for G-quadruplex structures are addressed in the next two articles. Iida et al. describe the synthesis of a dimeric macrocyclic hexaoxazole with enhanced affinity to telomeric DNA. Ferreira et al. describe the synthesis of dimeric and trimeric acridines with affinity to G-quadruplex structures found in promoter regions of oncogenes. Finally the interactions of porphyrin-Zinc (II) complexes with an intramolecular G-quadruplex have been analyzed by spectroscopic and docking methods by Ishikawa et al.

The editors of the issue would like to thank all the authors and referees involved in the production and evaluation of the manuscripts for their efforts in the preparation of this first special issue of the Journal of Nucleic Acids. This special issue shows the large interdisciplinarity and international scope of the research on G-quadruplex. Special thanks are given to the COST Action MP0802 entitled "Self-assembled guanosine structures for molecular electronic devices" (G4net, http://www.g4net.org/) for providing the "natural" forum of discussion and elaboration of ideas, as well as an excellent technical assistance, absolutely precious for the development of this special issue.

Ramon Eritja
Jean-Louis Mergny
Daniela Montesarchio
Lea Spindler
Mateus Webba da Silva

SAGE-Hindawi Access to Research
Journal of Nucleic Acids
Volume 2010, Article ID 938536, 9 pages
doi:10.4061/2010/938536

Research Article

Hierarchical Formation of Fibrillar and Lamellar Self-Assemblies from Guanosine-Based Motifs

Paolo Neviani,[1] Dominique Sarazin,[2] Marc Schmutz,[2] Christian Blanck,[2] Nicolas Giuseppone,[2,3] and Gian Piero Spada[1]

[1] *Dipartimento di Chimica Organica "A. Mangini", Alma Mater Studiorum—Università di Bologna, Via San Giacomo 11, 40126 Bologna, Italy*
[2] *Centre National de la Recherche Scientifique, Institut Charles Sadron, Université de Strasbourg, 23 Rue du Loess, BP 84087, 67034 Strasbourg cedex 2, France*
[3] *SAMS Research Group, icFRC, Centre National de la Recherche Scientifique, Université de Strasbourg, 23 Rue du Loess, BP 84087, 67034 Strasbourg cedex 2, France*

Correspondence should be addressed to Nicolas Giuseppone, giuseppone@unistra.fr and Gian Piero Spada, gianpiero.spada@unibo.it

Received 1 February 2010; Revised 7 April 2010; Accepted 27 May 2010

Academic Editor: Lea Spindler

Here we investigate the supramolecular polymerizations of two lipophilic guanosine derivatives in chloroform by light scattering technique and TEM experiments. The obtained data reveal the presence of several levels of organization due to the hierarchical self-assembly of the guanosine units in ribbons that in turn aggregate in fibrillar or lamellar soft structures. The elucidation of these structures furnishes an explanation to the physical behaviour of guanosine units which display organogelator properties.

1. Introduction

Supramolecular self-assembly represents a key technology for the spontaneous construction of nanoarchitectures and for the fabrication of materials with enhanced physical and chemical properties [1–4]. In addition, a significant asset of supramolecular self-assemblies rests on their reversible formation, thanks to the kinetic lability of their noncovalent interactions. This dynamic nature can be exploited for the development of "self-healing" and "smart" materials towards the tuning of their functional properties upon various external factors [5–8]. One particular intriguing objective in the field is to reach a high level of control over the shape and size of the supramolecular architectures, in order to produce well-defined functional nanostructures by rational design [9]. In this direction, many investigations have been pursued toward the construction of self-assembled objects from numerous low-molecular weight scaffolds [10–18], for instance, by exploiting multiple directional hydrogen-bonding interactions. In particular, nucleobases have been used as supramolecular synthons as a result of their efficiency to code for noncovalent interaction motifs [19]. Among nucleobases, guanine represents the most versatile one, because of its different H-bond donor (N^1H and N^2H) and acceptor sites (O^6, N^3, and N^7) which display self-complementary patterns of interactions. Interestingly, and depending on the environmental conditions, guanosine derivatives can form various types of structures. Most of the supramolecular architectures reported so far from guanosine derivatives require the presence of a cation (alkali metal, earth-alkali, or lanthanide ions) [20–31] which stabilizes, via dipole-ion interactions, the macrocyclic G-quartet that can, in turn, stack in columnar G-quadruplex arrangements (Figure 1(a)). In addition, guanosine can polymerize via hydrogen bonding to give a variety of supramolecular networks including linear ribbons such as A- and B-types (Figures 1(b) and 1(c)).

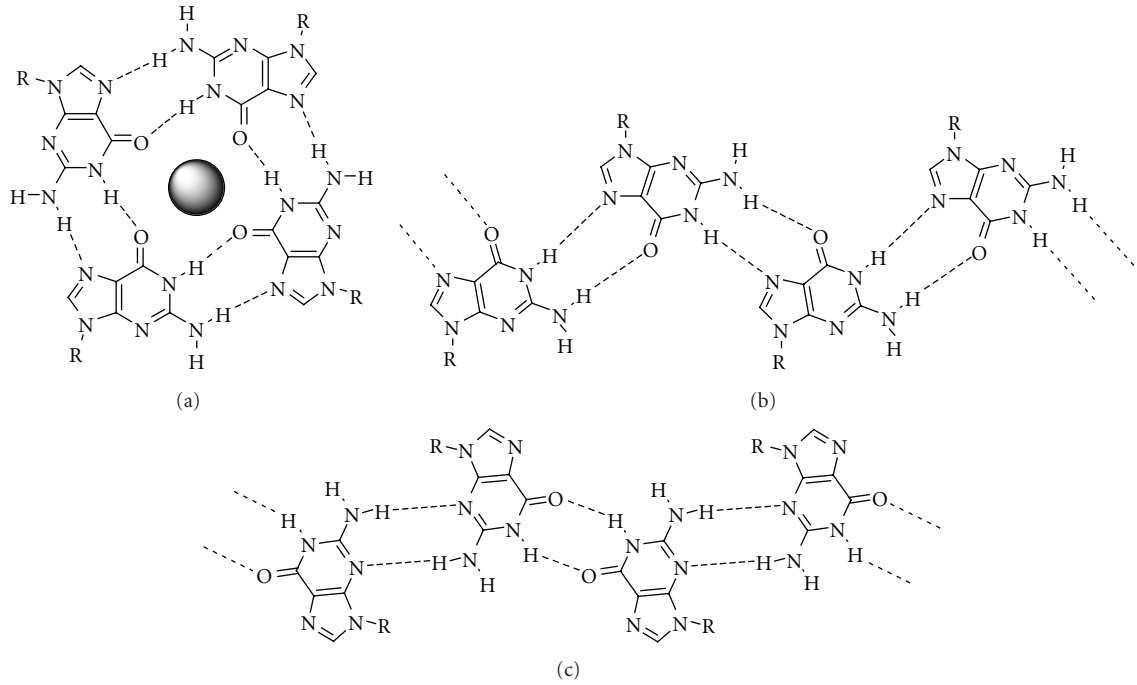

Figure 1: (a) G-quartet structure (the sphere indicates the central cation), (b) A-type ribbon, and (c) B-type ribbon.

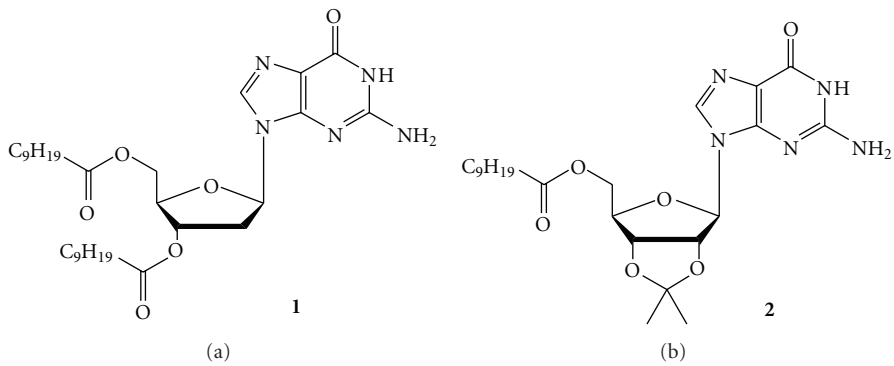

Figure 2: Structures of the two guanosine derivatives **1** and **2**.

This complex supramolecular behaviour confers to the guanine-guanine interactions their upper interest among all the homonucleobases studied [20, 32]. They have been subjected to intense investigations in various areas ranging from structural biology and medicinal chemistry—guanine-rich sequences are abundant in telomeric ends of chromosomes and promoter regions of DNA and are capable of forming G-quartet based structures [33–35]—to material science and nanotechnology [36, 37].

In 1998, it was reported [38] that, even in the absence of metal cations, lipophilic guanosine derivative **1** (Figure 2) is able to self-assemble in ribbon-like structures leading to the formation of a lyotropic liquid crystalline phase [39]. In the following years, the structures of the ribbons obtained from different guanosine derivatives have been characterized in solution (by NMR and ESI-MS), in the solid state (by X-ray diffraction and NMR), and at graphite-solution interface (by STM) [40–46]. Two different types of ribbons, with different patterns of hydrogen bonds, have been resolved in solution. The first species (ribbon-A, Figure 1(b)) is characterised by $N^2H\cdots O^6$ and $N^1H\cdots N^7$ hydrogen bonds, and the second one (ribbon-B, Figure 1(c)) by $N^1H\cdots O^6$ and $N^2H\cdots N^3$ hydrogen bonds. In the case of **1**, ribbon-A is detected in anhydrous chloroform solutions ($c > 10^{-2}$ M) soon after dissolving the polycrystalline powder but subsequently undergoes a structural transition towards a thermodynamically more stable ribbon-B [40]. Interestingly, in the case of the closely related chemical structure of **2**, only ribbon-B has been detected in chloroform solution (even soon after dissolution) [41]. For derivative **1**, the critical concentration for the formation of the gel-like phase was measured ≥ 0.596 M in chloroform, and for derivative **2** ≥ 0.125 M in the same solvent.

In both ribbon-like polymers A and B, the glycosidic bond adopts an *anti* conformation [42–46]. However, the two ribbons possess a different symmetry and, as a consequence, while ribbon-A does present a permanent dipole moment, it is not the case for ribbon-B. This feature has been exploited in organic electronic prototype devices [47–49], and more generally, linear ribbons from guanosine derivatives are considered as potential scaffolds for functional materials [50–54]. Although the formations of the linear ribbons and their H-bonding patterns have been demonstrated in solution [40, 41] (as well as in the crystal state and on graphite surface), only very few investigations have been performed so far toward the determination of the length of these supramolecular polymers, as well as on their possible hierarchical self-assemblies in higher scale structures. NMR spectroscopic indications of the supramolecular polymerisation only come from the shifting and broadening of the resonance signals upon concentration of the solution. In addition, the observation of negative enhancements (or positive cross-peaks) in NOE (or NOESY) experiments indicates that guanosine derivatives behave as large molecules with $M_W > 1000$ ($\omega\tau_c > 1$) [38–40].

In this paper we report on the investigation of the supramolecular polymerisation of **1** and **2** in chloroform by using light scattering technique as well as transmission electronic microscopy (TEM). This line of studies reveals the formation of supramolecular polymers with high molecular weights that produce hierarchical structuring of very soft self-assemblies displaying either fibrillar (**1**) or lamellar (**2**) organizations.

2. Results and Discussion

2.1. Static Light Scattering. The multiangle laser light scattering is the common technique [55, 56] for determining the shape of the polymers through the mean square radius of gyration $\langle R_g \rangle_z$ and their structure through the particle scattering factor $P_Z(q)$, the molecular weight M_W, and the second virial coefficient A_2. Theory took great interests long time ago giving statistical sense to these parameters [55–61]. When A_2 is near zero and solutions considered as athermal according to general polymer theories [61] one may deal with the apparent molecular weight $M_{w,\text{app}}$ and use the so-called statistical dimensions determined at discrete concentrations [59, 60] instead of the one extrapolated at $c \rightarrow 0$. Looking at the variation of $M_{w,\text{app}}$ versus concentration or temperature allows equilibrium constant K_0 to be evaluated which open fields to dynamics of the scaffolds and to their assembly ability. The form factor $P_Z(q)$ may be also useful to determine structural changes of the objects during the diffusion process of elementary unimers [59, 60]. The form factor may derive from calculations especially when the structure of the coil is well known. Theoretical aspects are shortly reviewed at the end of the paper (Section 4). There is shown typical processes for data calculations leading to Zimm plot which yields to the molecular dimensions and solution thermodynamics [55–58]. All the data obtained for guanosines **1** and **2** are summarized in Table 1.

Table 1: Molecular weights, radii of gyration, Virial coefficients, and Differential refraction indexes determined in chloroform solutions for guanosines **1** and **2**. The experimental errors were determined to be 2% on dn/dc, and 10% on A_2, $\langle R_g^2 \rangle_Z^{1/2}$, and $\langle M \rangle_W$.

	$\langle M \rangle_W$ g/mole	$\langle R_g^2 \rangle_Z^{1/2}$ nm	A_2 mol ml/g^2	dn/dc
Guanosine **1**	3620	57	$3.5\ 10^{-4}$	0.0769
Guanosine **2**	$5.93\ 10^4$	43	$-6.4\ 10^{-4}$	0.083

The Zimm plot obtained from guanosine **1** at 25°C in $CHCl_3$ for different concentrations is shown in Figure 3. In this range of concentration, the apparent molecular weight was determined to be relatively stable below the gelation threshold. The linear regression reveals a modest molecular weight of 3620 (corresponding to an aggregation number of 6 to 7 units) but with a radius of gyration of 57 nm which indicates the presence of large objects. The discrepancy between these two parameters is explained by the high polydispersity of the supramolecular polymer with an average of small ribbons together with a smaller population of large objects. Indeed, the gyration radius being determined from M_W, the importance of the large structures becomes predominant.

The molecular weight of the polymers depends largely on the concentration range and a study between $2.88\ 10^{-3}$ and $2.88\ 10^{-2}$ g·mL^{-1} reveals a power law of 0.75 (see Figure 4) which is higher than the value (0.6) for regular swollen coils and which is the signature for rigid objects of about 200 nm in length [57, 62].

Finally, the association constant K_0 between two monomers in the supramolecular B-type ribbon (see Figure 1(c)) was determined by plotting the apparent molecular weight as a function of the concentration (Figure 5) and shows a relatively small value $K_0 = 400\,\text{L mol}^{-1}$ [59, 60].

When the polymer is homogeneous, Flory Krigbaum [63] derived the more realistic model for A_2 introducing the κ enthalpy and ψ entropy parameter, respectively. By comparison with the Flory-Huggins theory [64] these parameters are seen to be related by $\psi - \kappa = (1/2) - \chi$ where χ is the Flory Huggins interaction parameters. For ideal behaviour $\psi = \kappa$ and $A_2 = 0$ so the theta point is reached, with theta temperature being given by $\theta = T(\kappa/\psi)$ where T is the absolute temperature. The theory leads to some basics which are the equivalent size of the solvent and monomers, respectively, and a number of association for statistical calculations.

These statistical basics hold for guanosine **2** but comments on guanosine **1** may lie in the expression of idealized lattice model for second virial coefficient. It is obvious that one of the optimal conditions for association is an athermal solution which is what we have found for guanosine **2** (Table 1). In the case of guanosine **2**, the light scattering reveals a quite different behavior of the self-assembly process. The Zimm plot in Figure 6 shows a smaller polidispersity

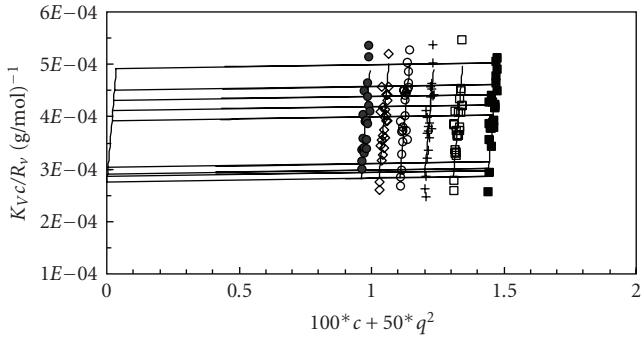

Figure 3: Zimm analysis by a two-power law linear regression (full line) which yields to the molecular size for molecule **1** from both extrapolations to $q, c \rightarrow 0$. M_W = 3620 dalton and $\langle R_g^2 \rangle_Z^{1/2}$ = 57 nmA_2 = 3.5 10^{-4} mol ml/g2 (■) = 1.44 10^{-2} g/ml; (□) = 1.31 10^{-2} g/ml; (+) =1.2 10^{-2} g/ml; (○) =1.11 10^{-2} g/ml; (◊) = 1.03 10^{-2} g/ml; (●) = 9.6 10^{-3} g/ml.

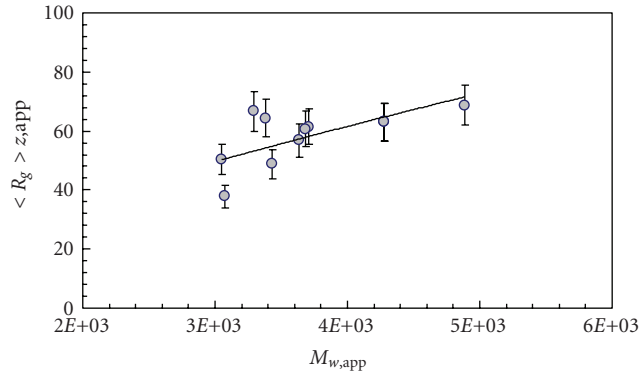

Figure 4: The experimental power law for guanosine **1** is 0.75, higher than the value for regular swollen coil 0.6 (for the apparent Molecular weight (●)) and is the signature for a rigid object (error bars of 10%). ⟨R*g*⟩*z*,app is a statistical value of the gyration radius depending on the mass and number of monomers in the polymer (see [64]).

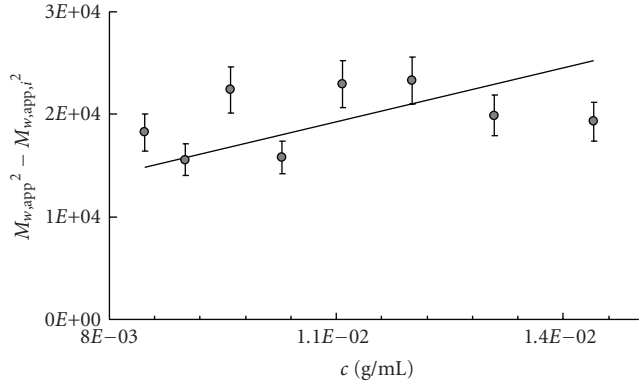

Figure 5: Determination of the equilibrium constant in the polymerization of **1**. $M_{w,\mathrm{app},i}$ is the molecular weight of the initial monomer **1** starting the association. The guiding line shows the experimental points' regular behaviour. From the straight line it is possible to calculate the equilibrium constant of the association K_0 = 400 L mol^{-1} (error bars of 10%).

than what is measured for guanosine **1** together with higher molecular weights (M_W = 5.93 10^4, and the degree of polymerisation D_p = 1250), but with a close radius of gyration (43 nm) which might correlate with the formation of more compact objects. This expectation is confirmed by plotting the M_W in the range of concentration 3.4 10^{-3} and 6.82 10^{-3} g · mL^{-1}. The experimentally determined power law of 0.3 (see Figure 7) is the signature for very compact objects such as spheres [57, 62]. Finally, the determination of the equilibrium constant [59, 60] for guanosine **2** shows a strong association process (K_0 = 6.75 10^5 L mol^{-1}) and a complex behaviour of a sigmoid type (Figure 8). This nonlinear effect indicates a cooperative process and the hierarchical association between the linear supramolecular ribbons with their organization in higher-ordered self-assembled structures that in turn stabilize the primary association.

2.2. Transmission Electron Microscopy. Structural observation of self-assembled system can easily be achieved by TEM approaches, as widely used and described in the literature [65, 66].

Guanosine derivative **1** in bromoform (1.44 10^{-2} g · mL^{-1}) forms small short fibers (Figure 9(a)). Bromoform was used for technical reasons regarding the evaporation rate at room temperature which is too high for chloroform thus changing the concentration of the sample during the preparation step. The dielectric constants are very close to each other for chloroform and bromoform (4,8 and 4,4 at 20°C, resp.), and the gelation concentration was observed to be similar in both cases. These fibers present a diameter of 6 nm and a length of approximatively 200 nm. Indeed, the precise length cannot be determined as the fibers present a high entanglement ratio. This length corresponds to the distance between the nodes of the networks and was also observed from time to time on individual filaments (see Figure 9(b)). It is also in agreement with the light scattering data. The small individual fibers self-assemble in larger ones to form bundles of 30 nm. These latter can be formed during the preparation step as the diameter of the bundles varies from one experiment to another. The distribution of the fibers within a clear network illustrates the organogelator properties of guanosine **1**.

Guanosine derivative **2** in bromoform (4 10^{-3} g · mL^{-1}) forms small aggregates and small lamellar structures. On Figure 10, large aggregates consisting of the superposition of small (100 nm) lamellar structures are observed (see arrows). These structures show no define contours and are the results of the aggregations of the smaller domains. No internal features inside the small domains are visible at the resolution of the technique. The aggregation within highly compact lamellar structures is also in good agreement with the light scattering experiments that indicate mainly the presence of pseudospherical objects with a strong cooperative effect occurring between the ribbons and their higher-scale self-assemblies.

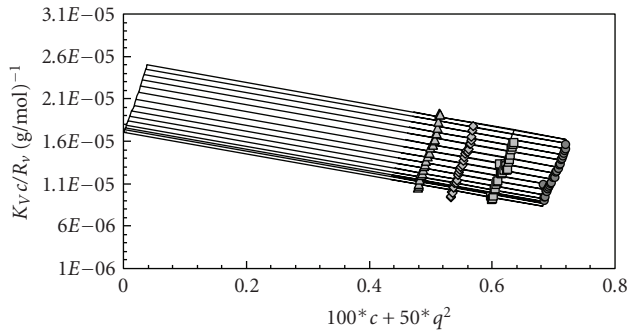

FIGURE 6: Zimm analysis by a two-power law linear regression (full line) which yields to the molecular size for molecule **2** from both extra polations to $q, c \rightarrow 0$. $M_W = 5.93\ 10^4$ Dalton and $\langle R_g^2 \rangle_Z^{1/2} = 43$ nm$A_2 = -6.4\ 10^{-4}$ mol ml/g^2 (●) = $6.82\ 10^{-3}$ g/ml; (■) = $5.97\ 10^{-3}$ g/ml; (♦) = $5.31\ 10^{-3}$ g/ml; (▲) = $4.78\ 10^{-3}$ g/ml.

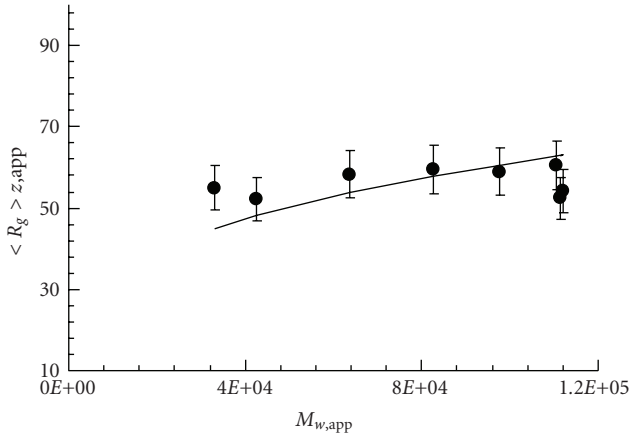

FIGURE 7: The experimental power law for guanosine **2** is 0.3 for the apparent Molecular weight (●). The result shows a signature of very compact object and is the value for an athermal binary solution as ascertained by the low value for A_2, the second virial coefficient (error bars of 10%).

3. Conclusions

We have determined the hierarchical polymeric natures of the self-assemblies obtained from the ribbon forming [40, 41] guanosine derivatives **1** and **2**. The light scattering measurements appeared as an appropriate technique for the molecular weight determination versus the structure of these objects that are both concentration sensitive. The main conclusions were confirmed by TEM. Lipophilic guanosine **1** forms very soft fibrillar objects of 6 nm of diameter and 200 nm in length and that in turn produces bundles of networked fibers with 30 nm of diameter. Despite its closely related structure, guanosine **2** forms much longer ribbons with molecular weights up to $6\ 10^5$ that in turn fold in very compact aggregates with lamellar structures. This process has been shown to be highly cooperative by the determination of the molecular weight as a function of the concentration.

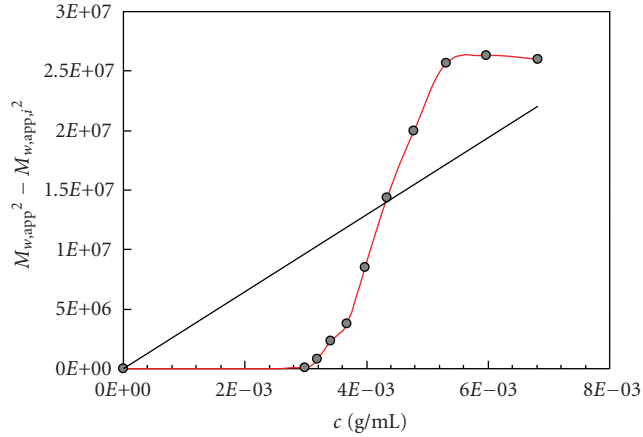

FIGURE 8: Determination of K_0 for compound **2**. $M_{w,\mathrm{app},i}$ is the molecular weight of the initial monomer starting the association [59, 60]. The red guiding line shows the experimental points' sigmoïdal behaviour. From the straight line, extrapolated for a noncooperative association, it is possible to calculate the mean equilibrium constant of the association $K_0 = 6.7\ 10^5$ L mol^{-1}.

Interestingly, while both derivatives show the same motif of H-bonding in the formation of the first level of supramolecular assembly (the B-type ribbon), their hierarchical organization is quite different. This finding points out the role of other structural aspects in addition to the H-bond recognition pattern (e.g., the number and length of tails) in determining the shape and dimension of the object obtained at the nanoscale level.

These investigations furnish an explanation to the gelation properties of these two derivatives and can be used to rationalize the synthesis of functional guanosine-based soft materials.

4. Materials and Methods

4.1. Experimental Details for the Synthesis of Guanosine Derivatives

3′,5′-O-Didecanoyl-2′-Deoxyguanosine ***1***. Compound **1** was prepared in 94% yield starting from 2′-deoxyguanosine (Fluka) (1 mmol) and decanoic anhydride (2.2 mmol) according to the literature procedure for 3′,5′-*O*-dipropanyl-2′-deoxyguanosine [67]. ^{1}H NMR (300 MHz, [D6]DMSO): $\delta = 0.84-0.86$ (tt, 6H; 2 CH3), 1.18−1.40 (m, 24H; 12 CH2), 1.40 − 1.60 (m, 4H; 2 CH2–CH2–CO), 2.35-2.36 (tt, 4H; 2 CH2–CO), 2.42 and 2.93 (mm, 2H, H-2′/H-2′′), 4.19 − 4.38 (m, 3H; H-4′/H-5′/H-5′′), 5.35 (m, 1H; H-3′), 6.17 (m, 1H; H-1′), 6.45 (bs, 2H; NH2), 7.9 (s, 1H; H-8), 10.65 (s, 1H; NH); ES-MS: m/z (%): 576.8 (100) [**1**$^+$+H].

2′,3′-O-Isopropylidene-5′-Decanoylguanosine ***2***. Compound **2** was prepared in 86% yield starting from 2′, 3′-*O*-isopropylideneguanosine (Sigma) (0.77 mmol) and decanoic anhydride (1.2 equiv) according to the literature procedure [41].

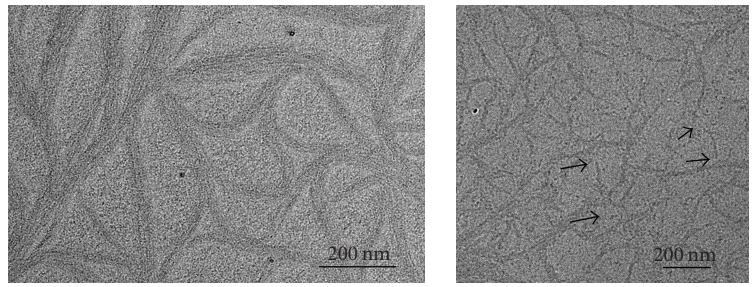

(a) (b)

Figure 9: (a) TEM image of guanosine derivative **1** showing bundles of fibers. (b) Picture of compound **1** of individual fibers observed in a more dispersed area. The length of the fibers, which is close to 200 nm, can only be measured on a very small number as they show a high tendency to fusion to form larger and entangled fibers.

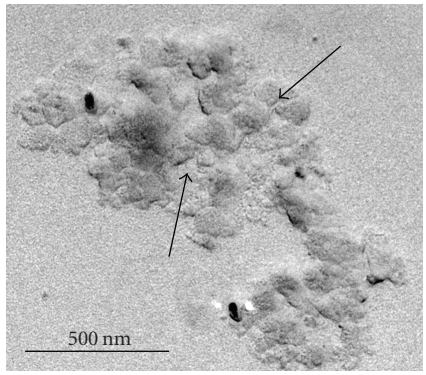

Figure 10: TEM image of guanosine derivative **2**.

4.2. Experimental Details Concerning the Static Light Scattering Technique. The light scattering experiments were carried out with an in-house apparatus [61] equipped with (i) a red He-Ne laser of wavelength $\lambda_0 = 632.8$ nm in vacuum, (ii) a discrete-angle goniometer acting within the range from 20° to 155°, (iii) a Hamamatsu type photomultiplier as detector, (iv) a photocounting device, and (v) a toluene matching bath. The vertical polarization of the incident beam with respect to the scattering plane has been used and is written V. The analyzer, arranged between the measuring cell and the photomultiplier, is vertically oriented and is written V_V. This optical setup allows measurement of the isotropic V_V scattering intensity [68]. The excess of light scattering intensity $V_V(q) = V_{V\text{solution}} - V_{V\text{solvent}}$ was measured as a function of scattering vector $q = (4\pi n/\lambda_0)\sin(\theta/2)$ with an accuracy of 1% (θ the scattering angle, n the solvent refractive index). The values of Rayleigh excess scattering intensity $R(q)$ were obtained through the calibration of $V_V(q)$ with a benzene standard. The intensities $V_V(q)$, after normalization of the raw data, can be written R_V for the vertically polarized scattering light through an analyzer.

Use the following formula for stray light R_v:

$$R_V = K_V * c * M_W * P(q) * S(q), \tag{1}$$

where M_W is the molecular weight, c is the concentration of the polymer, $P(q)$ is the form factor, and $S(q)$ the long range interference from distant scatterers, where for dilute solution $S(q) \sim 1$ and K_V is the optical factor for the system including the refractive index increment of the polymer as follows, where $K_V = K_{V\text{benzene}}(dn/dc)^2$ is the optical contrast calibrated with benzene standard (the suffix gives the polarization of incident beam and stray light).

The calibration of the spectrometer was made by evaluating the optical constant K_V or $K_{V,V}$ as follows:

$$K_V = \frac{4\pi^2 n_{\text{ref}}^2}{R_{V,\text{ref}} N_A \lambda_0^4}. \tag{2}$$

N_A is Avogadro Number, λ_0 is the wavelength in vacuum, n_{ref} is the benzene refractive index, and $R_{V,\text{ref}}$ is the benzene Rayleigh ratio for vertically polarised incident light.

The chloroform refractive index and the average refractive index increment of the assembly for **1** to $CHCl_3$ are equal to $n = 1.4459$ and $dn/dc = 0.0769$ ml/g, respectively.

The chloroform refractive index and the average refractive index increment of the assembly for **2** to $CHCl_3$ are equal to $n = 1.4459$ and $dn/dc = 0.0830$ ml/g respectively.

According to Yamakawa [62] the ratio $K_V c/R_V$ may be read versus q as

$$\frac{K_V c}{R_V} = \frac{1}{M_W P(q)}(1 + A_2 M_W c)^2, \tag{3}$$

where R_V is the normalized scattering intensity from vertically incident beam analyzed vertically, and A_2 is the second virial coefficient.

Using the formalism of Debye [55] and Zimm [56], (2) gives the following:

$$\frac{K_V c}{\Delta R_V} = M_W^{-1} P^{-1}(q) + 2A_2 c. \tag{4}$$

ΔR_v is the excess Rayleigh ratio of the polymer comparatively to the solvent. The inverse of the form factor $P^{-1}(q)$ leads after a MacLaurin transform at low q vector to (5). Here we get $\langle R_g^2 \rangle_z$ the second moment of the mass distribution which is the statistic z average mean radius of gyration [57, 58] as follows:

$$\frac{K_V c}{\Delta R_V} = M_W^{-1}\left(1 + \frac{q^2 \langle R^2 \rangle_z}{3} + \cdots\right) + 2A_2 c. \tag{5}$$

For extrapolation at $q^2 \to 0$ and $C \to 0$ (4) leads to the determination of the molecular mass and the second virial coefficient A_2. When the thermodynamic forces applied on the coil equilibrate, we can write $A_2 = 0$. This athermal condition for binary mixture allows the determination of the apparent molecular mass $M_{W,\text{app}}$ for each concentration [59, 60]:

$$\frac{K_V c}{\Delta R_V} = M_{w,\text{app}}^{-1}\left(1 + \frac{q^2\langle R^2\rangle_z}{3}\right) \pm \cdots . \tag{6}$$

Equation (6) contains all information on the shape and the conformation of the isolated polymer in solution. The determination of the radius of gyration is only valid in the guinier range $qR < 1$ where the architectures of the polymers are barely distinguishable.

The plot of (5) versus $k'q^2 + k''c$, called Zimm-plot, allows a simultaneous extrapolation to $q = 0$ and $c = 0$, which yields $M_W^{-1}(\text{g} \cdot \text{mol}^{-1})$ as the ordinate intercept and $\langle R_g^2\rangle_Z^{1/2}$ as the initial slope of (6) and the second viral coefficient A_2 from (5).

The value of the second viral coefficient A_2 is in our case of an athermal binary mixture and thus neglected:

$$\lim_{(q\to 0)} \frac{Kc}{\Delta R_V} = M_{w,\text{app}}^{-1}. \tag{7}$$

So we get a good evaluation of the variation for $M_{w,\text{app}}$ versus the concentration C.

Following the calculation of Huglin [59] and Elias [60] we obtain

$$M_{w,\text{app}}^2 - M_{w,\text{app},i}^2 = 4000\left(K_0 M_{w,\text{app},i}\right)c. \tag{8}$$

Here $M_{w,\text{app},i}$ is the molecular weight of the initial monomer and $M_{w,\text{app}}$ is the weight average molecular weight determined through (7).

Measurements of each sample have been carried out after various dilutions with precise volume of clarified solvent obtained by filtration through millipore filters size 0.45 μm. All the samples are directly processed in the measurements vial to avoid dust pollution.

4.3. Experimental Details Concerning the TEM Technique. The samples are prepared in standard conditions as described in literature [69].

Acknowledgments

This work was supported by the COST Network G4-NET (MPNS Action MP0802). P. Neviani thanks the University of Bologna for a Marco Polo Fellowship supporting his staying in Strasbourg. N. Giuseppone and M. Schmutz thank the icFRC for financial support.

References

[1] J.-M. Lehn, "Perspectives in supramolecular chemistry—from the lock-and-key image to the information," *Perspectives in Supramolecular Chemistry*, vol. 1, pp. 307–317, 1994.

[2] F. J. M. Hoeben, P. Jonkheijm, E. W. Meijer, and A. P. H. J. Schenning, "About supramolecular assemblies of π-conjugated systems," *Chemical Reviews*, vol. 105, no. 4, pp. 1491–1546, 2005.

[3] D. S. Lawrence, T. Jiang, and M. Levett, "Self-assembling supramolecular complexes," *Chemical Reviews*, vol. 95, no. 6, pp. 2229–2260, 1995.

[4] A. Ajayaghosh, S. J. George, and A. P. H. J. Schenning, "Hydrogen-bonded assemblies of dyes and extended π-conjugated systems," *Topics in Current Chemistry*, vol. 258, pp. 83–118, 2005.

[5] T. F. A. de Greef and E. W. Meijer, "Materials science: supramolecular polymers," *Nature*, vol. 453, no. 7192, pp. 171–173, 2008.

[6] P. Cordier, F. Tournilhac, C. Soulié-Ziakovic, and L. Leibler, "Self-healing and thermoreversible rubber from supramolecular assembly," *Nature*, vol. 451, no. 7181, pp. 977–980, 2008.

[7] R. Nguyen, E. Buhler, and N. Giuseppone, "Dynablocks: structural modulation of responsive combinatorial self-assemblies at mesoscale," *Macromolecules*, vol. 42, no. 16, pp. 5913–5915, 2009.

[8] L. Tauk, A. P. Schröder, G. Decher, and N. Giuseppone, "Hierarchical functional gradients of pH-responsive self-assembled monolayers using dynamic covalent chemistry on surfaces," *Nature Chemistry*, vol. 1, no. 8, pp. 649–656, 2009.

[9] M. Schmittel and V. Kalsani, "Functional, discrete, nanoscale supramolecular assimblies," *Topics in Current Chemistry*, vol. 245, pp. 1–53, 2005.

[10] S. Yagai, T. Seki, T. Karatsu, A. Kitamura, and F. Würthner, "Transformation from H- to J-aggregated perylene bisimide dyes by complexation with cyanurates," *Angewandte Chemie International Edition*, vol. 47, no. 18, pp. 3367–3371, 2008.

[11] P. G. A. Janssen, J. Vandenbergh, J. L. J. Van Dongen, E. W. Meijer, and A. P. H. J. Schenning, "ssDNA templated self-assembly of chromophores," *Journal of the American Chemical Society*, vol. 129, no. 19, pp. 6078–6079, 2007.

[12] A. Piermattei, M. Giesbers, A. T. M. Marcelis et al., "Induction of liquid crystallinity by self-assembled molecular boxes," *Angewandte Chemie International Edition*, vol. 45, no. 45, pp. 7543–7546, 2006.

[13] D. B. Amabilino and J. Veciana, "Supramolecular chiral functional materials," *Topics in Current Chemistry*, vol. 265, pp. 253–302, 2006.

[14] L. Brunsveld, B. J. B. Folmer, E. W. Meijer, and R. P. Sijbesma, "Supramolecular polymers," *Chemical Reviews*, vol. 101, no. 12, pp. 4071–4097, 2001.

[15] B. L. Feringa, R. A. Van Delden, N. Koumura, and E. M. Geertsema, "Chiroptical molecular switches," *Chemical Reviews*, vol. 100, no. 5, pp. 1789–1816, 2000.

[16] K. Kinbara and T. Aida, "Toward intelligent molecular machines: directed motions of biological and artificial molecules and assemblies," *Chemical Reviews*, vol. 105, no. 4, pp. 1377–1400, 2005.

[17] S. Yagai and A. Kitamura, "Recent advances in photoresponsive supramolecular self-assemblies," *Chemical Society Reviews*, vol. 37, no. 8, pp. 1520–1529, 2008.

[18] G. P. Spada, "Alignment by the convective and vortex flow of achiral self-assembled fibers induces strong circular dichroism effects," *Angewandte Chemie International Edition*, vol. 47, no. 4, pp. 636–638, 2008.

[19] S. Sivakova and S. J. Rowan, "Nucleobases as supramolecular motifs," *Chemical Society Reviews*, vol. 34, no. 1, pp. 9–21, 2005.

[20] J. T. Davis and G. P. Spada, "Supramolecular architectures generated by self-assembly of guanosine derivatives," *Chemical Society Reviews*, vol. 36, no. 2, pp. 296–313, 2007.

[21] G. Gottarelli, S. Masiero, and G. P. Spada, "Self-assembly in organic solvents of a deoxyguanosine derivative induced by alkali metal picrates," *Journal of the Chemical Society, Chemical Communications*, no. 24, pp. 2555–2557, 1995.

[22] J. T. Davis, S. Tirumala, J. R. Jenssen, E. Radler, and D. Fabris, "Self-assembled ionophores from isoguanosine," *Journal of Organic Chemistry*, vol. 60, no. 13, pp. 4167–4176, 1995.

[23] C. Arnal-Hérault, A. Banu, M. Barboiu, M. Michau, and A. van der Lee, "Amplification and transcription of the dynamic supra-molecular chirality of the guanine quadruplex," *Angewandte Chemie International Edition*, vol. 46, no. 23, pp. 4268–4272, 2007.

[24] S. Martic, X. Liu, S. Wang, and G. Wu, "Self-assembly of N^2-modified guanosine derivatives: formation of discrete G-octamers," *Chemistry*, vol. 14, no. 4, pp. 1196–1204, 2008.

[25] I. C. M. Kwan, A. Wong, Y.-M. She, M. E. Smith, and G. Wu, "Direct NMR evidence for Ca^{2+} ion binding to G-quartets," *Chemical Communications*, no. 6, pp. 682–684, 2008.

[26] M. Nikan and J. C. Sherman, "Template-assembled synthetic G-quartets (TASQs)," *Angewandte Chemie International Edition*, vol. 47, no. 26, pp. 4900–4902, 2008.

[27] L. Ma, M. Melegari, M. Colombini, and J. T. Davis, "Large and stable transmembrane pores from guanosine-bile acid conjugates," *Journal of the American Chemical Society*, vol. 130, no. 10, pp. 2938–2939, 2008.

[28] A. Likhitsup, S. Yu, Y.-H. Ng, C. L.L. Chai, and E. K.W. Tam, "Controlled polymerization and self-assembly of a supramolecular star polymer with a guanosine quadruplex core," *Chemical Communications*, no. 27, pp. 4070–4072, 2009.

[29] M. D. C. Rivera-Sánchez, I. Andújar-de-Sanctis, M. García-Arriaga, V. Gubala, G. Hobley, and J. M. Rivera, "Walking a supramolecular tightrope: a self-assembled dodecamer from an 8-aryl-2′-deoxyguanosine derivative," *Journal of the American Chemical Society*, vol. 131, no. 30, pp. 10403–10405, 2009.

[30] D. González-Rodriguez, J. L. J. van Dongen, M. Lutz, A. L. Spek, A. P. H. J. Schenning, and E. W. Meijer, "G-quadruplex self-assembly regulated by Coulombic interactions," *Nature Chemistry*, vol. 1, no. 2, pp. 151–155, 2009.

[31] S. Lena, P. Neviani, S. Masiero, S. Pieraccini, and G. P. Spada, "Triggering of guanosine self-assembly by light," *Angewandte Chemie International Edition*, vol. 49, no. 21, pp. 3657–3660, 2010.

[32] M. S. Kaucher, W. A. Harrell Jr., and J. T. Davis, "The G-quartet in supramolecular chemistry and nanoscience," in *Quadruplex Nucleic Acids*, S. Neidle and S. Balasubramanian, Eds., chapter 10, pp. 253–290, RSC Publishing, Cambridge, UK, 2006.

[33] S. Neidle and S. Balasubramanian, Eds., *Quadruplex Nucleic Acids*, RSC Publishing, Cambridge, UK, 2006.

[34] J. L. Huppert, "Four-stranded nucleic acids: structure, function and targeting of G-quadruplexes," *Chemical Society Reviews*, vol. 37, no. 7, pp. 1375–1384, 2008.

[35] D. Monchaud and M.-P. Teulade-Fichou, "A hitchhiker's guide to G-quadruplex ligands," *Organic and Biomolecular Chemistry*, vol. 6, no. 4, pp. 627–636, 2008.

[36] J. T. Davis, "G-quartets 40 years later: from 5′-GMP to molecular biology and supramolecular chemistry," *Angewandte Chemie International Edition*, vol. 43, no. 6, pp. 668–698, 2004.

[37] S. Lena, S. Masiero, S. Pieraccini, and G. P. Spada, "Guanosine hydrogen-bonded scaffolds: a new way to control the bottom-up realisation of well-defined nanoarchitectures," *Chemistry*, vol. 15, no. 32, pp. 7792–7806, 2009.

[38] G. Gottarelli, S. Masiero, E. Mezzina, G. P. Spada, P. Mariani, and M. Recanatini, "The self-assembly of a lipophilic deoxyguanosine derivative and the formation of a liquid-crystalline phase in hydrocarbon solvents," *Helvetica Chimica Acta*, vol. 81, no. 11, pp. 2078–2092, 1998.

[39] G. Gottarelli, S. Masiero, E. Mezzina, S. Pieraccini, G. P. Spada, and P. Mariani, "A new lyotropic liquid crystalline phase formed in hydrocarbon solvents by a deoxyguanosine derivative through extensive hydrogen bonding," *Liquid Crystals*, vol. 26, no. 7, pp. 965–971, 1999.

[40] G. Gottarelli, S. Masiero, E. Mezzina et al., "The self-assembly of lipophilic guanosine derivatives in solution and on solid surfaces," *Chemistry*, vol. 6, no. 17, pp. 3242–3248, 2000.

[41] T. Giorgi, F. Grepioni, I. Manet et al., "Gel-like lyomesophases formed in organic solvents by self-assembled guanine ribbons," *Chemistry*, vol. 8, no. 9, pp. 2143–2152, 2002.

[42] S. Lena, G. Brancolini, G. Gottarelli et al., "Self-assembly of an alkylated guanosine derivative into ordered supramolecular nanoribbons in solution and on solid surfaces," *Chemistry*, vol. 13, no. 13, pp. 3757–3764, 2007.

[43] T. N. Pham, J. M. Griffin, S. Masiero et al., "Quantifying hydrogen-bonding strength: the measurement of 2hJNN couplings in self-assembled guanosines by solid-state 15N spin-echo MAS NMR," *Physical Chemistry Chemical physics*, vol. 9, no. 26, pp. 3416–3423, 2007.

[44] S. A. Joyce, J. R. Yates, C. J. Pickard, and S. P. Brown, "Density functional theory calculations of hydrogen-bond-mediated NMR J coupling in the solid state," *Journal of the American Chemical Society*, vol. 130, no. 38, pp. 12663–12670, 2008.

[45] G. P. Spada, S. Lena, S. Masiero, S. Pieraccini, M. Surin, and P. Samorì, "Guanosine-based hydrogen-bonded scaffolds: controlling the assembly of oligothiophenes," *Advanced Materials*, vol. 20, no. 12, pp. 2433–2438, 2008.

[46] A. Ciesielski, S. Lena, S. Masiero, G. P. Spada, and P. Samorì, "Dynamers at the solid-liquid interface: controlling the reversible assembly/reassembly process between two highly ordered supramolecular guanine motifs," *Angewandte Chemie International Edition*, vol. 49, no. 11, pp. 1963–1966, 2010.

[47] G. Maruccio, P. Visconti, V. Arima, et al., "Field effect transistor based on a modified DNA base," *Nano Letters*, vol. 3, no. 4, pp. 479–483, 2003.

[48] R. Rinaldi, E. Branca, R. Cingolani, S. Masiero, G. P. Spada, and G. Gottarelli, "Photodetectors fabricated from a self-assembly of a deoxyguanosine derivative," *Applied Physics Letters*, vol. 78, no. 22, pp. 3541–3543, 2001.

[49] H. Liddar, J. Li, A. Neogi et al., "Self-assembled deoxyguanosine based molecular electronic device on GaN substrates," *Applied Physics Letters*, vol. 92, no. 1, Article ID 013309, 3 pages, 2008.

[50] K. Maekawa, D. Shiomi, T. Ise, K. Sato, and T. Takui, "A guanine-substituted nitronyl nitroxide radical forming a one-dimensional ferromagnetic chain," *Organic and Biomolecular Chemistry*, vol. 5, no. 10, pp. 1641–1645, 2007.

[51] A. M. S. Kumar, S. Sivakova, J. D. Fox, J. E. Green, R. E. Marchant, and S. J. Rowan, "Molecular engineering of supramolecular scaffold coatings that can reduce static platelet adhesion," *Journal of the American Chemical Society*, vol. 130, no. 4, pp. 1466–1476, 2008.

[52] K. Araki and I. Yoshikawa, "Nucleobase-containing gelators," *Topics in Current Chemistry*, vol. 256, pp. 133–165, 2005.

[53] K. Araki, R. Takasawa, and I. Yoshikawa, "Design, fabrication, and properties of macroscale supramolecular fibers consisted

of fully hydrogen-bonded pseudo-polymer chains," *Chemical Communications*, no. 18, pp. 1826–1827, 2001.

[54] A. M. S. Kumar, J. D. Fox, L. E. Buerkle, R. E. Marchant, and S. J. Rowan, "Effect of monomer structure and solvent on the growth of supramolecular nanoassemblies on a graphite surface," *Langmuir*, vol. 25, no. 2, pp. 653–656, 2009.

[55] P. Debye, "Molecular-weight determination by light scattering," *Journal of Physical and Colloid Chemistry*, vol. 51, no. 1, pp. 18–32, 1947.

[56] B. H. Zimm, "The scattering of light and the radial distribution function of high polymer solutions," *The Journal of Chemical Physics*, vol. 16, no. 12, pp. 1093–1099, 1948.

[57] H. C. Benoi and J. S. Higgins, *Polymers and Neutron Scattering*, Clarendon Press, Oxford, UK, 1994.

[58] B. Chu, *Laser Light Scattering*, Academic Press, London, UK, 2nd edition, 1991.

[59] M. B. Huglin, *Light Scattering from Polymer Solutions*, Academic Press, New York, NY, USA, 1972.

[60] H. G. Elias, "Specific refractive index increments," in *Light Scattering from Polymer Solutions*, M. B. Huglin, Ed., p. 428, Huglin Academic Press, London, UK, 1972.

[61] R. Libeyre, D. Sarazin, and J. François, "Automatized photogoniodiffusometer and coupling with automatized viscosimeter," *Polymer Bulletin*, vol. 4, no. 1-2, pp. 53–60, 1981.

[62] H. Yamakawa, *Modern Theory of Polymer Solution*, Harper and Row, New York, NY, USA, 1971.

[63] P. J. Flory and W. R. Krigbaum, "Statistical mechanics of dilute polymer solutions. II," *The Journal of Chemical Physics*, vol. 18, no. 8, pp. 1086–1094, 1950.

[64] P. J. Flory, *Principles of Polymer Chemistry*, Cornell University Press, New York, NY, USA, 1957.

[65] R. Schmidt, M. Schmutz, M. Michel, G. Decher, and P. J. Mésini, "Organogelation properties of a series of oligoamides," *Langmuir*, vol. 18, no. 15, pp. 5668–5672, 2002.

[66] A. Petitjean, L. A. Cuccia, M. Schmutz, and J.-M. Lehn, "Naphthyridine-based helical foldamers and macrocycles: synthesis, cation binding, and supramolecular assemblies," *Journal of Organic Chemistry*, vol. 73, no. 7, pp. 2481–2495, 2008.

[67] I. Manet, L. Francini, S. Masiero, S. Pieraccini, G. P. Spada, and G. Gottarelli, "An ESI-MS and NMR study of the self-assembly of guanosine derivatives," *Helvetica Chimica Acta*, vol. 84, no. 7, pp. 2096–2107, 2001.

[68] G. G. Fuller, *Optical Rheometry of Complex Fluids: Theory and Practice of Optical Rheometry*, Oxford University Press, Oxford, UK, 1995.

[69] V. Berl, M. J. Krische, I. Huc, J.-M. Lehn, and M. Schmutz, "Template-induced and molecular recognition directed hierarchical generation of supramolecular assemblies from molecular strands," *Chemistry*, vol. 6, no. 11, pp. 1938–1946, 2000.

SAGE-Hindawi Access to Research
Journal of Nucleic Acids
Volume 2010, Article ID 472478, 10 pages
doi:10.4061/2010/472478

Research Article

Guanosine Quadruplexes in Solution: A Small-Angle X-Ray Scattering Analysis of Temperature Effects on Self-Assembling of Deoxyguanosine Monophosphate

P. Mariani,[1] F. Spinozzi,[1] F. Federiconi,[1] M. G. Ortore,[1] H. Amenitsch,[2] L. Spindler,[3] and I. Drevensek-Olenik[4]

[1] *Physical Science Section, Research Unit of Ancona, SAIFET Department, CNISM, Marche Polytechnic University, Via Brecce Bianche, 60131 Ancona, Italy*
[2] *Institute of Biophysics and Nanosystems Research, Austrian Academy of Sciences, Schmiedlstrasse 6, 8042 Graz, Austria*
[3] *Faculty of Mechanical Engineering, University of Maribor, Smetanova 17, SI 2000 Maribor, and J. Stefan Institute, Jamova 39, SI 1000 Ljubljana, Slovenia*
[4] *Faculty of Mathematics and Physics, University of Ljubljana, Jadranska 19, and J. Stefan Institute, Jamova 39, SI 1000 Ljubljana, Slovenia*

Correspondence should be addressed to P. Mariani, mariani@univpm.it

Received 26 January 2010; Accepted 26 March 2010

Academic Editor: Mateus Webba da Silva

We investigated quadruplex formation in aqueous solutions of 2′-deoxyriboguanosine 5′-monophosphate, d(pG), which takes place in the absence of the covalent axial backbone. A series of in-solution small angle X-ray scattering experiments on d(pG) have been performed as a function of temperature in the absence of excess salt, at a concentration just above the critical one at which self-assembling occurs. A global fit approach has been used to derive composition and size distribution of the scattering particles as a function of temperature. The obtained results give thermodynamical justification for the observed phase-behavior, indicating that octamer formation is essential for quadruplex elongation. Our investigation shows that d(pG) quadruplexes are very suitable to assess the potential of G-quadruplex formation and to study the self-assembling thermodynamics.

1. Introduction

It is well known that guanosine-rich single stranded sequences of DNA, as found in telomeres and in other parts of the genome, especially in promoters [1, 2], can adopt various tertiary structures, including G-quadruplexes. G-quadruplexes are four-stranded helical structures, made by the stacking of planar quartets (also indicated as tetramers), arising from Hoogsten hydrogen-bonding between four guanines (G). The biological role of such sequences and the structural properties of G-quadruplexes have been extensively discussed [1, 3–6], and several reviews, focusing mainly on their topology [7–11] or on telomerase activity [12], have been published. However, the understanding of basic physical properties is still rather limited, even for short sequences comprising only 3 or 4 quartets. In particular, the mechanisms and the principles that govern quadruplex formation and stability in terms of sequence space and counter-ion effects, as expressed by thermodynamic and kinetic parameters, are still unknown.

Hence, in order to assess the potential of G-quadruplex formation and possible biological roles, the *in vitro* thermodynamic and kinetic properties of guanosine-rich sequences need to be investigated. The 2′-deoxyriboguanosine 5′-monophospate, d(pG), can be regarded as a useful model system for self-assembling studies. In fact, despite the absence of the sugar-phosphate axial backbone, d(pG) in aqueous solutions and in the presence of the proper counter-ion forms quadruplexes [13]. X-ray and neutron diffraction experiments showed that d(pG) quartets are stacked on the top of each other at the van der Waals distance of 3.4 Å and rotated with respect to each other by an angle of about 30°

[14–16]. The presence of monovalent cations was observed to be essential for the stability of these supramolecular aggregates: the cation, located between two G-quartets, stabilizes the hydrogen-bonded quartets by cation-dipole interactions with the O6 ketone groups of eight separate molecules of guanine, enhancing base-stacking interactions [17].

Depending on the concentration, d(pG) quadruplexes in water form cholesteric and hexagonal phases [13, 18, 19]. Extended analysis showed that the phase behavior depends on the length of the quadruplexes and on the nature and concentration of counterions [17–23]. Moreover, phase transitions and preferential (quadruplex lateral or axial) hydration were detected when high-pressure effects were considered [16]. Accordingly, temperature was suggested to induce quadruplex fragmentation [13].

The pathway that in dilute conditions governs the formation of d(pG) quadruplexes has been described as follows (see also Figure 1) [22, 24]:

$$4G + M \rightleftharpoons G_4M, \tag{1a}$$

$$2G_4M \rightleftharpoons G_8M + M, \tag{1b}$$

$$G_8M + G_4M \rightleftharpoons G_{12}M_2, \tag{1c}$$

$$\cdots \tag{1d}$$

$$G_{(n-1)4}M_{(n-2)} + G_4M \rightleftharpoons G_{4n}M_{(n-1)},$$

where M indicates the monovalent counter-ion and the index on the G symbol represents the aggregation state of d(pG) molecules (G is for monomer, G_4 for G-quartet, G_8 for dimer of G-quartets, etc.; note that in G_{4n}, n corresponds to the number of stacked quartets).

The first step is related to the quartet formation, which has been suggested to be strongly favored [20]. In the second step, a dimer of tetramers forms, associated with the releasing of one counter-ion. The formation of quadruplexes results from the successive addition of G-quartets to i-mer fragments, as indicated in (1c) and (1d). In these processes, no counter-ions are released.

The self-assembling of d(pG), in the form of ammonium salt, has been recently studied by in-solution small angle X-ray scattering (SAXS), both in the presence and in the absence of excess potassium ions [24]. A global fit analysis showed that the process is strongly modified by the excess potassium in solution, in full agreement with previous dynamic light scattering (DLS) and ^{31}P NMR measurements [25–27]. Accordingly, only a few aggregate forms (namely, G-quartets, G-octamers and monodisperse long G-quadruplexes) were detected in solution. In particular, SAXS experiments performed as a function of d(pG) concentration showed that the G-quartet-based self-assembling occurs above a critical guanosine concentration, c_0, of 4.5 wt%. Indeed, at this concentration, quadruplexes and G-octamers became detectable. Interestingly, the length of quadruplexes was observed to continuously increase with increasing concentration (n increases from 6 to 40 when concentration increases from 4.5 to 10 wt% [24]): as the amount of G_8 was detected to remain quite constant,

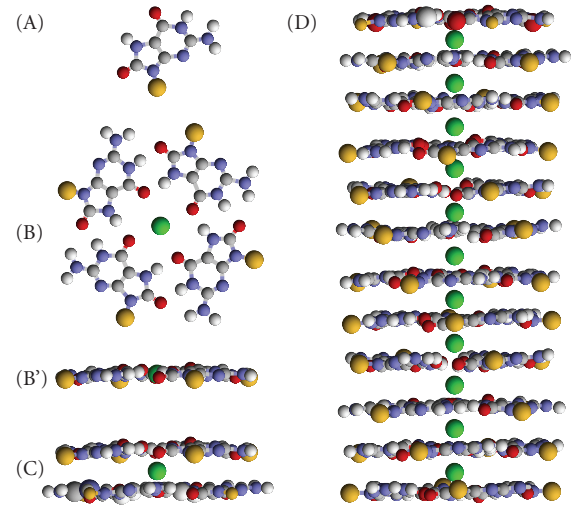

Figure 1: Representation of the aggregates formed by d(pG) in water (yellow and green beads represent the sugar-phosphate residue and the monovalent cation, resp.). (A) guanosine molecule; (B) and (B′) arrangement of four guanosine residues in a G-quartet (top and lateral views); K^+, Na^+, and NH_3^+ have the right size to occupy the tetramer inner cavity; (C) lateral view of the G-octamer, formed by two stacked quartets; the cation is located between the two quartets; (D) lateral view of the G-quadruplex, formed by stacking of discrete cation-bound quartets.

elongation was associated with a decrease of concentration of both free guanosine monomers and G-quartets. Excess K^+ in solution was observed to strongly induce quadruplex growth: indeed, very long aggregates form even below the critical concentration c_0 (at 0.2 M KCl, n around 160 was observed for c = 4 wt% [24]).

The thermodynamics of the process was explained in the framework of a nucleation-elongation model, where an unfavorable nucleation step, leading to G-octamers, is followed by a favorable spontaneous elongation, which rapidly progresses once a stable nucleus (the dodecamer, G_{12}) is achieved. Very interesting, no G_{12} species were detected in solution, probably because of their rapid elongation. To take into account the monodisperse length of the quadruplexes, two additional processes were included in the model: annealing, which favors longer particles, and fragmentation, which favors shorter ones. These processes were considered to balance and determine the final quadruplex length [24].

Quadruplex growth-in-length induced by concentration was demonstrated also by NMR and dynamic light scattering experiments performed on d(pG) in the form of sodium salt [28]. Two distinct types of aggregate species, consisting of stacked monomers and stacked G-quartets, were detected. Their length was found to increase with concentration but was insensitive to added NaCl. Moreover, the size of G-quartet aggregates was observed to be essentially independent on temperature, in contrast with the common temperature/concentration phase-diagram observed in several guanosine derivatives [13, 19].

Temperature dependence of the self-assembly of d(pG) was indeed controversial. At c = 5 wt%, DLS measurements

on d(pG) in the form of ammonium salt revealed the presence of self-assembled quadruplexes in addition to large globular aggregates. By increasing temperature, the number of quadruplexes was observed to abruptly decrease [29]. Such an abrupt transition between self-assembled and monomeric objects is however unusual for linear self-assembling systems [30]. DLS experiments were also performed on aqueous solutions of d(pG) and (pG), both in the form of ammonium salts, in the pretransitional region of the isotropic-to-cholesteric phase transition [31]. Even if d(pG) assembling occurs at lower concentrations and longer aggregates form, the aggregate melting curves of both derivatives were very similar. In particular, a low-temperature interaction-controlled region, an intermediate narrow region of intense aggregate dissociation, and a high-temperature region of dissociated species were identified. Besides, a DLS study on (pG) free acid solutions showed that self-assembled aggregates dissociate gradually on heating, and that the aggregation state of dissociated species is strongly related to guanosine concentration [32].

Due to contradictory findings reported in literature, temperature effects on the d(pG) self-assembling require further investigations. In this work, we report on a series of small-angle X-ray scattering experiments, which have been performed as a function of temperature on aqueous solutions of d(pG) in the form of ammonium salt. Samples were prepared in the absence of excess salt and at a d(pG) concentration just above the critical concentration at which self-assembling occurs. A global fit approach has been used to derive the composition and size distribution of the scattering particles as a function of temperature. The obtained results give thermodynamical justification for the observed phase-behavior.

2. Material and Methods

2′-deoxyriboguanosine 5’-monophosphate (Sigma, St. Louis, USA; 99% purity), in the form of ammonium salt, was obtained by exchanging sodium/ammonium cations using an Amberlite 200 ion exchange resin (Fluka, Deisenhofen, Germany) followed by subsequent lyophilization. To purify d(pG), the lyophilized powder was redissolved in pure water, precipitated by adding two or three volumes of 95% ethanol and collected by centrifugation in a microcentrifuge tube at high speed. The pellet was resuspended in distilled water and analyzed after an equilibration time of 24 hours at room temperature. To avoid the introduction of additional ions that can influence the self-assembling process, no buffers were used to adjust the pH of the solutions. The d(pG) weight concentration c of the investigated solutions was 50.8 mg/mL, which corresponds to 5 weight percent or to 0.15 M.

Small-angle X-ray scattering experiments were performed at the SAXS beamline at the Elettra Synchrotron (Trieste, Italy) [33]. The wavelength of the incident beam was $\lambda = 1.54$ Å and the explored Q-range extended from 0.05 to 0.4 Å^{-1} (Q is the modulus of the scattering vector, defined as $4\pi \sin\theta/\lambda$, where 2θ is the scattering angle).

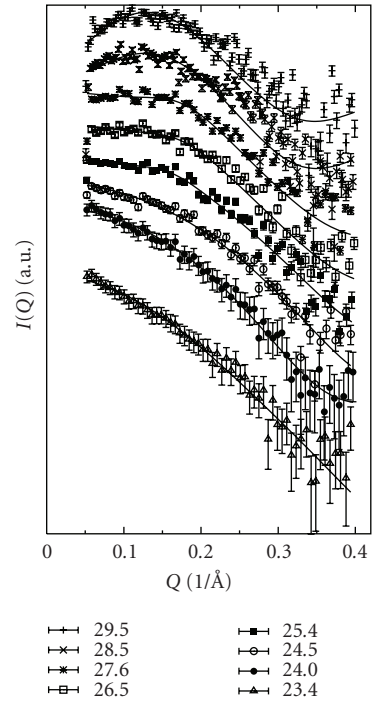

Figure 2: In-solution SAXS profiles observed for d(pG) concentration $c = 5$ wt% at different temperatures, as indicated. Best fitting curves obtained using the global fitting approach are shown as solid lines. Note that scattering curves have been scaled by a proper factor.

Guanosine solutions were measured using 1 mm thick quartz capillaries at different temperatures, from 23 to 30°C. Particular attention was paid to checking for equilibrium conditions and monitoring radiation damage. In a few tests, measurements were repeated several times (up to 10) at the same temperature to account for a constant scattering signal. Accordingly, to avoid radiation damage the exposure time was 300 s/frame, while to establish equilibrium condition the dead-time was around 5 minutes. Experimental intensities were corrected for background, solvent contributions, detector inhomogeneities, and sample transmission, as usual [34]. Unfortunately, no absolute scale calibration of the experimental data was available.

3. Results and Discussion

SAXS results are reported in Figure 2 and clearly show that the low angle scattering intensity decreases on heating, confirming that the self-assembling process is strongly related to temperature.

3.1. Guinier Analysis. A few structural data, obtained by a simple Guinier analysis of the experimental curves [21], are reported in Table 1. It should be mentioned that in the presence of a chemical equilibrium of different aggregate species (1a)–(1d), the application of the Guiner law can lead to unphysical averaged parameters. Nevertheless, from obtained data a few indications can be extracted. The radius of gyration R_g decreases as a function of temperature,

Table 1: Structural data obtained by Guinier analysis of the experimental SAXS curves. R_g is the particle gyration radius, while R_c is the gyration radius of the particle cross section [21, 35].

T	23.4°C	24.0°C	24.5°C	25.4°C	26.5°C	27.6°C	28.5°C	29.5°C
R_g (Å)	11.1 ± 0.3	8.9 ± 0.2	7.5 ± 0.3	6.7 ± 0.4	5.8 ± 0.8	5.6 ± 1.4	—	—
R_c (Å)	8.0 ± 0.1	8.1 ± 0.8	6.5 ± 1.5	—	—	—	—	—

indicating that the size of the aggregates reduces during heating. At temperatures higher than 28°C, the "melting" process seems to be completed, as no compact particles are any longer detected (in perfect agreement with DLS results obtained at the same concentration [31]). Likewise, the cross section gyration radius R_c can be determined only at low temperatures and its value remains rather constant. On one hand, this confirms the presence of cylindrical particles, whose section is fully compatible with the expected cross-section of the guanosine four-stranded helices; on the other hand, it can be inferred that the length of the quadruplexes becomes so short with increasing temperature that the Guiner approximation for tiny rods cannot be applied above 25°C.

3.2. Global Fitting Analysis. The temperature effects on particle size and composition were then derived by fitting simultaneously the whole set of experimental SAXS curves (8 scattering curves) [24, 36]. As the d(pG) solution contains randomly oriented scattering particles of different lengths, in equilibrium with each other and dispersed in a homogeneous solvent, the corresponding excess X-ray scattering intensity $I(Q)$ can be written as [35]

$$I(Q) = \kappa N_p P(Q) S_M(Q), \tag{2}$$

where N_p is the number density of the scattering particles, κ is a calibration factor (which, by comparing the experimental and the nominal sample concentrations, transforms the experimental intensities into scattering cross section in absolute units), and $P(Q)$ and $S_M(Q)$ are the effective particle form factor and the measured structure factor, respectively.

For an isotropic system containing particles with different aggregation state, the effective form factor depends on shape, size, and size-distribution of all the particles in solution. In the present case, $P(Q)$ can be written as a weighted sum of the form factors of all the guanosine aggregates eventually present in solution:

$$P(Q) = \sum_{n=0}^{N} x_{G_{4n}} P_{G_{4n}}(Q), \tag{3}$$

where $x_{G_{4n}}$ is the number fraction of the G_{4n} particle family and $P_{G_{4n}}(Q)$ is the corresponding form factor (notice that for $n = 0$, $x_{G_{4n}} = x_G$).

The form factor can be calculated from the molecular structure in the case of d(pG) and G-quartets, while for quadruplexes, a cylindrical model with two-electron density levels and a suitable length has been used (see [24]). On the other hand, $x_{G_{4n}}$ is related to both the particle number density N_p and the fraction of d(pG) molecules forming a particular aggregate, $\alpha_{G_{4n}}$. In fact,

$$N_p = \frac{10^{-3} N_A C}{\left(x_G + 4\sum_{n=1}^{N} n\, x_{G_{4n}}\right)},$$
$$\alpha_{G_{4n}} = \frac{4n\, x_{G_{4n}}}{\left(x_G + 4\sum_{n=1}^{N} n\, x_{G_{4n}}\right)}, \tag{4}$$

where N_A is the Avogadro's number and C is the nominal d(pG) molar concentration.

$S_M(Q)$ is the measured structure factor, related to eventual particle-particle interactions [37]. In dilute solutions, the structure factor is usually negligible ($S_M(Q) \approx 1$). In the present case, this approximation holds true for SAXS curves obtained below 26°C. At higher temperatures, the fitting based on $S_M(Q) = 1$ was very unsatisfactory, even assuming the contemporaneous presence of a variety of different aggregate forms, as stacked G-monomers (observed in [28]) or unstructured particles. Indeed, above 26°C, particle-particle interactions have to be considered, probably because of the increased number of scattering particles due to the thermal-induced aggregate dissociation. The corresponding $S_M(Q)$ factor was then calculated in the Random Phase Approximation [34, 38], considering the basic approximation of a two-body interaction potential described as the sum of a hard-sphere, a screened Coulombic, and a short-range Yukawian attractive potentials [39]. Details on potentials and form used for the structure factor can be found in [34]; here, it is important to note that the hard-sphere potential depends on the effective particle diameter, σ_{eff}, while the main terms determining the screened coulombic and the attractive potentials are the number of charges-per-particle Z and the pair of parameters J and d, which correspond to the attractive energy at the particle-particle contact and to its characteristic decay length, respectively [37].

According to (2), data analysis has been then performed by fitting all SAXS curves with an effective form factor, searching for the best structural parameters (namely, radii, electron densities, and length of the cylinders modeling the quadruplexes) and particle composition and concentration, which better described the observed scattering profiles. In agreement with our previous results [24], solutions characterized by the lower number of particle components were preferred. As explained, above 26°C, we also included a nonzero structure factor.

The GENFIT software was used (see details in [36]). Accordingly, the radius and shell thickness of the cylinder model, the corresponding electron densities, as well as the unique calibration factor κ were all considered as global parameters and were therefore obtained from the

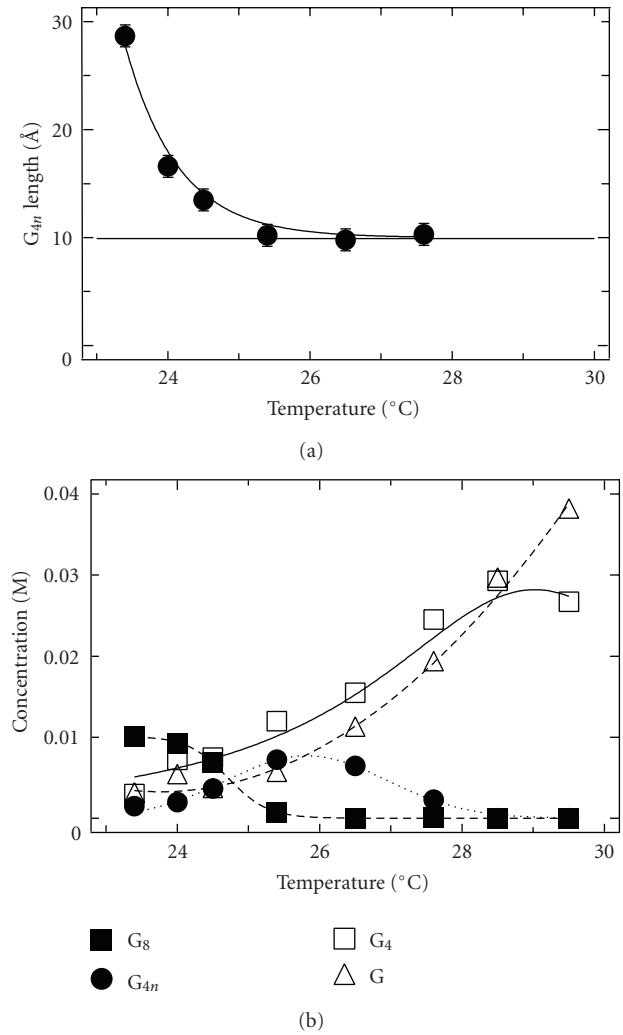

Figure 3: Fitting results. (a) Temperature dependence of the length of G-quadruplexes. (b) Temperature dependence of the concentration of the different aggregate species. Symbols are as in the text.

contemporaneous analysis of all the SAXS curves. On the contrary, the pairs n and $x_{G_{4n}}$, which are related to the experimental conditions, were obtained from the analysis of each single curve. As dependency of parameters σ_{eff}, Z, J, and d on temperature is unknown, they were handled as single curve fitting parameters.

Best-fitting curves are superposed to experimental data in Figure 2, while the fitting parameters are reported in Table 2 and shown in Figure 3. It can be noticed that all curves are very well reproduced by considering the presence of at least 4 different kinds of scattering particles (namely, free d(pG) monomers, G-quartets, G-octamers, and monodisperse G-quadruplexes). The use of polydispersion models (as Gaussian, log-normal, or Lorentzian) to describe the quadruplex lengths and the inclusion of particles made by stacked d(pG) molecules did not improve the fitting results, not even at the higher investigated temperatures.

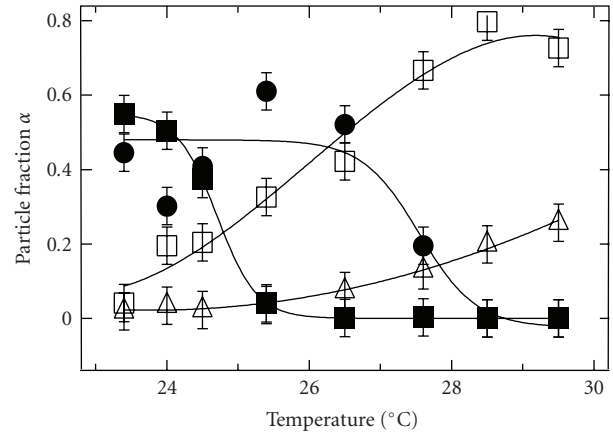

Figure 4: Fitting results. Temperature dependence of the fraction of particles assembled in different forms. Symbols are as in Figure 3.

A confirmation of the quality of the global approach is given by the determination of a unique calibration factor: indeed, the whole scattering data have been found to be consistent with the nominal, constant sample composition. Moreover, all the other common parameters are in very good agreement with previous reported structural data [17–19, 21, 24, 25, 27]. As expected, the main structural parameters of G-quadruplexes do not depend on the experimental conditions.

3.3. Temperature Effects on Self-Assembling: Aggregate Structure and Concentration. The temperature dependence of the aggregate composition and of the length of quadruplexes (G_{4n} particles) is reported in Figure 3. Concerning the length of quadruplexes, it can be observed that heating induces particle shortening; however, shortening is rather sharp up to 25°C, after which a constant length of about 10 Å is reached. This length indicates the presence of dodecamers (G_{12}). The analysis of the particle composition indicates that octamers are stable only up to 25°C, while longer particles disappear around 28°C, with a curious temperature dependence. On the other hand, the amount of both free d(pG) molecules and G-tetramers continuously increases by heating. Noticeably, the concentration of tetramers starts to decrease at the higher investigated temperatures, even if a "melting" temperature cannot be derived.

The fraction of guanosine molecules assembled in different forms, calculated by (4), is reported in Figure 4 as a function of temperature. Because of compensation between quadruplex length and concentration, the number of guanosine molecules assembled as quadruplexes is rather constant with temperature (or only slighting increasing) until abruptly decreases at some critical point. The corresponding melting temperature is 27.6°C. In contrast, the fraction of molecules present as G_8 shows a temperature dependence which perfectly reproduces the thermal behavior observed for its concentration. An octamer melting temperature of 24.7°C is derived by sigmoid data fitting. Therefore, the general features actually indicate the presence of two

Table 2: Single and common parameters obtained by the global-fitting procedure applied to the 8 experimental SAXS curves shown in Figure 2. Symbols are as in the text.

T(°C)	23.4	24.0	24.5	25.4	26.5	27.6	28.5	29.5
σ_{eff} (Å)	—	—	—	—	8.6 ± 0.2	9.0 ± 0.9	9 ± 2	9 ± 2
Z	—	—	—	—	6.9 ± 0.3	6.5 ± 0.5	4 ± 1	3 ± 1
J (kcal/mol)	—	—	—	—	32 ± 12	28 ± 12	30 ± 12	25 ± 15
d (Å)	—	—	—	—	2.6 ± 0.2	2.6 ± 0.2	1.1 ± 0.8	1.7 ± 0.5
R (Å)					12.2 ± 0.5			
r_{core} (Å)					1.9 ± 0.1			
ρ_{shell} (e Å^{-3})					0.43 ± 0.01			
ρ_{core} (e Å^{-3})					0.325 ± 0.005			
κ					(1.6 ± 0.1) 10^{-3}			

melting processes, that can be attributed to the complex two-step mechanism for guanosine self-assembling. However, the temperature dependence of the fraction of guanosine molecules assembled as tetramers evidences that at high temperature a further melting process occurs: the complete dissociation of G-quartet.

Because the measured structure factor has been calculated considering a number of effective interacting objects in solution [39], the fitted interaction potential parameters should be discussed taking into account the derived particle composition. As shown in Table 2, the average effective particle diameter and the attractive potential parameters can be considered fairly constant within the estimated errors, while the effective particle charge clearly reduces at increasing temperatures. Indeed, in the temperature range where the measured structure factor, and then the interparticle interaction potentials, cannot be neglected (above 26.5°C), the interacting particles are mainly represented by G-quartets, whose dimensions do not depend on temperature. On the other hand, the variation of the effective particle charge is probably related to a temperature-dependent condensation of counter-ions on the particle surface. In particular, the number of total counter-ions presents in solution is essentially determined by the aggregation state, and, for example, octamer disaggregation produces a smaller number of free counter-ions in solution, while tetramer melting increases this number. From (1a)–(1d), it is then clear that temperature will strongly influence the counter-ion-charge balance. The last comment concerns the values of the two parameters describing the attractive potential. The very small value of d indicates that attraction is short-range. By contrast, J values are surprisingly large, but comparable to interaction energies predicted for G-G stacking (9.5 kcal/mol of guanosine [40]) or for the G-quartet stacking in the presence of potassium (40 kcal/mol of G_4 [41]). Such a result then suggests that the observed short-range attractive term is mainly related to guanosine stacking interactions.

3.4. Temperature Effects on Self-Assembling: Thermodynamics. To derive thermodynamic data on the d(pG) self-assembling, the behavior described in Figure 3 should be further analyzed. Indeed, two different quadruplex unfolding equilibria, one below and the other above the octamer dissociation

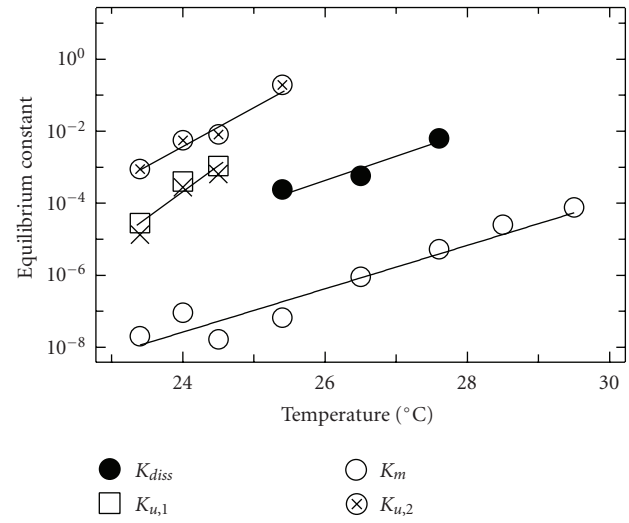

Figure 5: Temperature dependence of the equilibrium dissociation constants. Symbols are as in the text. The corresponding reactions are shown in (5).

temperature, exist. In particular, the following dissociation equilibria are suggested to establish at each temperature:

$$\begin{aligned} G_{4n} &\overset{K_{u,1}}{\rightleftharpoons} \left(\frac{n}{2}\right) G_8 \overset{K_{u,2}}{\rightleftharpoons} n G_4 \overset{K_m}{\rightleftharpoons} 4n G \quad \text{for } T < 25^\circ\text{C}, \\ G_{4n} &\overset{K_{\text{diss}}}{\rightleftharpoons} n G_4 \overset{K_m}{\rightleftharpoons} 4n G \quad \text{for } T > 25^\circ\text{C}. \end{aligned} \tag{5}$$

Equilibrium constants have been derived from aggregate concentrations and their temperature dependence is shown in Figure 5. Note that data concerning quadruplex thermal disaggregation are reported with two different symbols, as they refer to the quadruplex dissociation to octamers (that we identify as the first step in the quadruplex unfolding occurring at low temperature) and directly to tetramers (that we identify as a dissociation process occurring at higher temperature), respectively.

Equilibrium constants increase with temperature, indicating that dissociation of all aggregate species is favored by heating: because equilibrium constant units are different, a direct comparison would be inappropriate, but data

in Figure 5 suggest that aggregates have different stability (among them, quartets are relatively stable). Noticeable is the strong temperature dependence observed for the equilibrium constant for quadruplex dissociation to octamers, $K_{u,1}$.

In fact, the increase of $K_{u,1}$ on heating is higher than those observed for the other equilibrium constants and cannot be explained considering classical temperature effects. A recent analysis on the temperature-dependent self-assembly of π-conjugated molecules into helical supramolecular fibrillar structures revealed distinct hierarchical stages that govern the formation process [42]. In particular, short oligo *p*-phenylenevinylenes were observed to occur in two different states in dodecane solution, mainly discrete monomeric or hydrogen-bonded dimeric species at high temperature and mainly helical aggregates at low temperature. A nucleation-growth pathway, based on the Oosawa-Kasai behavior for thermally activated equilibrium polymerization [43], was considered to describe the self-assembling process. In the proposed model, a nonisodesmic helical assembly (characterized by an activation step and subsequent propagation steps) is preceded by an isodesmic assembly of nonhelical preaggregate structures and the two kinds of assemblies are linked through equilibrium between nonhelical and helical assemblies of a critical size. Accordingly, a simple relationship connecting the average aggregation number of the helical assemblies (N) with the equilibrium constants of the elongation process (K_e) and the equilibrium constant of the activation step (K_a, i.e., the equilibrium constant between the active and nonactive state, active meaning the state that can initiate the elongation) was derived [42]:

$$K_e = 1 - N^{-1} + K_a N(N-1). \tag{6}$$

A similar aggregate particle thermal profile is observed here (Figure 4); moreover, a nucleation-elongation mechanism was already proposed to analyze SAXS data on guanosine self-assembling as a function of concentration [24]. Therefore, the model presented in [42] has been tentatively applied to describe the thermally induced quadruplex dissociation. In Figure 5, X-shaped symbols indicate the theoretical values for the dissociation constant (i.e., the inverse of the elongation constant K_e) calculated by (6) at any step of quadruplex aggregation (see also Figure 3) using $K_{u,2}$ as reference (note that $K_{u,2}$ is the inverse of the dimerization constant, and that the formation of octamers is then considered the activation step, i.e., $K_a = 1/K_{u,2}$). The agreement with the experimental data is compelling.

Taking into account the absence of quadruplex elongation above 25°C, a hierarchical pathway for the self-assembly of guanosine into helical structures upon cooling a solution of dissolved monomers can be proposed. At first, monomers form G-quartets via Hoogsteen hydrogen bonding. On cooling, quartets are brought together via an isodesmic pathway, forming short stacked preaggregates (dodecamers) which, probably, show thermal disorder both in the stacking direction and in the respective quartet orientation. Elongation is not activated. Upon further cooling, the quartes in the preaggregates become more restricted in relative position via a cooperative process. Moreover, at $T \simeq 25°C$, chiral nuclei (octamers) start to form and the elongation-growth pathway sets in. The rapid growth from helical nuclei and helical preaggregates is caused by the many reinforcing noncovalent interactions and is probably enthalpy-driven.

From data interpolated at 25°C, the free energy changes, $\Delta G_{25°C}$, have been obtained, while plotting data as Van't Hoff isochores ($\ln(K)$ versus $1/T$), and under the approximation that standard entropy and enthalpy changes are temperature independent, their values ΔH^0 and ΔS^0 have been determined. Results are reported in Table 3. Such a result deserves for a few general comments.

First, free energy changes range around the values observed for the unfolding of quadruplexes made by telomeric or model sequences. ΔG values extending from 1 to 16 kcal mol^{-1} per quadruplex, variably depending on loop length or cation, were reported, for example, in [1, 44] (data at 20°C) and [45] (data at 27°C), while $\Delta G_{25°C}$ and ΔH^0 values per quartet around 2 to 3 kcal mol^{-1} and 20 to 30 kcal mol^{-1}, respectively, were indicated in [46]. Notice that ΔG values for quadruplex structures found in literature seem to be constantly higher than values here reported for d(pG) aggregation. The absence of the covalent axial sugar-phosphate backbone could explain the difference. *Second*, both ΔH^0 and ΔS^0 are positive, indicating that the reverse process, namely, the self-assembling, results from the characteristic compensation of favorable enthalpies of formation (around -30 kcal per mol of guanosine) with unfavorable entropy contributions (around -130 cal/K per mol of guanosine). Once more, it is proved that self-assembling is the result of a delicate balance between sometimes opposing forces: the favorable ΔH^0 values result from the formation of hydrogen bonds and tetramer stacks, whereas the unfavorable entropies indicate the ordering of the guanines and the uptake of counter-ions and water molecules. *Third*, thermodynamic parameters provide no evidence (or even provide counter evidence) that tetramer stacking is driven by classical hydrophobic interactions, even if it has often been suggested that this effect is important for quadruplex formation. *Fourth*, free energy changes associated to quadruplex and octamer unfolding are small and rather similar, and they compare well with the free energy change associated to the dodecamer dissociation. Indeed, $\Delta G_{\text{dis}} \simeq \Delta G_{u,1} + \Delta G_{u,2}$, indicating that at 25°C, G_{4n} and G_{12} forms have the same thermodynamic stability with respect to the G-quartet. However, very different enthalpy and entropy contributions characterize the G_{12} dissociation: the suggested disorder in the quartet stacking and a binding energy so low that elongation is inhibited are confirmed. *Fifth*, G-quartets are very stable. Dissociation implies the removal of a coordinated ion. This step is then analogous to the dissociation of an ion from a crown ether, which costs ca. 2.5 kcal mol^{-1} ion [1], but also includes the favorable free energy of solvation of the counterion and any contingent conformational rearrangement of G_4M to G_4. Accordingly, it is plausible that the energy of counter-ion binding accounts for a substantial fraction of net favorable free energy. Indeed, quartet melting is realized by the breaking of 8 hydrogen bonds. As the strength of a hydrogen bond is between 2 and 10 kcal mol^{-1} [47], the observed thermodynamic

Table 3: Thermodynamic parameters for the different chemical equilibria described by (5). Data are reported on a *per mole of guanosine* basis.

Reaction	$\Delta G_{25^\circ C}$ kcal mol^{-1}	ΔH^0 kcal mol^{-1}	ΔS^0 cal mol^{-1}K^{-1}
Quadruplex dissociation to octamers	0.18 ± 0.05	37 ± 8	122 ± 26
Octamer unfolding to G-quartets	0.26 ± 0.03	45 ± 6	149 ± 20
Quadruplex unfolding to G-quartets	0.45 ± 0.05	22 ± 10	73 ± 34
G-quartet melting to free d(pG)	2.36 ± 0.04	64 ± 7	205 ± 22

parameters suggest that H-bonds contribute positively to quartet stabilization, but concurrent hydrogen bonds to water and the processes just above discussed should play the main role.

4. Conclusions

In order to be able to assess the potential function of G-quadruplexes in a biological system, the self-assembling of deoxyguanosine monophosphate in dilute solution has been studied by SAXS as a function of temperature, from 23 to 30°C. Samples were prepared in the absence of excess salt, at a concentration of 50.8 mg/mL, just above the critical concentration at which self-assembling occurs [24]. To derive composition and size distribution of the scattering particles, SAXS curves were analyzed by using a global fit approach [36]. As a result, the presence of only a few aggregate forms, namely, free d(pG) molecules, G-quartets, G-octamers, and monodisperse G-quadruplexes, was detected, and their respective concentrations were observed to strongly depend on temperature. In particular, heating induces shortening of G-quadruplexes, that finally disappear around 28°C, while octamers are stable only up to 25°C. On the other side, the tetramer melting very probably starts at the higher investigated temperatures, even if a G_4 "melting" temperature was unfortunately not reached in our experiment.

The thermodynamics of the self-assembling process of d(pG) was further analyzed in the framework of a nucleation-elongation model. The unfavorable nucleation step has been clearly identified with the formation of G-octamers and a hierarchical pathway for the self-assembly of guanosine into helical structures upon cooling proposed. On decreasing temperature, G-quartets form by extended guanosine hydrogen bonding. Through an isodesmic pathway, quartets form stacked dodecamers, which probably show thermal disorder both in stacking direction and in quartet orientation, so that elongation is not activated. Upon further cooling, preaggregates become ordered and chiral nuclei form. The elongation-growth pathway sets in: the rapid growth from the helical nuclei is enthalpy-driven.

To some extent, the picture seems clear, but to derive a complete description of quadruplex formation in the absence of the covalent axial sugar-phosphate backbone, such results should be compared with self-assembling processes occurring in the presence of excess cations, as Na^+, K^+, and NH_4^+. Indeed, concerning the stability of G-quadruplexes formed by oligonucleotides, NMR measurements have shown that the melting kinetics of non-terminal G quartets in a structure containing four G-quartets are very slow (months), whereas they are rapid (minutes) in structures containing only three G-quartets [48]. By comparison, the melting kinetics of Watson-Crick base pairs are in the order of a few milliseconds. Clearly, G-quadruplexes are relatively stable structures, but the number of G-quartets present in a quadruplex dramatically affects its stability. The crucial role that counter-ions could play in driving the formation of stable, long quadruplexes still remains to be investigated.

Acknowledgment

P. Mariani thanks the Italian MIUR for financial support in the frame of Italia-Slovenia Bilateral project.

References

[1] A. N. Lane, J. B. Chaires, R. D. Gray, and J. O. Trent, "Stability and kinetics of G-quadruplex structures," *Nucleic Acids Research*, vol. 36, no. 17, pp. 5482–5515, 2008.

[2] Y. Qin and L. H. H. Hurley, "Structures, folding patterns, and functions of intramolecular DNA G-quadruplexes found in eukaryotic promoter regions," *Biochimie*, vol. 90, no. 8, pp. 1149–1171, 2008.

[3] S. Chan and E. H. Blackburn, "Telomeres and telomerase," *Philosophical Transactions of the Royal Society B*, vol. 359, no. 1441, pp. 109–121, 2004.

[4] T. R. Cech, "Beginning to understand the end of the chromosome," *Cell*, vol. 116, no. 2, pp. 273–279, 2004.

[5] N. I. N. Borovok, D. Zikich, J. Ghabboun, G. I. Livshits, D. Porath, and A. B. Kotlyar, "Assembling of G-strands into novel tetra-molecular parallel G4-DNA nanostructures using avidin-biotin recognition," *Nucleic Acids Research*, vol. 36, no. 15, pp. 5050–5060, 2008.

[6] H. J. Lipps and D. Rhodes, "G-quadruplex structures: in vivo evidence and function," *Trends in Cell Biology*, vol. 19, no. 8, pp. 414–422, 2009.

[7] D. J. Patel, A. T. Phan, and V. Kuryavyi, "Human telomere, oncogenic promoter and 5′-UTR G-quadruplexes: diverse higher order DNA and RNA targets for cancer therapeutics," *Nucleic Acids Research*, vol. 35, no. 22, pp. 7429–7455, 2007.

[8] S. Burge, G. N. Parkinson, P. Hazel, A. K. Todd, and S. Neidle, "Quadruplex DNA: sequence, topology and structure," *Nucleic Acids Research*, vol. 34, no. 19, pp. 5402–5415, 2006.

[9] M. W. da Silva, "NMR methods for studying quadruplex nucleic acids," *Methods*, vol. 43, no. 4, pp. 264–277, 2007.

[10] D. Sen and W. Gilbert, "The structure of telomeric DNA: DNA quadriplex formation," *Current Opinion in Structural Biology*, vol. 1, no. 3, pp. 435–438, 1991.

[11] A. T. Phan, V. Kuryavyi, and D. J. Patel, "DNA architecture: from G to Z," *Current Opinion in Structural Biology*, vol. 16, no. 3, pp. 288–298, 2006.

[12] J.-L. Mergny, J.-F. Riou, P. Mailliet, M.-P. Teulade-Fichou, and E. Gilson, "Natural and pharmacological regulation of telomerase," *Nucleic Acids Research*, vol. 30, no. 4, pp. 839–865, 2002.

[13] G. Gottarelli, G. Spada, and P. Mariani, "The self-assembly of guanosine derivatives and folic acid," in *Crystallography of Supramolecular Compounds*, Kluwer Academic Publishers, Dordrecht, The Netherlands, 1996.

[14] P. Mariani and L. Saturni, "Measurement of intercolumnar forces between parallel guanosine four-stranded helices," *Biophysical Journal*, vol. 70, no. 6, pp. 2867–2874, 1996.

[15] P. Mariani, F. Ciuchi, and L. Saturni, "Helix-specific interactions induce condensation of guanosine four- stranded helices in concentrated salt solutions," *Biophysical Journal*, vol. 74, no. 1, pp. 430–435, 1998.

[16] P. Ausili, M. Pisani, S. Finet, H. Amenitsch, C. Ferrero, and P. Mariani, "Pressure effects on columnar lyotropics: anisotropic compressibilities in guanosine monophosphate four-stranded helices," *Journal of Physical Chemistry B*, vol. 108, no. 5, pp. 1783–1789, 2004.

[17] F. Federiconi, P. Ausili, G. Fragneto, C. Ferrero, and P. Mariani, "Locating counterions in guanosine quadruplexes: a contrast-variation neutron diffraction experiment in condensed hexagonal phase," *Journal of Physical Chemistry B*, vol. 109, no. 21, pp. 11037–11045, 2005.

[18] P. Mariani, C. Mazabard, A. Garbesi, and G. P. Spada, "A study of the structure of the lyomesophases formed by the dinucleoside phosphate d(GpG). An approach by X-ray diffraction and optical microscopy," *Journal of the American Chemical Society*, vol. 111, no. 16, pp. 6369–6373, 1989.

[19] H. Franz, F. Ciuchi, G. D. Nicola, M. D. Morais, and P. Mariani, "Unusual lyotropic polymorphism of deoxyguanosine-5′-monophosphate: X-ray diffraction analysis of the correlation between self-assembling and phase behavior," *Physical Review E*, vol. 50, no. 1, pp. 395–402, 1994.

[20] C. Detellier and P. Laszlo, "Role of alkali metal and ammonium cations in the self-assembly of the 5′-guanosine monophosphate dianion," *Journal of the American Chemical Society*, vol. 102, no. 3, pp. 1135–1141, 1980.

[21] F. Carsughi, M. Ceretti, and P. Mariani, "Structural organization of guanosine derivatives in dilute solutions: small angle neutron scattering analysis," *European Biophysics Journal*, vol. 21, no. 2, pp. 155–161, 1992.

[22] T. J. Pinnavaia, C. L. Marshall, C. Mettler, C. Fisk, H. Miles, and E. Becker, "Alkali metal ion specificity in the solution ordering of a nucleotide, 5′-guanosine monophosphate," *Journal of the American Chemical Society*, vol. 100, no. 11, pp. 3625–3627, 1978.

[23] A. Wong and G. Wu, "Selective binding of monovalent cations to the stacking G-quartet structure formed by guanosine 5′-monophosphate: a solid-state NMR study," *Journal of the American Chemical Society*, vol. 125, no. 45, pp. 13895–13905, 2003.

[24] P. Mariani, F. Spinozzi, F. Federiconi, H. Amenitsch, L. Spindler, and I. Drevenšek-Olenik, "Small angle X-ray scattering analysis of deoxyguanosine 5′-monophosphate self-assembing in solution: nucleation and growth of G-quadruplexes," *Journal of Physical Chemistry B*, vol. 113, no. 22, pp. 7934–7944, 2009.

[25] L. Spindler, I. Drevenšek-Olenik, M. Čopič, et al., "Dynamic light scattering and 31P NMR spectroscopy study of the self-assembly of deoxyguanosine 5′-monophosphate," *European Physical Journal E*, vol. 7, no. 1, pp. 95–102, 2002.

[26] L. Spindler, I. Drevenšek-Olenik, M. Čopič, and P. Mariani, "Effect of added Ions on the self-assembly of guanosine," *Molecular Crystals & Liquid Crystals*, vol. 395, p. 317, 2003.

[27] L. Spindler, I. Drevenšek-Olenik, M. Čopič, J. Cerar, J. Škerjanc, and P. Mariani, "Dynamic light scattering and 31P NMR study of the self-assembly of deoxyguanosine 5′-monophosphate: the effect of added salt," *European Physical Journal E*, vol. 13, no. 1, pp. 27–33, 2004.

[28] A. Wong, R. Ida, L. Spindler, and G. Wu, "Disodium guanosine 5′-monophosphate self-associates into nanoscale cylinders at pH 8: a combined diffusion NMR spectroscopy and dynamic light scattering study," *Journal of the American Chemical Society*, vol. 127, no. 19, pp. 6990–6998, 2005.

[29] L. Spindler, I. Drevenšek-Olenik, M. Čopič, and P. Mariani, "The effect of temperature on the self-assembly of deoxyguanosine 5′-monophosphate in pretransitional region of the I-CH phase transition," *Molecular Crystals and Liquid Crystals*, vol. 409, pp. 43–50, 2004.

[30] M. P. Taylor and J. Herzfeld, "Liquid-crystal phases of self-assembled molecular aggregates," *Journal of Physics: Condensed Matter*, vol. 5, no. 17, pp. 2651–2678, 1993.

[31] L. Spindler, F. Federiconi, P. Mariani, et al., "Melting of self-Assembled columnar aggregates formed in aqueous solutions of deoxy- and guanosine 5′-monophosphate," *Molecular Crystals & Liquid Crystals*, vol. 435, pp. 661–672, 2005.

[32] H. Jurga-Nowak, E. Banachowicz, A. Dobek, and A. Patkowski, "Supramolecular guanosine 5′-monophosphate structures in solution. Light scattering study," *Journal of Physical Chemistry B*, vol. 108, no. 8, pp. 2744–2750, 2004.

[33] H. Amenitsch, S. Bernstorff, M. Kriechbaum, et al., "Performance and first results of the ELETTRA high-flux beamline for small-angle X-ray scattering," *Journal of Applied Crystallography*, vol. 30, pp. 872–672, 1997.

[34] L. R. S. Barbosa, M. G. Ortore, F. Spinozzi, P. Mariani, S. Bernstorff, and R. Itri, "The importance of protein-protein interactions on the pH-induced conformational changes of bovine serum albumin: a small-angle X-ray scattering study," *Biophysical Journal*, vol. 98, no. 1, pp. 147–157, 2010.

[35] A. Guinier and G. Fournet, *Small Angle Scattering of X-Ray*, John Wiley & Sons, New York, NY, USA, 1955.

[36] F. Spinozzi, P. Mariani, L. Saturni, et al., "Met-myoglobin association in dilute solution during pressure-induced denaturation: an analysis at pH 4.5 by high-pressure small-angle X-ray scattering," *Journal of Physical Chemistry B*, vol. 111, no. 14, pp. 3822–3830, 2007.

[37] F. Spinozzi, D. Gazzillo, A. Giacometti, P. Mariani, and F. Carsughi, "Interaction of proteins in solution from small-angle scattering: a perturbative approach," *Biophysical Journal*, vol. 82, no. 4, pp. 2165–2175, 2002.

[38] J. Narayanan and X. Y. Liu, "Protein interactions in undersaturated and supersaturated solutions: a study using light and X-ray scattering," *Biophysical Journal*, vol. 84, no. 1, pp. 523–532, 2003.

[39] C. L. P. Oliveira, M. A. Behrens, J. S. Pedersen, K. Erlacher, D. Otzen, and J. S. Pedersen, "A SAXS study of glucagon fibrillation," *Journal of Molecular Biology*, vol. 387, no. 1, pp. 147–161, 2009.

[40] J. Šponer, H. A. Gabb, J. Leszczynski, and P. Hobza, "Base-base and deoxyribose-base stacking interactions in B-DNA and Z-

DNA: a quantum-chemical study," *Biophysical Journal*, vol. 73, no. 1, pp. 76–87, 1997.

[41] A. Calzolari, R. D. Felice, E. Molinari, and A. Garbesi, "Electron channels in biomolecular nanowires," *Journal of Physical Chemistry B*, vol. 108, no. 8, pp. 2509–2515, 2004.

[42] P. Jonkheijm, P. van der Schoot, A. P. H. J. Schenning, and E. W. Meijer, "Probing the solvent-assisted nucleation pathway in chemical self-assembly," *Science*, vol. 313, no. 5783, pp. 80–83, 2006.

[43] F. Oosawa and M. Kasai, "A theory of linear and helical aggregations of macromolecules," *Journal of Molecular Biology*, vol. 4, pp. 10–21, 1962.

[44] C. M. Olsen, H.-T. Lee, and L. A. Marky, "Unfolding thermodynamics of intramolecular G-quadruplexes: base sequence contributions of the loops," *Journal of Physical Chemistry B*, vol. 113, no. 9, pp. 2587–2595, 2009.

[45] N. Kumar and S. Maiti, "A thermodynamic overview of naturally occurring intramolecular DNA quadruplexes," *Nucleic Acids Research*, vol. 36, no. 17, pp. 5610–5622, 2008.

[46] V. A. Bloomfield, D. M. Crothers, and I. Tinoco, *Nucleic Acids: Structures, Properties and Functions*, University Science Book, Sausalito, Calif, USA, 2000.

[47] J. N. Israelachvili, *Intermolecular and Surface Forces*, Academic Press, London, UK, 1992.

[48] Y. Wang and D. J. Patel, "Guanine residues in d(T2AG3) and d(T2G4) form parallel-stranded potassium cation stabilized G-quadruplexes with anti glycosidic torsion angles in solution," *Biochemistry*, vol. 31, no. 35, pp. 8112–8119, 1992.

SAGE-Hindawi Access to Research
Journal of Nucleic Acids
Volume 2010, Article ID 431651, 8 pages
doi:10.4061/2010/431651

Research Article

Effect of Base Sequence on G-Wire Formation in Solution

Lea Spindler,[1,2] Martin Rigler,[3] Irena Drevenšek-Olenik,[2,3] Nason Ma'ani Hessari,[4] and Mateus Webba da Silva[4]

[1] *Faculty of Mechanical Engineering, University of Maribor, Smetanova 17, 2000 Maribor, Slovenia*
[2] *J. Stefan Institute, Jamova 39, 1000 Ljubljana, Slovenia*
[3] *Faculty of Mathematics and Physics, University of Ljubljana, Jadranska 19, 1000 Ljubljana, Slovenia*
[4] *Faculty of Life and Health Sciences, University of Ulster, Cromore Road, Northern Ireland, Coleraine BT52 1SA, UK*

Correspondence should be addressed to Lea Spindler, lea.spindler@uni-mb.si

Received 1 February 2010; Accepted 22 March 2010

Academic Editor: R. Eritja

The formation and dimensions of G-wires by different short G-rich DNA sequences in solution were investigated by dynamic light scattering (DLS) and polyacrilamide gel electrophoresis (PAGE). To explore the basic principles of wire formation, we studied the effects of base sequence, method of preparation, temperature, and oligonucleotide concentration. Both DLS and PAGE show that thermal annealing induces much less macromolecular self-assembly than dialysis. The degree of assembly and consequently length of G-wires (5-6 nm) are well resolved by both methods for DNA sequences with intermediate length, while some discrepancies appear for the shortest and longest sequences. As expected, the longest DNA sequence gives the longest macromolecular aggregates with a length of about 11 nm as estimated by DLS. The quadruplex topologies show no concentration dependence in the investigated DNA concentration range (0.1 mM–0.4 mM) and no structural change upon heating.

1. Introduction

The construction of specific surface architectures via controlled self-assembly is a key goal in the design of nanoscale molecular electronic devices. In this respect, biomolecular self-assembly of the strongly interacting DNA bases provides a promising avenue. Particularly, attractive candidates are guanine (G) and its derivatives, which are unique among the DNA constituents for their propensity to form quadruplex structures, known to be stabilized through Hoogsteen and Watson-Crick base pairing [1, 2]. Moreover, guanine has a low ionization potential due to which it plays a key role in electrical conductivity of DNA-based materials.

Various research groups have recently reported on the evolution of the "art" of making surface deposited 1-dimensional (1D) structures known as guanosine wires (G-wires) [3–12]. However, despite the promising experimental results, basic processes responsible for wire formation are still far from being fully understood. Two main steps are fundamental to drive the topic from a laboratory curiosity towards the technologically relevant G-wire engineering: (a) achieving control of self-folding and self-stimulated end-to-end fusion of the macromolecular quadruplexes in solution as a function of their molecular composition (i.e., base sequence) and solution conditions, and (b) understanding the effect of surface interactions on material deposition from solution phase onto the solid substrate.

In this work, we report on how particular modifications of the base sequence of a G-rich oligonucleotide, which are supposed to affect the folding geometry of the quadruplex [13], affect its ability to form G-wires in solution phase. The idea of wire formation is based on the previously established finding that GC "sticky ends" may be used to link quadruplexes into longer 1D aggregates [14]. A series of oligonucleotide sequences with one or two GC ends and central sequences of different length were designed for this purpose (see Table 1). The folding topology [14, 15] has been previously investigated, and quadruplex formation has been recently studied by Mergny et al. [16]. In these studies, length and nature of propeller loops were studied, but end-to-end fusion of the quadruplexes was not considered. Here, we focused on end-to-end fusion of these quadruplex folds.

Polyacrilamide gel electrophoresis (PAGE) is a conventional tool to differentiate between macromolecular objects of different length. During migration through the gel, breakage of bonds and smearing of bands may happen. Thus, weakly linked aggregates are difficult to be identified. An alternative noninvasive method for determining the size of macromolecular objects is dynamic light scattering (DLS). This method was extensively applied to study DNA molecules over a wide range of sizes [17–21]. Specifically, it has been used to characterize G-quartet stacking in solutions of single guanosine molecules [22–26], and for studying formation of G-quadruplexes [27–30]. Protozanova and Macgregor [29] compared the use of DLS and PAGE on sequences with long terminal tracks. These tracks were based on sequences such as $d(A_{15}G_{15})$ and $d(A_{13}G_{15}TC)$, which form frayed wires with a G-quadruplex stem and nonguanine portions reaching out as single-stranded arms. These frayed wires can be considerably long and have a rather broad size distribution. Thus, specific effects of base sequence on wire length were not evident.

We investigated the formation and dimensions of the supramolecular objects formed in aqueous solution of specially designed G-rich DNA sequences (Table 1) by combining DLS and PAGE measurements. We studied the effects of temperature, oligonucleotide concentration, method of preparation, and base sequence to explore the basic principles of G-wire formation.

2. Experimental

2.1. Material. Oligonucleotides (see Table 1) were ordered from Eurogentec (Belgium) as 40 nM desalted syntheses and reconstituted in water. Oligonucleotides were folded utilising either dialysis or heat treatment. Dialysis was performed at a concentration of 100 μM DNA in the presence of 100 mM NaCl buffered with 10 mM NaPi at pH 6.8, then diluted in same concentration of buffer or H_2O to specified concentrations immediately prior to measurements. Where heat treatment is specified, oligonucleotides at 100 μM DNA in presence of 100 mM NaCl, 10 mM NaPi (pH 6.8) were heated to 93°C for ten minutes and left to cool in heating block to room temperature prior to experiment. For DLS measurements, the oligonucleotides with a 0.4 mM concentration were used. For the concentration dependence studies the initial solutions were dissolved by the corresponding buffer.

2.2. PAGE. Gel electrophoresis experiments were performed on 15% native bis/acrylamide gels, utilising 1X TBE running buffer supplemented with 5 mM $NaBO_2$ to retain folded architectures. Oligonucleotide samples were prepared to a final concentration of 2 μM DNA in presence of 100 mM NaCl buffered with 10 mM NaPi at pH 6.8 with 5% sucrose to facilitate sample loading. Gels were run at 120 V and 4°C for a maximum of 2 hours and stained with 1X SYBR gold (Invitrogen, Paisley, UK) in 1X TBE buffer. In order to compare migration rates between different oligonucleotide samples, a GeneRuler Ultra Low Range (10–200 bps) DNA Ladder (Fermentas, York, UK) was used.

Table 1: The investigated G-rich DNA sequences.

Designation	Sequence
Sequence 1	GCGGTCGGGGTCGGGGTCGG
Sequence 2	GCGGAGGCG
Sequence 3	GCGGTGGCG
Sequence 4	GCGGTGGGGTGGCG
Sequence 5	GCGGTGGGGTGGGGTGGGGTGGGGTGGCG
Sequence 6	GCGGTGGGGTGGGGTGGCG

2.3. Dynamic Light Scattering. Dynamic light scattering experiments (DLS) were performed using a digital correlator (ALV-Laser Vertriebgesellschaft), a goniometer, and a photomultiplier detector. The light source was a frequency doubled Nd:YAG laser with a wavelength of 532 nm. The incident laser beam was linearly polarized in the direction perpendicular to the scattering plane. The scattered light of the same polarization was detected at scattering angles $50^\circ \leq \theta \leq 130^\circ$. The capillary containing the sample had an inner diameter of 5 mm and was immersed in an index matching bath with a diameter of 10 cm to minimize stray light from the outer capillary wall.

We measured the autocorrelation function $g_2(t) = \langle I(0)I(t)\rangle/\langle I\rangle^2$ of the average scattered light intensity I [31]. Most of the measurements were performed in a mixed regime, in which the intensity autocorrelation function is related to the field correlation function $g_1(t)$ by the relation [32]

$$g_2(t) = 1 + 2(1 - j_d)\, j_d g_1(t) + {j_d}^2 {g_1}^2(t), \tag{1}$$

with j_d being the ratio between the intensity of the light that is scattered inelastically and the total scattered intensity. The field correlation function $g_1(t)$ for systems with a polydisperse size distribution can be expressed by stretch exponential functions [33]

$$g_1(t) = \sum_i A_i \exp\left(\frac{-t}{\tau_i}\right)^{\beta_i}, \tag{2}$$

where A_i is the amplitude of the ith relaxation mode and the stretch exponent lies in the range $0 \leq \beta_i \leq 1$. The average relaxation time of the ith relaxation mode is given by

$$\langle \tau_i \rangle = \frac{\tau_i}{\beta_i}\Gamma\left(\frac{1}{\beta_i}\right), \tag{3}$$

where $\Gamma(1/\beta_i)$ is the gamma function. The parameter β_i is a measure of the width of the distribution of relaxation times. Very narrow distributions correspond to $\beta_i \sim 1$, while smaller values of β_i indicate broader distributions. The characteristic relaxation times of the observed dynamic modes were obtained by fitting the measured autocorrelation curves $g_2(t)$ to (1) and (2).

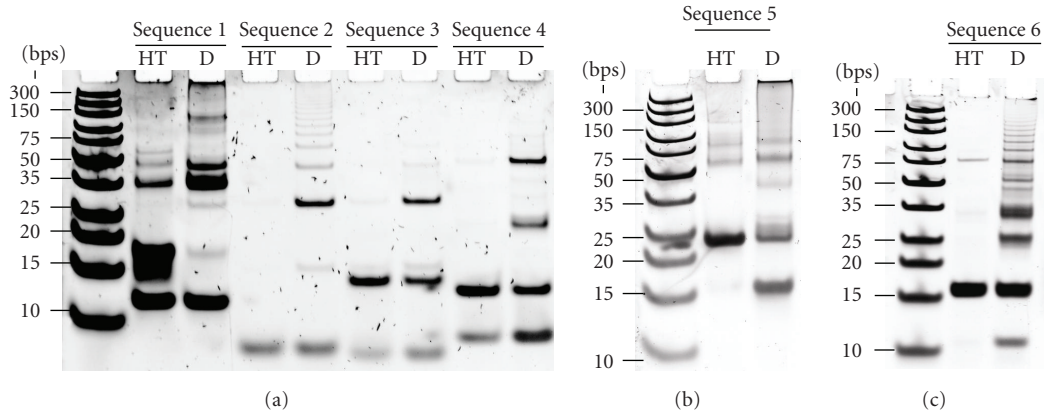

Figure 1: PAGE shows that heat treatment (HT) mainly gives short aggregates, while preparation by dialysis (D) results in higher degree of assembly. Most profound multistep assembling is observed for dialysed sequences 1, 5, and 6.

According to the polarized scattering (so called VV scattering) detected in our experiments, the translational diffusion coefficients were calculated as

$$D_i = \frac{1}{\langle \tau_i \rangle q^2}, \tag{4}$$

where q is the scattering wave vector given as $q = (4\pi n/\lambda)\sin(\theta/2)$ with $n = 1.33$ being the solution refractive index, λ the laser wavelength and θ the scattering angle. In most cases, two diffusive modes were detected. Several correlation curves were measured for every solution and averaged values of the fitting parameters were taken for further consideration.

From the translational diffusion coefficients, the dimensions of the scattering objects in solutions can be estimated. The corresponding hydrodynamic radius is calculated as

$$r_H = \frac{k_B T}{6\pi\eta D}, \tag{5}$$

with k_B being the Boltzmann constant, T the absolute temperature, and η the solvent viscosity. For dilute solutions of rod-like particles the hydrodynamic theory of Tirado and Garcia de la Torre [34–36] can be applied as long as the ratio of length to diameter $p = L/d$ is in the range $2 \le p \le 30$. The translational diffusion coefficient in this theory is given by

$$D = \frac{k_B T}{3\pi\eta L}(\ln p + \nu), \tag{6}$$

where ν is the end-effect correction term given as $\nu = 0.312 + 0.565/p - 0.100/p^2$. Knowing the diameter of the studied rod-like assembly, thus the length of the objects can be estimated.

3. Results

3.1. PAGE. The sequences were first investigated by PAGE to check for folding of oligonucleotides into higher order architectures. Samples prepared by heat treatment show a lesser degree of macromolecular assembly as compared to dialysed samples for all investigated oligonucleotides (Figure 1). The formation of macromolecular assemblies should indeed take more time. The band with the highest mobility in each lane corresponds to a bistranded monomeric unit. The shortest dialysed sequences (sequences 2 and 3) show only few albeit sharp bands pointing to the formation of smaller discrete stable species and a very low degree of macromolecular self-assembly. The longer sequences 1, 5 and 6, on the other hand, indicate possible stepwise assembly into large aggregates.

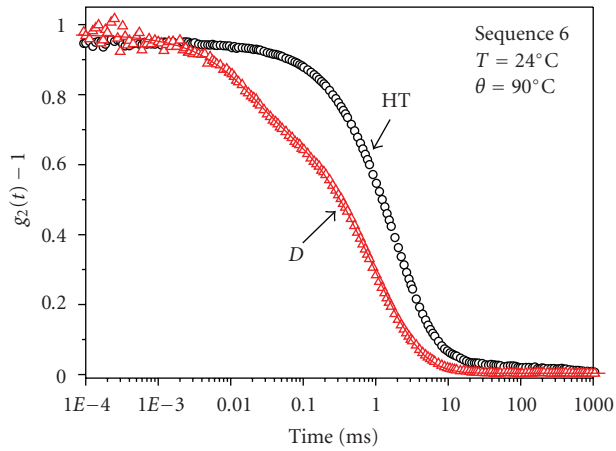

Figure 2: Typical DLS autocorrelation functions detected for heat treated (HT) and dialysed (D) samples. The slow diffusive mode (correlation time in the range of 1–10 ms at $\theta = 90°$) is observed for both samples, while the fast diffusive mode (correlation time in the range of 0.01–0.1 ms at $\theta = 90°$) is observed only for the dialysed sample. The fast mode is assigned to quadruplex motion, while the slow mode presumably arises from dynamics of loose polyion associates.

3.2. DLS. In all investigated samples, we detected a slow diffusive mode with correlation times in the range of 1–10 ms (at $\theta = 90°$) (Figures 2 and 3). Such a mode corresponds to translational motion of large globular aggregates with hydrodynamic radii in the range of micrometers. Similar slow modes are typically observed in DNA and many other

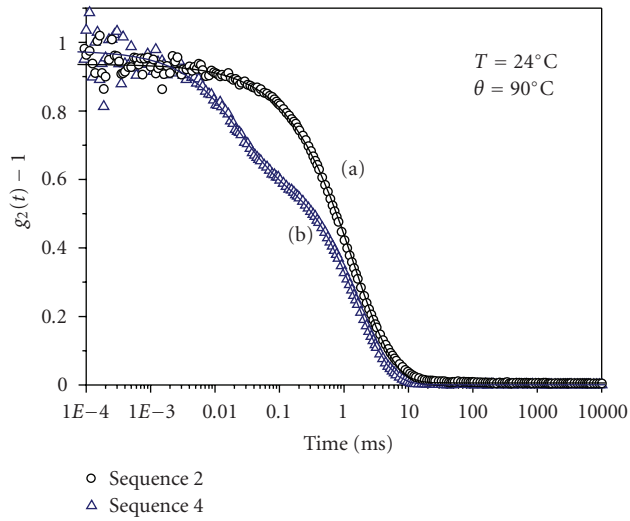

Figure 3: Typical autocorrelation functions of short (a) and long (b) oligonucleotide solutions prepared by dialysis method (c = 0.4 mM).

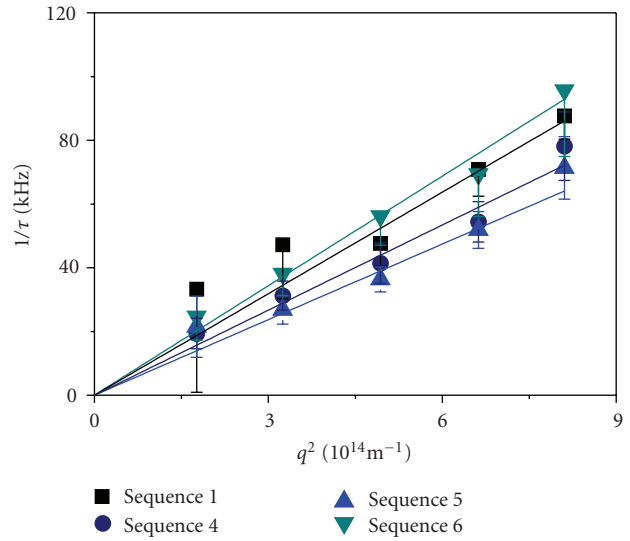

Figure 4: Dispersion relation of the fast diffusive mode for dialysed solutions of sequences 1, 4, 5, and 6 at $T = 24°$C. Solid lines are fits to (4). Error bars were obtained by fitting experimental correlation functions $g_2(t)$ to (1) taking into account (2).

Table 2: Hydrodynamic parameters obtained from DLS measurements in dialysed samples at 0.4 mM DNA concentration and room temperature. The length of the quadruplex L is estimated from (6) using d = 2.6 nm for the quadruplex diameter [26, 39]. For comparison, the length of extended oligonucleotides L_{oligo} is estimated by multiplying the number of bases with 0.34 nm, the average base distance.

Designation	D_f (10^{10} m^2/s)	r_H (nm)	Length (nm)	L_{oligo} (nm)
Sequence 1	1.06 ± 0.037	2.26 ± 0.034	6.1 ± 0.5	6.8
Sequence 2	—	—	—	3.1
Sequence 3	3.0 ± 0.30	0.78 ± 0.08	—	3.1
Sequence 4	0.89 ± 0.040	2.69 ± 0.044	8.8 ± 0.8	4.8
Sequence 5	0.79 ± 0.008	3.03 ± 0.062	11.0 ± 0.2	9.9
Sequence 6	1.15 ± 0.041	2.09 ± 0.036	5.0 ± 0.4	6.5

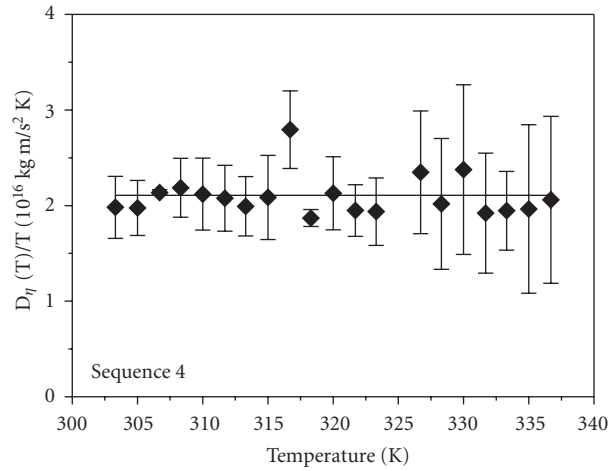

Figure 5: The values of the diffusion coefficient of the fast mode D_f normalised by solution temperature T and solvent viscosity $\eta(T)$ show no modifications with temperature. This suggests that the associated quadruplex structure is stable in the whole investigated temperature range.

polyelectrolyte solutions. They are usually attributed to the presence of loose multichain associates formed due to electrostatic interactions, but their nature is still not quite resolved [20, 37, 38]. As these aggregates are to our opinion not connected with G-wire formation, they will not be further considered.

In all heat treated samples, only the above mentioned "slow mode" exists, so they will not be further discussed. Solely the "slow mode" is observed also in the dialysed sequence 2 (Figure 3(a)), which is the only sequence containing adenine base. In dialysed sequence 3, an additional fast diffusive mode can be faintly resolved at large scattering angles ($\theta > 90°$). The corresponding diffusion coefficient calculated from (4) has a value of $D_f = 3.0 \pm 0.3 \cdot 10^{-10}$ m^2/s (Table 2), which indicates fast translational motion of very small scattering objects, most probably single oligonucleotides. In dialysed sequence 4, the fast mode is more profound and can be clearly resolved (Figure 3(b)).

The DLS autocorrelation functions of dialysed sequences containing GGGG repeats (sequences 1, 5, and 6) all show two relaxation modes. The angular dependence of the inverse relaxation time of the fast mode (Figure 4) reveals quadratic dispersion as given by (4). The resultant diffusion coefficients D_f obtained for solution concentration of 0.4 mM are listed in Table 2. The obtained values suggest that the fast mode is most probably associated with translational motion of oligonucleotides assembled into G-quadruplex structures.

The dialysed sequence 4 at 0.4 mM DNA was also used to investigate the temperature dependence of the fast diffusive

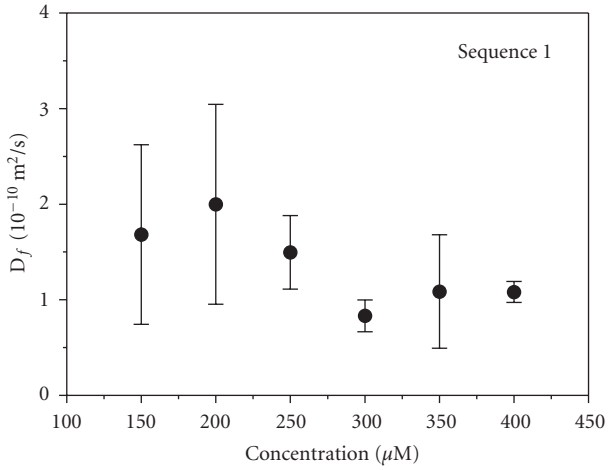

Figure 6: Diffusion coefficient of the fast diffusive mode as a function of oligonucleotide concentration. Measurements for dialysed sequence 1.

mode (Figure 5). The sample was slowly heated from $T = 300$ K towards higher temperatures. A relative amplitude of the fast mode decreased with increasing temperature and for $T > 338$ K the fast mode could not be resolved anymore. However, the slow mode remained. To reveal possible temperature-induced structural changes of the scattering objects, the values of diffusion coefficient D_f obtained at different temperatures were divided by temperature T and multiplied by the corresponding solvent viscosity $\eta(T)$. The resulting values of $D_f\eta(T)/T$ as a function of temperature are shown in Figure 5. One can notice that they remain constant throughout the investigated temperature range, which indicates that no structural modification of the scattering objects (quadruplexes) takes place.

The effect of oligonucleotide concentration on the value of D_f was investigated for dialyzed sequence 1 (Figure 6). Although it appears that the values decrease with increasing concentration, no precise conclusion can be drawn due to the large uncertainty of the measured data points. At low solution concentrations and short relaxation times, DLS measurements typically exhibit relatively large noise level. This has been previously observed in studies on short DNA sequences [19]. However, for DNA concentrations below 1 mM, which was the case in all our measurements, the effect of electrostatic interactions on solution dynamics is usually negligible and so the solution can be considered as infinitely dilute. Consequently, the value of the diffusion coefficient is expected to be constant.

4. Discussion

Both, PAGE and DLS analysis, reveal that the method of sample preparation is essential for the level of self-assembly in solution. We observe formation of slower migrating species for all oligonucleotides in PAGE for the dialysis treated samples. Sequences 1, 2, 5, and 6 appear to form larger assemblies, whilst sequences 3 and 4 do not. The most striking results are for sequences 2 and 6, where one or two species of lower molecular weight were formed in the annealing treatment versus numerous larger species through dialysis.

PAGE comparison between sequences 2 and 3 shows that there are sequence effects in the kinetics of formation for the same topology. When comparing dialysis, a band appearing at nominal 15 bp in sequence 3 appears only very faintly in sequence 2, while a faster, and a slower, migrating bands appear quite distinctively in both. The effect of "sticky ends" is also shown when comparing sequences 1 and 6. While between nominal 10 and 35 bp they have the same number of bands appearing in approximately the same positions, their intensities vary substantially. For these particular sequences, the difference in the annealing treatment is greater, with sequence 6 showing a very strong fast migrating band at nominal 16 bp. In contrast, the fastest migrating band for seq1 is at nominal 12 bp. In general, and as expected, it is apparent that the greater the oligonucleotide length the longer the species formed. Indeed, it is apparent for the longest oligonucleotide sequence (sequence 5) that the macromolecular DNA objects break into smaller units in a less discrete manner than for the other sequences. The smear for low migrating DNA in sequence 5 may thus be due to steric hindrance by the pore size of the gel.

For the shortest of the dialysed sequences, sequences 2 and 3, the absence of any measurable fast DLS mode for the former and the observation of a faint extremely fast mode for the latter, can be explained only by the presence of very small scattering objects, most probably single oligonucleotide molecules. This finding is not consistent with PAGE results (Figure 1), which reveal additional slower diffusing species resulting in sharp bands, probably signifying multimers. Similar discrete bands are seen also in the picture of PAGE for dialysed sequence 4. For this sequence, the PAGE result is in better agreement with the DLS results. The diffusion coefficient of the fast DLS mode gives quadruplex length of 8.8 ± 0.8 nm (Table 2), which is considerably larger than the length of a single oligonucleotide strand (about 4.8 nm). This signifies formation of assemblies formed from several oligonucleotides.

The two dialysed intermediate-length sequences (sequences 1 and 6) both exhibit the same PAGE band attributed to fast migrating monomers and a strong band at about 35 bps (accordingly to the reference duplex DNA ladder). The main difference between the two oligonucleotides is in the formation of two intermediate bands for sequence 6, while sequence 1 forms no intermediate species. Interestingly, the two strong bands (at 35 bps) very well agree with the quadruplex length L estimated from the DLS measurements, which is 5.0 ± 0.4 nm for sequence 6 and 6.1 ± 0.5 nm for sequence 1, respectively. The smaller apparent length of sequence 6 can be explained by the presence of the intermediate species contributing to the scattering. The diffusion coefficient measured for sequence 1 ($D_f = 1.06 \pm 0.037$) is in very good agreement with the values obtained for similar folded structures by hydrodynamic modelling [30].

The longest oligonucleotide, sequence 5, forms the largest aggregates. In PAGE, the majority of the material is so slowly migrating through the gel, that just a broad smearing is observed. Therefore, a formation of very long structures is expected. DLS measurements, on the other hand, reveal the presence of supramolecular assemblies with the length of 11.0 ± 0.2 nm, which is only slightly larger than the length of a single strand. In contrast to PAGE, DLS also reveals a relatively narrow distribution of aggregate lengths. This is seen from the DLS stretch exponent factor for the fast mode, which is in the range $0.9 < \beta_f < 1$, thus excluding a broad distribution of the dimensions of the scattering objects. Also for other sequences, the values of β_f were very close to 1.

The origin of the differences between the PAGE and the DLS results is not clear. On the basis of the PAGE results, sequences 1, 5, and 6 are all supposed to form some long wire-like assemblies, but DLS measurements do not support this expectations. Accordingly to the DLS results, the highest level of self-assembly is expected for sequence 4, which exhibits the largest length of the scattering objects with respect to the length of the single strand. One possible reason for the discrepancies might be quite different solution concentrations used for the two experiments. PAGE is usually performed with concentrations $c \sim 10\,\mu$M, while DLS gives reasonable signals. Yet for $c > 100\,\mu$M, this is not consistent with what we intuitively know, that is, higher concentrations tend to favour multimer formation. Another aspect arises from the slow DLS mode, which signifies that in addition to wire-like assemblies there are also some other aggregate types present in solution. These aggregates, most probably loose multipolyion associates, might correspond to the slow diffusing objects observed in PAGE.

DLS experiments bring also information on temperature and concentration dependence of the self-assembly. The temperature dependence (Figure 5) shows that up to $T = 65^\circ$C the length of the self-assembled objects remains constant. Nevertheless, the amplitude of the fast DLS mode strongly decreases by increasing temperature, while the overall scattering intensity is only slightly reduced. This signifies that the slow mode, which mainly contributes to the scattering intensity, is not much affected by heating. But relatively to it, the scattering intensity related to the fast mode becomes more and more weak. This can be explained by temperature-driven dissociation of the self-assembled structures of well-defined size into much smaller single oligonucleotides, which are practically invisible by DLS.

Dependence of the fast DLS mode on the concentration of the solution (Figure 6) also supports the idea of formation of the self-assembled structures with well-defined length, which are not affected by modifications of the solution concentration. On the contrary to wire-like assemblies formed from single guanosine molecules (GMP), it seems that formation of supramolecular assemblies of G-rich oligonucleotides, does not exhibit any critical solution concentration, at which the assembling would become profound.

5. Conclusions

A series of G-rich oligonucleotides was studied by PAGE and DLS to investigate the formation and dimensions of G-quadruplexes. Both methods show that thermal annealing induces much less macromolecular self-assembly than the dialysis method. This demonstrates that not only the base sequence, but also the folding kinetics play an important role in the self-assembly process. On one hand, this makes the phenomenon very complex, but on the other hand it provides a possibility for fine tuning of the assembling features via external stimuli. Further studies are needed to find the source of the differences and how they can be modulated.

PAGE and DLS show the best agreement on quadruplex dimensions for sequences of intermediate length (sequences 1, 4 and 6). The last band of sequence 4 coincides with the DLS signal arising from aggregates of a 9 nm length. The two similar sequences 1 and 6 give also aggregates of similar length 5–6 nm and these agree with a strong PAGE band observed for both sequences.

For the shortest sequences 2 and 3, PAGE suggest the formation of multimers not detected by DLS. The only DLS signal comes from very fast diffusing objects with effective dimensions below 1 nm pointing to single oligonucleotides. For the largest sequence, on the other hand, PAGE suggests very long aggregates giving a broad smeared band at the beginning of the lane. In DLS instead, a well defined fast mode is attributed to a species with the length of about 11 nm.

Because we are able to assess intermediate lengths, we are currently investigating the mechanism of self-assembly of these wires by combining both methods. Thus, the combination provides valuable information on the G-quadruplex formation towards control of its length.

Acknowledgment

The authors acknowledge the financial support of COST Action MP0802 in scope of Short Term Scientific Missions.

References

[1] J. R. Williamson, "G-quartet structures in telomeric DNA," *Annual Review of Biophysics and Biomolecular Structure*, vol. 23, pp. 703–730, 1994.

[2] J. T. Davis, "G-quartets 40 years later: from 5′-GMP to molecular biology and supramolecular chemistry," *Angewandte Chemie International Edition*, vol. 43, no. 6, pp. 668–698, 2004.

[3] T. C. Marsh and E. Henderson, "G-wires: self-assembly of a telomeric oligonucleotide, d(GGGGTTGGGG), into large superstructures," *Biochemistry*, vol. 33, no. 35, pp. 10718–10724, 1994.

[4] M. Weglarz, J. Vesenka, W. Fritzsche, S. Yerkes, and E. Kmiec, "Analysis of G-5x Quadruplex DNA," in *International Symposium on DNA-Based Nanodevices*, vol. 1062 of *AIP Conference Proceedings*, pp. 123–128, 2008.

[5] J. Vesenka, D. Bagg, A. Wolff, A. Reichert, R. Moeller, and W. Fritzsche, "Auto-orientation of G-wire DNA on mica," *Colloids and Surfaces B*, vol. 58, no. 2, pp. 256–263, 2007.

[6] K. Kunstelj, F. Federiconi, L. Spindler, and I. Drevenšek-Olenik, "Self-organization of guanosine 5′-monophosphate on mica," *Colloids and Surfaces B*, vol. 59, no. 2, pp. 120–127, 2007.

[7] M. A. Batalia, E. Protozanova, R. B. Macgregor Jr., and D. A. Erie, "Self-assembly of frayed wires and frayed-wire networks: nanoconstruction with multistranded DNA," *Nano Letters*, vol. 2, no. 4, pp. 269–274, 2002.

[8] T. C. Marsh, J. Vesenka, and E. Henderson, "A new DNA nanostructure, the G-wire, imaged by scanning probe microscopy," *Nucleic Acids Research*, vol. 23, no. 4, pp. 696–700, 1995.

[9] N. Borovok, N. Iram, D. Zikich, et al., "Assembling of G-strands into novel tetra-molecular parallel G4-DNA nanostructures using avidin-biotin recognition," *Nucleic Acids Research*, vol. 36, no. 15, pp. 5050–5060, 2008.

[10] I. Lubitz, N. Borovok, and A. Kotlyar, "Interaction of monomolecular G4-DNA nanowires with TMPyP: evidence for intercalation," *Biochemistry*, vol. 46, no. 45, pp. 12925–12929, 2007.

[11] K. Kunstelj, L. Spindler, F. Federiconi, M. Bonn, I. Drevenšek-Olenik, and M. Čopič, "Sum-frequency generation spectroscopy of self-assembled structures of Guanosine 5′-monophosphate on mica," *Chemical Physics Letters*, vol. 467, no. 1–3, pp. 159–163, 2008.

[12] J. B. Hightower, D. R. Olmos, and J. A. Walmsley, "Supramolecular structure and polymorphism of alkali metal salts of guanosine 5′-monophosphate: SEM and NMR study," *Journal of Physical Chemistry B*, vol. 113, no. 36, pp. 12214–12219, 2009.

[13] M. Webba da Silva, "Geometric formalism for DNA quadruplex folding," *Chemistry*, vol. 13, no. 35, pp. 9738–9745, 2007.

[14] M. Webba da Silva, "Association of DNA Quadruplexes through G:C:G:C tetrads. Solution structure of d(GCGGTGGAT)," *Biochemistry*, vol. 42, no. 49, pp. 14356–14365, 2003.

[15] M. Webba da Silva, "Experimental demonstration of T:(G:G:G:G):T hexad and T:A:A:T tetrad alignments within a DNA quadruplex stem," *Biochemistry*, vol. 44, no. 10, pp. 3754–3764, 2005.

[16] J.-L. Mergny, A. De Cian, S. Amrane, and M. Webba da Silva, "Kinetics of double-chain reversals bridging contiguous quartets in tetramolecular quadruplexes," *Nucleic Acids Research*, vol. 34, no. 8, pp. 2386–2397, 2006.

[17] J. Seils and R. Pecora, "Dynamics of a 2311 base pair superhelical DNA in dilute and semidilute solutions," *Macromolecules*, vol. 28, no. 3, pp. 661–673, 1995.

[18] H. Tj. Goinga and R. Pecora, "Dynamics of low molecular weight DNA fragments in dilute and semidilute solutions," *Macromolecules*, vol. 24, no. 23, pp. 6128–6138, 1991.

[19] H. Liu, L. Skibinska, J. Gapinski, A. Patkowski, E. W. Fischer, and R. Pecora, "Effect of electrostatic interactions on the structure and dynamics of a model polyelectrolyte. I. Diffusion," *Journal of Chemical Physics*, vol. 109, no. 17, pp. 7556–7566, 1998.

[20] L. Skibinska, J. Gapinski, H. Liu, A. Patkowski, E. W. Fischer, and R. Pecora, "Effect of electrostatic interactions on the structure and dynamics of a model polyelectrolyte. II. Intermolecular correlations," *Journal of Chemical Physics*, vol. 110, no. 3, pp. 1794–1800, 1999.

[21] A. Wilk, J. Gapinski, A. Patkowski, and R. Pecora, "Self-diffusion in solutions of a 20 base pair oligonucleotide: effects of concentration and ionic strength," *Journal of Chemical Physics*, vol. 121, no. 21, pp. 10794–10802, 2004.

[22] W. Eimer and Th. Dorfmüller, "Self-aggregation of guanosine 5′-monophosphate studied by dynamic light scattering techniques," *Journal of Physical Chemistry*, vol. 96, no. 16, pp. 6790–6800, 1992.

[23] L. Spindler, I. Drevenšek-Olenik, M. Čopič, et al., "Dynamic light scattering and ^{31}P NMR spectroscopy study of the self-assembly of deoxyguanosine 5′-monophosphate," *European Physical Journal E*, vol. 7, no. 1, pp. 95–102, 2002.

[24] L. Spindler, I. Drevenšek-Olenik, M. Čopič, J. Cerar, J. Škerjanc, and P. Mariani, "Dynamic light scattering and ^{31}P NMR study of the self-assembly of deoxyguanosine 5′-monophosphate: the effect of added salt," *European Physical Journal E*, vol. 13, no. 1, pp. 27–33, 2004.

[25] H. Jurga-Nowak, E. Banachowicz, A. Dobek, and A. Patkowski, "Supramolecular guanosine 5′-monophosphate structures in solution. Light scattering study," *Journal of Physical Chemistry B*, vol. 108, no. 8, pp. 2744–2750, 2004.

[26] A. Wong, R. Ida, L. Spindler, and G. Wu, "Disodium guanosine 5′-monophosphate self-associates into nanoscale cylinders at pH 8: a combined diffusion NMR spectroscopy and dynamic light scattering study," *Journal of the American Chemical Society*, vol. 127, no. 19, pp. 6990–6998, 2005.

[27] M. Bolten, M. Niermann, and W. Eimer, "Structural analysis of G-DNA in solution: a combination of polarized and depolarized dynamic light scattering with hydrodynamic model calculations," *Biochemistry*, vol. 38, no. 38, pp. 12416–12423, 1999.

[28] A. Włodarczyk, J. Gapiński, A. Patkowski, and A. Dobek, "Structural polymorphism of telomeres studied by photon correlation spectroscopy," *Acta Biochimica Polonica*, vol. 46, no. 3, pp. 609–613, 1999.

[29] E. Protozanova and R. B. Macgregor Jr., "Thermal activation of DNA frayed wire formation," *Biophysical Chemistry*, vol. 84, no. 2, pp. 137–147, 2000.

[30] A. Włodarczyk, P. Grzybowski, A. Patkowski, and A. Dobek, "Effect of ions on the polymorphism, effective charge, and stability of human telomeric DNA. Photon correlation spectroscopy and circular dichroism studies," *Journal of Physical Chemistry B*, vol. 109, no. 8, pp. 3594–3605, 2005.

[31] B. J. Berne and R. Pecora, *Dynamic Light Scattering*, Wiley, New York, NY, USA, 1976.

[32] A. Mertelj, L. Cmok, and M. Čopič, "Anomalous diffusion in ferrofluids," *Physical Review E*, vol. 79, no. 4, Article ID 041402, 2009.

[33] K. S. Schmitz, *An Introduction to Dynamic Light Scattering by Macromolecules*, Academic Press, San Diego, Calif, USA, 1990.

[34] M. M. Tirado and J. Garcia de la Torre, "Translational friction coefficients of rigid, symmetric top macromolecules. Application to circular cylinders," *The Journal of Chemical Physics*, vol. 71, no. 6, pp. 2581–2587, 1979.

[35] M. M. Tirado and J. Garcia de la Torre, "Rotational dynamics of rigid, symmetric top macromolecules. Application to circular cylinders," *The Journal of Chemical Physics*, vol. 73, no. 4, pp. 1986–1993, 1980.

[36] M. M. Tirado, C. Lopez Martinez, and J. Garcia de la Torre, "Comparison of theories for the translational and rotational diffusion coefficients of rod-like macromolecules. Application to short DNA fragments," *The Journal of Chemical Physics*, vol. 81, no. 4, pp. 2047–2052, 1984.

[37] M. Sedlak, "Long-time stability of multimacroion domains in polyelectrolyte solutions," *Journal of Chemical Physics*, vol. 116, no. 12, pp. 5246–5255, 2002.

[38] M. Sedlak, "Mechanical properties and stability of multimacroion domains in polyelectrolyte solutions," *Journal of Chemical Physics*, vol. 116, no. 12, pp. 5236–5245, 2002.

[39] M. S. Kaucher, W. A. Harrell Jr., and J. T. Davis, "A unimolecular G-quadruplex that functions as a synthetic transmembrane Na^+ transporter," *Journal of the American Chemical Society*, vol. 128, no. 1, pp. 38–39, 2006.

SAGE-Hindawi Access to Research
Journal of Nucleic Acids
Volume 2010, Article ID 468017, 6 pages
doi:10.4061/2010/468017

Research Article

Structure and Stability of a Dimeric G-Quadruplex Formed by Cyclic Oligonucleotides

Joan Casals,[1] Júlia Viladoms,[1,2] Enrique Pedroso,[1] and Carlos González[3]

[1] *Departament de Química Orgànica, Universitat de Barcelona, C/. Martí i Franquès 1, 08028 Barcelona, Spain*
[2] *The Skaggs Institute for Chemical Biology, The Scripps Research Institute, 10550 North Torrey Pines Road, La Jolla, CA 92037, USA*
[3] *Instituto de Química Física "Rocasolano", CSIC, C/. Serrano 119, 28006 Madrid, Spain*

Correspondence should be addressed to Enrique Pedroso, epedroso@ub.edu and Carlos González, cgonzalez@iqfr.csic.es

Received 15 January 2010; Accepted 12 March 2010

Academic Editor: Daniela Montesarchio

We have studied the structure and stability of the cyclic dodecamer d<pGGGTTAGGGTTA>, containing two copies of the human telomeric repeat. In the presence of sodium, NMR data are consistent with a dimeric structure of the molecule in which two cycles self-associate forming a quadruplex with three guanine tetrads connected by edgewise loops. The two macrocycles are arranged in a parallel way, and the dimeric structure exhibits a high melting temperature. These results indicate that cyclization of the phosphodiester chain does not prevent quadruplex formation, although it affects the global topology of the quadruplex.

1. Introduction

One of the most studied noncanonical DNA motifs is the G-quadruplex, where four guanines are paired through their Watson-Crick and Hoogsteen sides [1–3]. These structures are receiving substantial attention in research areas ranging from molecular biology to structural and analytical chemistry [4–6]. It has been suggested that G-quadruplexes play a role in several biological processes, such as telomere integrity, genetic recombination, transcription, or replication. In addition, they are attractive targets for drug design, especially in cancer chemotherapy [7–11]. Clear evidence of quadruplex formation in vivo has been found recently [12–14].

G-quadruplexes can fold in many ways that differ in their chain number and orientation. Whereas single G_n tracks arrange in parallel structures, multiple G_n repeats fold with different topologies that are influenced mainly by the nucleotide sequence between G_n repeats as well as by the kind of counterion. In occasions, different topologies have been found for the same oligonucleotide in solid and solution studies.

On the other hand, cyclic oligonucleotides have emerged as interesting molecules in research for diagnosis and as therapeutic agents due to their increased nuclease resistance relative to their linear analogues [15, 16]. These molecules are also interesting for structural studies since the conformational constraint induced by cyclization of the chain may increase the relative stability of the structure of interest [17–21]. G-quadruplexes have been used as templates for enhancing the efficiency of the synthesis of cyclic oligonucleotides. This approach takes advantage of the proximity between the two oligonucleotide termini in some quadruplex topologies to improve phosphodiester ligation [22–24].

G-quadruplex forming cyclic oligonucleotides may be interesting in a number of applications. For example, these nuclease resistant oligonucleotides can be very useful probes to study G-quadruplex interacting proteins. However, the conformational constraint induced by cyclization affects the range of structures that a G-quadruplex can adopt. For example, diagonal loops or double-chain-reversal loops are not possible in quadruplexes formed by cyclic oligonucleotides.

To gain insight on the effect of cyclization on the structure of G-quadruplexes, we have studied the structure and stability of the cyclic dodecamer d<pGGGTTAGGGTTA>, containing two copies of the human telomeric repeat. The analogous linear oligonucleotide d(TAGGGTTAGGGT) forms two interconverting dimeric structures in solution: a parallel quadruplex with double-chain-reversal loops, and

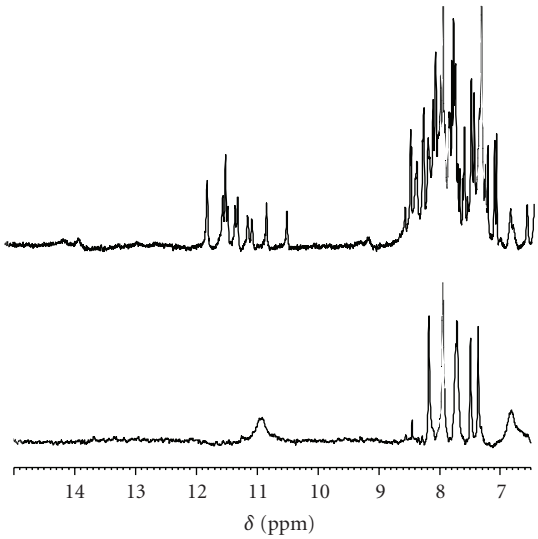

Figure 1: One-dimensional NMR spectra of d<pGGGTTA-GGGTTA> in H_2O at 60 μM (bottom) and 600 μM (top) oligonucleotide concentrations (buffer conditions: 100 mM NaCl, 25 mM sodium phosphate pH 7, $T = 5°C$).

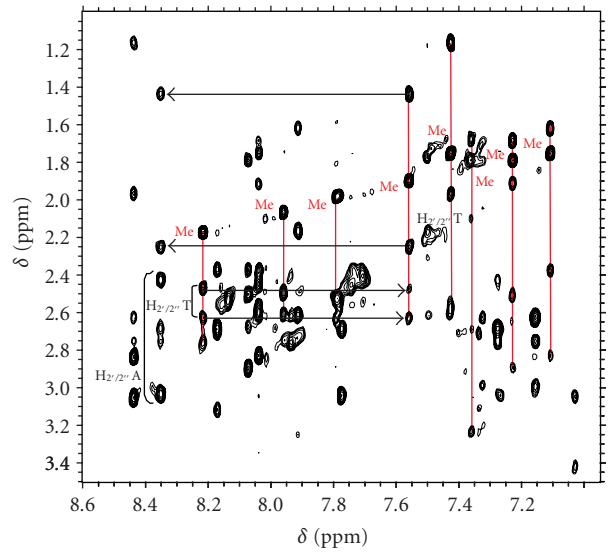

Figure 2: NOESY spectra of d<pGGGTTAGGGTTA> in D_2O (200 ms mixing time) at 600 μM oligonucleotide concentration (same buffer conditions as in Figure 1). The eight thymine signals are indicated together with some informative sequential NOE contacts.

an antiparallel quadruplex with edgewise loops [25]. On the other hand, the same sequence forms a parallel quadruplex with double-chain-reversal loops in the crystal (in presence of K^+) [26]. A similar structural diversity has also been observed in an oligonucleotide containing four copies of the human telomeric repeat, which in K^+ forms an intramolecular parallel quadruplex in the crystal [26] and an antiparallel quadruplex with a diagonal and two edgewise loops in Na^+-containing solution [27]. Other quadruplex topologies have been observed in a variety of oligonucleotides containing different number of telomeric repeats [28–31] (see [32] for a recent review on these studies).

2. Materials and Methods

The synthesis of d<pGGGTTAGGGTTA> was carried out following previously reported methods [33]. Samples for NMR experiments were prepared in 100 mM NaCl, 25 mM sodium phosphate buffer pH 7, with an oligonucleotide concentration ranging from 60 to 600 μM. NMR spectra were acquired in a Bruker AVANCE spectrometer operating at 600 MHz and equipped with a cryoprobe. Two-dimensional experiments (NOESY, TOCSY, and DQF-COSY) were carried out at 5°C in either D_2O or in H_2O/D_2O 9:1. NOESY spectra were acquired with mixing times of 50, 100, and 200 ms, and TOCSY spectra were recorded with standard MLEV-17 spin-lock sequence, and 80 ms mixing time. NOESY spectra in H_2O were acquired with 50 and 150 ms mixing times. In 2D experiments in H_2O, water suppression was achieved by including a WATERGATE [34] module in the pulse sequence prior to acquisition. The spectra were processed with Topspin software and analyzed with the program Sparky [35].

CD spectra were obtained following the change of ellipticity from 220 nm to 320 nm at different temperatures on a Jasco spectropolarimeter equipped with a Peltier temperature control used to set the temperature between 5°C and 90°C. The changes in ellipticity versus temperatures were plotted and used to obtain the melting temperature. Melting experiments were recorded at 0.5°C/min at the maximum wavelength. CD spectra were recorded at oligonucleotide concentrations ranging from 5 to 50 μM. The spectra were normalized to facilitate comparisons.

3. Results and Discussion

NMR spectra change dramatically upon oligonucleotide concentration. At low concentration, only six H6/H8 aromatic signals are detected (as a logical consequence of the repetitive sequence), and the exchangeable proton spectrum is very broad (see Figure 1). However, at high oligonucleotide concentration the exchangeable proton spectra shows 12 narrow signals between 10.0 and 12.0 ppm, and 24 aromatic signals (corresponding to H6/H8 protons) are observed in the non-exchangeable proton spectrum (see Figure 2). These data indicate the formation of an asymmetric dimer. Two fragments of the NOESY spectra in D_2O are shown in Figures 2 and 3. The NMR spectrum in these conditions exhibits narrow and well dispersed signals, which indicates that the oligonucleotide adopt a well-defined structure. However, the NMR spectra of this molecule could not be unambiguously assigned due to its highly repetitive sequence. In spite of this, many structural features can be spotted from this spectrum. First, the cross-peaks of the imino and amino protons are consistent with the presence of three G-tetrads. Secondly, as shown in Figure 3, six

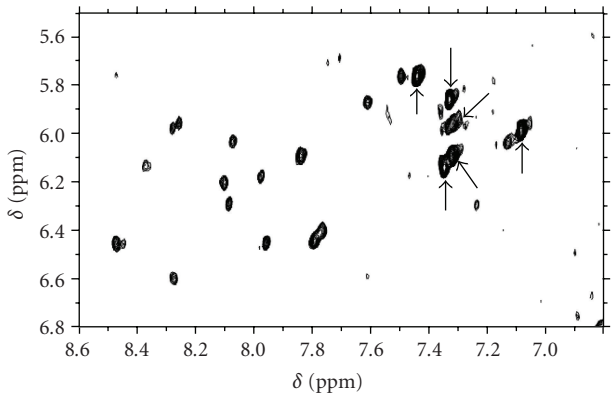

FIGURE 3: NOESY spectra of d<pGGGTTAGGGTTA> in D_2O (200 ms mixing time) at 600 μM oligonucleotide concentration (same buffer conditions as in Figure 1). Strong H1′-H8 cross-peaks, characteristic of *syn* guanines, are indicated.

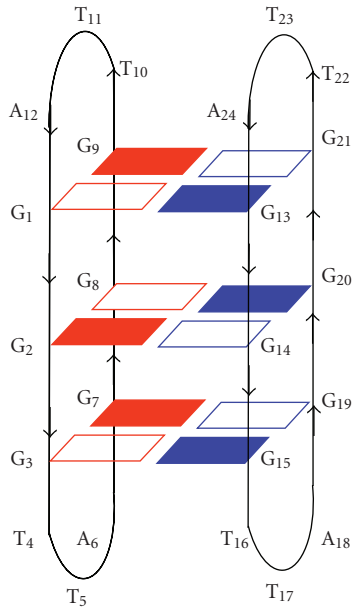

FIGURE 4: Schematic model of the dimeric structure of d<pGGGTTAGGGTTA>, consistent with the experimental data in Na^+ buffer. Guanines *syn* and *anti* are indicated with open and solid rectangles, respectively.

strong H1′-H8 cross-peaks are observed, indicating that the glycosidic angle of the corresponding guanines is in a *syn* conformation (Gs). The six remaining guanines are in an *anti* conformation (Ga). Moreover, the occurrence of four steps Gs-Ga can be established from the sequential H1′ → H8 NOEs steps. Finally, no Ga-Ga steps are present in this structure since no sequential NOEs are observed between guanines in *anti*.

All these data, together with symmetry considerations, led us to suggest a model for this structure in which two cyclic dodecamers self-associate forming an antiparallel quadruplex with three G-tetrads (Figure 4). The two macrocycles are arranged in a parallel way. Overall, the structure is similar to antiparallel quadruplexes resulting from a head-to-head association of two hairpins with "edgewise" loops.

It is interesting to compare these results with other structures of quadruplexes formed by linear oligonucleotides containing repeats of the human telomeric sequence. Different groups have shown that linear oligonucleotides containing two repeats tend to adopt antiparallel quadruplex structures in sodium buffer [25, 36]. In the case of d(UAGGGT^{Br}UAGGGT) the structure is an asymmetric dimer [25], but the relative orientation of the two molecules is different than in the dimeric structure of d<pGGGTTAGGGTTA>. The distribution of *syn* and *anti* guanines is also different in both cases. In the presence of K^+, linear oligonucleotides containing two repeats of the human telomere have the propensity to adopt parallel-stranded structures [25, 36], which are obviously impossible in the case of the cyclic analogues. We must conclude that the conformational constraint induced by cyclization of the phosphodiester chain affects the topology of the quadruplex. This result is not surprising since cyclization is formally equivalent to introducing an additional nonnative loop in the sequence. The effect of loop variations in the structure and topology of quadruplex has been extensively studied by several groups [37–39].

Since many oligonucleotides containing human telomeric repeats tend to adopt different structures in presence of K^+ or Na^+ cations, we tackled the study of the effect of these two cations on the structure of d<pGGGTTAGGGTTA>. The profile of the CD spectra in Na^+ buffer was consistent with an antiparallel G-quartet architecture characterized by a positive band at 248 nm, a positive maximum at 295 nm, and a negative maximum at 265 nm (Figure 5(a)). However, in presence of K^+ the CD spectra of d<pGGGTTAGGGTTA> changes dramatically (Figure 5(b)). The negative band at 265 nm disappears, and the minimum around 235 nm is more pronounced. In these experimental conditions the CD spectrum is not consistent with a pure antiparallel or parallel G-quadruplex, the latter presenting a characteristic positive maximum at 265 nm [36]. The experimental CD spectrum suggests the presence of several conformations in equilibrium. NMR spectra conducted at 500 μM oligonucleotide concentration in K^+ buffer exhibit very broad signals (data not shown), in agreement with the occurrence of multiple conformations or aggregation. This result is not unexpected since it is well documented that K^+ cations favour the parallel-stranded structures, which in this case are impeded by the cyclization of the phosphodiester chain.

The thermal stability of this structure has been studied by NMR and CD experiments. CD spectra of d<pGGGTTAGGGTTA> in Na^+ are characteristic of antiparallel quadruplexes (see Figure 5). Melting curves were recorded at different oligonucleotide concentrations, and thermodynamic parameters were obtained from the variation of the melting temperature with the concentration [40]. Thermodynamic parameters for dimer formation in 100 mM NaCl buffer solution are $\Delta H^0 = -35$ kcal/mol, $\Delta S^0 = -92$ cal/mol, and $\Delta G^0_{298} = -8$ kcal/mol. It is interesting to compare these parameters with the values for the unimolecular quadruplex formed by analogous linear oligonucleotides

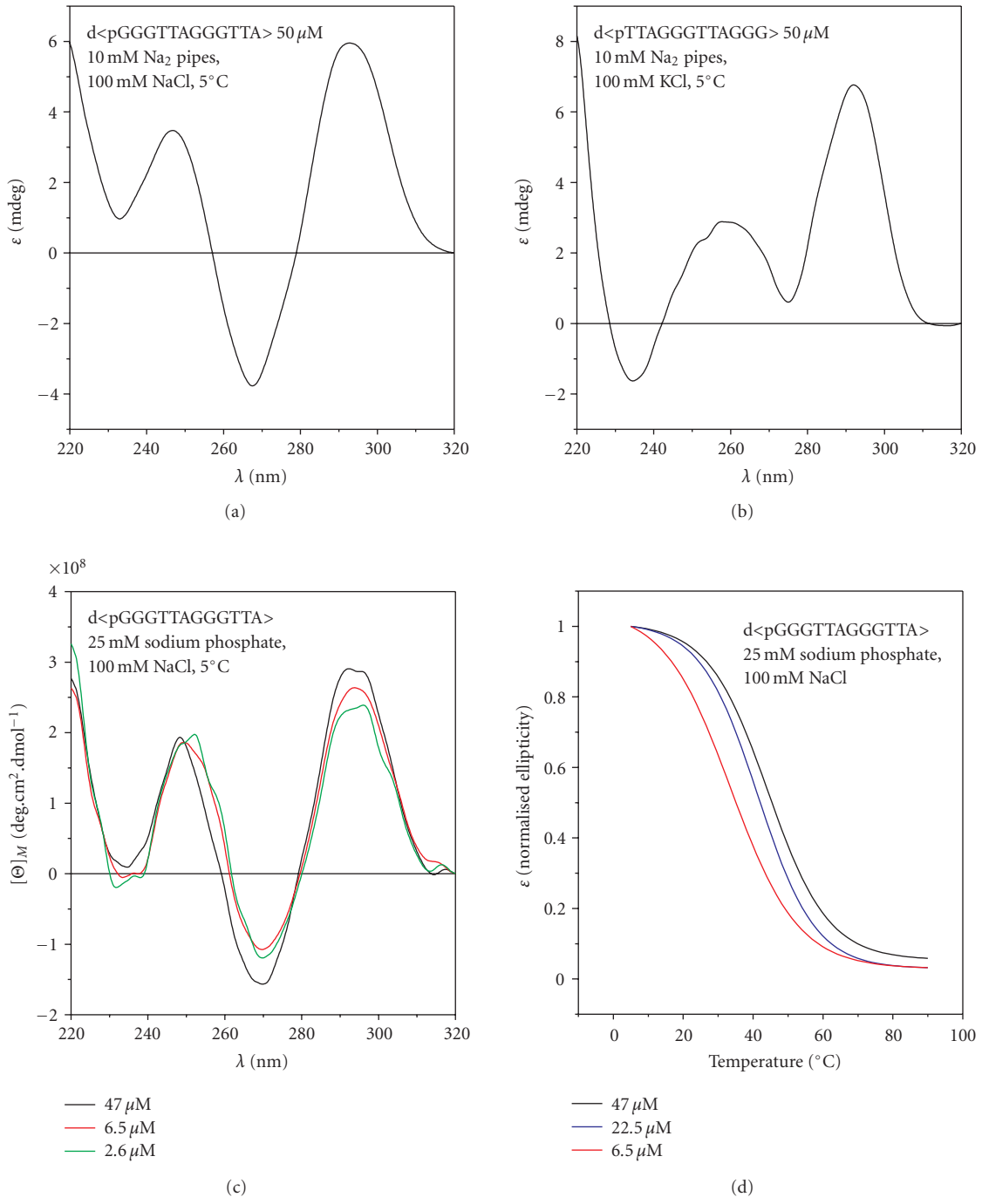

FIGURE 5: CD spectra of d<pGGGTTAGGGTTA> in media containing Na^+ (a) or K^+ (b). Converted to molar ellipticity CD spectra (c) and normalized melting curves (d) at different oligonucleotide concentrations in the same buffer conditions as NMR experiments.

containing four repeats of the human telomere. For example, the thermodynamic parameters for d(AGGGTTAGGGTTAGGGTTAGGG), under the same buffer conditions, are $\Delta H^0 = -54$ kcal/mol, $\Delta S^0 = -163$ cal/mol, and $\Delta G^0_{298} = -5.4$ kcal/mol [41]. Interestingly, formation-free energy is lower for the quadruplex formed by two cyclic oligonucleotides than for the quadruplex formed by the "native" sequence with four telomeric repeats. The larger stability of the former is entropic in nature. The lower formation enthalpy in the dimer is probably a consequence of the constraint in the loops induced by the cyclization. We can conclude that "native" loops are enthalpically more stable. However, the entropic cost of forming the quadruplex through the self-association of two cyclic oligonucleotides with two repeats is lower than in the case of the folding of a linear oligonucleotide with four telomere repeats.

4. Conclusions

In summary, we have shown that guanine-rich cyclic oligonucleotides can form dimeric quadruplex structures. The conformational constraint induced by cyclization of the chain does not prevent quadruplex formation but has a profound influence in the global topology and stability of the structure. Such effect must be taken into account in the potential application of cyclic G-quadruplex as molecular probes.

Acknowledgments

This work was supported by the Spanish Ministry of Science and Innovation Grant CTQ2007-68014-C02-01/02, COST project (G4-net, MP0802) and Generalitat de Catalunya grants 2009 SGR 208 and XRB.

References

[1] S. Burge, G. N. Parkinson, P. Hazel, A. K. Todd, and S. Neidle, "Quadruplex DNA: sequence, topology and structure," *Nucleic Acids Research*, vol. 34, no. 19, pp. 5402–5415, 2006.

[2] P. Bates, J.-L. Mergny, and D. Yang, "Quartets in G-major. The first international meeting on quadruplex DNA," *EMBO Journal*, vol. 8, no. 11, pp. 1003–1010, 2007.

[3] J. L. Huppert, "Four-stranded nucleic acids: structure, function and targeting of G-quadruplexes," *Chemical Society Reviews*, vol. 37, no. 7, pp. 1375–1384, 2008.

[4] J. T. Davis, "G-quartets 40 years later: from 5′-GMP to molecular biology and supramolecular chemistry," *Angewandte Chemie International Edition*, vol. 43, no. 6, pp. 668–698, 2004.

[5] D. Margulies and A. D. Hamilton, "Protein recognition by an ensemble of fluorescent DNA G-quadruplexes," *Angewandte Chemie International Edition*, vol. 48, no. 10, pp. 1771–1774, 2009.

[6] P. Alberti, A. Bourdoncle, B. Saccà, L. Lacroix, and J.-L. Mergny, "DNA nanomachines and nanostructures involving quadruplexes," *Organic and Biomolecular Chemistry*, vol. 4, no. 18, pp. 3383–3391, 2006.

[7] S. Balasubramanian and S. Neidle, "G-quadruplex nucleic acids as therapeutic targets," *Current Opinion in Chemical Biology*, vol. 13, no. 3, pp. 345–353, 2009.

[8] M. A. Blasco, "Telomeres and human disease: ageing, cancer and beyond," *Nature Reviews Genetics*, vol. 6, no. 8, pp. 611–622, 2005.

[9] D. J. Patel, A. T. Phan, and V. Kuryavyi, "Human telomere, oncogenic promoter and 5′-UTR G-quadruplexes: diverse higher order DNA and RNA targets for cancer therapeutics," *Nucleic Acids Research*, vol. 35, no. 22, pp. 7429–7455, 2007.

[10] D. Monchaud and M.-P. Teulade-Fichou, "A hitchhiker's guide to G-quadruplex ligands," *Organic and Biomolecular Chemistry*, vol. 6, no. 4, pp. 627–636, 2008.

[11] B. Gatto, M. Palumbo, and C. Sissi, "Nucleic acid aptamers based on the G-quadruplex structure: therapeutic and diagnostic potential," *Current Medicinal Chemistry*, vol. 16, no. 10, pp. 1248–1265, 2009.

[12] K. Paeschke, T. Simonsson, J. Postberg, D. Rhodes, and H. J. Lipps, "Telomere end-binding proteins control the formation of G-quadruplex DNA structures in vivo," *Nature Structural and Molecular Biology*, vol. 12, no. 10, pp. 847–854, 2005.

[13] M. L. Duquette, P. Handa, J. A. Vincent, A. F. Taylor, and N. Maizels, "Intracellular transcription of G-rich DNAs induces formation of G-loops, novel structures containing G4 DNA," *Genes and Development*, vol. 18, no. 13, pp. 1618–1629, 2004.

[14] N. Maizels, "Dynamic roles for G4 DNA in the biology of eukaryotic cells," *Nature Structural and Molecular Biology*, vol. 13, no. 12, pp. 1055–1059, 2006.

[15] E. T. Kool, "Circular oligonucleotides: new concepts in oligonucleotide design," *Annual Review of Biophysics and Biomolecular Structure*, vol. 25, pp. 1–28, 1996.

[16] E. T. Kool, "Recognition of DNA, RNA, and proteins by circular oligonucleotides," *Accounts of Chemical Research*, vol. 31, no. 8, pp. 502–510, 1998.

[17] G. W. Ashley and D. M. Kushlan, "Chemical synthesis of oligonucleotide dumbbells," *Biochemistry*, vol. 30, pp. 2927–2933, 1991.

[18] J. H. Ippel, V. Lanzotti, A. Galeone, et al., "Conformation of the circular dumbbell d<pCGC-TT-GCG-TT>: structure determination and molecular dynamics," *Journal of Biomolecular NMR*, vol. 6, no. 4, pp. 403–422, 1995.

[19] C.-T. Lin, Y. L. Lyu, and L. F. Liu, "A cruciform-dumbbell model for inverted dimer formation mediated by inverted repeats," *Nucleic Acids Research*, vol. 25, no. 15, pp. 3009–3016, 1997.

[20] N. Escaja, E. Pedroso, M. Rico, and C. González, "Dimeric solution structure of two cyclic octamers: four-stranded DNA structures stabilized by A:T:A:T and G:C:G:C tetrads," *Journal of the American Chemical Society*, vol. 122, no. 51, pp. 12732–12742, 2000.

[21] J. Viladoms, N. Escaja, M. Frieden, I. Gomez-Pinto, E. Pedroso, and C. González, "Self-association of short DNA loops through minor groove C:G:G:C tetrads," *Nucleic Acids Research*, vol. 37, no. 10, pp. 3264–3275, 2009.

[22] J. Qi and R. H. Shafer, "Covalent ligation studies on the human telomere quadruplex," *Nucleic Acids Research*, vol. 33, no. 10, pp. 3185–3192, 2005.

[23] T. Zhou, G. Chen, Y. Wang, Q. Zhang, M. Yang, and T. Li, "Synthesis of unimolecularly circular G-quadruplexes as prospective molecular probes," *Nucleic Acids Research*, vol. 32, no. 21, article e173, 2004.

[24] J. Chen, D. Liu, A. H. F. Lee, J. Qi, A. S. C. Chan, and T. Li, "Formation of circular oligodeoxyribonucleotides on the structural basis of G-quadruplex and product analysis," *Chemical Communications*, pp. 2686–2687, 2002.

[25] A. T. Phan and D. J. Patel, "Two-repeat human telomeric d(TAGGGTTAGGGT) sequence forms interconverting parallel and antiparallel G-quadruplexes in solution: distinct topologies, thermodynamic properties, and folding/unfolding kinetics," *Journal of the American Chemical Society*, vol. 125, no. 49, pp. 15021–15027, 2003.

[26] G. N. Parkinson, M. P. H. Lee, and S. Neidle, "Crystal structure of parallel quadruplexes from human telomeric DNA," *Nature*, vol. 417, no. 6891, pp. 876–880, 2002.

[27] Y. Wang and D. J. Patel, "Solution structure of the human telomeric repeat d[AG3(T2AG3)3] G-tetraplex," *Structure*, vol. 1, no. 4, pp. 263–282, 1993.

[28] N. Zhang, A. T. Phan, and D. J. Patel, "(3 + 1) assembly of three human telomeric repeats into an asymmetric dimeric G-quadruplex," *Journal of the American Chemical Society*, vol. 127, no. 49, pp. 17277–17285, 2005.

[29] A. T. Phan, V. Kuryavyi, K. N. Luu, and D. J. Patel, "Structure of two intramolecular G-quadruplexes formed by natural human telomere sequences in K^+ solution," *Nucleic Acids Research*, vol. 35, no. 19, pp. 6517–6525, 2007.

[30] A. T. Phan, K. N. Luu, and D. J. Patel, "Different loop arrangements of intramolecular human telomeric (3+1) G-quadruplexes in K^+ solution," *Nucleic Acids Research*, vol. 34, no. 19, pp. 5715–5719, 2006.

[31] J. Dai, M. Carver, C. Punchihewa, R. A. Jones, and D. Yang, "Structure of the hybrid-2 type intramolecular human telomeric G-quadruplex in K^+ solution: insights into structure polymorphism of the human telomeric sequence," *Nucleic Acids Research*, vol. 35, no. 15, pp. 4927–4940, 2007.

[32] A. T. Phan, "Human telomeric G-quadruplex: structures of DNA and RNA sequences," *FEBS Journal*, vol. 277, no. 5, pp. 1107–1117, 2010.

[33] E. Alazzouzi, N. Escaja, A. Grandas, and E. Pedroso, "A straightforward solid-phase synthesis of cyclic oligodeoxyribonucleotides," *Angewandte Chemie International Edition*, vol. 36, no. 13-14, pp. 1506–1508, 1997.

[34] M. Piotto, V. Saudek, and V. Sklenář, "Gradient-tailored excitation for single-quantum NMR spectroscopy of aqueous solutions," *Journal of Biomolecular NMR*, vol. 2, no. 6, pp. 661–665, 1992.

[35] D. T. Goddard and G. Kneller, *SPARKY 3*, University of California, San Francisco, Calif, USA, 2003.

[36] I. N. Rujan, J. C. Meleney, and P. H. Bolton, "Vertebrate telomere repeat DNAs favor external loop propeller quadruplex structures in the presence of high concentrations of potassium," *Nucleic Acids Research*, vol. 33, no. 6, pp. 2022–2031, 2005.

[37] M. Webba da Silva, M. Trajkovski, Y. Sannohe, N. Ma'ani Hessari, H. Sugiyama, and J. Plavec, "Design of a G-quadruplex topology through glycosidic bond angles," *Angewandte Chemie International Edition*, vol. 48, no. 48, pp. 9167–9170, 2009.

[38] P. Hazel, G. N. Parkinson, and S. Neidle, "Predictive modelling of topology and loop variations in dimeric DNA quadruplex structures," *Nucleic Acids Research*, vol. 34, no. 7, pp. 2117–2127, 2006.

[39] N. Smargiasso, F. Rosu, W. Hsia, et al., "G-quadruplex DNA assemblies: loop length, cation identity, and multimer formation," *Journal of the American Chemical Society*, vol. 130, no. 31, pp. 10208–10216, 2008.

[40] K. J. Breslauer, "Extracting thermodynamic data from equilibrium melting curves for oligonucleotide order-disorder transitions," *Methods in Enzymology*, vol. 259, pp. 221–242, 1995.

[41] J.-L. Mergny, A.-T. Phan, and L. Lacroix, "Following G-quartet formation by UV-spectroscopy," *FEBS Letters*, vol. 435, no. 1, pp. 74–78, 1998.

SAGE-Hindawi Access to Research
Journal of Nucleic Acids
Volume 2010, Article ID 841932, 8 pages
doi:10.4061/2010/841932

Research Article

Thrombin-Binding Aptamer Quadruplex Formation: AFM and Voltammetric Characterization

Victor Constantin Diculescu,[1] Ana-Maria Chiorcea-Paquim,[1] Ramon Eritja,[2] and Ana Maria Oliveira-Brett[1]

[1] *Departamento de Quimica, Faculdade de Ciências e Tecnologia, Universidade de Coimbra, 3004-535 Coimbra, Portugal*
[2] *Institute for Research in Biomedicine, IQAC-CSIC, CIBER-BBN Networking Centre on Bioengineering, Biomaterials and Nanomedicine, 08028 Barcelona, Spain*

Correspondence should be addressed to Ana Maria Oliveira-Brett, brett@ci.uc.pt

Received 15 January 2010; Accepted 29 March 2010

Academic Editor: Lea Spindler

The adsorption and the redox behaviour of thrombin-binding aptamer (TBA) and extended TBA (eTBA) were studied using atomic force microscopy and voltammetry at highly oriented pyrolytic graphite and glassy carbon. The different adsorption patterns and degree of surface coverage were correlated with the sequence base composition, presence/absence of K^+, and voltammetric behaviour of TBA and eTBA. In the presence of K^+, only a few single-stranded sequences present adsorption, while the majority of the molecules forms stable and rigid quadruplexes with no adsorption. Both TBA and eTBA are oxidized and the only anodic peak corresponds to guanine oxidation. Upon addition of K^+ ions, TBA and eTBA fold into a quadruplex, causing the decrease of guanine oxidation peak and occurrence of a new peak at a higher potential due to the oxidation of G-quartets. The higher oxidation potential of G-quartets is due to the greater difficulty of electron transfer from the inside of the quadruplex to the electrode surface than electron transfer from the more flexible single strands.

1. Introduction

Since it has been recognized that G-rich nucleic acid sequences can adopt intermolecular and intramolecular quadruplex structures stabilized by G-quartets [1], Scheme 1, there is substantial interest in the role of quadruplex formation, largely as a consequence of the identification of G-quadruplex-forming sequences in the genome (e.g., telomers, several oncogenes and aptamers) [2–4]. Despite the intensive studies on the role of G-quartet formation in vivo, there is considerable interest in the therapeutic potential of quadruplex oligodeoxynucleotides (ODNs).

Aptamers are nucleic acid sequences (DNA or RNA) selected in vitro from large combinatorial pools to bind to specific targets [5–7]. Aptamers exhibit a strong and specific binding affinity towards their targets and can be simply synthesized via cost-effective and readily automated routes [8, 9]. More important, the structure and conformation of aptamers can be rationally designed and tailor-made to be selectively responsive to various kinds of targets ranging from small molecules [9] to biological molecules [7, 10, 11] and even cells [12, 13]. Aptamers possess significant advantages over other recognition molecules, such as antibodies, due to their small size, chemical simplicity, and flexibility.

One of the most preeminent examples of the in vitro selection of DNA oligonucleotides for targeting a specific protein is the thrombin-binding aptamer (TBA), Scheme 2. Thrombin is a serine protease and a coagulation protein in the blood stream that has many effects in the coagulation mechanism. Activation of thrombin is crucial in physiological and pathological coagulation. Various rare diseases involving thrombin have been described. Blood from a ruptured cerebral aneurysm clots around a cerebral artery and releases thrombin, which can induce an acute and prolonged narrowing of the blood vessel, potentially resulting in cerebral ischemia and infarction (stroke). Because of its importance in anticlotting therapeutics, TBA has

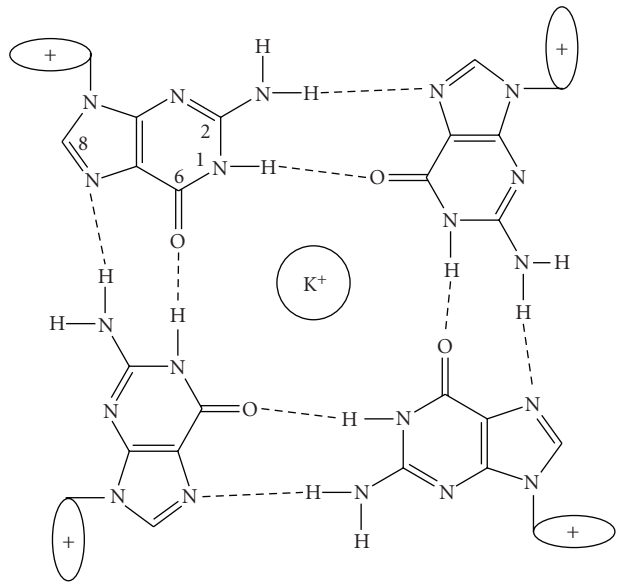

Scheme 1: Schematic representation of the G-quartet.

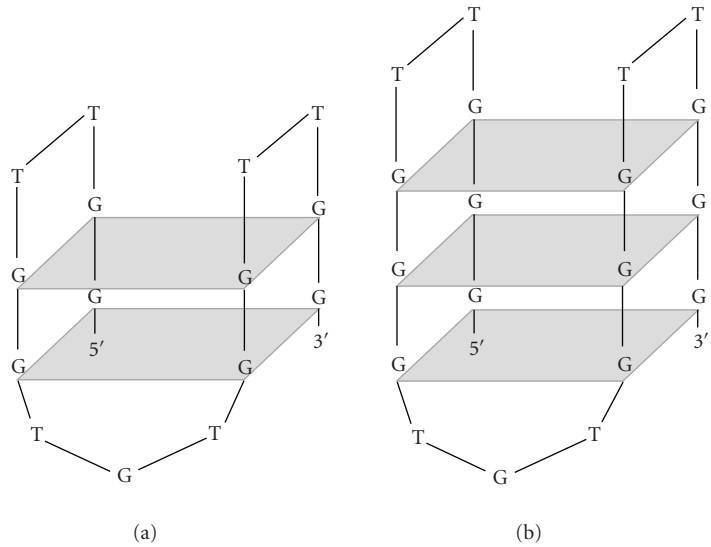

Scheme 2: Schematic representation of the antiparallel G-quadruplex structures of (a) TBA and (b) eTBA.

been studied extensively. It has been shown that in the presence of alkali metals [4, 7, 14], TBA forms an antiparallel intramolecular quadruplex consisting of two G-quartets connected by two TT loops and one TGT loop. TBA has also been used for development of electrochemical biosensors for the detection of thrombin [10]. However, no publication has shown the adsorption and voltammetric behaviour of these G-quartet forming ODNs.

The present paper is the first report of a voltammetric and atomic force microscopy (AFM) study of two different thrombin-binding aptamer sequences. The process of adsorption of TBA (5′-GGTTGGTGTGGTTGG-3′) and extended TBA (eTBA, 5′-GGGTTGGGTGTGGGTTGGG-3′) was studied on a highly oriented pyrolytic graphite (HOPG) electrode using acoustic AC mode AFM (AAC Mode AFM). The electrochemical oxidation of these TBA sequences has been also performed by differential pulse (DP) voltammetry using a glassy carbon (GC) electrode.

2. Experimental

2.1. Materials and Reagents. The ODN sequences TBA (5′-GGTTGGTGTGGTTGG-3′) and eTBA (5′-GGGTTG-GGTGTGGGTTGGG-3′), Scheme 2, were synthesized on an ABI 3400 DNA Synthesizer (Applied Biosystems, Foster City, CA, USA) using the 200-nmol scale synthesis cycle [7]. All

solutions were prepared using analytical grade reagents and purified water from a Millipore Milli-Q system (conductivity $\leq 0.1\,\mu S\,cm^{-1}$). Stock TBA and eTBA solutions were prepared in Milly Q water and kept at 4°C. Before each experiment, solutions of either TBA or eTBA were freshly prepared by dilution of the appropriate quantity in pH 7.0 0.1 M phosphate buffer (0.2 M Na_2HPO_4+ 0.2 M NaH_2PO_4).

Microvolumes were measured using EP-10 and EP-100 Plus Motorized Microliter Pippettes (Rainin Instrument Co. Inc., Woburn, USA). The pH measurements were carried out with a Crison micropH 2001 pH-meter with an Ingold combined glass electrode. All experiments were done at room temperature (25 ± 1°C).

2.2. Atomic Force Microscopy. HOPG, grade ZYB of dimensions $15 \times 15 \times 2\,mm^3$, from Advanced Ceramics Co., USA, was used as a substrate in the AFM study. The HOPG was freshly cleaved with adhesive tape prior to each experiment and imaged by AFM in order to establish its cleanliness.

AFM was performed in the AAC mode AFM, with a PicoScan controller from Agilent Technologies, Tempe, AZ, USA. All the AFM experiments were performed with a CS AFM S scanner with a scan range of 6 μm in x-y and 2 μm in z, from Agilent Technologies. AppNano type FORT of 225 μm length, $3.0\,N\,m^{-1}$ spring constants, and 47–76 kHz resonant frequencies in air (Applied NanoStructures, Inc., USA) were used. All AFM images were topographical and were taken with 256 samples/line × 256 lines and scan rates of 0.8–2.0 lines s^{-1}. When necessary, the AFM images were processed by flattening in order to remove the background slope and the contrast and brightness were adjusted.

2.3. Sample Preparation for AFM. The TBA and eTBA modified HOPG surfaces were obtained by spontaneous adsorption, by depositing 200 μL samples of $1\,\mu g\,mL^{-1}$ TBA or eTBA solutions in pH 7.0 0.1 M phosphate buffer onto the freshly cleaved HOPG surface, during 3 minutes. The excess of solution was gently cleaned with a jet of Millipore Milli-Q water, and the HOPG with adsorbed ODN molecules was then dried in a sterile atmosphere and imaged by AAC Mode AFM in air.

2.4. Voltammetric Parameters and Electrochemical Cells. Voltammetric experiments were carried out using a μAutolab running with GPES 4.9 software, Eco-Chemie, The Netherlands. Measurements were carried out using a GC(d = 1.5 mm) working electrode, a Pt wire counter electrode, and a Ag/AgCl as reference, in a 0.25 mL electrochemical cell. The experimental conditions for DP voltammetry were pulse amplitude 50 mV, pulse width 70 ms, scan rate $5\,mV\,s^{-1}$.

The GC electrode was polished using diamond spray (particle size 1 μm) before each experiment. After polishing, the electrode was rinsed thoroughly with Milli-Q water and placed in supporting electrolyte and various DP voltammograms were recorded until a steady state baseline voltammogram was obtained. This procedure ensured very reproducible experimental results.

2.5. Acquisition and Presentation of Voltammetric Data. The DP voltammograms were baseline-corrected using the moving average with a step window of 2 mV included in GPES version 4.9 software. This mathematical treatment improves the visualization and identification of peaks over the baseline without introducing any artefact, although the peak height is in some cases reduced (<10%) relative to that of the untreated curve. Nevertheless, this mathematical treatment of the original voltammograms was used in the presentation of all experimental voltammograms for a better and clearer identification of the peaks. The values for peak current presented in all graphs were determined from the original untreated voltammograms after subtraction of the baseline.

3. Results and Discussion

3.1. AFM Characterisation of Spontaneously Adsorbed TBA and eTBA. The capacity of TBA and eTBA molecules to interact and adsorb spontaneously on the HOPG electrode forming different morphological films was investigated by AFM in air. The spontaneous adsorption of the ODN sequences was obtained using concentrations of $1\,\mu g\,mL^{-1}$ TBA or eTBA in pH 7.0 0.1 M phosphate buffer as described in Section 2.3. The relationship between the degree of surface coverage with adsorbed molecules, the base composition in the ODN sequence and the presence/absence of K^+ cations will be discussed.

An atomically flat HOPG electrode was used as a substrate with less than 0.06 nm of root-mean-square (*r.m.s.*) roughness for a $1000 \times 1000\,nm^2$ surface area. The GC electrode used for the voltammetric characterisation was much rougher, with 2.10 nm *r.m.s.* roughness for the same surface area, therefore unsuitable for AFM surface characterisation. Furthermore, the experiments using GC and HOPG electrodes showed similar electrochemical behaviour.

AFM topographical images in air of the TBA modified HOPG electrode showed that the TBA adsorbs spontaneously onto HOPG, showing the formation of two different adsorbed structures: a thin and incomplete network film, Figure 1(a), and aggregates with spherical and rod-like shapes, marked with white arrows in the images, Figure 1(b). The network was composed of small molecules adsorbed side by side that formed close-packed "polymer-like" chains, with many pores, corresponding to the dark regions in the images, and exposed HOPG surface at the bottom of the pores, Figure 1(a). The measured thickness of the TBA layer was calculated from cross section analysis as being 0.8 ± 0.1 nm. The average height and standard deviation of the spherical aggregates was 1.9 ± 0.5 nm, Figure 1(b), higher than the values obtained for the TBA lattices.

Similar results were obtained for the eTBA molecules, which present four extra guanines in the base sequence. The AFM images in air also showed a densely packed 0.8 ± 0.1 nm height self-assembled network with looped arms, Figure 2(a), and small TBA fragments of 0.8 ± 0.1 nm height with embedded 1.5 ± 0.2 nm height aggregates (marked with white arrows), Figure 2(b).

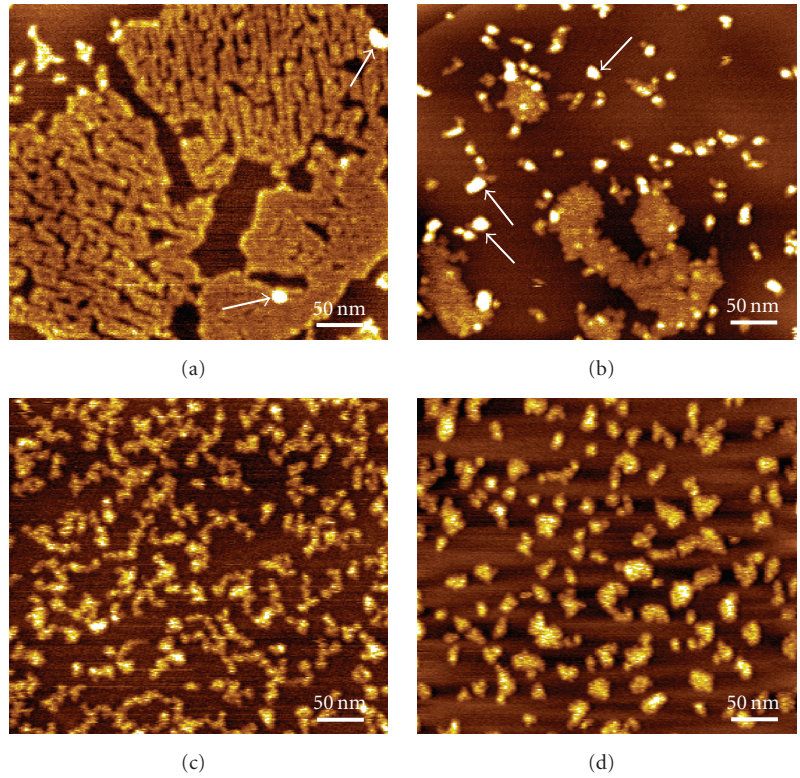

Figure 1: AFM topographical images in air of TBA molecules, immobilized onto HOPG by spontaneous adsorption during 3 minutes, from solutions of 1 μg mL^{-1} TBA in pH 7.0 0.1 M phosphate buffer: (a, b) in the absence and (c, d) in the presence of 100 mM K^+, after (c) 1 hour and (d) 24 hours of incubation.

The adsorption mechanism of the nucleic acid molecules onto HOPG is mainly driven by hydrophobic interactions [15], being strongly influenced by the hydrophobicity of the constituent nucleotides, the ODN molecular mass and the formation of secondary structures. As expected, the eTBA presents an increased adsorption onto HOPG when compared with TBA, due to an enhanced hydrophobic character given by the larger number of guanine bases, especially at the molecule extremities.

Additionally, G-rich ODN sequences that contain sections of guanines can form G-quadruplex structures comprised of stacked tetrads, each one of the tetrads formed by a planar association of four guanines by Hoogsteen hydrogen bonding. Therefore, the guanine bases that enter in the TBA and eTBA composition influence the ODN hydrophobicity directly, through the intrinsic hydrophobic character of the aromatic ring, and indirectly, by allowing the ODN sequences to establish quadruplex conformations. In this context, the interaction of the single-stranded molecules with HOPG is facilitated because they have the bases exposed to the solution and free to undergo hydrophobic interactions, when compared to the ODNs with quadruplex morphology that have the bases protected by the sugar-phosphate backbones. Indeed, the AFM images of the TBA and eTBA modified HOPG surfaces show the formation of 1.5–1.9 nm height spherical and rod-like shape aggregates due to the adsorption of ODNs presenting G-quartet configurations, as also observed for telomeric G-rich sequences on mica [16]. The adsorption of single-stranded molecules led to the formation of polymeric structures and films of approximately 0.8 nm height.

The stabilisation of the quadruplex structures requires the presence of metal ions, in particular alkali metals, and the order of preference is $K^+ > Na^+$. The ions are positioned in the interior channel that is formed at the centre of each G-quartet, coordinating the O6 atoms of the guanines. The AFM results previously described were obtained in the presence of Na^+ ions (pH 7.0 0.1 M phosphate buffer solutions). In order to establish how the presence of K^+ ions influences the formation and stabilisation of TBA and eTBA quadruplexes and therefore modifies their pattern of adsorption onto HOPG, the morphological characteristics of the HOPG modified by spontaneous adsorption from 1 μg mL^{-1} TBA or eTBA in pH 7.0 0.1 M phosphate buffer after incubation with 100 mM and 200 mM KCl during different periods of time, were also analysed.

AFM images of the TBA modified HOPG obtained after incubation of TBA with 100 mM K^+ during 1 hour showed tilted polymeric structures of 0.8 ± 0.2 nm height, Figure 1(c). A dramatically reduced adsorption was observed in the presence of K^+, when compared with the adsorption of TBA from solutions containing only Na^+ cations,

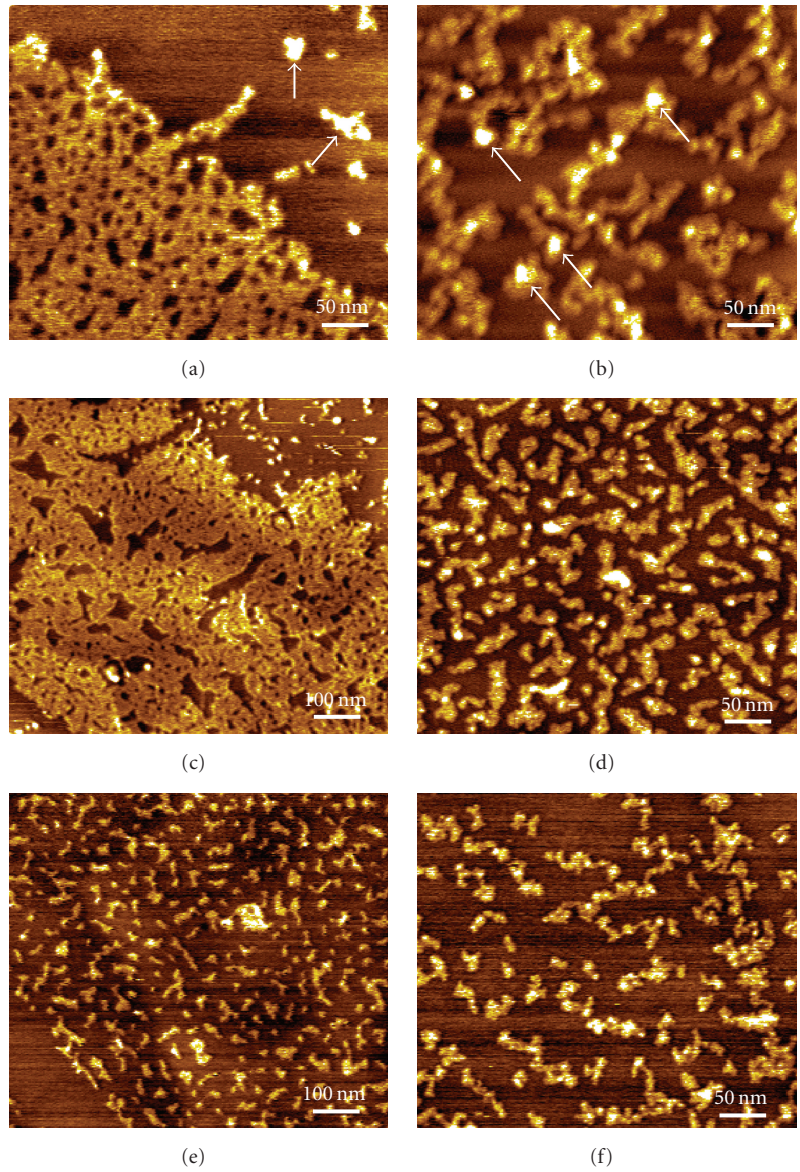

FIGURE 2: AFM topographical images in air of eTBA molecules, immobilized onto HOPG by spontaneous adsorption during 3 minutes, from solutions of 1 μg mL^{-1} eTBA in pH 7.0 0.1 M phosphate buffer: (a, b) in the absence and (c–f) in the presence of (c, d) 100 mM and (e, f) 200 mM K^+, after (c, e) 1 hour and (d, f) 24 hours of incubation.

Figures 1(a) and 1(b). The adsorption decreased further after 24 hours incubation with K^+ and the adsorbed TBA fragments presented heights of 0.9 ± 0.3 nm, Figure 1(d).

AFM images of the eTBA modified HOPG obtained from solutions of eTBA incubated with 100 mM K^+ during 1 hour, Figure 2(c), showed 0.8 ± 0.1 nm height network films and small spherical and rod-like shape aggregates, similar to what was obtained with eTBA in the presence of only Na^+, Figures 2(a) and 2(b). After 24 hours incubation in the presence of K^+ the HOPG coverage decreased significantly, Figure 2(d), although the observed 0.8 ± 0.1 nm eTBA lattice still presented small embedded 1.5 nm height aggregates, corresponding to molecules in G-quartet configurations. AFM images of the eTBA modified HOPG obtained after incubation with 200 mM K^+ during 1 hour, Figure 2(e), and 24 hours, Figure 2(f), showed, as expected, an even more reduced adsorption, and the fragments observed in the images presented heights of 0.8 ± 0.1 nm, corresponding only to the adsorption of single-stranded molecules.

AFM images demonstrated that, after the interaction with K^+ ions during long incubation times, the adsorption pattern of both TBA and eTBA molecules corresponded only to the spontaneous adsorption of a small number of single-stranded molecules present in solution, while no quadruplex TBA/eTBA was observed. This is due to the fact that, in the presence of K^+ cations, TBA and eTBA form very stable and rigid intramolecular quadruplex configurations, which prevent the interaction of the hydrophobic bases with

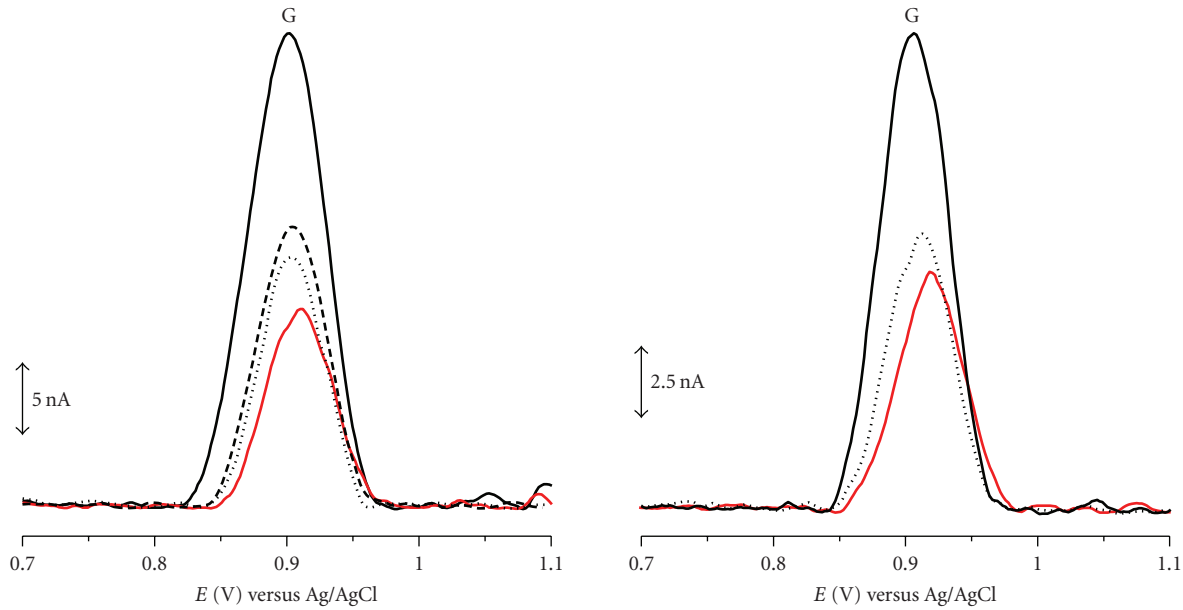

Figure 3: Baseline corrected DPV obtained with the GC electrode in a solution of 1 μg mL^{-1} TBA in pH 7.0 0.1 M phosphate buffer: (a) (solid line) in the absence and in the presence of 100 mM KCl after (dashed line) 0 hour, (dotted line) 1 hour and (red line) 24 hours of incubation and (b) in the presence of (solid line) 50, (dotted line) 100 and (red line) 200 mM KCl after 24 hours of incubation.

the HOPG. On the contrary, the presence of only Na^+ cations from the solutions of TBA/eTBA in pH 7.0 0.1 M phosphate buffer led to the formation of less stable quadruplex TBA/eTBA morphologies that are locally destabilised by the HOPG hydrophobic surface, inducing their consequent adsorption.

3.2. Voltammetric Characterisation of TBA and eTBA. DP voltammograms were recorded in solutions containing 1 μg mL^{-1} TBA in pH 7.0 0.1 M phosphate buffer before and after incubation with 100 mM K^+ ions during different periods of time, Figure 3(a). Between measurements, the GC electrode surface was always polished in order to ensure a clean surface to avoid possible problems from the adsorption of TBA. On the voltammograms obtained in the solution containing only TBA, one main anodic peak G occurred at E_{pa} = +0.91 V. This peak is due to the oxidation of guanine residues, since the oxidation of thymine occurs at much higher positive potential, near the potential of oxygen evolution and therefore it is more difficult to detect [17]. Upon addition of K^+ ions, a decrease of the guanine oxidation peak occurred in a time-dependent manner reaching constant currents after 24 hours of incubation, Figure 3(a). This process is related to a decrease of the concentration of free/uncomplexed guanine residues available for oxidation and can be explained considering the TBA quadruplex structure in the presence of K^+ ions. Upon the formation of G-quartets, the guanine electroactive centers are hidden inside the rigid quadruplex being unable to reach the GC electrode surface and consequently unavailable for electrochemical oxidation. Thus, the occurrence of a smaller guanine oxidation peak with increasing incubation time is attributed to guanine molecules that were not involved in the formation of G-quartets.

A similar experiment was carried out in which 1 μg mL^{-1} TBA in pH 7.0 0.1 M phosphate buffer was incubated during 24 hours with different concentrations of K^+ ions. The DP voltammograms recorded in these solutions, Figure 3(b), showed a decrease of the guanine oxidation peak dependent on the K^+ ions concentration, relative to the guanine oxidation peak obtained in a solution containing only TBA. Thus, by increasing the K^+ ions concentration, the guanine oxidation peak recorded after 24 hours of incubation gradually decreased and its potential become more positive (~10 mV) in agreement with a greater difficulty for the transition of electrons after the formation of more complex structures.

DP voltammograms were recorded in solutions containing 1 μg mL^{-1} eTBA in pH 7.0 0.1 M phosphate buffer before and after incubation with 100 mM K^+ ions during different periods of time, Figure 4(a). Between measurements, the GC electrode surface was always polished in order to ensure a clean surface to avoid possible problems from the adsorption of eTBA. The voltammograms obtained in the solution containing only eTBA, showed only the guanine oxidation peak G, at E_{pa} = +0.91 V. DP voltammograms were also recorded after 0 hour, 1 hour and 24 hours of incubation. It was observed that, upon addition of K^+ ions, a decrease of guanine oxidation peak occurred in a time-dependent manner reaching constant currents after 24 hours of incubation, Figure 4(a). As in the case of TBA, the occurrence of a smaller guanine oxidation peak with increasing incubation time is attributed to guanine molecules that were not involved in the formation of G-quartets.

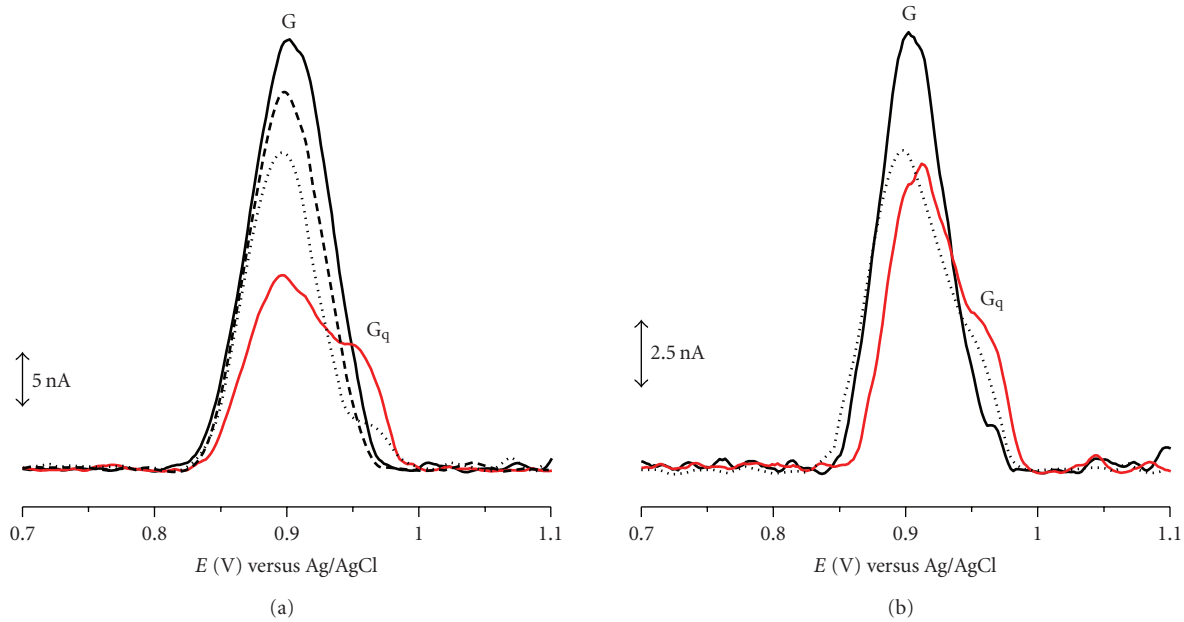

FIGURE 4: Baseline corrected DPV obtained with the GC electrode in a solution of 1 μg mL^{-1} eTBA in pH 7.0 0.1 M phosphate buffer: (a) (solid line) in the absence and in the presence of 100 mM KCl after (dashed line) 0 hour, (dotted line) 1 hour and (red line) 24 hours of incubation and (b) in the presence of (solid line) 50, (dotted line) 100 and (red line) 200 mM KCl after 24 hours of incubation.

On the other hand, on the voltammograms obtained after 1 hour of incubation of eTBA with K^+ ions, a new small peak G_q appeared at E_{pa} = +0.97 V and its current increased with incubation time reaching constant values after 24 hours of incubation, Figure 4(a). This new peak is attributed to the oxidation of G-quartets and its higher potential value relative to guanine itself can be explained considering the greater difficulty for the transition of electrons from the inside of the rigid quadruplex to the GC electrode surface than from the more flexible form of single stranded eTBA where guanine residues can reach the surface leading to higher peak currents [17]. Although this peak did not appear during the experiments with TBA, this can be due to the formation of G-quartets below the detection limit of the technique. On the contrary, in the case of eTBA a higher number of guanine residues are available and thus a higher number of G-quartets are expected, which leads to the occurrence of larger oxidation peaks.

In another experiment, 1 μg mL^{-1} eTBA in pH 7.0 0.1 M phosphate buffer was incubated during 24 hours with different concentrations of K^+ ions, Figure 4(b). The DP voltammograms recorded in these conditions showed the decrease of guanine peak current G with increasing K^+ concentration up to 200 mM where it reached a constant value. On the other hand, peak G_q occurred with a small current after incubation with low K^+ ions and also increased with increasing K^+ concentration.

4. Conclusions

The redox behaviour and adsorption process of two thrombin-binding aptamer sequences were studied at room temperature, using AFM and voltammetry at HOPG and GC electrodes, in the presence/absence of Na^+ and K^+ cations.

Due to the formation of very stable and rigid intramolecular quadruplex configurations in the presence of K^+ cations, both TBA and eTBA adsorb less onto HOPG, compared to the adsorption in the presence of only Na^+ cations present in the pH 7.0 0.1 M phosphate buffer. This is due to the fact that a larger number of intramolecular quadruplexes is formed, which were more stable due to the incorporation of K^+, which prevents their hydrophobic interaction with HOPG. On the contrary, the presence of only Na^+ cations led to the formation of less stable quadruplexes that are locally destabilised by the HOPG hydrophobic surface, inducing their adsorption together with single-stranded sequences.

Voltammetric studies showed that both TBA and eTBA are oxidized at GC electrode and the only electrochemical signal is due to the oxidation of guanine residues. Upon addition of K^+ ions, both TBA and eTBA folded into G-quadruplex structures and this process was observed by the decreasing of the guanine oxidation peak and the occurrence of a new peak at higher potential values due to the oxidation of G-quartets. The difference in the oxidation potential of guanine and G-quartets is attributed to the difficulty of the transition of electrons from the inside of the rigid quadruplex to the GC electrode surface than from the more flexible form of single-stranded ODNs whose guanine residues can reach the surface leading to higher peak currents.

Acknowledgments

Financial support from Fundação para a Ciência e Tecnologia (FCT), Post-Doctoral Grant SFRH/BPD/36110/2007 (V. C.

Diculescu), projects PTDC/QUI/65255/2006 and PTDC/QUI/098562/2008, POCI 2010 (cofinanced by the European Community Fund FEDER), CEMUC-R (Research Unit 285), and COST Action MP0802 (Self-assembled guanosine structures for molecular electronic devices (G4-net)) is gratefully acknowledged.

References

[1] V. Dapić, V. Abdomerović, R. Marrington, et al., "Biophysical and biological properties of quadruplex oligodeoxyribonucleotides," *Nucleic Acids Research*, vol. 31, no. 8, pp. 2097–2107, 2003.

[2] L. Oganesian and T. M. Bryan, "Physiological relevance of telomeric G-quadruplex formation: a potential drug target," *BioEssays*, vol. 29, no. 2, pp. 155–165, 2007.

[3] S. Cogoi and L. E. Xodo, "G-quadruplex formation within the promoter of the KRAS proto-oncogene and its effect on transcription," *Nucleic Acids Research*, vol. 34, no. 9, pp. 2536–2549, 2006.

[4] R. F. Macaya, P. Schultze, F. W. Smith, J. A. Roe, and J. Feigon, "Thrombin-binding DNA aptamer forms a unimolecular quadruplex structure in solution," *Proceedings of the National Academy of Sciences of the United States of America*, vol. 90, no. 8, pp. 3745–3749, 1993.

[5] A. D. Ellington and J. W. Szostak, "In vitro selection of RNA molecules that bind specific ligands," *Nature*, vol. 346, no. 6287, pp. 818–822, 1990.

[6] M. K. Beissenhirtz and I. Willner, "DNA-based machines," *Organic and Biomolecular Chemistry*, vol. 4, no. 18, pp. 3392–3401, 2006.

[7] M. del Toro, R. Gargallo, R. Eritja, and J. Jaumot, "Study of the interaction between the G-quadruplex-forming thrombin-binding aptamer and the porphyrin 5,10,15,20-tetrakis-(N-methyl-4-pyridyl)-21,23H-porphyrin tetratosylate," *Analytical Biochemistry*, vol. 379, no. 1, pp. 8–15, 2008.

[8] Z. Tang, D. Shangguan, K. Wang, et al., "Selection of aptamers for molecular recognition and characterization of cancer cells," *Analytical Chemistry*, vol. 79, no. 13, pp. 4900–4907, 2007.

[9] B. Chakraborty, Z. Jiang, Y. Li, and H.-Z. Yu, "Rational design and performance testing of aptamer-based electrochemical biosensors for adenosine," *Journal of Electroanalytical Chemistry*, vol. 635, no. 2, pp. 75–82, 2009.

[10] E. Torres-Chavolla and E. C. Alocilja, "Aptasensors for detection of microbial and viral pathogens," *Biosensors and Bioelectronics*, vol. 24, no. 11, pp. 3175–3182, 2009.

[11] A. Numnuam, K. Y. Chumbimuni-Torres, Y. Xiang, et al., "Aptamer-based potentiometric measurements of proteins using ion-selective microelectrodes," *Analytical Chemistry*, vol. 80, no. 3, pp. 707–712, 2008.

[12] C. Wang, M. Zhang, G. Yang, et al., "Single-stranded DNA aptamers that bind differentiated but not parental cells: subtractive systematic evolution of ligands by exponential enrichment," *Journal of Biotechnology*, vol. 102, no. 1, pp. 15–22, 2003.

[13] K. N. Morris, K. B. Jensen, C. M. Julin, M. Weil, and L. Gold, "High affinity ligands from in vitro selection: complex targets," *Proceedings of the National Academy of Sciences of the United States of America*, vol. 95, no. 6, pp. 2902–2907, 1998.

[14] J. A. Kelly, J. Feigon, and T. O. Yeates, "Reconciliation of the X-ray and NMR structures of the thrombin-binding aptamer d(GGTTGGTGTGGTTGG)," *Journal of Molecular Biology*, vol. 256, no. 3, pp. 417–422, 1996.

[15] A.-M. Chiorcea Paquim, T. S. Oretskaya, and A. M. Oliveira Brett, "Adsorption of synthetic homo- and hetero-oligodeoxynucleotides onto highly oriented pyrolytic graphite: atomic force microscopy characterization," *Biophysical Chemistry*, vol. 121, no. 2, pp. 131–141, 2006.

[16] T. C. Marsh, J. Vesenka, and E. Henderson, "A new DNA nanostructure, the G-wire, imaged by scanning probe microscopy," *Nucleic Acids Research*, vol. 23, no. 4, pp. 696–700, 1995.

[17] A. M. Oliveira Brett, V. C. Diculescu, A. M. Chiorcea-Paquim, and S. H. P. Serrano, "Chapter 20 DNA-electrochemical biosensors for investigating DNA damage," *Comprehensive Analytical Chemistry*, vol. 49, pp. 413–437, 2007.

SAGE-Hindawi Access to Research
Journal of Nucleic Acids
Volume 2010, Article ID 564946, 6 pages
doi:10.4061/2010/564946

Review Article

A Toolbox for Predicting G-Quadruplex Formation and Stability

Han Min Wong,[1] Oliver Stegle,[2] Simon Rodgers,[3] and Julian Leon Huppert[1]

[1] *Cavendish Laboratory, University of Cambridge, JJ Thomson Avenue, Cambridge CB3 0HE, UK*
[2] *Max-Planck-Institutes Tübingen, Spemanstraße 38, 72076 Tübingen, Germany*
[3] *Thaze Ltd, 121 Mowbray Road, Cambridge CB1 7SP, UK*

Correspondence should be addressed to Julian Leon Huppert, jlh29@cam.ac.uk

Received 1 February 2010; Accepted 24 March 2010

Academic Editor: Jean Louis Mergny

G-quadruplexes are four stranded nucleic acid structures formed around a core of guanines, arranged in squares with mutual hydrogen bonding. Many of these structures are highly thermally stable, especially in the presence of monovalent cations, such as those found under physiological conditions. Understanding of their physiological roles is expanding rapidly, and they have been implicated in regulating gene transcription and translation among other functions. We have built a community-focused website to act as a repository for the information that is now being developed. At its core, this site has a detailed database (QuadDB) of predicted G-quadruplexes in the human and other genomes, together with the predictive algorithm used to identify them. We also provide a QuadPredict server, which predicts thermal stability and acts as a repository for experimental data from all researchers. There are also a number of other data sources with computational predictions. We anticipate that the wide availability of this information will be of use both to researchers already active in this exciting field and to those who wish to investigate a particular gene hypothesis.

1. Introduction

It was observed in 1910 [1] that a sufficiently high concentration of guanosine could form a gel, unlike the other nucleobases, and in 1962 [2] it was discovered that four guanosine can self-assemble to form a hydrogen-bonded square, with bonds between the N_1–O_6 and N_2–N_7 positions. This structure is known as a G-tetrad or G-quartet. Like any nucleobase, there is also a strong propensity for these structures to stack on each other via π-π interactions, forming four-stranded helices called G-quadruplexes, with the phosphate backbone perpendicular to the plane of the G-quartets. The four strands may be from separate molecules, or they may be from only 2 or 1, with loops joining them together [3–7].

They form with great thermal stability, [8] and have been found experimentally to form from genomic sequences in critical regions such as telomeres, gene promoters and UTRs, [9, 10] and to have physiological effects in each of these regions. In telomeres, their formation reduces the activity of telomerase, the upregulation of which has been associated with 85% of cancers, and has led to much pharmaceutical interest [11]. G-quadruplexes in gene promoters, such as the oncogenes c-myc and c-kit, [12, 13] have been shown to control transcriptional activity in vitro, although interestingly their formation can lead to the increase or decrease of activity in different systems. It has been shown that G-quadruplex formation in the 5′ UTR can decrease translational activity, [14] and there have been suggestions of other physiological effects. A wide variety of proteins have been found to interact specifically with them, [15] and they have been shown experimentally to form in vivo [16–18].

G-quadruplexes have also been employed as biosensors (e.g., for thrombin[19]) and in other nanotechnological applications (e.g., [20, 21]). Some of these uses are reviewed in [5].

In parallel with the experimental work being developed, computational techniques have also been developed to predict which sequences will form G-quadruplexes [22–24]. There are a variety of different algorithmic rules that can be used to predict which sequences can form G-quadruplexes, [25, 26] although some are more widely used and accepted.

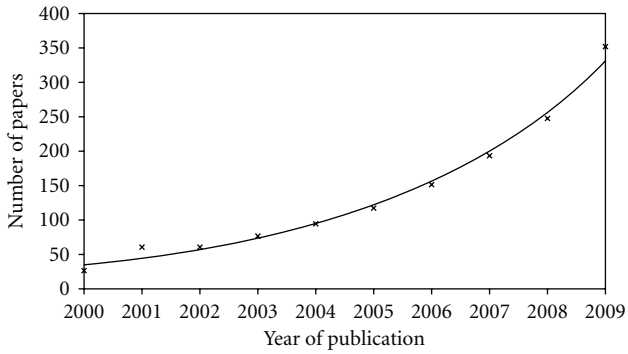

Figure 1: Annual publication rate in the G-quadruplex field in the past decade. Data obtained from the Web of Knowledge, searching for the term "G-quadruplex" or "G-tetraplex." The solid line is an exponential fit to the data.

There is not sufficient evidence for any of them to be held as absolutely true, and it is only recently that any work has been done to try to predict relative stabilities of possible G-quadruplex structures, rather than just whether they could form or not.

Despite this limitation, computational methods have led to a number of discoveries, including the observations that G-quadruplexes are relatively rare in the human genome, but more prevalent than expected in gene promoters [27]. Some of the computational discoveries have been recently reviewed [25, 26].

The field as a whole has grown very significantly in recent times, with a roughly exponential rise in publications (see Figure 1), including over 350 in 2009. A dedicated book has been produced, [28] together with special issues of some journals focused on this topic, and some databases on particular aspects of G-quadruplexes. A few G-quadruplex based drugs have also entered clinical trials. A series of International Conferences has been initiated, the first two hosted in Louisville, KY [29, 30]. At the first of these, it was suggested that a central and coherent website to store and provide data related to G-quadruplexes should be produced, and we volunteered to provide such a repository [29], hosted at the URL http://www.quadruplex.org/.

Here, we describe the features available at that website, and in particular the core databases to describe predicted G-quadruplexes, and a new tool to estimate the thermal stability of these structures computationally. We also describe the other online sources of predictive data for G-quadruplexes, so that researchers may chose the most appropriate tool for their work.

2. QuadDB—A Database of G-Quadruplex Predictions

The core quadruplex database (QuadDB, http://www.quadruplex.org/?view=quadbase) provides both static and searchable data for researchers on computationally predicted G-quadruplexes (Putative Quadruplex Sequences, PQS). These have been generated as previously described [22], using our favoured predictive algorithm, which identifies sequences on either strand of the form ($G_{3+}N_{1-7}G_{3+}N_{1-7}G_{3+}N_{1-7}G_{3+}$). This has been shown experimentally to be a good predictor of in vitro G-quadruplex formation [31]. It aims to identify specific G-quadruplexes that may form, providing a testable in vitro hypothesis that can be tested using simple biophysical methods.

2.1. Quadparser. For any researcher interested in identifying PQS in specific sequences, we provide the *quadparser* program pre-compiled for MS Windows and Mac OS X with detailed instructions. The program is customisable, so that different patterns can be searched for. Different loop length constraints, G-tract lengths and so forth may all be set, so that the algorithm can be adjusted to fit with the particular context desired. *Quadparser* has a variety of output styles for different uses, and reads sequence data in FASTA format.

2.2. Data Search. The Data search section allows a researcher to identify any PQS in gene promoters (defined as the 1 kb upstream of the TSS) or UTRs for their gene of interest. The genes may be identified by ensembl ID, HGNC code or description. The output provides full details of the gene, including genomic parameters, and the location and sequence of PQS in the appropriate regions of every transcript of the gene. Links are also provided to Ensembl so the PQS may be seen in context. Figure 2 displays the output when searching the human genome for PQS in the promoter or UTRs of c-kit (HGNC nomenclature KIT). Currently, searches may be performed against the human, chimpanzee and mouse genomes.

2.3. Data Download. As a convenient alternative to gene-by-gene searches or using the quadparser program, we also provide a downloadable listing of every PQS identified in various genomes. We currently offer this data for human (builds 34, 35 and 36 for back compatibility), chimpanzee (2.1), mouse (37), rat (3.4), dog (2), chicken (2), zebrafish (7), fruitfly (5.4), roundworm (180) and yeast (1.01) genomes. In each case the data provides a genomic coordinates for each PQS, together with the strand, sequence and a unique identifier. Data may be taken altogether or by chromosome.

3. Quadpredict—Predicting G-Quadruplex Stability

The thermal stability of G-quadruplexes varies with the concentration of monovalent cations, specifically Na^+ and K^+. However, even for fixed concentrations, the exact details of the sequence, and hence the structure formed, make a very large difference. G-quadruplexes can vary from those which are too unstable to form at 5°C to those which will resist temperatures above 95°C [31]. It is therefore necessary not just to predict which sequences can form G-quadruplexes at all, but also the stability with which such sequences can form. Such experiments are relatively easy to perform, and have led to a series of studies of different aspects of the relationship

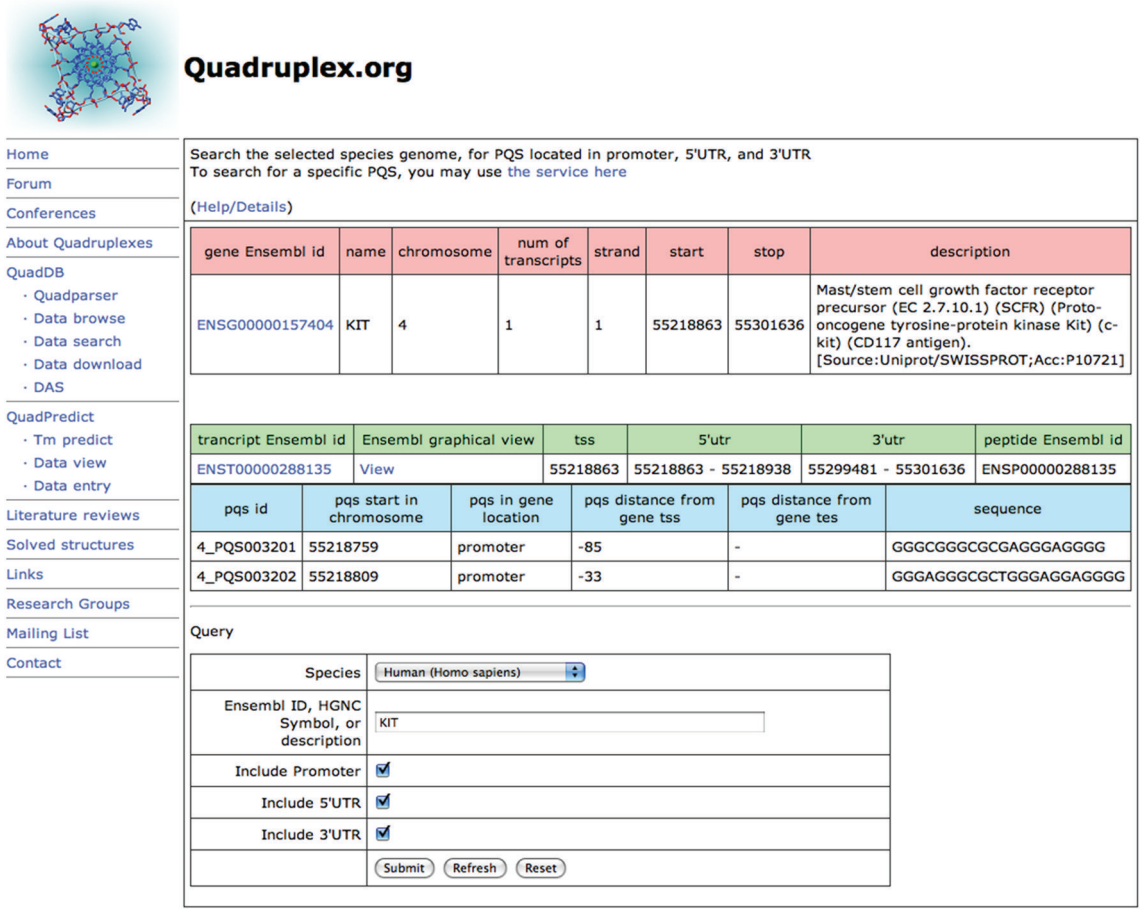

Figure 2: Sample output from the data search component of Quadbase. The search query is shown at the bottom of the figure.

between sequence and stability [31–34]. However, this does not enable prediction of unmeasured sequences, forcing researchers to make informed guesses as to the stability of novel sequences.

We recently developed [35] a Bayesian learning algorithm that is capable of making accurate predictions of thermal stability for new sequences, having been trained on a collection of measured sequences. Full details of the methodology and the parameters considered are available elsewhere [35]. We provide an interface to this system at http://www.quadruplex.org/?view=quadpredict, enabling researchers to make easy predictions of melting temperatures under various conditions for any desired sequence. Figure 3 gives an example of such predictions.

One feature of the Bayesian inference we use is that in addition to predictions of the melting temperature, we also provide uncertainties in the values for each sequence. In general, the uncertainty increases for sequences that are highly unlike those in our training set. This therefore enables researchers to decide rationally how much faith to place in a particular prediction.

We intend to develop the training data further, and have already employed a rational active learning protocol to collect more data and reduce the uncertainties below that originally presented. We will continue to do this, and also provide an opportunity for researchers to contribute their own data, so that the Bayesian inference can be increasingly accurate. We hope that depositing data publicly may become a standard requirement for publication of G-quadruplex thermal data.

We allow researchers to discover whether particular sequences they are interested in are already in our database of measurements, with information about exactly how such an experiment was performed. We hope that these facilities will prove useful to all those working in this field. As well as those interested in biological aspects of G-quadruplexes, we feel this facility may be particularly helpful for those working in nanotechnology or materials science, providing them with a method of rationally selecting G-quadruplex-forming oligonucleotides.

4. Other G-Quadruplex Computational Tools

There are a number of other tools that may be used to predict the existence of G-quadruplexes in DNA, and links to these are provided from http://www.quadruplex.org/. Bagga and coworkers use a similar algorithm to *quadparser* called

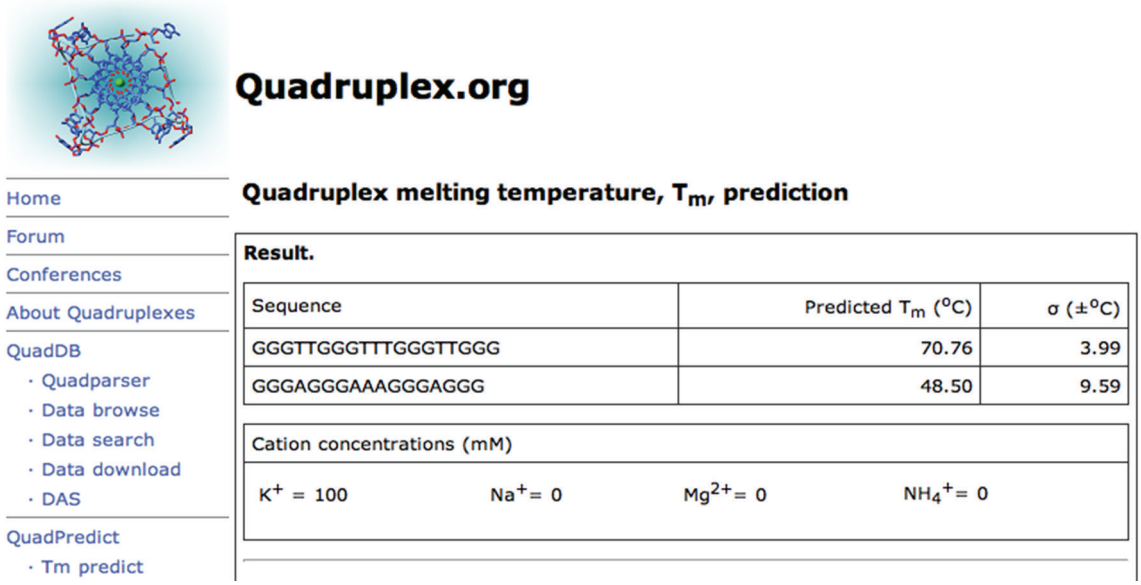

Figure 3: Sample predictions from QuadPredict, using Bayesian inference to calculate predicted melting temperatures together with predicted uncertainties.

QGRS mapper [36]. It has different default parameters, in particular looking at sequences with fewer consecutive guanines and longer loops, but essentially looks for much the same sequences. Interestingly, it includes a scoring parameter for different possible G-quadruplexes that can be formed. Although this is loosely based on empiric evidence, it is not clear how the "G-score" produced, which ranges up to a maximum of 105, relates to stability. To the best of our knowledge, no empiric tests have been performed testing the validity of the G-score even as a ranking list, but it is still a useful formulation of established rules of thumb. As well as the QGRS mapper, which also provides the facility to search by genes, they also provide specialised databases, GRSDB2 and GRS_UTRdb, [37] for searching pre-mRNAs and UTR sequences.

Maiti and coworkers offer a site called Quadfinder, [38] which implements essentially the same algorithm as *quadparser*. (At the time of writing it does not appear to be functioning.) At the same institute, Chowdhury and coworkers have a site called QuadBase, [39] again using essentially the same algorithm. They focus on cross-species analysis, offering an ortholog analysis for finding conserved G-quadruplexes, across either prokaryotes (ProQuad) (and see [40]) or eukaryotes (EuQuad). It should be noted that the conservation required is by presence, and no sequence comparison is performed.

Lastly in this category is the Greglist database of potential G-quadruplex regulated genes, which lists all human genes that have a G-quadruplex in the 1 kb region upstream of the transcription start site. The *quadparser* algorithm is used to predict these sequences [41].

A completely different approach to G-quadruplex prediction is taken by the Maizels lab [42, 43]. Whereas other methods aim to predict specific G-quadruplex sequences, largely driven by the desire of structural biologists to have structures to study, and by the desire of medicinal chemists to have a defined form to target, the G4 calculator from Eddy and Maizels accepts that many of these structures are highly polymorphic in vivo. As a result, they do not aim to predict individual structures but look at the density of sequences likely to lead to G-quadruplex structures. Given that this is an entirely orthogonal approach, it is striking that in many cases, particularly working on the gene functions that are likely to be regulated by G-quadruplexes, very similar conclusions arise from using this approach as the *quadparser* model. We strongly recommend that for any large-scale genomic studies, both approaches are used to corroborate the results found.

5. Conclusions

Computational methods have been of great use in understanding the role that G-quadruplexes may play in biology, unveiling their function in gene promoters [27, 42] and in regulating translation [44]. They have also revealed that stable G-quadruplexes are generally located in nucleosome-free regions [45]. Stability predictions have been used to develop experimental methods to directly visualise G-quadruplexes using AFM [46]. We anticipate that greater availability of ever more reliable tools will both improve the quality of informatic research in this area and make it increasingly easy for experimentalists to access computational results.

Acknowledgment

The fourth author is a Research Councils UK Academic Fellow. This work was supported by the Isaac Newton Trust.

References

[1] I. Bang, "Untersuchungen über die Guanylsäre," *Biochemisce Zeitschrift*, vol. 26, pp. 293–311, 1910.

[2] M. Gellert, M. N. Lipsett, and D. R. Davies, "Helix formation by guanylic acid," *Proceedings of the National Academy of Sciences of the United States of America*, vol. 48, pp. 2013–2018, 1962.

[3] T. Simonsson, "G-quadruplex DNA structures—variations on a theme," *Biological Chemistry*, vol. 382, no. 4, pp. 621–628, 2001.

[4] D. Sen and W. Gilbert, "Guanine quartet structures," *Methods in Enzymology*, vol. 211, pp. 191–199, 1992.

[5] J. T. Davis, "G-Quartets 40 Years Later: from 5′-GMP to molecular biology and supramolecular chemistry," *Angewandte Chemie—International Edition*, vol. 43, no. 6, pp. 668–698, 2004.

[6] J. L. Huppert, "Four-stranded nucleic acids: structure, function and targeting of G-quadruplexes," *Chemical Society Reviews*, vol. 37, no. 7, pp. 1375–1384, 2008.

[7] S. Burge, G. N. Parkinson, P. Hazel, A. K. Todd, and S. Neidle, "Quadruplex DNA: sequence, topology and structure," *Nucleic Acids Research*, vol. 34, no. 19, pp. 5402–5415, 2006.

[8] J.-L. Mergny, A.-T. Phan, and L. Lacroix, "Following G-quartet formation by UV-spectroscopy," *FEBS Letters*, vol. 435, no. 1, pp. 74–78, 1998.

[9] D. J. Patel, A. T. Phan, and V. Kuryavyi, "Human telomere, oncogenic promoter and 5′-UTR G-quadruplexes: diverse higher order DNA and RNA targets for cancer therapeutics," *Nucleic Acids Research*, vol. 35, no. 22, pp. 7429–7455, 2007.

[10] J. L. Huppert, "Four-stranded DNA: cancer, gene regulation and drug development," *Philosophical transactions. Series A*, vol. 365, no. 1861, pp. 2969–2984, 2007.

[11] L. Oganesian and T. M. Bryan, "Physiological relevance of telomeric G-quadruplex formation: a potential drug target," *BioEssays*, vol. 29, no. 2, pp. 155–165, 2007.

[12] S. Rankin, A. P. Reszka, J. Huppert, et al., "Putative DNA quadruplex formation within the human c-*kit* oncogene," *Journal of the American Chemical Society*, vol. 127, no. 30, pp. 10584–10589, 2005.

[13] H. Fernando, A. P. Reszka, J. Huppert, et al., "A conserved quadruplex motif located in a transcription activation site of the human c-kit oncogene," *Biochemistry*, vol. 45, no. 25, pp. 7854–7860, 2006.

[14] S. Kumari, A. Bugaut, J. L. Huppert, and S. Balasubramanian, "An RNA G-quadruplex in the 5′ UTR of the NRAS proto-oncogene modulates translation," *Nature Chemical Biology*, vol. 3, no. 4, pp. 218–221, 2007.

[15] M. Fry, "Tetraplex DNA and its interacting proteins," *Frontiers in Bioscience*, vol. 12, pp. 4336–4351, 2007.

[16] C. Schaffitzel, I. Berger, J. Postberg, J. Hanes, H. J. Lipps, and A. Plückthun, "In vitro generated antibodies specific for telomeric guanine-quadruplex DNA react with Stylonychia lemnae macronuclei," *Proceedings of the National Academy of Sciences of the United States of America*, vol. 98, no. 15, pp. 8572–8577, 2001.

[17] K. Paeschke, T. Simonsson, J. Postberg, D. Rhodes, and H. J. Lipps, "Telomere end-binding proteins control the formation of G-quadruplex DNA structures in vivo," *Nature Structural and Molecular Biology*, vol. 12, no. 10, pp. 847–854, 2005.

[18] M. L. Duquette, P. Handa, J. A. Vincent, A. F. Taylor, and N. Maizels, "Intracellular transcription of G-rich DNAs induces formation of G-loops, novel structures containing G4 DNA," *Genes and Development*, vol. 18, no. 13, pp. 1618–1629, 2004.

[19] K. Y. Wang, S. McCurdy, R. G. Shea, S. Swaminathan, and P. H. Bolton, "A DNA aptamer which binds to and inhibits thrombin exhibits a new structural motif for DNA," *Biochemistry*, vol. 32, no. 8, pp. 1899–1904, 1993.

[20] T. C. Marsh, J. Vesenka, and E. Henderson, "A new DNA nanostructure, the G-wire, imaged by scanning probe microscopy," *Nucleic Acids Research*, vol. 23, no. 4, pp. 696–700, 1995.

[21] M. Inoue, D. Miyoshi, and N. Sugimoto, "Development of molecular logic gates using the structural switch of telomere DNAs," *Nucleic Acids Symposium Series*, no. 50, pp. 315–316, 2006.

[22] J. L. Huppert and S. Balasubramanian, "Prevalence of quadruplexes in the human genome," *Nucleic Acids Research*, vol. 33, no. 9, pp. 2908–2916, 2005.

[23] A. K. Todd, M. Johnston, and S. Neidle, "Highly prevalent putative quadruplex sequence motifs in human DNA," *Nucleic Acids Research*, vol. 33, no. 9, pp. 2901–2907, 2005.

[24] L. D'Antonio and P. Bagga, "Computational methods for predicting intramolecular G-quadruplexes in nucleotide sequences," in *Proceedings of the IEEE Computational Systems Bioinformatics Conference (CSB '04)*, pp. 590–591, 2004.

[25] J. L. Huppert, "Hunting G-quadruplexes," *Biochimie*, vol. 90, no. 8, pp. 1140–1148, 2008.

[26] A. K. Todd, "Bioinformatics approaches to quadruplex sequence location," *Methods*, vol. 43, no. 4, pp. 246–251, 2007.

[27] J. L. Huppert and S. Balasubramanian, "G-quadruplexes in promoters throughout the human genome," *Nucleic Acids Research*, vol. 35, no. 2, pp. 406–413, 2007.

[28] S. Neidle and S. Balasubramanian, *Quadruplex Nucleic Acids*, RSC Publishing, Cambridge, UK, 2006.

[29] P. Bates, J.-L. Mergny, and D. Yang, "Quartets in G-major. The first international meeting on quadruplex DNA," *EMBO Reports*, vol. 8, no. 11, pp. 1003–1010, 2007.

[30] W. D. Wilson and H. Sugiyama, "First international meeting on quadruplex DNA," *ACS Chemical Biology*, vol. 2, no. 9, pp. 589–594, 2007.

[31] P. Hazel, J. Huppert, S. Balasubramanian, and S. Neidle, "Loop-length-dependent folding of G-quadruplexes," *Journal of the American Chemical Society*, vol. 126, no. 50, pp. 16405–16415, 2004.

[32] A. Risitano and K. R. Fox, "Influence of loop size on the stability of intramolecular DNA quadruplexes," *Nucleic Acids Research*, vol. 32, no. 8, pp. 2598–2606, 2004.

[33] P. A. Rachwal, T. Brown, and K. R. Fox, "Sequence effects of single base loops in intramolecular quadruplex DNA," *FEBS Letters*, vol. 581, no. 8, pp. 1657–1660, 2007.

[34] J. Gros, F. Rosu, S. Amrane, et al., "Guanines are a quartet's best friend: impact of base substitutions on the kinetics and stability of tetramolecular quadruplexes," *Nucleic Acids Research*, vol. 35, no. 9, pp. 3064–3075, 2007.

[35] O. Stegle, L. Payet, J.-L. Mergny, D. J. C. MacKay, and J. L. Huppert, "Predicting and understanding the stability of G-quadruplexes," *Bioinformatics*, vol. 25, no. 12, pp. 374–382, 2009.

[36] O. Kikin, L. D'Antonio, and P. S. Bagga, "QGRS mapper: a web-based server for predicting G-quadruplexes in nucleotide sequences," *Nucleic Acids Research*, vol. 34, pp. W676–W682, 2006.

[37] O. Kikin, Z. Zappala, L. D'Antonio, and P. S. Bagga, "GRSDB2 and GRS_UTRdb: databases of quadruplex forming G-rich sequences in pre-mRNAs and mRNAs," *Nucleic Acids Research*, vol. 36, pp. D141–D148, 2008.

[38] V. Scaria, M. Hariharan, A. Arora, and S. Maiti, "Quadfinder: server for identification and analysis of quadruplex-forming motifs in nucleotide sequences," *Nucleic Acids Research*, vol. 34, pp. 683–685, 2006.

[39] V. K. Yadav, J. K. Abraham, P. Mani, R. Kulshrestha, and S. Chowdhury, "QuadBase: genome-wide database of G4 DNA—occurrence and conservation in human, chimpanzee, mouse and rat promoters and 146 microbes," *Nucleic Acids Research*, vol. 36, pp. 381–385, 2008.

[40] P. Rawal, V. B. R. Kummarasetti, J. Ravindran, et al., "Genome-wide prediction of G4 DNA as regulatory motifs: role in *Escherichia coli* global regulation," *Genome Research*, vol. 16, no. 5, pp. 644–655, 2006.

[41] R. Zhang, Y. Lin, and C.-T. Zhang, "Greglist: a database listing potential G-quadruplex regulated genes," *Nucleic Acids Research*, vol. 36, pp. 372–376, 2008.

[42] J. Eddy and N. Maizels, "Gene function correlates with potential for G4 DNA formation in the human genome," *Nucleic Acids Research*, vol. 34, no. 14, pp. 3887–3896, 2006.

[43] J. Eddy and N. Maizels, "Conserved elements with potential to form polymorphic G-quadruplex structures in the first intron of human genes," *Nucleic Acids Research*, vol. 36, no. 4, pp. 1321–1333, 2008.

[44] J. L. Huppert, A. Bugaut, S. Kumari, and S. Balasubramanian, "G-quadruplexes: the beginning and end of UTRs," *Nucleic Acids Research*, vol. 36, no. 19, pp. 6260–6268, 2008.

[45] H. M. Wong and J. L. Huppert, "Stable G-quadruplexes are found outside nucleosome-bound regions," *Molecular BioSystems*, vol. 5, no. 12, pp. 1713–1719, 2009.

[46] K. J. Neaves, J. L. Huppert, R. M. Henderson, and J. M. Edwardson, "Direct visualization of G-quadruplexes in DNA using atomic force microscopy," *Nucleic Acids Research*, vol. 37, no. 18, pp. 6269–6275, 2009.

SAGE-Hindawi Access to Research
Journal of Nucleic Acids
Volume 2010, Article ID 489736, 6 pages
doi:10.4061/2010/489736

Research Article

A Comparative Study of the Impact of G-Stack Probes on Various Affymetrix GeneChips of Mammalia

Farhat Naureen Memon, Graham J. G. Upton, and Andrew P. Harrison

Departments of Mathematical Sciences and Biological Sciences, University of Essex, Wivenhoe Park, Colchester, Essex CO4 3SQ, UK

Correspondence should be addressed to Farhat Naureen Memon, fnmemo@essex.ac.uk

Received 1 December 2009; Revised 11 February 2010; Accepted 22 April 2010

Academic Editor: Jean Louis Mergny

We have previously discovered that probes containing runs of four or more contiguous guanines are not reliable for measuring gene expression in the Human HG_U133A Affymetrix GeneChip data. These probes are not correlated with other members of their probe set, but they are correlated with each other. We now extend our analysis to different 3′ GeneChip designs of mouse, rat, and human. We find that, in all these chip designs, the G-stack probes (probes with a run of exactly four consecutive guanines) are correlated highly with each other, indicating that such probes are not reliable measures of gene expression in mammalian studies. Furthermore, there is no specific position of G-stack where the correlation is highest in all the chips. We also find that the latest designs of rat and mouse chips have significantly fewer G-stack probes compared to their predecessors, whereas there has not been a similar reduction in G-stack density across the changes in human chips. Moreover, we find significant changes in RMA values (after removing G-stack probes) as the number of G-stack probes increases.

1. Introduction

A sequence of nucleotides having frequent occurrences of runs of guanines is capable of forming unusual four-stranded structures called G-quadruplex structures. These are a result of the Hoogesteen hydrogen bond that binds two guanines at close to 90 degrees. These structures not only form in a single sequence of nucleotides but two or four parallel sequences can also collectively form a G-quadruplex structure. We are investigating the effect of these unusual structures on gene expression measurements using microarrays.

Microarray technology is an effective way of gene expression profiling. Affymetrix GeneChips are the most popular type of array for many model organisms. GeneChip arrays are composed of 25-base long sequences that are known as probes. These probes are arranged in the form of pairs; each pair consists of a perfect match (PM) probe and a mismatch (MM) probe. The PM probe contains the same sequence of bases as appears in the gene; whilst MM is identical to PM except that the central base (13th position base) is the complement of that in the PM probe. Each probe belongs to a particular probe set and similarly each probe set represents a particular gene; however, some genes are represented by more than one probe set.

As a probe set corresponds to a particular gene, it is therefore expected that all the probes of a probe set should be correlated with each other if the particular gene that is represented by that probe set is expressed. However, [1] previously discovered that probes containing G-stacks behaved abnormally with respect to other probes in their probe sets. In our previous work [2], we confirmed the findings of [1], but we also went further in discovering that the G-stack probes are highly correlated with each other. This indicates that they cannot be measuring gene expression but instead suggests a biophysical process occurring on the surface of GeneChips, which we associate with the formation of G-quadruplexes. The probes on a GeneChip are grown through photolithography and this results in many single-stranded DNA sequences being held in close proximity [3]. Probes are readily able to physically touch their neighbouring probes, each of which shares the same sequence. It is expected that if these closely placed parallel probes contain runs of guanines then they may form G-quadruplex structures. In [2], we have also shown that

the value of the correlation coefficient changes according to the location of G-stack within the probes (using a popular human chip, the HG_U133A array).

We are now investigating different GeneChip designs for two issues.

(1) The effect of the position of guanine run within the G-stack probes with an expectation that G-stack probes are highly correlated with each other. We provide a detailed discussion on this topic in Section 3.1.

(2) The position of the G-stack with the highest correlation coefficient value with an expected result that this will be position 1. Position 1 is at the free end of the probe so it can more readily come into contact with its neighbouring probes (discussed in Section 3.2).

For this study we have selected chip designs that are used to study the transcriptome of the mammalian family. We have generated contour plots to show overviews of the entire correlation surface for each of these chip designs.

2. Materials and Methods

The GeneChip data consist of CEL files that report the average intensity of each probe of a microarray. These fluorescent intensities are read through the Affymetrix scanners after the target sequences are hybridised to a microarray. The data from many tens of thousands of GeneChip arrays are freely available in public domains in the form of CEL files. We have downloaded CEL files from the NCBI GEO (Gene Expression Omnibus) repository [4].

We have focused on the mammalian family and have selected GeneChip data for Homo Sapiens (Human), Mus Musculus (Mouse), and Rattus Norvegicus (Rat). For each organism, three or more different chip designs have been used. We have used data from 352 randomly chosen CEL files for most of the chip designs except for a mouse chip design MG_U74Bv2 (280 CEL files) and two of the human chips, HG_U95D (87 CEL files), and HG_U95E (86 CEL files).

We have adopted a pipeline for which a number of in-house informatics tools have been developed. The pipeline performs the following tasks.

2.1. To Generate Contour Plots

(1) We selected probes having exactly one G-stack of length four from the probe sequence (.tab) file of the particular chip design. The.tab file, which contains the probe annotation which includes probe set ID, x and y coordinates and probe sequence with some other information is available at the Affymetrix website [5].

(2) We separated out the filtered list of G-stack probes into groups according to the position of the guanine-run (G-stack) within the G-stack probes. The possible position of a G-stack having exactly four guanines within a probe could be $P = 1, 2, 3, \ldots, 22$. In this way, we have generated 22 groups of G-stack probes. For instance, group 1 represents to all the G-stack probes in which G-stack is at position one.

(3) Rather than using the observed intensities, we used the normalised CEL files.

(4) We produced lookup tables of the x and y coordinates for each of the 22 groups.

(5) As we have generated 22 groups of G-stack probes, a 22 by 22 matrix (M) is generated in which each element represents the average correlation coefficient of two groups of probes; probes that are members of one specified group with probes that are members of another specified group. For instance, element $M[5, 12]$ of the matrix represents the average correlation between G-stack probes in groups 5 and 12.

(6) As a final step, the matrix M is used to generate a contour plot of the correlation surface.

2.2. To Analyse RMA Values with the G-Stack Probes Included and Excluded

(1) In R with Bioconductor, we used RMA [6] to obtain a set of values for each probe set in each of 352 CEL file using the standard CDF file of the specific chip. This set of RMA values reflects to the values of the probe sets with the G-stack probes included.

(2) We then masked all the G-stack probes using the code supplied by NASC [7] in order to generate a new CDF file without G-stack probes.

(3) We again used RMA with the new CDF file to obtain another set of values of the probe sets with the G-stack probes masked.

(4) These two sets of RMA values were used to analyse the effect of removing G-stack probes on RMA values (discussed in Section 3.3).

3. Result and Discussion

A list of chip designs involved in this study is shown in Table 1. The table also shows the chip size, the number of annotated probes, the number of G-stack probes, and the number of affected probe sets in each chip design. The lists of G-stack probes and the lists of affected probe sets (along with the number of G-stack probes in those probe sets) for the arrays analysed are available at http://bioinformatics.essex.ac.uk/users/fnmemo/G-Tract.html.

3.1. Effect of the Position of G-Stack within the Probes. The contour plot for human chip HG_U133A, Figure 1, is almost identical to our previous work, with the discrepancy arising because of the different datasets used in the two studies. The density of G-stack probes differs according to the position of G-stack within the probes (see Table 2). The correlation coefficients of G-stack probes in all the human chips are quite high with the most marked correlation values at their diagonals.

Human arrays show a fairly constant fraction of G-stack probes across different designs. For instance, for

Table 1: List of organisms and their chip designs used in this study. The number of annotated probes and the number of G-stack probes include both the main and control probes.

Organism	Chip Design	Chip size	No. of annotated Probes	No. of G-stack Probes	No. of Affected Probe Sets
Humans	HG_U133_Plus_2	1164 ∗ 1164	604,258	24,980	16,254
(Homo_Sapiens)	HG_U133A	712 ∗ 712	247,965	12,868	8,298
	HG_U95A	640 ∗ 640	201,807	7,329	3,733
	HG_U95B	640 ∗ 640	201,862	6,334	3,240
	HG_U95D	640 ∗ 640	201,858	7,198	3,227
	HG_U95E	640 ∗ 640	201,863	7,880	3,514
Mouse	MOE430A	712 ∗ 712	249,958	372	314
(Mus Musculus)	MOE430B	712 ∗ 712	248,704	252	203
	MG_U74Av2	640 ∗ 640	197,993	7,360	3,556
	MG_U74Bv2	640 ∗ 640	197,131	7,006	3,614
Rat	RAE230A	602 ∗ 602	175,477	81	58
(Rattus Norvegicus)	Rat230_2	834 ∗ 834	342,410	208	163
	RG_U34A	534 ∗ 534	140,317	3,691	2,104

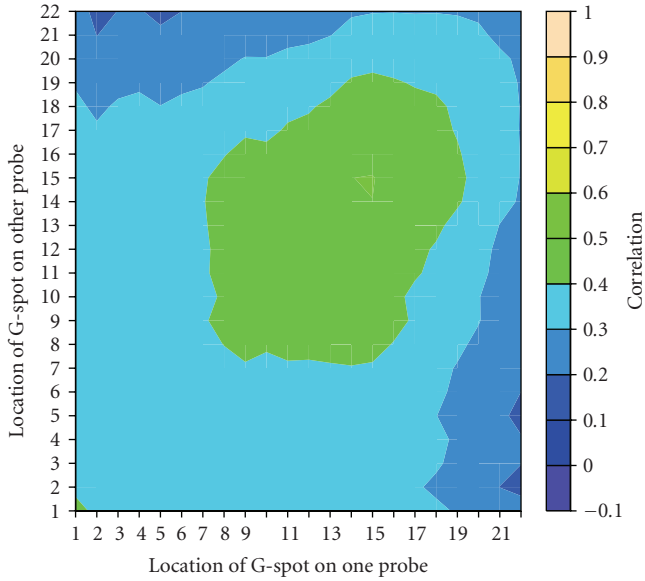

Figure 1: Contour plot illustrating that in human chip HG_U133A, the average correlation coefficient values changes according to the position of G-stack (with four Gs only) for a group of probes.

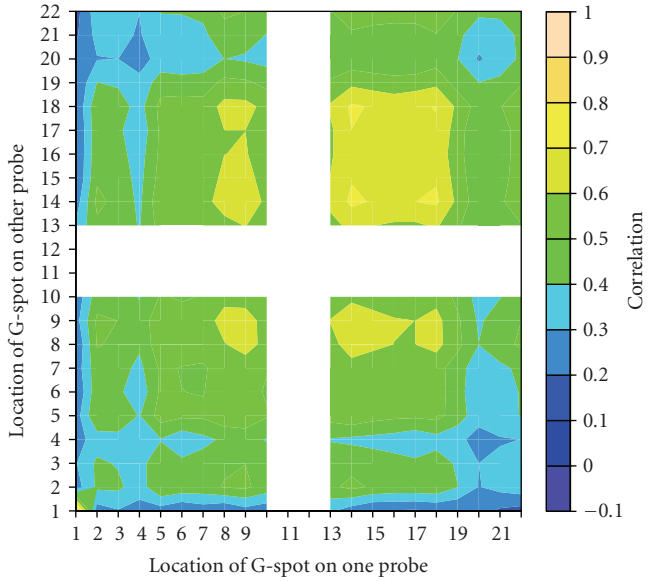

Figure 2: Contour plot illustrating that in mouse chip MOE430B, the average correlation coefficient values changes according to the position of G-stack (with four Gs only) for a group of probes.

a recent human chip design, HG_U133_Plus_2, 4.1% (24,980/604,258) of the annotated probes contain a G-stack. On the older HG_U95A design 3.6% (7,329/201,807) of the annotated probes contain a G-stack.

In contrast to the human results, the mouse and rat chips show large changes in G-stack probe density across different designs, with significantly smaller fractions being found on the latest designs. Of the four mouse chips used in this study, the older designs MG_U74Av2 and MG_U74Bv2 have over an order of magnitude more G-stack probes than do the newer chip designs, MOE430A and MOE430B. We found that 0.15% (372/249,958) and 0.1% (252/248,704) of the annotated probes contain a G-stack in MOE430A and MOE430B, respectively. Whereas the percentages of annotated G-stack probes in MG_U74Av2 and MG_U74Bv2 are 3.72% (7,360/197,993) and 3.6% (7,006/197,131), respectively. Moreover, both the chips, MOE430A and MOE430B, also have an absence of G-stack probes in their middle (see Table 2) which is reflected in the contour plot of chip MOE430B in Figure 2. As with the human data, the locations for which there are probes indicate that G-stacks probes are highly correlated on mouse designs. Furthermore, the correlation is also highest when comparing two probes that have G-stacks at the same location within the probe.

We also used three chip designs for rat (Rattus Norvegicus). The RG_U34A chip is the oldest design and we find

Table 2: In G-stack probes, the effect of the position of G-stack on the average correlation coefficient value, (n is the number of affected probes and $\bar{r}$ is the average correlation between these n probes).

		Position of G-stack										
		1	2	3	4	5	6	7	8	9	10	11
HG_U133A	n	871	449	548	583	664	546	599	604	531	471	458
	$\bar{r}$	0.51	0.32	0.36	0.36	0.34	0.34	0.36	0.40	0.44	0.42	0.44
HG_U133_Plus_2	n	1758	925	1072	1170	1234	1087	1214	1093	1049	923	903
	$\bar{r}$	0.29	0.15	0.17	0.18	0.19	0.18	0.18	0.23	0.26	0.22	0.27
HG_U95A	n	398	297	255	271	315	308	367	448	417	47	47
	$\bar{r}$	0.40	0.28	0.30	0.31	0.31	0.29	0.33	0.35	0.40	0.42	0.39
HG_U95B	n	314	267	237	261	282	293	326	375	339	19	23
	$\bar{r}$	0.66	0.51	0.54	0.55	0.56	0.57	0.58	0.64	0.67	0.63	0.68
HG_U95D	n	293	278	243	272	284	311	381	471	478	56	73
	$\bar{r}$	0.60	0.36	0.37	0.39	0.38	0.41	0.42	0.44	0.50	0.41	0.47
HG_U95E	n	346	323	317	285	350	363	398	532	559	73	57
	$\bar{r}$	0.54	0.29	0.32	0.35	0.34	0.33	0.41	0.41	0.46	0.39	0.47
MOE430A	n	15	19	16	14	15	22	36	12	12	13	0
	$\bar{r}$	0.51	0.26	0.32	0.30	0.15	0.28	0.27	0.33	0.33	0.40	—
MOE430B	n	4	13	14	13	16	13	22	4	9	8	0
	$\bar{r}$	0.92	0.42	0.39	0.31	0.54	0.50	0.49	0.60	0.62	0.49	—
MG_U74Av2	n	357	315	259	292	292	349	349	428	431	39	46
	$\bar{r}$	0.29	0.15	0.17	0.18	0.19	0.18	0.18	0.23	0.26	0.22	0.27
MG_U74Bv2	n	326	286	246	257	271	298	369	436	496	17	14
	$\bar{r}$	0.54	0.33	0.33	0.35	0.39	0.40	0.42	0.46	0.54	0.61	0.63
RG_U34A	n	194	148	145	126	166	160	183	176	144	94	85
	$\bar{r}$	0.33	0.23	0.21	0.24	0.28	0.29	0.32	0.32	0.41	0.38	0.36
		Position of G-stack										
		12	13	14	15	16	17	18	19	20	21	22
HG_U133A	n	491	424	523	580	592	604	650	615	737	611	689
	$\bar{r}$	0.45	0.47	0.50	0.50	0.47	0.43	0.41	0.38	0.34	0.29	0.26
HG_U133_Plus_2	n	949	872	1009	1140	1098	1193	1271	1185	1310	1192	1308
	$\bar{r}$	0.29	0.32	0.39	0.42	0.39	0.41	0.39	0.38	0.32	0.27	0.24
HG_U95A	n	33	37	631	417	384	388	359	433	467	399	570
	$\bar{r}$	0.42	0.49	0.54	0.55	0.55	0.57	0.55	0.57	0.55	0.54	0.54
HG_U95B	n	15	18	555	336	350	342	340	383	390	365	463
	$\bar{r}$	0.77	0.84	0.81	0.79	0.81	0.81	0.81	0.80	0.77	0.78	0.75
HG_U95D	n	72	74	832	364	357	337	330	391	426	334	500
	$\bar{r}$	0.43	0.54	0.64	0.64	0.66	0.75	0.69	0.70	0.74	0.71	0.75
HG_U95E	n	61	73	833	412	378	371	354	420	434	370	530
	$\bar{r}$	0.39	0.47	0.62	0.61	0.66	0.64	0.67	0.68	0.67	0.69	0.65
MOE430A	n	2	25	16	15	27	20	19	18	8	14	7
	$\bar{r}$	0.37	0.33	0.40	0.42	0.37	0.36	0.26	0.29	0.31	0.10	0.07
MOE430B	n	0	7	10	19	23	12	10	10	6	6	6
	$\bar{r}$	—	0.55	0.72	0.66	0.62	0.68	0.70	0.45	0.28	0.32	0.48
MG_U74Av2	n	42	51	682	434	388	373	362	457	471	357	545
	$\bar{r}$	0.29	0.32	0.39	0.42	0.39	0.41	0.39	0.38	0.32	0.27	0.24
MG_U74Bv2	n	6	11	790	404	392	336	326	443	419	357	465
	$\bar{r}$	0.78	0.54	0.68	0.67	0.67	0.69	0.62	0.62	0.57	0.56	0.55
RG_U34A	n	82	76	182	185	214	200	204	215	213	202	268
	$\bar{r}$	0.47	0.43	0.46	0.49	0.46	0.42	0.42	0.45	0.34	0.26	0.21

Table 3: The effect on RMA of removing G-stack probes from probe sets. Subtraction of the original RMA value from the RMA value after removal of G-stack probes gives the quantity d. Entries are column percentages.

No. of G-stack probes:	0	1	2	3	4	5	6
No. of probe sets:	38,422	10,216	4,192	1,280	384	121	36
$d > 2.0$	0	0	0	0	0	0	2
$1.0 < d \leq 2.0$	0	0	1	1	3	3	9
$0.5 < d \leq 1.0$	0	1	4	5	7	6	11
Between −0.5 and 0.5	100	94	76	61	51	46	34
$-0.5 > d \geq -1.0$	0	5	14	21	19	19	10
$-1.0 > d \geq -2.0$	0	0	5	11	17	21	18
$d < -2.0$	0	0	0	1	2	5	16

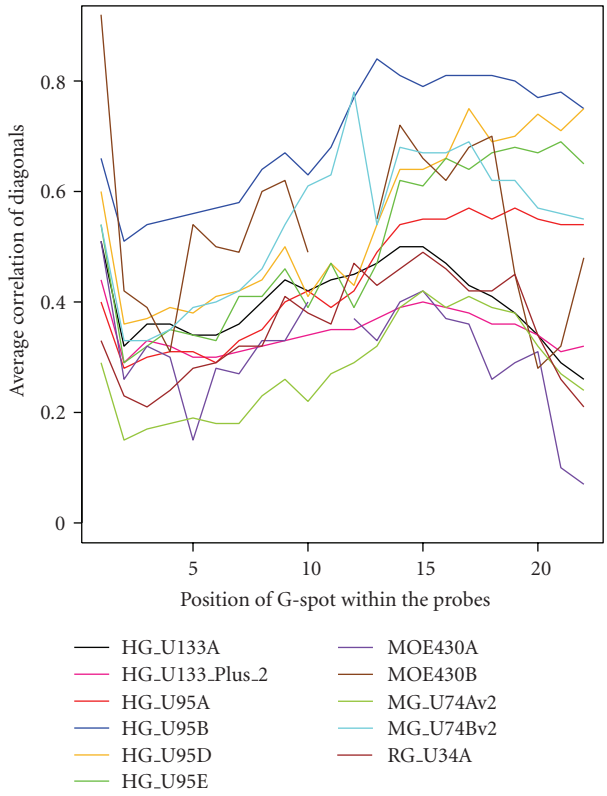

Figure 3: The plot shows that diagonal correlation coefficient values of each chip design. Diagonal values represent correlation among the same group of probes.

that it has over an order of magnitude more G-stack probes than do the new chip designs, Rat230_2 and RAE230A. We found 0.05% (81/175,477) of the annotated probes contain a G-stack in chip design RAE230A. Similarly chip design Rat230_2 has 0.06% (208/342,410) of the annotated probes contain a G-stack. Whereas, the old Rat chip RG_U34A contains 2.6% G-stack probes (3,691/140,317).

Due to the small number of G-stack probes in the new chips of rat and mouse, we expect that the gene expression measurement in these new chip designs will be less affected by G-stack probes.

3.2. Position of the G-Stack with the Highest Correlation Coefficient Value. We have also checked whether there is any specific position of G-stack where the correlation is always most marked. We were expecting that the correlation could be highest at the 5′ end of the probes, as is the case for HG-U133A in our previous work [2]. The 5′ end of the probe is free and so it has a greater tendency to come into physical contact with adjacent probes. However, we find that there is no specific position of G-stack where correlation coefficient is most marked in all the chips. Furthermore, the diagonal values in the contour plot are almost always showing the highest correlation. Table 2 provides the details of diagonal values of matrix M (M is explained in Section 2.1) for all the chips analysed which is graphically illustrated in Figure 3.

3.3. Effect of Removing G-Stack Probes on RMA Values. To examine the effect of removing G-stack probes, we used RMA to obtain values for each probe set in each of 352 HG_U133_Plus_ 2 CEL files. We then obtained revised RMA values with the G-stack probes masked. In Table 3, we report the results in terms of a summary of the values obtained for d, which we define as the revised RMA value minus the original value. In the table there are separate columns to summarise the effects on probe sets having varying numbers of G-stack probes. The percentages reported are based on the number of probe sets shown in the second row of the table and are averaged over the 352 CEL files.

As one would hope, there are no major changes on probe sets that have no G-stack probes. As the number of G-stack probes increases, so the changes become potentially much more serious, and the effects are more variable. On average G-stack probes have higher values than other probes, so that, the majority of RMA values are reduced by the removal of the G-stack probes. However, there are also many instances where the RMA value is appreciably increased by removal of G-stack probes.

4. Conclusion

G-stack probes behave as outliers within their probe sets because they are usually poorly correlated with other members of their probe sets while they are highly correlated with each other. We have illustrated that this is true in

various chip designs of different mammalia. Therefore, as we suggested before in our previous work [2], these probes should not be included within a calculation of the gene expression measurement. Due to the previous work, we were expecting that the correlation among the G-stack probes is at its highest when the runs of guanines start from position 1 (5′ end) within the probes. It was our expectation that as the 5′ end is the free/moving end, so there are more changes for the G-stack probes to attach with the neighbouring probe's G-stack at this end. Although it is true for some chip designs, for instance HG_U133A, MOE430A and MOE430B, it is not true for all of them. Thus, in general, we did not find a common position of G-stack where the correlation coefficient value is high in all the chips. We also found that a much smaller fraction of G-stack probes are present in the new chip designs of rat and mouse compared to the original designs. This suggests that the change in design protocol led to a significant removal of probes which we now believe to be misinformative. It is surprising that such a change in design did not lead to a significant reduction in the amount of G-stack probes in human 3′ array.

Furthermore, we find that the changes in RMA values (after removing the G-stack probes) become more serious as the number of G-stack probes increases.

Acknowledgments

Memon is funded by a scholarship from the University of Sindh (NO.SU/PLAN/F.SCH/611). The authors are grateful to Dr. Neil S. Graham and Dr. Olivia Sanchez-Graillet for help with software.

References

[1] C. Wu, H. Zhao, K. Baggerly, R. Carta, and L. Zhang, "Short oligonucleotide probes containing G-stacks display abnormal binding affinity on Affymetrix microarrays," *Bioinformatics*, vol. 23, no. 19, pp. 2566–2572, 2007.

[2] G. J. G. Upton, W. B. Langdon, and A. P. Harrison, "G-spots cause incorrect expression measurement in Affymetrix microarrays," *BMC Genomics*, vol. 9, article 613, 2008.

[3] W. B. Langdon, G. J. G. Upton, and A. P. Harrison, "Probes containing runs of guanines provide insights into the biophysics and bioinformatics of Affymetrix GeneChips," *Briefings in Bioinformatics*, vol. 10, no. 3, pp. 259–277, 2009.

[4] T. Barrett, T. O. Suzek, D. B. Troup et al., "NCBI GEO: mining millions of expression profiles - Database and tools," *Nucleic Acids Research*, vol. 33, pp. D562–D566, 2005.

[5] Affymetrix, http://www.affymetrix.com/index.affx.

[6] R. A. Irizarry, B. Hobbs, F. Collin et al., "Exploration, normalization, and summaries of high density oligonucleotide array probe level data," *Biostatistics*, vol. 4, no. 2, pp. 249–264, 2003.

[7] NASC's International Affymetrix Service, http://affymetrix.arabidopsis.info/xspecies/.

SAGE-Hindawi Access to Research
Journal of Nucleic Acids
Volume 2010, Article ID 820356, 8 pages
doi:10.4061/2010/820356

Research Article

Evaluation of Human Telomeric G-Quadruplexes: The Influence of Overhanging Sequences on Quadruplex Stability and Folding

Viktor Viglasky,[1] Lubos Bauer,[1] Katarina Tluckova,[1] and Peter Javorsky[2]

[1] *Department of Biochemistry, Institute of Chemistry, Faculty of Sciences, P. J. Safarik University, Moyzesova 11, 04154 Kosice, Slovakia*
[2] *Institute of Animal Physiology, Slovak Academy of Sciences, Šoltésovej 4-6, 04001 Košice, Slovakia*

Correspondence should be addressed to Viktor Viglasky, viktor.viglasky@upjs.sk

Received 11 January 2010; Revised 21 March 2010; Accepted 11 May 2010

Academic Editor: Mateus Webba da Silva

To date, various G-quadruplex structures have been reported in human telomeric sequences. Human telomeric repeats can form many topological structures depending on conditions and on base modification; parallel, antiparallel, and hybrid forms. The effect of salts and some specific ligands on conformational switches between different conformers is known, but the influence of protruding sequences has rarely been discussed. In this paper, we analyze different quadruplex-forming oligomers derived from human telomeric sequences which contain 3′- and 5′-protruding nucleotides, not usually associated with the G-quadruplex motif. The study was performed using electrophoresis, CD, and UV spectroscopies. The major findings are (i) protruding nucleotides destabilize the G-quadruplex structure, and (ii) overhanging sequences influence the folding of the quadruplex.

1. Introduction

There is currently tremendous interest in understanding G-quadruplex formation from G-rich sequences. To date, more than 1600 scientific articles concerning the quadruplex problem have been published; more than 1200 of them are focused on quadruplexes which potentially occur in humans and approximately half of these are interested in quadruplex formation in telomeres. Telomeres are structures at the end of chromosomes which protect chromosomal DNA from degradation and recombination [1, 2]. Eukaryotic telomeres consist of tandem repeats of G-rich sequences, for example, $(TTAGGG)_n$ repeats in human. Several kilobases of that sequence are paired with a complementary strand to form duplex DNA, but approximately 100–200 nucleotides of the sequence remain unpaired and form a single-stranded overhang. These G-rich ends can fold into four-stranded G-quadruplex structures containing G-tetrads, paired by intra- or intermolecular Hoogsteen bonds; they are held together by π-π stacking interactions [3]. This noncanonical DNA secondary structure has been postulated as being involved in a variety of biological functions; it is suggested that they may also be important causal factors in cell aging and human diseases such as cancer [1, 2]; G-quadruplexes formed by these sequences represent attractive anticancer targets [4, 5]. There is supporting evidence that telomeres also serve as a biological clock, as telomere structures appear to shorten with each successive cell cycle. In immortalized cells and in cancer cells however, telomerase is activated to maintain the length of the telomere [6]. Specific proteins interact with the overhang and regulate telomerase activity. There is supporting evidence that quadruplex structures occur *in vivo* [7], and recent evidence suggests that quadruplexes form in telomeric DNA at specific times in the cell cycle [8]. However, G-rich DNA sequences can form a large number of structurally diverse G-quadruplex structures in the presence of monovalent ions, for example potassium and sodium [9]. Much still remains unclear about the condition and driving forces of quadruplex topology.

Repeats of the 5′-TTAGGG sequence spontaneously form intramolecular quadruplex structures in solution, with a variety of folded morphologies. Different conformations of human telomeric oligomers in water solution and in crystals have been reported by a number of authors [3, 10, 11]. In addition, one conformation of G-quadruplex can transform to another, for example, parallel-to-antiparallel

form. Quadruplex folding depends on many factors; the DNA sequence, the presence of ions, the temperature, and the presence of various ligands [12, 13]. Recently, four-repeats of human telomere sequences have been shown to form two very similar intramolecular (3 + 1) G-quadruplexes in solutions containing K^+ ion (hybrid form 1 and 2) [14–16]. Both structures contain the (3 + 1) G-tetrad core with one double-chain-reversal (DCR) and two edgewise loops (EW), but differ in the order of loop appearance within the G-quadruplex scaffold. In addition, a basket-type G-quadruplex with only two G-tetrad layers was detected where loops are successively edgewise, diagonal, and edgewise. Despite the presence of only two G-tetrads in the core, this structure is more stable than the three-G-tetrad intramolecular G-quadruplexes previously observed in human telomeric sequences in potassium solution. This novel structure highlights the conformational heterogeneity of human telomeric DNA [17]. Studies have also revealed a crystal structure of the human telomere sequence which has a unique symmetrical propeller-type structure with all parallel G-tetrads and three double-chain-reversal loops [3]. This structure does not seem to be the prevalent form in solution [11]. However, recent experiments show that the human telomeric repeats can form parallel G-quadruplex structures in crowding conditions simulated with polyethylene glycol and ethanol [18–20].

In this study, we analyze the human telomeric sequence 3′-$G_3(TTAG_3)_3$-5′ containing various overhangs at 3′- and 5′-ends, Table 1. The effect of thymine tract length has previously been studied for different shorter sequences which form dimeric and tetrameric quadruplex molecules [21]. However, for the first time we focus on monomolecular quadruplexes containing longer protruding sequences of more than 7 nucleotides. It has been widely documented that changes of only one base in the sequence at the 3′- or 5′- end can drastically modify quadruplex topology [15]. Our goal was to choose sequences in which overhangs do not form any secondary structures, because additional secondary motifs can significantly affect CD spectra and can complicate spectra interpretation. Therefore, only one random protruding sequence was analyzed to avoid any unexpected interactions of overhanging guanines with parts of the sequence forming a core of G-quadruplex; other sequences in overhangs do not contain guanine and cytosine bases. Thus, $d(T)_n$ and $d(TTA)_m$ have been analyzed, where $n = 7$ and 11 and $m = 1$ and 6. The second goal was to use sequences which cannot form or associate to other quadruplex motifs, as for example, in the *TEL2* sequence used here. Recent evidence suggests the existence of intramolecular quadruplex-quadruplex interactions between two contiguous quadruplex motifs in another quadruplex forming sequence, which can influence their overall structure [22]. These oligomeric sequences forming G-quadruplexes serve as a model of the arrangement of quadruplexes in telomeres in cellular conditions because G-rich islands are always associated with another part of telomeric DNA, mainly at 5′-end, where the telomeric sequence occurs as double-stranded DNA. Electrophoresis, CD and UV spectroscopies have been used for this purpose.

2. Materials and Methods

2.1. Material and Equipments. All chemical and reagents were obtained from commercial sources. Acrylamide : bisacrylamide (19 : 1) solution and ammonium persulfate were purchased from Bio-Rad, polyethylene glycol—PEG 200 and N,N,N′,N′-tetramethyl- ethylenediamine were purchased from Fisher Slovakia. DNA oligomers (sequences shown in Table 1) were obtained from Sigma Genosys and Biosearch Technologies, Inc. All DNA oligomers were PAGE purified and dissolved in double-distilled water before use. Single-strand DNA concentrations were determined by measuring the absorbance (260 nm) at high temperature. The concentration of DNA was determined by UV measurements carried out on a Varian Cary 100 UV-visible spectrophotometer (Amedis, Slovakia). Cells with optical path lengths of 10 mm were used, and the temperature of the cell holder was controlled with an external circulating water bath (Varian).

2.2. Circular Dichroism Spectroscopy. CD spectra were recorded on a Jasco J-810 spectropolarimeter (Easton, MD, USA) equipped with a PTC-423L temperature controller using a quartz cell of 1 mm optical path length in a reaction volume of 300 μl and an instrument scanning speed of 100 nm/min, 1 nm pitch, and 1 nm bandwidth, with a response time of 2 s, over a wavelength range of 220–320 nm. The scan of the buffer was subtracted from the average scan for each sample. All DNA samples were dissolved and diluted in suitable buffers containing appropriate concentrations of ions. The amount of DNA oligomers used in the experiment was kept close to ~2.5 μM. The normalized CD spectra were compared. DNA samples were annealed at 95°C for 5 minutes then allowed to cool down to the initial temperature as at the beginning of the experiment for ~2 hours. CD data represents three averaged scans taken at a temperature range of 20°C. The Britton-Robinson buffer was used in all experiments: 25 mM H_3PO_4, 25 mM Boric acid, 25 mM acetic acid, and supplemented by 50 mM of KCl, pH was adjusted by Tris to the final value of 7.0.

2.3. Melting Curves. The CD melting profiles were collected at 265 and at 295 nm. The thermal stability of different antiparallel quadruplexes was also measured by recording UV absorbance and the CD ellipticity at 295 nm as a function of temperature, by a method similar to that published previously [23, 24]. The temperature ranged from 20 to 100°C, the heating rate was 0.25°C per minute. The melting temperature (T_m) was defined as the temperature of the midtransition point. This T_m value was used as an initial parameter of van't Hoff analysis [24].

2.4. Electrophoresis. Native polyacrylamide gel electrophoresis (PAGE) was run in a temperature-controlled vertical electrophoretic apparatus (Z375039-1EA; Sigma-Aldrich, San Francisco, CA). Gel concentration was 16% (19 : 1 monomer to bis ratio, Applichem, Darmstadt). About two micrograms of DNA (~1/5 of DNA as used in the CD experiments) was

loaded on 14 × 16 × 0.1 cm gels. Electrophoresis was run at 20°C for 4 hours at 126 V (~8 V·cm^{-1}). DNA oligomers were visualized with silver after the electrophoresis, and the electrophoretic record was photographed by an Olympus Camedia 3000 camera [25].

3. Results and Discussion

3.1. CD Spectroscopy. Although CD spectra are routinely used to assign DNA folds [11], the interpretation of optical properties such as hypochromicity or the shape and sign of CD bands can be controversial [26]. G-tetrad stacking and the polarity of DNA strands are determining factors in the intensity and shape of the CD spectrum, and specifically the rotation angle between the stacks. It is well known that parallel G-quadruplex structures give a positive band ~265 nm and a negative band ~240 nm, while antiparallel G-quadruplex structures, such as the basket and chair forms, show two positive bands ~295 and ~245 nm and a negative band ~260 nm [26]. These spectral features are mainly attributed to the specific guanine stacking in various G-quadruplex structures [24, 27].

Figure 1 shows CD spectra of oligomers, the sequences of which are summarized in Table 1. CD measurements were performed in a Britton-Robinson buffer containing 50 mM of KCl. These measurements clearly show that protruding nucleotides have a considerable impact on the profile of spectra; longer protrusions have an even more significant influence. The positive CD band of *TEL1* and *TEL2* at 293 nm associated with a ~265 nm positive shoulder (red and black lines in Figure 1(a)), correspond to the antiparallel hybrid forms in K^+ solution [28]. *TEL1* in the presence of 50% PEG 200 folds into a parallel conformer, which the CD spectrum shows as no peak at ~295 nm, red-dashed line in Figure 1(a). The spectra of *TEL1-3-5-T-7* and *TEL1-5-T-11* are in principle the same which is why only one spectrum is presented in Figure 1(b). Prolongation of the quadruplex overhanging sequence increases the negative and positive signals at ~250 nm and 265 nm, respectively, Figures 1(b) and 1(c). These results indicate that tails of G-quadruplexes can influence the quadruplex topology. Our data also supports the suggestions made by other authors that even small changes to flanking sequences can disturb the equilibrium between different coexisting G-quadruplex forms. In a recent study, two separated bands of comparable magnitude were observed at ~270 and ~295 nm for $A_3G_3(T_2AG_3)3A_2$ oligomer [20]. Similar features of spectra were observed to that of *TEL1-3-5-TTA-18, TEL1-5-TTA-18,* and *TEL1-3-5-A-7* in K^+ solution. In addition, a study of $A_3G_3(T_2AG_3)3A_2$ using NMR confirmed a hybrid 2 of quadruplex structure [16]. The flanking nucleotides resulted in a shoulder on the short wavelength side of the 295 nm CD band. The height of this shoulder increased with the number of flanking nucleotides. A similar CD spectrum was observed for $G_3(T_2AG_3)_4$, which contains one redundant T_2AG_3 repeat [18].

The presence of multiple G-quadruplex conformations in K^+ solution makes structural interpretation difficult under conditions of NMR measurements [15]. To date, only two hybrid conformers have been clearly confirmed by NMR. However, Phan et al. have detected a small population of other (3 + 1) hybrids containing two DCR loops [29]. Our hypotheses explaining the relative increase and decrease of peaks at ~270 nm and ~295 nm, respectively, is as follows; increasing the number of protruding nucleotides shifts the equilibrium from a hybrid with one DCR towards the (3 + 1) arrangement containing two DCR loops. The subsequent introduction of crowding conditions causes a propeller-like parallel arrangement of G-quadruplex to develop

$$\begin{aligned}\text{hybrid } 1,2\ (1\text{xDCR}) &\longrightarrow \text{hybrid } (2\text{xDCR})\\ &\longrightarrow \text{propeller } (3\text{xDCR})\end{aligned} \tag{1}$$

However, our hypothesis has to be verified with NMR at corresponding condition. Interestingly, the CD pattern of *TEL1-ran* (green line) shows a maximum of ellipticity at ~262 nm associated with ~295 nm positive shoulder. This oligomer supports and confirms our previous suggestions. However, when a protruding sequence is able to form an additional quadruplex, as for example, the *TEL2* oligomer used in this study, then two tandemic quadruplexes are more likely to be formed. The same spectral features are to be observed in both *TEL1* and *TEL2* [26, 30, 31]. Nevertheless, a significant destabilization of *TEL2* quadruplex structure can also be observed, Table 2. These results are in agreement with previous studies [26].

3.2. Electrophoretic Analysis. The overhanging sequences significantly influence the mobility of DNA samples. Frequently, the unusually small value of mobility of the parallel conformers which does not correspond to their size can be explained by a higher molecularity. It has been suggested that the mobility of antiparallel and parallel conformers depends only on the number of molecules associated with the formation of its structure [26]. However, in a nondenaturing condition the mobility depends not only on the molecular mass and the charge of macromolecules, but is also strongly determined by topology [24]. Figure 2 displays electrophoretic records of native 16% polyacrylamide gels illustrating the relative mobilities of the oligomers in the presence of 50 mM KCl. The electrophoretic mobilities of *TEL1* and their derivatives are clearly visible.

Random 20-mer and 40-mer were used as DNA standards. The fastest electrophoretic mobility is exhibited by the *TEL1* oligomer (line 1); it is consistent with the mobility of monomolecularly folded G-quadruplexes [24, 26, 30]. The mobility retardation caused by the overhanging nucleotides of *TEL1* oligomer is evident. The electrophoresis did not confirm any anomalous mobility of oligomers; sequences with the same length move equally and longer oligomers more slowly. For example, the mobilities of *TEL1-ran* and *TEL1-5-TTA-18* sequences are comparable in the given conditions due to similarities in their lengths. The CD spectra of oligomers *TEL1, TEL1-3-T-7, TEL1-5-T-7, TEL1-3-T-11, TEL1-5-T-11,* and *TEL2* show similar profiles, suggesting that all these sequences form a topologically equivalent core of quadruplex, and then their mobilities depend on the

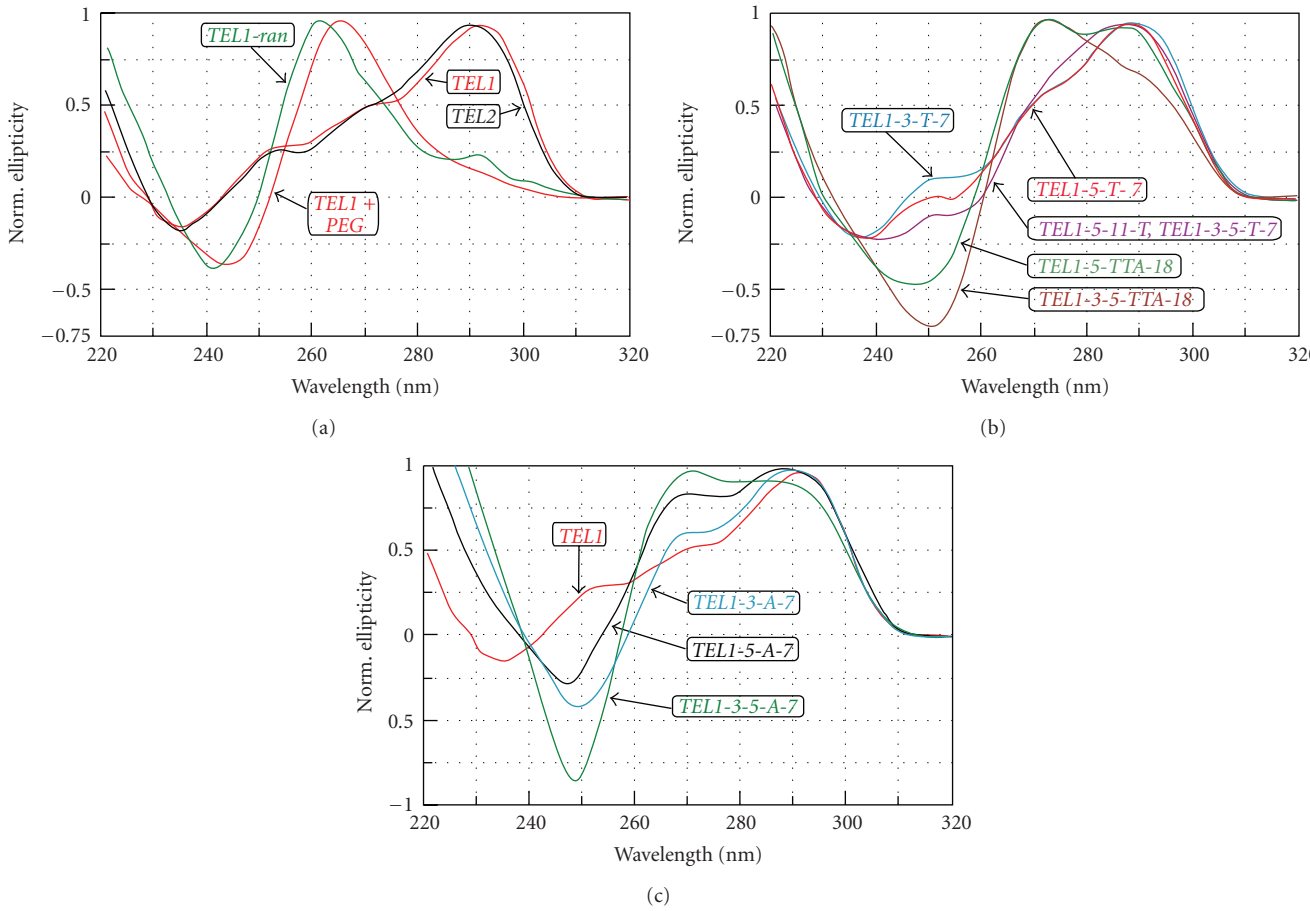

Figure 1: Normalized CD spectra of G-quadruplex-forming sequences in Britton-Robinson buffer containing 50 mM KCl, pH 7.0 distinguished by different color: *TEL1*, *TEL2*, and *TEL1* in the presence of 50% PEG-200 and *TEL1-ran* in (a); *TEL1-3-T-7*, *TEL1-5-T-7*, *TEL1-3-5-T-7*, *TEL1-5-T-11*, *TEL1-5-TTA-18*, *TEL1-3-5-TTA-18* in (b), and *TEL1-3-A-7*, *TEL1-5-A-7*, *TEL1-3-5-A-7*, and *TEL1* in (c).

Table 1: Oligodeoxynucleotides and their sequences used in this study.

Name	N. nt.	Sequence 5′ → 3′
TEL1	21	**GGGTTAGGGTTAGGGTTAGGG**
TEL1-TTA	24	**GGGTTAGGGTTAGGGTTAGGG**TTA
TEL2	45	**GGGTTAGGGTTAGGGTTAGGG**TTA**GGGTTAGGGTTA GGG TTAGGG**
TEL1-5-T-7	28	TTTTTTT-**GGGTTAGGGTTAGGGTTAGGG**
TEL1-3-T-7	28	**GGGTTAGGGTTAGGGTTAGGG**-TTTTTTT
TEL1-5-A-7	28	AAAAAAA- **GGGTTAGGGTTAGGGTTAGGG**
TEL1-3-A-7	28	**GGGTTAGGGTTAGGGTTAGGG**-AAAAAAA
TEL1-5-T-11	32	TTTTTTTTTTT-**GGGTTAGGGTTAGGGTTAGGG**
TEL1-3-T-11	32	**GGGTTAGGGTTAGGGTTAGGG**-TTTTTTTTTTT
TEL1-3-TTA-11	32	**GGGTTAGGGTTAGGGTTAGGG**-TTATTATTATT
TEL1-5-TTA-11	32	TTATTATTATT **GGGTTAGGGTTAGGGTTAGGG**-
TEL1-3-5-T-7	35	TTTTTTT-**GGGTTAGGGTTAGGGTTAGGG**-TTTTTTT
TEL1-3-T-18	39	**GGGTTAGGGTTAGGGTTAGGG**-TTTTTTTTTTTTTTTTTT
TEL1-5-T-18	39	TTTTTTTTTTTTTTTTTT-**GGGTTAGGGTTAGGGTTAGGG**
TEL1-3-5-A-7	39	AAAAAAA- **GGGTTAGGGTTAGGGTTAGGG**-AAAAAAA
TEL1-5-TTA-18	39	TTATTATTATTATTATTA-**GGGTTAGGGTTAGGGTTAGGG**
TEL1-3-5-TTA-18	57	TTATTATTATTATTATTA-**GGGTTAGGGTTAGGGTTA GGG**-TTATTATTATTATTATTA
TEL1-ran	39	GATCCCAGATCTTC-**GGGTTAGGGTTAGGGTTAGGG** -CAGA

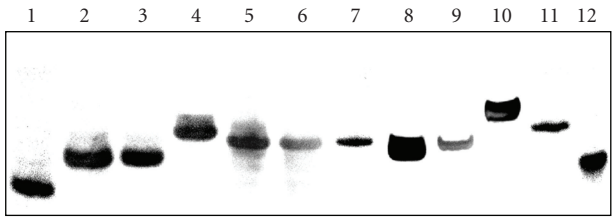

Figure 2: Electrophoresis at 20°C in 16% polyacrylamide gels in 25 mM Britton-Robinson buffer (pH 7.0) containing 50 mM KCl. Each well contains ~0.5 μM of oligomer. In lines 1–10 there were loaded *TEL1*, *TEL1-3-T-7*, *TEL1-5-T-7*, *TEL1-3-5-T-7*, *TEL1-3-T-11*, *TEL1-5-T-11*, *TEL1-ran*, *TEL2*, *TEL1-5-TTA-18*, and *TEL1-3-5-TTA-18* oligomers. Random 20- and 40-mer are loaded in lines 11 and 12.

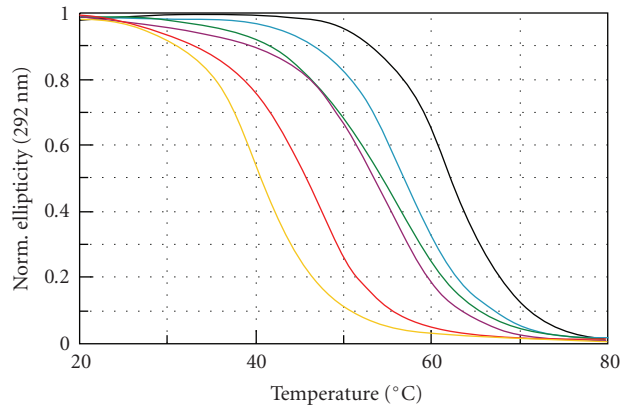

Figure 3: Normalized melting curves of *TEL1* (black), *TEL2* (green), *TEL1-3-T-7* (blue), *TEL1-5-T-11* (magenta), *TEL1-3-5-7-T* (red), and *TEL1-3-5-TTA-18* (orange) at pH 7.0 obtained by CD spectroscopy collected at 293 nm.

length of protruding sequences and not on DNA topology. Though *TEL1-ran*, *TEL1-5-TTA-18*, and *TEL1-3-5-TTA-18* oligomers show the most intensive peaks at range of 262–272 nm, their mobility is not anomalous to the oligomers discussed above. Therefore, we suggest that the topology of the (3 + 1) hybrid arrangement did not have to be disturbed. However, we cannot decide based on CD and electrophoretic experiment unambiguously whether the arrangement of *TEL1-ran* is still a hybrid or parallel form. Nevertheless, the *TEL2* consists of 45 nucleotides, but this oligomer moves faster than other "tailed" but shorter oligomers; *TEL1-3-5-T-7* (35 nt), *TEL1-5-T-11*, and *TEL1-3-T-11* (32 nt). Thus, we suggest that based on CD spectra and electrophoresis, this oligomer forms two quadruplexes within a (3 + 1) hybrid topology ordered in tandem [26].

However, we cannot exclude the possibility of a mixed population of parallel and antiparallel conformers in a solution containing potassium, because both corresponding peaks/shoulders (265 and 295 nm) were observed in some sequences. Electrophoresis excludes a mix of topologically different conformers because only one clear band is detected, although thermodynamically transient conformers can cause smears in certain lines during the electrophoretic separation [24]. The silver staining procedure is highly sensitive in DNA visualization; the advantage is that it allows us to detect even very small populations of structural forms [25].

3.3. Analysis of Melting Curves. Melting curve analysis can help to clarify some other aspects concerning quadruplex stability. Nonsigmoidal shapes of the melting curve have been reviewed by many authors, in particular those concerning quadruplex evaluation [32]. Although van't Hoff's evaluation of melting curves can offer important information, inappropriate use of the application can also lead to incorrect interpretations. This analysis can only offer relevant results for two-state mechanisms, as described by the following scheme: $F \leftrightarrow U$, where F and N represent the folded and unfolded states of molecule, respectively. Chaires have critically reviewed a routine application of van't Hoff analysis to a number of melting curves [33]. The following methods should be used to verify a two-state mechanism; (i) dual-wavelength parametric test [34], (ii) detection of whole-scale spectra at each temperature, for example, detection of isoelliptic and isosbestic points [12, 23, 33], and (iii) so-called *singular value decomposition* (SVD) analysis which allows us to detect the presence of kinetically stable intermediate species in the process of quadruplex formation [12, 35]. The dual-wavelength parametric test and detection of isoelliptic and isosbestic points gave ambiguous results concerning a two-state mechanism of quadruplex unfolding (not shown). Only the *TEL1-ran*, *TEL1-3-5-TTA-18*, and *TEL-5-A-7* oligomers used in this work show signs of two-state melting behavior, therefore the result of van't Hoff enthalpy, entropy, and Gibbs energy change, summarized in Table 2, are provided for information purposes and might be verified by microcalorimetry.

The effect of quadruplex destabilization by tails could be partially explained with analogy to a negatively charged head and a whip. Local thermal fluctuations cause a different movement of the tail and of the head of quadruplex in solution, which can result in a destabilization of the proximal G-tetrad, Figure 3. It appears that 5′-tail destabilizes *TEL1* slightly more than 3′-overhanging nucleotides, Table 2. This fact confirms that the folding topology of human quadruplexes, the arrangements of DCR and EW loops in (3 + 1) hybrid conformers, governs a structural stability of G-quadruplex. It seems that the melting temperature and other thermodynamic parameters are affected by protruding nucleotides. However, it is impossible to describe the destabilization effect using simple formulae, because the effect depends on at least two factors: (i) the sequence of overhanging sequence and (ii) the length of DNA overhanging. The random overhanging sequence of *TEL-ran* presented here provides a noteworthy effect. Its melting temperature is comparable with *TEL1-5-TTA-18* oligomer of the same nucleotide size, but the shift of the main CD peak towards lower wavelengths is more evident in comparison with other sequences, Figure 1. The *TEL2* oligomer also shows destabilization, although the CD spectrum is in principle equivalent to *TEL1*. The CD spectrum of *TEL2* agrees with the spectrum obtained by Petraccone at al. for $(TTAG_3)_8TT$ [31], where the CD spectrum of the dimer

Table 2: Thermodynamic parameters obtained from CD and UV melting curves. UV melting curves were obtained at ~293 nm in the presence of 50 mM KCl. Values in which a two-state mechanism was clearly confirmed by dual-wavelength parametric test are highlighted by bold font.

Oligomer	Protrusion [nt.]	CD				UV			
		T_m [°C]	ΔH [kcal · mol^{-1}]	ΔS [cal·mol^{-1}·K^{-1}]	ΔG^{o}_{37} [kcal · mol^{-1}]	T_m [°C]	ΔH [kcal · mol^{-1}]	ΔS [cal·mol^{-1}·K^{-1}]	ΔG^{o}_{37} [kcal · mol^{-1}]
TEL1	0–0	64.7	59.3	207	4.9	65.3	58.8	205	4.9
TEL2	0-3-0	55.9	**39.5**	135	2.3	55.3	34.0	116	1.9
5′-overhang									
TEL1-5-TTA	3–0	57.6	57.9	198	3.6	57.8	58.7	201	3.7
TEL1-5-T-7	7–0	53.6	51.4	174	2.6	50.6	39.2	132	1.6
TEL1-5-A-7	7–0	54.8	**39.0**	133	2.1	56.0	41.8	143	2.4
TEL1-5-T-11	11–0	55.1	51.6	175	2.8	54.9	60.7	206	3.3
TEL1-5-TTA-11	11–0	54.8	50.6	172	2.7	53.9	58.1	197	3.0
TEL1-5-T-18	18–0	51.2	43.4	143	1.9	nd	nd	nd	nd
TEL1-5-TTA-18									
293 nm	18–0	51.0	**42.4**	137	1.8	nd	nd	nd	nd
263 nm		52.3	**42.8**	144	2.0	nd	nd	nd	nd
3′-overhang									
TEL1-3-TTA	0–3	59.6	55.9	193	3.8	58.9	61.6	212	4.1
TEL1-3-T-7	0–7	56.8	52.8	181	3.2	55.4	59.1	201	3.3
TEL1-3-A-7	0–7	59.8	50.5	174	3.5	59.3	50.7	175	3.4
TEL1-3-T-11	0–11	57.9	57.5	197	3.6	56.1	26.8	92	1.6
TEL1-3-TTA-11	0–11	57.7	55.5	190	3.5	57.1	46.8	160	2.8
TEL1-3-T-18	0–18	53.4	45.8	155	2.3	nd	Nd	nd	Nd
3′- and 5′-overhangs									
TEL1-3-5-T-7	7–7	47.5	55.9	186	1.8	48.3	39.5	132	1.4
TEL1-3-5-A-7	7–7	51.3	46.8	158	2.1	52.6	52.4	179	3.1
TEL1-ran 263 nm	14–4	53.5	**37.5**	127	1.9	nd	Nd	nd	nd
TEL1-3-5-TTA-18									
290 nm	18–18	40.5	49.5	161	0.5	nd	nd	nd	nd
265 nm		40.9	**37.6**	129	0.5	nd	nd	nd	nd

closely matches the sum of the CD spectra of hybrid 1 and hybrid 2 monomers. According to the analysis of human telomeric quadruplex multimers by molecular dynamics, it has been shown that quadruplexes behave as two independent subunits connected by a TTA linker. The TTA linker loop also loses all of its original conformational features and becomes extended [36]. Therefore, we suggest here that when two thermodynamically equivalent quadruplex units of *TEL1* in *TEL2* connected by a TTA loop are exhibited to thermal fluctuations in solution, the proximal guanines in G-tetrads might be preferentially destabilized in comparison with *TEL1* oligomer. Our suggestion is also supported by previous studies where there is shown that the number of TTAG3 repeats influences the quadruplex thermostability and enthalpy [26]. 5′-protruding nucleotides partially model the end of telomere. We can extrapolate our results and suggest that the 5′-overhanging sequence forces contiguous G-quadruplex to fold into conformers where the positive CD signal at 265–270 nm, originally only being a shoulder in *TEL1*, is dominant. This can be compared to the "mild" crowding condition, in which DNA oligomer is forced to fold into similar conformers at the presence of potassium and certain concentration of PEG [30, 37].

Interestingly, the van't Hoff enthalpies for *TEL1-ran* and *TEL1-3-5-TTA-18* agree with the calorimetric measurements obtained for *TEL1* [35]. However, Antonacci et al. reported an unfolding process involving a three-state mechanism for the sequence $(TTAGGG)_4$ with a total enthalpy change of two transitions ranging from 32.1 to 36.3 $kcal \cdot mol^{-1}$ depending on salt concentration; two clear transitions were clearly distinguished. The difference between melting temperatures of both transitions is about 12°C. One of the possible explanations why we observe a process that fits a two-state mechanism is as follows. Based on CD melting experiments at different wavelengths we are suggesting that unpaired overhangs decrease the melting temperature difference which does not allow distinguishing between the transitions. It could mean that in solution there either occur two topological isoforms with the same mobilities before temperature unfolding and similar unfolding energies or a transition of one topological structure is governed by a three-state mechanism but with proximal melting temperatures. Recently we have discussed in detail a similar effect observed for intermolecular and intramolecular G-quadruplexes formed from various G-rich repetitive sequences, two melting curves at different wavelengths and at least two electrophoretic bands [24]. Therefore, we presume that "tailed" monomolecular quadruplexes might occur in two different structural forms with the same electrophoretic mobility, and the melting process in each of them is governed by a two-state mechanism as illustrated by the example of *TEL1-3-5-TTA-18* where two different enthalpy values of 49.5 and 37.6 are reported in Table 2.

4. Conclusions

The human overhanging sequence on the 3′-end consists of 100–200 nucleotides forming G-quadruplexes [2, 3]. 21 nucleotides are consumed in the formation of one quadruplex subunit and three additional nucleotides are necessary for the connection of two neighboring quadruplexes. Therefore, the end of telomere can contain no more than 4–8 tandem quadruplexes.

The favorable formation of a G-quartet stack is enthalpy-driven, and this favorable enthalpy is compensated by an unfavorable entropy contribution, consistent with the immobilization of counterions [37]. A decrease in degree of freedom is normally associated with the entropy changes. Overhanging sequences at 3′- and/or 5′-end cause a decrease in the degree of freedom of DNA folding; this effect is the most evident for longer quadruplex protrusions and can be compared with the *TEL2* oligomer, however, in case the protruding sequence again consists of telomeric repeats able to form an additional quadruplex structure [26]. Our results confirm that the 3′- and 5′-overhangs in human telomeric quadruplexes are not equivalent due to the arrangement of DCR and EW loops.

Abbreviations

DCR: Double-chain-reversal loop
EW: Edgewise loops
nt: Nucleotide
PEG: Polyethylene glycol.

Acknowledgments

This study was supported by grants from the Slovak Grant Agency (1/0153/09), the Science and Technology Assistance Agency (APVT-20-006604), and COST action MP0802. The authers would like to thank L. Sieber and G. W. Cowper for a critical paper proofreading.

References

[1] N. Grandin and M. Charbonneau, "Protection against chromosome degradation at the telomeres," *Biochimie*, vol. 90, no. 1, pp. 41–59, 2008.

[2] M. J. McEachern, A. Krauskopf, and E. H. Blackburn, "Telomeres and their control," *Annual Review of Genetics*, vol. 34, pp. 331–358, 2000.

[3] G. N. Parkinson, M. P. H. Lee, and S. Neidle, "Crystal structure of parallel quadruplexes from human telomeric DNA," *Nature*, vol. 417, no. 6891, pp. 876–880, 2002.

[4] D. Sun, B. Thompson, B. E. Cathers et al., "Inhibition of human telomerase by a G-quadruplex-interactive compound," *Journal of Medicinal Chemistry*, vol. 40, no. 14, pp. 2113–2116, 1997.

[5] J.-L. Mergny and C. Hélène, "G-quadruplex DNA: a target for drug design," *Nature Medicine*, vol. 4, no. 12, pp. 1366–1367, 1998.

[6] J. A. Londoño-Vallejo, "Telomere instability and cancer," *Biochimie*, vol. 90, no. 1, pp. 73–82, 2008.

[7] C. Granotier, G. Pennarun, L. Riou et al., "Preferential binding of a G-quadruplex ligand to human chromosome ends," *Nucleic Acids Research*, vol. 33, no. 13, pp. 4182–4190, 2005.

[8] K. Paeschke, S. Juranek, T. Simonsson, A. Hempel, D. Rhodes, and H. J. Lipps, "Telomerase recruitment by the telomere end binding protein-β facilitates G-quadruplex DNA unfolding in

ciliates," *Nature Structural and Molecular Biology*, vol. 15, no. 6, pp. 598–604, 2008.

[9] N. Smargiasso, F. Rosu, W. Hsia et al., "G-quadruplex DNA assemblies: loop length, cation identity, and multimer formation," *Journal of the American Chemical Society*, vol. 130, no. 31, pp. 10208–10216, 2008.

[10] Y. Wang and D. J. Patel, "Solution structure of the human telomeric repeat $d[AG_3(T_2AG_3)_3]$ G-tetraplex," *Structure*, vol. 1, no. 4, pp. 263–282, 1993.

[11] J. Li, J. J. Correia, L. Wang, J. O. Trent, and J. B. Chaires, "Not so crystal clear: the structure of the human telomere G-quadruplex in solution differs from that present in a crystal," *Nucleic Acids Research*, vol. 33, no. 14, pp. 4649–4659, 2005.

[12] R. D. Gray, J. Li, and J. B. Chaires, "Energetics and kinetics of a conformational switch in G-quadruplex DNA," *Journal of Physical Chemistry B*, vol. 113, no. 9, pp. 2676–2683, 2009.

[13] R. D. Gray and J. B. Chaires, "Kinetics and mechanism of K^+- and Na^+-induced folding of models of human telomeric DNA into G-quadruplex structures," *Nucleic Acids Research*, vol. 36, no. 12, pp. 4191–4203, 2008.

[14] A. T. Phan, V. Kuryavyi, K. N. Luu, and D. J. Patel, "Structure of two intramolecular G-quadruplexes formed by natural human telomere sequences in K^+ solution," *Nucleic Acids Research*, vol. 35, no. 19, pp. 6517–6525, 2007.

[15] A. Ambrus, D. Chen, J. Dai, T. Bialis, R. A. Jones, and D. Yang, "Human telomeric sequence forms a hybrid-type intramolecular G-quadruplex structure with mixed parallel/antiparallel strands in potassium solution," *Nucleic Acids Research*, vol. 34, no. 9, pp. 2723–2735, 2006.

[16] J. Dai, C. Punchihewa, A. Ambrus, D. Chen, R. A. Jones, and D. Yang, "Structure of the intramolecular human telomeric G-quadruplex in potassium solution: a novel adenine triple formation," *Nucleic Acids Research*, vol. 35, no. 7, pp. 2440–2450, 2007.

[17] K. W. Lim, S. Amrane, S. Bouaziz et al., "Structure of the human telomere in K^+ solution: a stable basket-type G-quadruplex with only two G-tetrad layers," *Journal of the American Chemical Society*, vol. 131, no. 12, pp. 4301–4309, 2009.

[18] Y. Xue, Z.-Y. Kan, Q. Wang et al., "Human telomeric DNA forms parallel-stranded intramolecular G-quadruplex in K^+ solution under molecular crowding condition," *Journal of the American Chemical Society*, vol. 129, no. 36, pp. 11185–11191, 2007.

[19] K. W. Zheng, Z. Chen, Y. H. Hao, and Z. Tan, "Molecular crowding creates an essential environment for the formation of stable G-quadruplexes in long double-stranded DNA," *Nucleic Acids Research*, vol. 38, no. 1, pp. 327–338, 2009.

[20] D. Renčiuk, I. Kejnovská, P. Školáková, K. Bednářová, J. Motlová, and M. Vorlíčková, "Arrangements of human telomere DNA quadruplex in physiologically relevant K^+ solutions," *Nucleic Acids Research*, vol. 37, no. 19, pp. 6625–6634, 2009.

[21] Q. Guo, M. Lu, and N. R. Kallenbach, "Effect of thymine tract length on the structure and stability of model telomeric sequences," *Biochemistry*, vol. 32, no. 14, pp. 3596–3603, 1993.

[22] J. D. Schonhoft, R. Bajracharya, S. Dhakal, Z. B. Yu, H. B. Mao, and S. Basu, "Direct experimental evidence for quadruplex-quadruplex interaction within the human ILPR," *Nucleic Acids Research*, vol. 37, no. 10, pp. 3310–3320, 2009.

[23] J.-L. Mergny, A.-T. Phan, and L. Lacroix, "Following G-quartet formation by UV-spectroscopy," *FEBS Letters*, vol. 435, no. 1, pp. 74–78, 1998.

[24] V. Víglaský, L. Bauer, and K. Tlučková, "Structural features of intra- and intermolecular G-quadruplexes derived from telomeric repeats," *Biochemistry*, vol. 49, no. 10, pp. 2110–2120, 2010.

[25] B. J. Bassam and P. M. Gresshoff, "Silver staining DNA in polyacrylamide gels," *Nature Protocols*, vol. 2, no. 11, pp. 2649–2654, 2007.

[26] M. Vorlíčková, J. Chládková, I. Kejnovská, M. Fialová, and J. Kypr, "Guanine tetraplex topology of human telomere DNA is governed by the number of (TTAGGG) repeats," *Nucleic Acids Research*, vol. 33, no. 18, pp. 5851–5860, 2005.

[27] D. M. Gray, J.-D. Wen, C. W. Gray et al., "Measured and calculated CD spectra of G-quartets stacked with the same or opposite polarities," *Chirality*, vol. 20, no. 3-4, pp. 431–440, 2008.

[28] J. Kypr, I. Kejnovská, D. Renčiuk, and M. Vorlíčková, "Circular dichroism and conformational polymorphism of DNA," *Nucleic Acids Research*, vol. 37, no. 6, pp. 1713–1725, 2009.

[29] A. T. Phan, K. N. Luu, and D. J. Patel, "Different loop arrangements of intramolecular human telomeric (3+1) G-quadruplexes in K^+ solution," *Nucleic Acids Research*, vol. 34, no. 19, pp. 5715–5719, 2006.

[30] D. Miyoshi, A. Nakao, and N. Sugimoto, "Molecular crowding regulates the structural switch of the DNA G-quadruplex," *Biochemistry*, vol. 41, no. 50, pp. 15017–15024, 2002.

[31] L. Petraccone, J. O. Trent, and J. B. Chaires, "The tail of the telomere," *Journal of the American Chemical Society*, vol. 130, no. 49, pp. 16530–16532, 2008.

[32] A. N. Lane, J. B. Chaires, R. D. Gray, and J. O. Trent, "Stability and kinetics of G-quadruplex structures," *Nucleic Acids Research*, vol. 36, no. 17, pp. 5482–5515, 2008.

[33] J. B. Chaires, "Human telomeric G-quadruplex: thermodynamic and kinetic studies of telomeric quadruplex stability," *FEBS Journal*, vol. 277, no. 5, pp. 1098–1106, 2010.

[34] P. Wallimann, R. J. Kennedy, J. S. Miller, W. Shalongo, and D. S. Kemp, "Dual wavelength parametric test of two-state models for circular dichroism spectra of helical polypeptides: anomalous dichroic properties of alanine-rich peptides," *Journal of the American Chemical Society*, vol. 125, no. 5, pp. 1203–1220, 2003.

[35] C. Antonacci, J. B. Chaires, and R. D. Sheardy, "Biophysical characterization of thehuman telomeric (TTAGGG)4 repeat in a potassium solution," *Biochemistry*, vol. 46, no. 15, pp. 4654–4660, 2007.

[36] H.-Q. Yu, D. Miyoshi, and N. Sugimoto, "Characterization of structure and stability of long telomeric DNA G-quadruplexes," *Journal of the American Chemical Society*, vol. 128, no. 48, pp. 15461–15468, 2006.

[37] C. M. Olsen, W. H. Gmeiner, and L. A. Marky, "Unfolding of G-quadruplexes: energetic, and ion and water contributions of G-quartet stacking," *Journal of Physical Chemistry B*, vol. 110, no. 13, pp. 6962–6969, 2006.

SAGE-Hindawi Access to Research
Journal of Nucleic Acids
Volume 2010, Article ID 525862, 19 pages
doi:10.4061/2010/525862

Review Article

"*One Ring to Bind Them All*"—Part I: The Efficiency of the Macrocyclic Scaffold for G-Quadruplex DNA Recognition

David Monchaud,[1,2] Anton Granzhan,[1] Nicolas Saettel,[1] Aurore Guédin,[3,4] Jean-Louis Mergny,[4] and Marie-Paule Teulade-Fichou[1]

[1] *Section Recherche, Institut Curie, CNRS UMR176, Centre Universitaire Paris XI, Batiment 110, 91405 Orsay, France*
[2] *Institut de Chimie Moléculaire, CNRS UMR5260, Université de Bourgogne, 21000 Dijon, France*
[3] *Acides Nucléiques : Dynamique, Ciblage et Fonctions Biologiques, Laboratoire des Régulations et Dynamique du Génome, CNRS, UMR5153, INSERM U565, Muséum National d'Histoire Naturelle USM 503, 43 Rue Cuvier, 75005 Paris, France*
[4] *Institut Européen de Chimie et Biologie, INSERM U869, Université de Bordeaux, 33607 Pessac Cedex, France*

Correspondence should be addressed to Marie-Paule Teulade-Fichou, mp.teulade-fichou@curie.fr

Received 29 January 2010; Accepted 18 February 2010

Academic Editor: R. Eritja

Macrocyclic scaffolds are particularly attractive for designing selective G-quadruplex ligands essentially because, on one hand, they show a poor affinity for the "standard" B-DNA conformation and, on the other hand, they fit nicely with the external G-quartets of quadruplexes. Stimulated by the pioneering studies on the cationic porphyrin TMPyP4 and the natural product telomestatin, follow-up studies have developed, rapidly leading to a large diversity of macrocyclic structures with remarkable-quadruplex binding properties and biological activities. In this review we summarize the current state of the art in detailing the three main categories of quadruplex-binding macrocycles described so far (telomestatin-like polyheteroarenes, porphyrins and derivatives, polyammonium cyclophanes), and in addressing both synthetic issues and biological aspects.

1. Introduction

G-rich DNA strands are naturally involved in duplex-DNA architecture through association with their complementary C-rich DNA strands by the canonical Watson-Crick pairing [1–3]. However, a growing body of evidence currently testifies that this canonical association is not the unique mode of stabilization of G-rich DNA in cells. Indeed, given that four guanine residues can self-associate in a planar arrangement through a Hoogsteen-type hydrogen-bonding network [4] to form a structure called G-quartet, G-rich strands can adopt a peculiar three-dimensional arrangement called G-quadruplex DNA [5–9] resulting from the stacking of several contiguous G-quartets (Figure 1).

The formation of G-quadruplex DNA is easily conceivable in DNA sequences that are present as single strands in cells, such as the telomeric overhang. The structural and functional integrity of this overhang is based on its association with a constellation of specific proteins, some of them belonging to the shelterin complex [10]. Altogether, this nucleoproteic assembly caps the chromosomes, protects their integrity, and is also deeply involved in the telomeric replication process [11–13]. Numerous studies currently suggest that quadruplex formation in this overhang alters the structure and function of telomeres, inducing a damage response and rapid apoptosis in particular in cancer cells [14–24]. Thus, over the past decade telomeric G-quadruplex DNA has been thoroughly studied with an initial focus on the possible interferences with telomerase activity [25].

The existence of G-quadruplex DNA is also heavily implied in the promoter region of genes and oncogenes, and is thus assumed to play an important regulatory role in their transcription [26]. It has been indeed demonstrated that the involvement of G-rich sequences in duplex architecture is compatible with their folding into quadruplex structures, thanks to the breathing of duplex DNA [27]. Nevertheless, we have to keep in mind that these G-quadruplex-forming

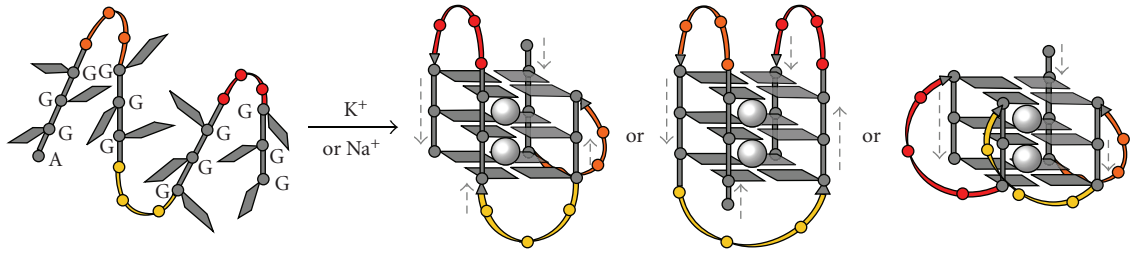

FIGURE 1: Schematic representation of the folding of an oligonucleotide that mimics the human telomeric sequence ($d[AG_3(T_2AG_3)_3]$). The polymorphism of the quadruplex is represented through the various possible structures, namely, the hybrid (left), antiparallel (centre), and parallel (right) forms; these structures differ by strand orientation (grey dashed arrows) and loop arrangement (represented in orange, yellow, and red).

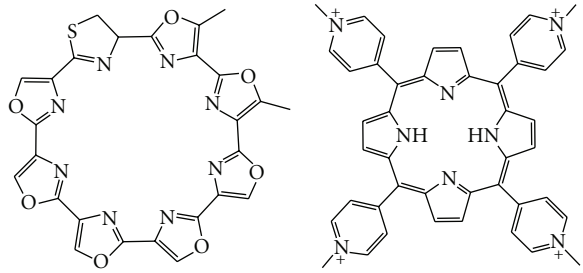

Telomestatin **TMPyP4**

(a) (b)

FIGURE 2: Chemical structures of **telomestatin** and **TMPyP4** (with p-$CH_3(C_6H_4)SO_3^-$ as counterions).

sequences although transiently single-stranded are *a priori* not as easily accessible as the telomeric sequences, due to the presence of the transcription machinery [28].

Stabilization of quadruplex architecture by small molecules is thus emerging as a potential anticancer approach since it is thought to interfere with oncogenic expression and telomeric maintenance in cancer cells [11–13]. Interestingly, several classes of small molecules have been developed that efficiently target G-quadruplex DNA [29–32]. Among them, macrocycles rapidly became popular for recognition of quadruplexes motivated by the fact that **telomestatin** is one of the most active known G-quadruplex ligands [33]. This natural 8-ring 24-membered macroheterocycle (Figure 2) displays high affinity for quadruplex and most importantly has no affinity for duplex DNA (*vide infra*). Nevertheless, apart from several reports on **telomestatin**-like molecules, true polyheteroaryl analogues are still scarce, essentially because of the difficulty to synthesise such molecules. Another well-known G-quadruplex ligand—and arguably one of the most studied—is **TMPyP4** [34, 35], a tetramethylpyridinium porphyrin (Figure 2). This molecule has been widely used, essentially due to its great affinity for several quadruplex targets, as well as its commercial availability. However, the interest in employing **TMPyP4** is somewhat counterbalanced by its lack of quadruplex selectivity (*vide infra*).

These two examples illustrate the main reasons that made the macrocyclic scaffold particularly interesting for targeting G-quadruplex DNA: (i) a broad aromatic surface that favours the stacking interactions with the external G-quartets of the quadruplex, (ii) a rigid structure that maximizes the quartet overlap and, combined with their large size, impedes intercalation into duplex DNA, and (iii) in the case of **TMPyP4**, a cationic charge that promotes the electrostatic interactions with the negatively charged biopolymer. Unfortunately, the high cationic charge of **TMPyP4** represents both an advantage and a drawback due to the nonspecificity of electrostatic interactions which promote association with any form of DNA, but in particular duplex DNA, thereby decreasing the binding selectivity (*vide infra*).

A great deal of research effort around the macrocyclic scaffold was thus motivated by these two examples. The macrocyclic systems described up to now as G-quadruplex ligands can be divided in three different categories: (i) **telomestatin** like (i.e., neutral and rigid macrocycles), (ii) porphyrin (**TMPyP4**) like (i.e., cationic and rigid macrocycles), and (iii) the less studied family of **flexible polyammonium macrocycles** (i.e., cationic and non planar), which will be described herein also in the companion paper, "*One Ring to Bind Them All*"—Part II, by A. Granzhan et al.) in the present issue.

2. Telomestatin-Like Macrocycles

Telomestatin is the benchmark compound in terms of G-quadruplex recognition (Figure 2). This natural compound was isolated from *Streptomyces anulatus* in 2001 by Shinya's group [33], and has been extensively studied due to its outstanding selectivity for G-quadruplex and highly promising biological properties.

One general method to quantify the DNA affinity of a given molecule is to perform thermal denaturation experiments, either in a UV-monitored melting assay [36] or in the so-called "FRET-melting" assay. Here the thermal unfolding of the quadruplex-forming oligonucleotide F21T (*FAM*-$G_3[T_2AG_3]_3$-*Tamra*), doubly labelled with a complementary pair of FRET donor and acceptor (*FAM*: 6-carboxyfluorescein and *Tamra*: 6-carboxytetramethylrhodamine), is monitored *via* FRET (*fluorescence resonance*

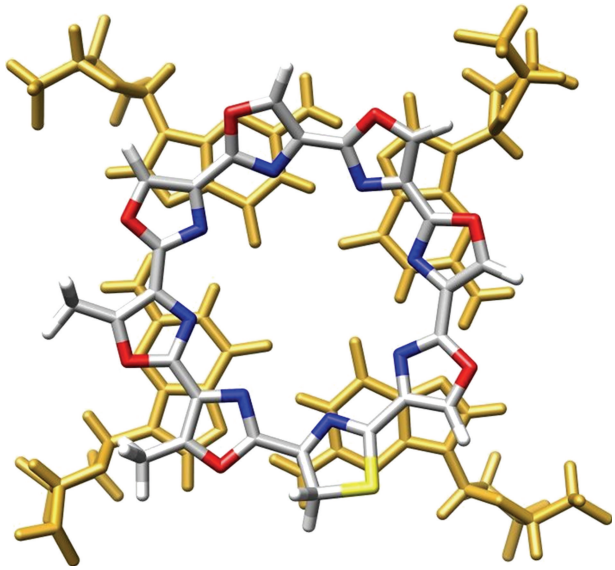

Figure 3: Qualitative in silico superposition of **telomestatin** and a G-tetrad (extracted from PDB entry: 2A5R); guanine residues appear in gold; the carbon, nitrogen, oxygen, sulphur, and hydrogen atoms of **telomestatin** appear in grey, blue, red, yellow, and white, respectively.

energy transfer) [37]. Semiquantitative evaluation of ligand-binding affinity is obtained by measuring the increase in melting temperature induced by the ligand ($\Delta T_{1/2}$). The quadruplex-over-duplex-DNA selectivity may then be established *via* competitive FRET melting which is carried out in presence of competitive duplex DNA (ds26). In the presence of **telomestatin**, the increase in melting temperature is very large ($\Delta T_{1/2} = 24^{\circ}$C), and since this value is unaffected by the presence of up to 50 equiv. of competitive duplex DNA (herein ds26, the self-complementary sequence 5′-$CA_2TCG_2ATCGA_2T_2CGATC_2GAT_2$G-3′), **telomestatin** stands among the most selective of G-quadruplex ligands. This property has been subsequently confirmed by independent studies using various evaluation techniques.

The enthusiasm for **telomestatin** was also justified by its ability to inhibit telomerase [38], with the reported IC_{50} value lying, impressively, in the nanomolar range (IC_{50}-TRAP = 5 nM) [33]. However, the relationship between TRAP assay and telomerase inhibition was recently challenged on the grounds that this assay does not actually reflect the influence of the ligand on the activity of the enzyme but rather the ability of the ligand to inhibit the PCR amplification step [25]. The direct assay, a more constraining method based on the telomerase elongation of a telomeric primer with incorporation of [α-^{32}P]dGTP, provides a more reliable estimation of the telomerase inhibition ability [25]. Interestingly, **telomestatin** is still highly active, staying among the best reported inhibitors, with an IC_{50} value of 58 nM.

The structure of **telomestatin** is quite unusual since it is a neutral polycyclic compound, composed of five oxazole, two methyloxazole, and one thiazoline rings, whose overall flatness is impeded by the presence of an sp^3 carbon within the thiazoline ring (Figure 2). Whether this molecule is aggregated in water is yet not known; however, it is likely that the strong hydrophobic character of the molecule should reinforce the hydrophobic forces that contribute to stacking interactions, and so explain its exceptional effectiveness in binding G-quadruplex. This efficiency is also assumed to rely on a perfect shape adaptation between the macrocycle and a G-quartet (Figure 3) [39].

Abundant biophysical and biological investigations have been performed with **telomestatin**. For example, it exhibits an antiproliferative activity against a wide variety of cancer cell lines with IC_{50} values between 0.1 and 5 μM, including human pancreatic carcinoma [40], myeloid leukaemia [41, 42], breast cancer [43], cervical [43], tumoral HT1080 [44], telomerase-transformed SW39 [45], ALT-transformed SW26 [45], immortalized EcR293 [46], and a panel of myeloma [47] and neuroblastoma lines [48]. Remarkably, **telomestatin** does not affect normal cell lines, with no effect observed at 5 μM on fibroblast MRC-5 cells [43]. This observation has recently been substantiated by the finding that **telomestatin** does not interfere with telomere replication in normal cells [49]. **Telomestatin** was also a tool of choice to investigate the biological role of G-quadruplex ligands in cells by suggesting that effects of ligands might originate essentially from the disruption of the telomeric structure with subsequent displacement of protective proteins (shelterin complex) rather than in telomerase inhibition [44, 46]. **Telomestatin** was used to investigate the role of putative quadruplex formation within the promoter region of genes like VEGF [50] and hTERT [51] or oncogenes like c-Myc [52], Bcl-2 [53], and RET [54], whose corresponding proteins are overexpressed in some cancers. Recently, **telomestatin** was shown to interfere with the ability of helicases to unwind G-quadruplex structures [55], and to affect the growth of telomerase-negative ALT (Alternative Lengthening of Telomeres) cell lines via an indirect interaction with a proteinic complex comprised of the shelterin component TRF2, the helicase BLM, and the enzyme Topoisomerase IIIα [56]. The reason why **telomestatin**—or more generally G-quadruplex ligands—selectively affects tumour cell lines is yet not fully understood. However, differences in plasmic membrane permeability between normal and cancer cells or in the accessibility of the telomere and in particular variations in the composition of the shelterin complex have been proposed; even if the accessibility is identical, one can imagine that the cellular responses are different.

Unexpectedly, only two studies have addressed in detail the actual binding mode of **telomestatin** to G-quadruplex using in silico investigations [57, 58]. This is particularly surprising, given that there are no structural characterizations of this interaction (NMR, X-ray crystallography) available to date. These studies support concomitant double endstacking on quartets, with a preference for the parallel conformation of the human telomeric quadruplex. This conclusion is somewhat in contradiction with those of other studies based on CD spectroscopy [59] or ^{125}I-radioprobing [60], underlining that further efforts are required to clarify the interaction mode of **telomestatin** with quadruplexes.

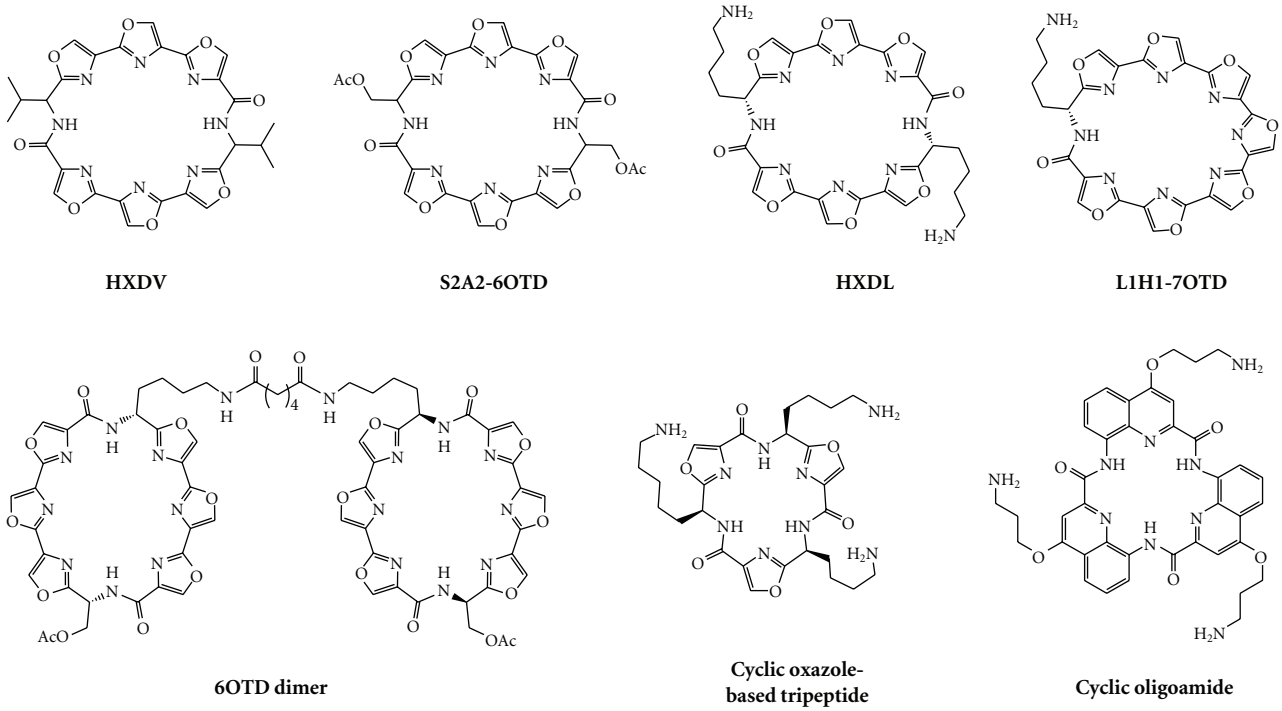

Figure 4: Chemical formulae of **telomestatin**-related macrocycles.

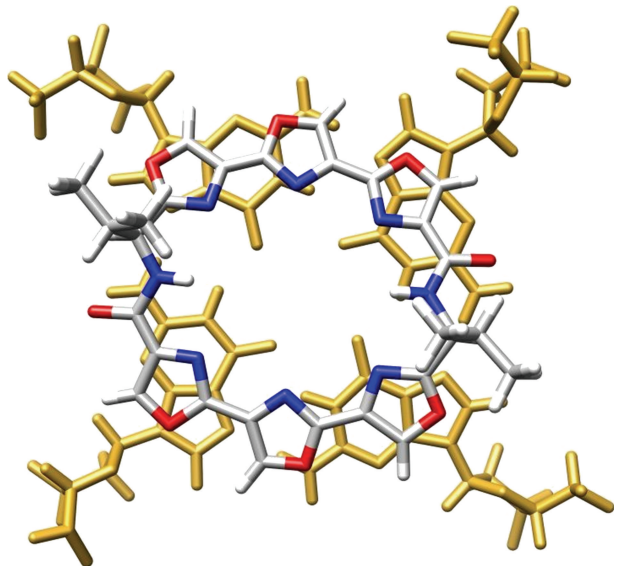

Figure 5: Qualitative in silico superposition of **HXDV** and a G-tetrad (extracted from PDB entry: 2A5R); guanine residues appear in gold, the carbon, nitrogen, oxygen, and hydrogen atoms of **HXDV** in grey, blue, red and white, respectively.

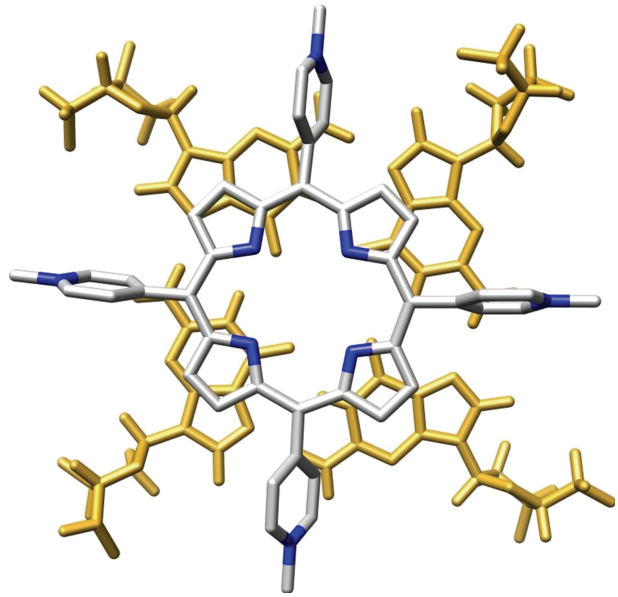

Figure 6: Interaction of **TMPyP4** and a G-tetrad (adapted from PDB entry: 2A5R); guanine residues appear in gold; the carbon, nitrogen, oxygen, and hydrogen atoms of **TMPyP4** appear in grey, blue, red, and white, respectively.

Nevertheless, one major concern is that **telomestatin** is difficult to synthesise. Despite considerable synthetic efforts to obtain either fragments of **telomestatin** or **telomestatin**-like arrays of polyoxazoles [61–65], its total synthesis has been reported only recently [66], and the complexity of the proposed pathway is incompatible with large-scale preparation. This can explain why, whilst the excellence of **telomestatin** towards quadruplex-recognition can hardly be exaggerated, relatively few reports on **telomestatin**-like compounds have appeared in the literature. Among them, two hexaoxazole macrocyclic ligands have been independently reported by Rice et al. [67, 68] and by Shin-ya, Nagasawa

et al. [69]. The structure of these macrocycles was based on the dimeric association of two symmetrical trioxazole moieties through an amino-acid linker, either a valine (for **HXDV**, Figure 4) or a protected serine (for **S2A2-6OTD**, Figure 4), respectively.

HXDV has been widely investigated and found to profoundly stabilize the telomeric G-quadruplex structure by UV-melting assay ($\Delta T_m = 24^\circ C$), without any significant binding to duplex DNA [67, 68]. Its association with a quadruplex-forming sequence mimicking the human telomeric sequence has recently been confirmed to be based on external stacking, with occupancy of both external G-quartets. Interestingly, the high quadruplex selectivity of **HXDV** is assumed to originate from its particular **telomestatin**-like concave shape since the two planes defined by the trioxazole moieties present an angle of ~30°, along with the disposition of the two amino-acid residues on the same face of the cycle, thereby optimizing stacking interaction with quartets (Figure 5) [39]. The biological effects of **HXDV** have been investigated on human lymphoblastoma (RPM1) and murine leukaemia (P388) cell lines, with IC_{50} values for inhibition of the population doubling in the low micromolar range (0.4 and 0.5 μM, resp.) [67, 68]. Very interestingly, it has also been shown recently that **HXDV** elicits antiproliferative effect on both telomerase-positive (HeLa, A875, PC3-1 with IC_{50} between 0.2 and 0.6 μM) and telomerase-negative cell lines (like SAOS2 or GM847 with IC_{50} between 0.4 and 0.5 μM) mainly through an M-phase inhibitory effect, thereby contributing to the elucidation of the actual biological effects of G-quadruplex ligands [70].

Interestingly, to circumvent the solubility problems, various **HXDV** derivatives have been prepared based on the modification of the nature of the side chain(s), from two valine residues (for **HXDV**), to only one valine [71], one valine and one protected lysine (**HXLV-AC**) [72], and two lysine residues (**HXDL**, Figure 4) [73]. Of all these derivatives, **HXDL** appeared as the most promising, whilst it is not neutral at physiological pH (due to protonation of both terminal amine groups, whose pK_a values are estimated as 9.9 and 10.5) [74] and the characteristics of its association with quadruplex are impressive in terms of both affinity ($\Delta T_m = 49^\circ C$) and selectivity, since only residual stabilization of salmon testes duplex-DNA is observed. This gain in efficiency is assumed to originate in a higher solubility and in enhanced interactions with quadruplex-DNA, mixing both tetrad-stacking and electrostatic interactions.

The success obtained with **HXDL** was concomitantly—and independently—confirmed by Nagasawa et al., who developed a series of G-quadruplex binding macrocyclic hexaoxazoles (6OTD for 6-Oxazole **Telomestatin** Derivatives). The very first example of this series, **S2A2-6OTD** (Figure 4), [69] was rapidly surpassed by more active compounds, in which the serine residues of the side chain were replaced by lysine (**L2H2-6OTD,** also called **HXDL** by Rice et al.) or arginine residues (**L2G2-6OTD**) [75]. Both compounds were found to be active in vitro in a range similar to that of **telomestatin**, notably via PCR stop assay (IC_{50} down to 0.64 μM), TRAP assay (IC_{50} down to 20 nM), and inhibition of the growth of HeLa cells (IC_{50} down to 0.5 μM). Current strategies for improvement include the dimerisation of the 6OTD scaffold (**6OTD dimer**, Figure 4) [76], using a bisamide linker between the two 6OTD moieties, which is long enough to span the thickness of the quadruplex architecture (~15 Å). Unexpectedly the affinity of the dimer so obtained is not significantly increased as compared with the corresponding monomer, as judged by FRET-melting data (ΔT_m = 25.1 versus 25.0°C, resp.) and PCR stop assays (IC_{50} = 3.0 versus 2.9 μM, resp.). On the other hand, the dimer is more selective than the monomer since a ~10-fold improvement is obtained when comparing the inhibitory IC_{50} values measured by PCR stop assay allowing the authors to claim a 800-fold selectivity. The fact that the dimer is able to form a unique 1 : 1 complex with G-quadruplex, as shown by ESI-MS analysis, added to a proven inability to interact with duplex-DNA, implies that this dimeric scaffold is optimized for quadruplex recognition. Further improvement was found by replacing the hexaoxazole scaffold by the more planar heptaoxazole analogue (**L1H1-7OTD**, Figure 4) [77]. This compound was shown to interact strongly with quadruplex DNA (as judged by PCR stop assay, IC_{50} = 0.67 μM), with a fair quadruplex-over-duplex DNA selectivity (~8-fold). Furthermore, it displays a selective cytotoxicity toward telomerase-positive cells (HeLa, IC_{50} = 2.2 μM) as compared to telomerase-negative cells (Saos-2, $IC_{50} > 30\,\mu$M). It is thus highly probable that a dimeric version of the 7OTD scaffold will appear in a near future and that it will help this scaffold to improve its quadruplex-over-duplex DNA selectivity.

Other series of oxazole-based macrocycles have been investigated as G-quadruplex binders and notably macrocycles whose structure is based on a trisoxazole [78], trisfuran, or tetrafuran scaffolds [79] (Figure 4). Amino-terminated chains have been introduced to improve water solubility and favour electrostatic interactions with DNA (the pK_a values of the amino side chains depicted in Figure 4 standing in the 8.8–10.7 range) [74], with the chain length finely tuned to reach the quadruplex grooves. The intrinsic qualities of these compounds have been evaluated through FRET-melting assay, and whilst modest results were obtained with the oxazole-based tripeptide ($\Delta T_{1/2} = 6.4^\circ C$), moderate ($\Delta T_{1/2} = 10^\circ C$) to good ($\Delta T_{1/2} = 17^\circ C$) results were obtained with furan-based tri- and tetrapeptides, respectively. Interestingly, when performed with duplex DNA, no stabilization occurred in any case, thus inferring a high quadruplex-selectivity of this series of ligands. But a real breakthrough was achieved in increasing the aromatic surface of the ligands, since stabilizations higher than 30°C were obtained with the aminoquinoline-based **cyclic oligoamide** depicted in Figure 4 [80, 81]. Once more, this compound retains a high selectivity for quadruplex DNA, since no stabilization was detected when a FRET-melting assay was performed with duplex hairpin-DNA. It is worth noting that this compound is also able to discriminate various types of quadruplex DNA (human telomeric versus oncogenic c-kit), thus opening perspectives for discovery of a novel generation of selective and specific G-quadruplex ligands. Additionally, the very attractive in vitro biophysical results were also

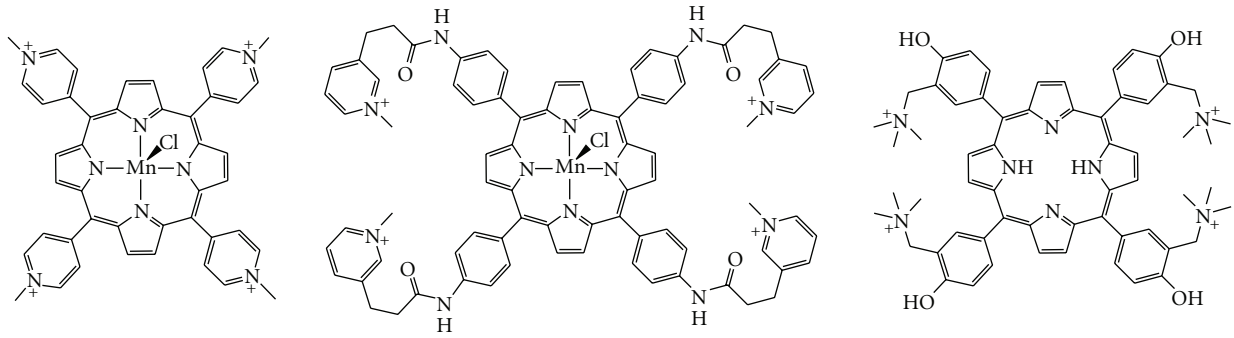

Figure 7: Chemical formulae of porphyrin-based G-quadruplex ligands.

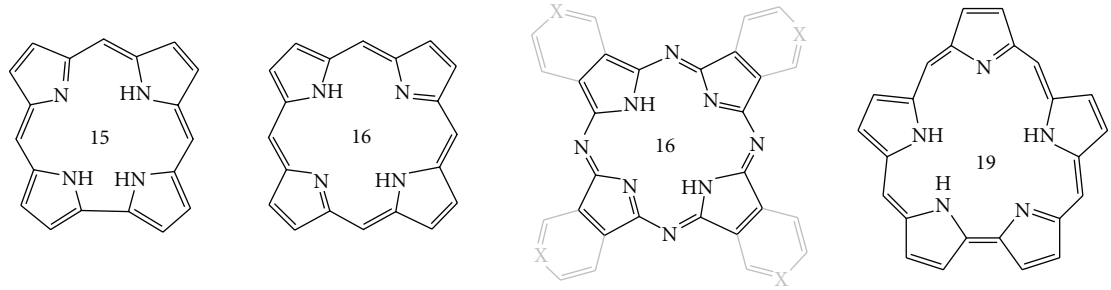

Figure 8: Polyheterocyclic macrocyclic cores used in the structures of G-quadruplex ligands. The number in the center corresponds to the number of atoms in the central ring.

complemented by the low general cytotoxicity of the cyclic oligopeptides.

Despite the real viability of the neutral macrocyclic scaffold for G-quadruplex recognition, the equilibrium between hydrosolubility and activity is difficult to achieve. One improvement has been the introduction of amino side chains that increase water-solubility and electrostatic attraction with the DNA target without altering the duplex-versus-quadruplex selectivity of the ligand, which relies on the shape and rigidity of the polyhetroaryl cyclic scaffold itself. Such molecular designs have thus to be further investigated, in order to gain more insights in terms of bioavailability and selective cytotoxicity.

3. Porphyrin- (TMPyP4-) Like Macrocycles

Along with neutral and cationic cyclic polyheteroarenes, cationic porphyrins are probably the most widely used macrocyclic G-quadruplex ligands. **TMPyP4** (for 5,10,15,20-tetra(*N*-methyl-4-pyridyl)porphyrin) [34, 35] is a representative example of this family of ligands (Figures 2 and 6) [39]. The ability of **TMPyP4** to interact with DNA was first mentioned 30 years ago [82–84] whilst its use as a G-quadruplex ligand was reported for the first time twenty years later [34, 35, 85]. Since these seminal reports, this tetracationic porphyrin has been extensively studied: it has demonstrated a high affinity for G-quadruplex DNA (as monitored by FRET-melting assay, $\Delta T_{1/2} = 17^{\circ}$C) [86], but with low selectivity [86–91]. **TMPyP4** has been particularly used as a tool to investigate the possibility of downregulating the expression of genes due to quadruplex formation or induction (like c-myc [92–100], RET [54], HIF-1α [101], VEGF [50, 102, 103], Bcl-2 [53, 104, 105], KRAS [106], PDGF-A [107], c-kit [108], and even hTERT genes [51]). The biological behaviour of **TMPyP4** has also been investigated in vitro against a broad variety of tumor cell lines (with IC_{50} between 23 and 310 μM), including human pancreatic [40], breast [85], and prostate carcinomas [85], lymphoma [85], retinoblastoma [109], leukaemia [110] and human gastrointestinal stromal tumor [108] cell lines, as well as telomerase-transformed SW39 [45], ALT-transformed SW26 [45], transformed human breast [85] and HeLa cell lines [111]. **TMPyP4** has also been tested on normal cell lines (human fibroblast and breast cell lines) [85], in which it demonstrated moderate to acute cytotoxicity (IC_{50} down to 13 μM). It has also been used as an in vitro tool for more prospective and fundamental studies [112–115], sometimes exhibiting some unexpected behaviour, including quadruplex-unfolding activity on both quadruplex-forming DNA (d(CGG) repeats [116], or antithrombin

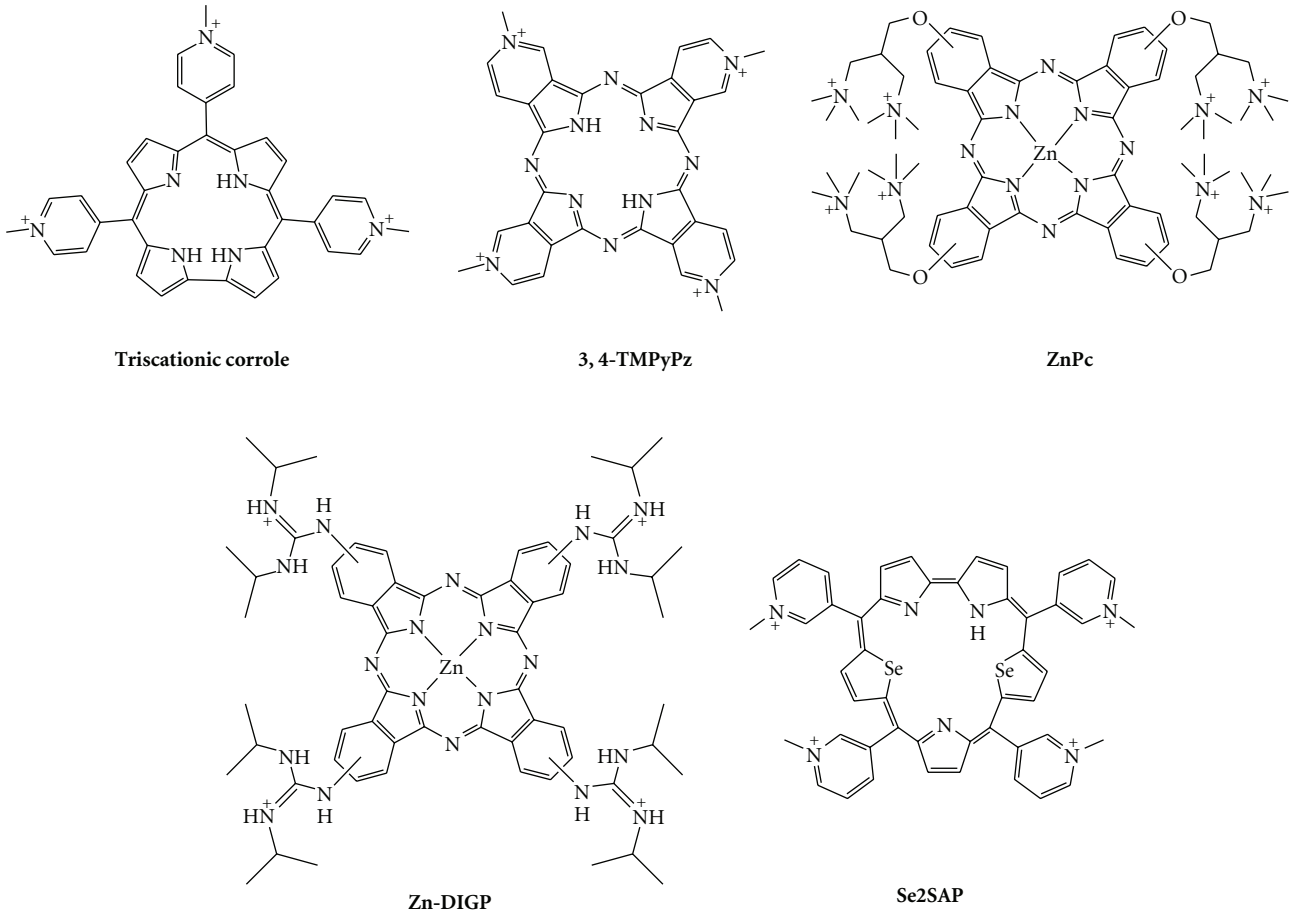

Figure 9: Chemical structures of corrole-, porphyrazine-, phthalocyanine-, and sapphyrin-based G-quadruplex ligands.

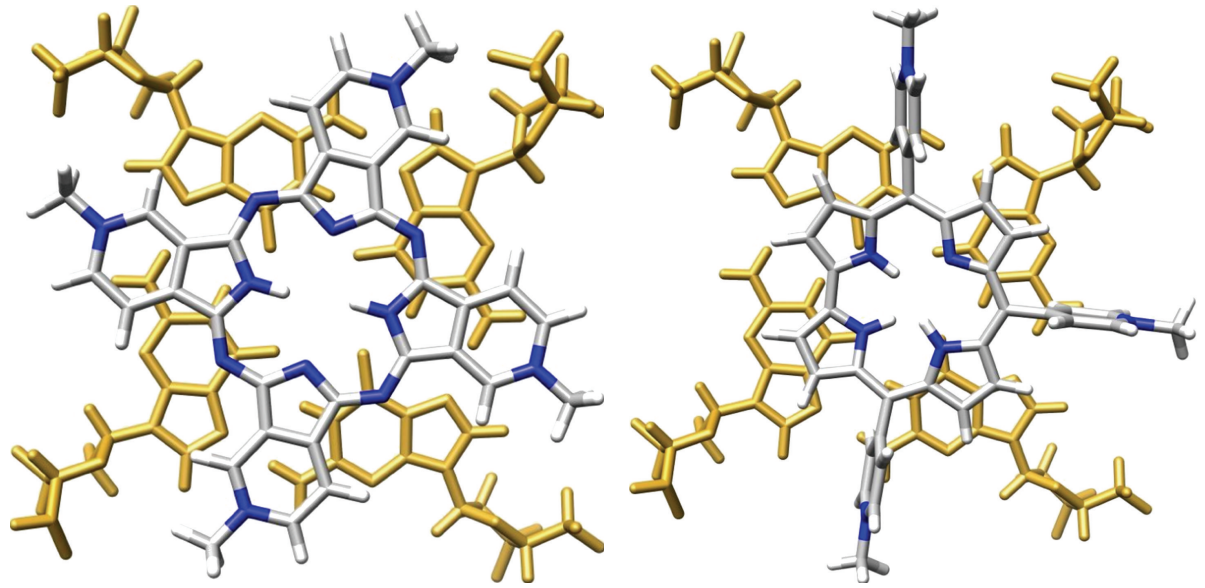

Figure 10: Qualitative in silico superposition of **3,4-TMPyPz** (a) and **corrole** (b) and a G-tetrad (extracted from PDB entry: 2A5R); guanine residues appear in gold; the carbon, nitrogen, oxygen, and hydrogen atoms of the ligands in grey, blue, red, and white, respectively.

aptamer) [117] and RNA sequences (r(CGG) repeats) [118].

Interestingly, despite the fact that it was quickly acknowledged that **TMPyP4** has poor selectivity for quadruplex structures [86–91], this ligand is still the focus of an intense research interest. Notably, a lot of structural studies are currently undertaken to investigate its binding mode with quadruplex DNA; interestingly, **TMPyP4** displays various quadruplex-interactions, ranging from intercalation between adjacent G-quartets (as suggested via Raman spectroscopy studies) [119] to the more expected stacking on the external G-quartet (demonstrated by NMR studies) [120], passing by a mode totally devoid of direct contacts with G-quartets (shown by X-ray analysis of obtained crystal structures) [121], without excluding the possibility of combining several binding modes during a single recognition process (*vide infra*). These efforts are also currently completed by investigations dedicated to the understanding of the nature of the interaction between **TMPyP4** and G-quadruplex, either in silico [100, 122, 123] or *via* established biophysical methods, UV-Vis [105], steady-state or time-resolved fluorescence [124–127], CD [128–130] or Raman spectroscopies [119], as well as ITC [99, 131–133], ESI-MS [134], DSC [135], SPR [90], or even HPLC methods [136], on a broad variety of quadruplex architectures, for example, telomeric [90, 119, 125, 127, 128, 130–133, 135], c-myc [99], c-kit [108], Bcl-2 [105, 134], TBA [136], the bimolecular $(G_4T_4G_4)_2$ [124], or the tetramolecular $(TG_4T)_4$ quadruplexes [126], and even G-wires [129]. Nevertheless, it is worth pointing out that a vast majority of these studies have been carried out in in vitro conditions that have to be considered as "dilute" as compared to the crowded environment within a living cell (due to the presence of naturally occurring proteins, nucleic acids, sugars, etc.). Interestingly, when the conditions are artificially crowded (using molecular crowding agents such as ethylene glycol [130] or poly(ethylene glycol) [125, 132], **TMPyP4** displays a higher affinity (for quadruplex-DNA) [125, 130] and selectivity (with regard to duplex DNA) [132] than in dilute conditions, on the basis of a different recognition process (the crowded conditions influencing both the quadruplex DNA structures and the **TMPyP4** stacking interactions, becoming multiple but stepwise [125, 132]). Given that crowded conditions are more biologically relevant, these results indicate that **TMPyP4** may be more selective than anticipated in cells, and these observations will certainly revitalize **TMPyP4**-related researches.

Thus, the current status of **TMPyP4** is the opposite of **telomestatin**; it is both commercially and synthetically accessible and its interaction with quadruplexes, although multiple, is fully characterized. Finally, the simple geometric comparison allowed by the overlaps shown in Figures 3 and 6 strongly suggests that the tetrapyrrolic macrocycle is much less suitable than the octacyclic ring for optimizing aromatic-aromatic interactions with a G-quartet. In conclusion, although **TMPyP4** remains an interesting tool that has contributed to the understanding of the ligand–quadruplex interactions and to their complexity, its biological use for probing the involvement of quadruplex in biological assays is questionable.

With an inner cavity particularly suited to coordination of a metal, **TMPyP4** (and other porphyrins, *vide infra*) has been also widely exploited to form metal complexes. Given the well-known modulation of DNA association by metallation, this modification was thus performed in order to improve the DNA recognition [82–84]. **TMPyP4** has now been used to prepare Pt(II), Cu(II), In(III), Zn(II), Co(II), Fe(III), Ni(II), Mn(III), Mg(II), and Pd(II) complexes [34, 137–142]. Among them, **Mn-TMPyP4** (Figure 7) deserves particular attention since it showed a strong improvement in terms of quadruplex-versus-duplex selectivity.

The porphyrin core, as clearly demonstrated with **TMPyP4**, has been extensively explored as a macrocyclic scaffold for the design of G-quadruplex ligands. Among the numerous examples that have been reported, either as metal free or in a complexed state, the most interesting ligands are presented in Figure 7. Even if the methods for analyzing G-quadruplex affinity and selectivity are not yet standardised, the nature of the side arms that surround the porphyrin core is unmistakably crucial. Indeed, while the above mentioned **Mn-TMPyP4** was able to interact with G-quadruplex 10 times faster than with duplex DNA, a 10,000-fold difference was obtained by moving the *N*-methylpyridinium moieties from the close vicinity of the porphyrin core to the termini of flexible arms [143]. This modification is assumed to greatly improve the electrostatic interaction with quadruplex grooves, while impeding intercalation into duplex DNA. This kinetic difference was evaluated through biosensor-surface plasmon resonance (SPR) measurements. The SPR technique, based on the use of surface-immobilized oligonucleotides, enables a quantitative analysis of the binding parameters, that is, thermodynamic (equilibrium constant, Gibbs energy of binding, and stoichiometry) and kinetic (k_{on}/k_{off}) parameters of the interaction of small molecules with the target DNA [90, 144]. In the present case, the affinity constant determined with duplex DNA lies in the $10^4\,M^{-1}$ range, reaching up to $10^8\,M^{-1}$ with quadruplex-DNA. Even if more modest, similar observations were made with **TQMP**, a porphyrin in which *N*-methylpyridinium substituents were replaced by (trimethylammonium)methylphenol arms (Figure 7) [91]. In this case, an ~100-fold difference in the kinetics of the association with duplex ($10^4\,M^{-1}\cdot s^{-1}$ range) and quadruplex DNA ($10^6\,M^{-1}\cdot s^{-1}$ range) was obtained. Finally, knowing that the nature and number of the surrounding side arms can be finely tuned in the case of **TMPyP4** [145, 146], interesting perspectives exist to modify porphyrin-based G-quadruplex ligands in this way. It is, however, worth noting that the equilibrium between affinity and selectivity is difficult to access with the **TMPyP4** scaffold, as demonstrated by a recent study in which a **TMPyP4**-related compound was included in a high-order supramolecular architecture (ruthenium coordination cubes) [147], on the basis of the elegant idea to use the metal itself to build the macrocyclic scaffold [148]. These cubic complexes were indeed shown to strongly bind not only quadruplex-DNA but also duplex-DNA, despite their peculiar molecular volume. This lack of selectivity may originate in their highly cationic nature (eight positive charges).

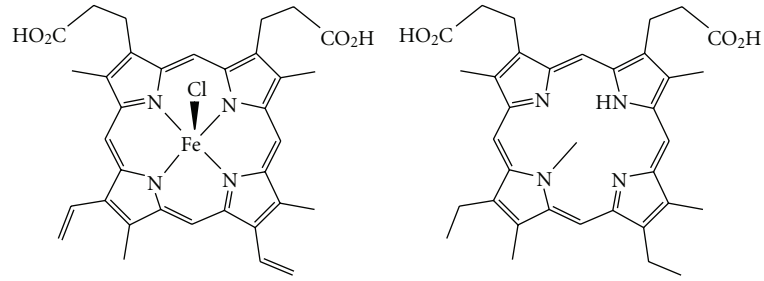

Hemin (a) **NMM** (b)

Figure 11: Chemical formulae of **Hemin** (a) and **NMM** (b).

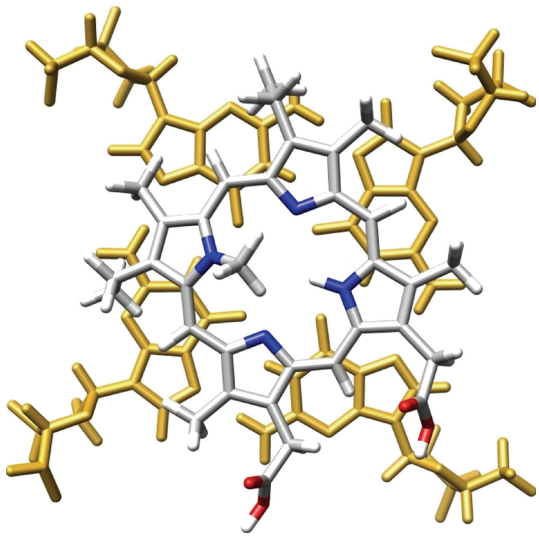

Figure 12: Qualitative in silico superposition of **NMM** and a G-tetrad (extracted from PDB entry: 2A5R); guanine residues appear in gold; the carbon, nitrogen, oxygen, and hydrogen atoms of **NMM** in grey, blue, red, and white, respectively.

A large number of structural analogues of **TMPyP4** have been recently described in the literature, differing notably by the nature of the side-arms (*N*-methylpyridinium groups have, for example, been replaced by *N*-propylpyridinium [126], *N*-methylquinolinium [149], and phenyl groups with short [150] or long aminoalkyl arms [151], and even endowed with fluorescent reporters) [152]. The extensive family of ring-size analogues of the 16-membered porphyrins are exemplified in Figure 8, including the 15-membered corrole, 16-membered phthalocyanine or porphyrazine, and the 19-membered sapphyrin, which have all been employed for the construction of G-quadruplex ligands.

Corroles are tetrapyrrolic macrocyclic structures, lacking one bridging sp^2 carbon with respect to porphyrins. Interestingly, the resulting **TMPyP4** analogue, which is substituted with *N*-methylpyridium groups (Figure 9) [153], is only trisubstituted, with a peculiar spatial disposition of pyridinium moieties relative to each other (Figure 10) [39]. This corrole efficiently stabilizes quadruplex DNA, as judged from CD-melting experiments (T_m increase of 36°C), with a fair selectivity, judged by SPR measurements (affinity constants in the range of 10^5 and $10^6\,M^{-1}$ for duplex- and quadruplex-DNA, resp.). Copper corroles have also been studied and proved to be good stabilizing agents for quadruplexes formed from sequences of both the human telomere and the c-myc promoter [154]. Porphyrazine, the polyaza tetra(pyrrolopyridine) analogue of porphyrin (Figures 8 and 9), has also been widely used in the design of G-quadruplex ligands, because of its steric properties (close to those of the porphyrin), but also because its synthesis opens novel perspectives for structural diversity. It enables, for example, to fuse the pyridinium moieties with the cyclic scaffold, thereby leading to a flat, electron-deficient and structurally frozen macrocycle, with an excellent overlap of a G-tetrad (Figure 10) [39]. **3,4-TMPyPz**, used either as metal-free or as Zn complex, shows a high affinity and selectivity for quadruplex DNA, as demonstrated by UV-Vis and SPR experiments (affinity constants in the range of $10^6\,M^{-1}$ for quadruplex DNA and $<10^5$ for duplex-DNA), with a refined binding mode, since a unique binding site was determined using both of these techniques [155]. It is worth noting that **3,4-TMPyPz** has also been used as a tool to investigate the role of G-quadruplex ligands in a totally telomere-independent mechanism, that is, an innovative gene-silencing strategy based on the control by a G-quadruplex ligand of the dicing of quadruplex-forming short hairpin RNAs that actively participate to the RNA interference (RNAi) pathway [156].

Phthalocyanines are structurally close to porphyrazines, with the pyridine rings that compose the porphyrazine scaffold replaced by benzene rings. The zinc phthalocyanine complex **ZnPc** (Figure 9) [157, 158] carries the classical amino side chains in the close vicinity of the macrocyclic scaffold. The results are interesting, since they demonstrate that a highly charged compound (up to 8 positive charges), whilst presenting an expected high degree of quadruplex affinity, can concomitantly retain a satisfactory level of selectivity (on the basis of SPR and CD-melting data), the difference in kinetic parameters with duplex-versus-quadruplex DNA being in the range of one order of magnitude. When the aminoalkyl side arms of **ZnPc** are

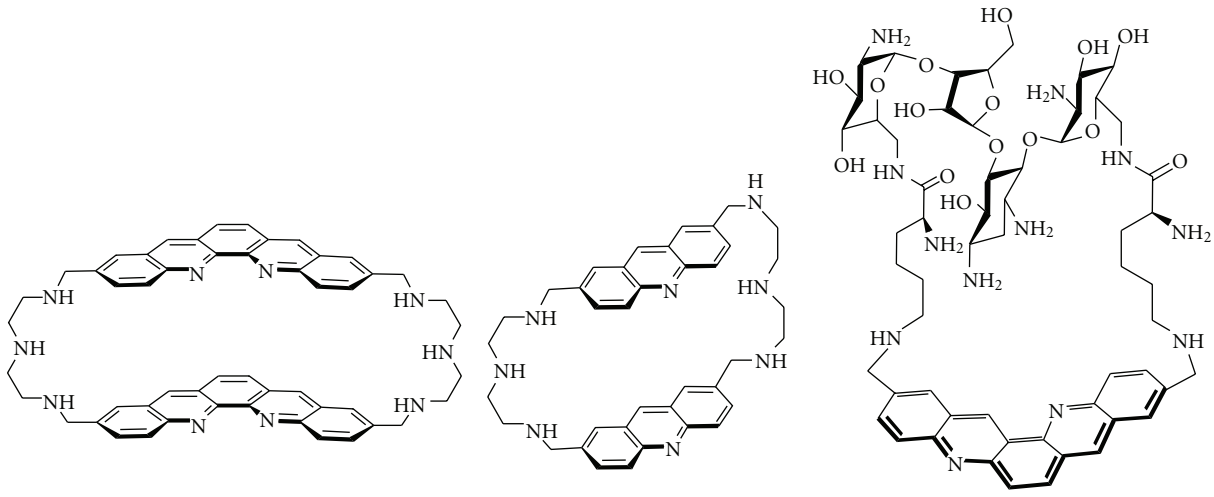

(a) (b) (c)

Figure 13: Chemical formulae of nonplanar macrocyclic G-quadruplex ligands: **BOQ$_1$** (a), **BisA** (b), and the neomycin-capped scaffold **NCQ** (c).

replaced by guanidinium moieties, the corresponding **Zn-DIGP** (for tetrakis-(diisopropylguanidinio) zinc phthalocyanine, Figure 9) elicits quite exceptional properties, both in terms of quadruplex affinity (K_d < 2 nM for c-myc quadruplex) and quadruplex-versus-duplex DNA selectivity (**Zn-DIGP** displays a 5000-fold higher affinity for c-myc quadruplex than for calf thymus DNA). In addition, **Zn-DIGP** exhibits "turn-on" fluorescent properties, making it a particularly interesting quadruplex-selective dye [159]. Very recent studies have substantiated the interest in this series of molecules, confirming their good cellular uptake and inhibition of promoter-quadruplex-mediated genes (KRAS) [160].

The expanded diselenosapphyrin **Se2SAP** (Figure 9) represents a novel class of chemically challenging compounds but with a very interesting ability to interact only with its preferential target, the oncogenic c-myc-derived quadruplex [52, 59]. Indeed, **Se2SAP** discerns, firstly, among the DNAs of various nature (duplex and quadruplex DNA, with a selectivity factor of ~600 as judged by a competitive Taq polymerase assay), and secondly, among quadruplex DNA of various structures (**Se2SAP** binds specifically c-myc, as compared to human telomeric quadruplex, but displays also a higher affinity for the quadruplex found in the promoter region of VEGF) [102]. The substitution of nitrogen by selenium atoms in the backbone of the ligand was motivated by the decrease of the known photocytotoxicity of the porphyrins, as confirmed by the low general cytotoxicity of **Se2SAP** in HeLa cells (no effect at 200 μM dose). One major drawback to the use of **Se2SAP** in cells stands in its limited bioavailability, which remains to be improved for further biological investigations.

A further noteworthy family of porphyrins is **hemin** and related compounds. **Hemin**, also known as Fe(III)-protoporphyrin IX (Figure 11), is the oxidized version of heme (Fe(II)-protoporphyrin IX), widely known as a cofactor of hemoglobin (and myoglobin) that actively participates in the reversible binding of dioxygen. Since the pioneering work of Sen et al. [161–165], **hemin** is known to bind tightly to quadruplex architecture; however, **hemin** has not been investigated as a G-quadruplex ligand per se, but has been thoroughly investigated for its DNAzyme activity when bound to quadruplex. Indeed, the **hemin**/quadruplex complex acquires the ability to catalyze the H_2O_2-mediated oxidation of precursors such as ABTS (2,2′-azino-bis(3-ethylbenzothiozoline-6-sulfonic acid) [161–165], luminol [166–168], or TMB (3,3′,5,5′-tetramethylbenzidine) [169, 170], therefore causing an easily detectable color change. This particular activity has found numerous applications, including the detection of telomerase activity [167, 168], single-stranded DNA [171], SNP (single-nucleotide polymorphism) [172], DNA [173] and DNA analytes [174], proteins (like nucleolin [175], lysozyme [176], or thrombin [177]), various cations (such as Cu^{2+} [169], Hg^{2+} [178, 179], Pb^{2+} [180], or K^+) [181], or enzyme cofactors (like L-histidine) [180], as well as a use for constructing DNA logic gates [182, 183], and it has been also implied in the development of novel in vitro assays for screening G-quadruplex ligands [184, 185].

A hemin-related porphyrin, **NMM** (or *N*-methyl mesoporphyrin IX) has also been thoroughly investigated for its ability to interact with G-quadruplex. **NMM** (Figure 11) is interesting as the unique representative of the negatively charged macrocyclic G-quadruplex ligands (its two carboxylic groups being deprotonated at physiological pH) [74, 186–188]. **NMM** was initially studied since it behaves as stable transition-state analogue for ferrochelatase enzyme, which catalyzes the insertion of Fe^{2+} ions into protoporphyrin in the final step of the heme biosynthesis [161–165]. Whilst **NMM** became rapidly known as highly quadruplex

selective [87, 189], it was only sparingly studied due to a moderate affinity for its DNA target, despite an excellent overlap with the G-tetrad (Figure 12). However, in recent studies in yeast, it has shown a very interesting ability to control the regulation of genes in direct connection with the probability of quadruplex formation in their promoters [190, 191]. Additionally, given that the effect of **NMM** is felt at both telomeres and loci throughout the genome, this study provides novel lines of evidence of the possible in vivo roles of G-quadruplexes. Finally, **NMM** has also been used as a novel tool for isolating G-quadruplex DNA from a mixture of nucleic acids derived from in vivo sources, *via* its grafting on a sepharose resin, thus offering an innovative way to determine whether or not the in silico detected putative quadruplex-forming sequences (QFSs) [192–194] exist in the cellular context as quadruplex DNA [195].

4. Polyammonium Cyclophane-Type Macrocycles

As compared to the **telomestatin**, porphyrins, and related compounds, polyammonium cyclophane-type macrocycles have not been extensively studied as G-quadruplex ligands. Mainly two types of cyclophane-like macrocycles have been studied for their interaction with quadruplexes: the cyclobisintercalator family (CBI, Figure 13) and the neomycin-capped aromatic platforms (exemplified by **NCQ**, Figure 13).

The CBI macrocycles contain two flat aromatic units, usually derived from simple intercalators linked together by polyamine chains. This particular scaffold is highly soluble at physiological pH thanks to protonation of the four benzylic nitrogen atoms of the linkers [196]. With regard to DNA binding, the CBIs present unique features that are (i) a strong association with DNA bases *via* aromatic π-π interactions and (ii) a very low affinity for duplex-DNA. This family of compounds has already been studied for its recognition of various unusual DNA structures, mainly mismatch-containing DNA [197–200], abasic sites [201], and trinucleotide repeats [202]. However, only two members of this family, namely, **BOQ$_1$** (for Bis-Ortho-Quinacridine, Figure 13) [203–205] and **BisA** (for Bis-Acridine, Figure 13), [206] have been already evaluated for their ability to interact with quadruplex-DNA.

BisA and more particularly **BOQ$_1$** display promising G-quadruplex-binding properties. Both compounds are composed of two large polycyclic aromatic moieties, namely, acridine [207–209] or quinacridine [210–212], that enable efficient π-stacking interactions with nucleic bases in particular guanines [213]. These dimeric macrocycles were found to bind much better to quadruplexes than their planar monomeric acyclic counterparts [203–206]. This strong association has been demonstrated by numerous techniques, including FRET-melting assay, SPR, and equilibrium dialysis: **BOQ$_1$** and **BisA** efficiently induce thermal stabilization of the human telomeric quadruplex ($\Delta T_{1/2}$ = 28 and 15°C, resp.) displaying high affinity for this target ($K_a = 1.2 \times 10^7\,M^{-1}$ for **BOQ$_1$** measured by SPR and $1.1 \times 10^5\,M^{-1}$ for **BisA**, estimated by dialysis) [203–206]. The difference between the two compounds clearly demonstrates the importance of the size of the aromatic unit in the binding interaction with the quadruplex structure.

Most interestingly the two compounds exhibit a high selectivity for quadruplex over duplex DNA attributed to their particular topology. CBIs are clearly distinct from the planar rigid macrocycles mentioned precedently since they exist in a semiclosed conformation with the two aromatic units facing each other in more or less parallel planes (Figures 13 and 14) [39]. This particular nonplanar conformation impedes binding to duplex-DNA, both for steric reasons and because the length of the linkers does not enable bisintercalation between contiguous base pairs due to the neighbour-exclusion principle [214, 215]. In the case of **BOQ$_1$**, this particular topology was found both in the free state (Figures 14(a)–14(c)) and in the complex formed with the human telomeric quadruplex (Figure 14(d)) [205], meaning that there is little conformational change upon binding. This would suggest that the ligand is already preorganized to fit into the quadruplex target resulting in a gain in the binding entropy. In addition, the modelling studies performed both with the telomeric and with the c-myc quadruplex demonstrate that the semiclosed conformation of **BOQ$_1$** enables interaction *via* a mixed binding mode, combining G-quartet and loop (Figure 14(d), c-myc not shown) [205]. In fact, careful examination of this complex strongly suggests the occurrence of electrostatic and H-bonding interactions between the linkers and the loop backbone (Figure 14(d)).

The second category of polyammonium cyclophane-type macrocycles, namely, the neomycin-capped macrocycles was developed with the goal to validate the ditopic interactive design. To this aim three aromatic platforms (acridine, phenanthroline, and quinacridine) able to stack on a G-quartet were combined with a well-known loop-binding motif, that is, the aminoglycoside neomycin. The most active prototype of this series is the quinacridine derivative **NCQ** shown in Figure 13 [216, 217]. This ligand that has a high degree of molecular flexibility is a potent binder of the telomeric quadruplex as shown by the FRET melting assay ($\Delta T_{1/2}$ = 15°C) whereas it elicits a poor affinity for duplex-DNA. Most importantly **NCQ** elicits a high degree of selectivity for looped quadruplex (i.e., intramolecular telomeric quadruplex), compared with the tetramolecular quadruplex lacking the loop motifs. The preference for intramolecular over tetramolecular quadruplexes confirms the potential of the multitopic approach and altogether this work proposes a new innovative design for achieving intra-quadruplex selectivity. Subsequent studies have since then fully supported this approach using various G-quadruplex recognition scaffolds, including a macrocyclic oxazole-based tripeptide [218] or a small-molecule ligand (acridine) [219] equipped with loop and/or groove recognition elements like carbohydrates [218] or peptides [219].

In conclusion, polyammonium cyclophane-type macrocycles have been only sparingly studied as G-quadruplex ligands. They are able to establish various types of interaction with their DNA target, thereby opening the innovative perspective of a selective interaction with quadruplex DNA

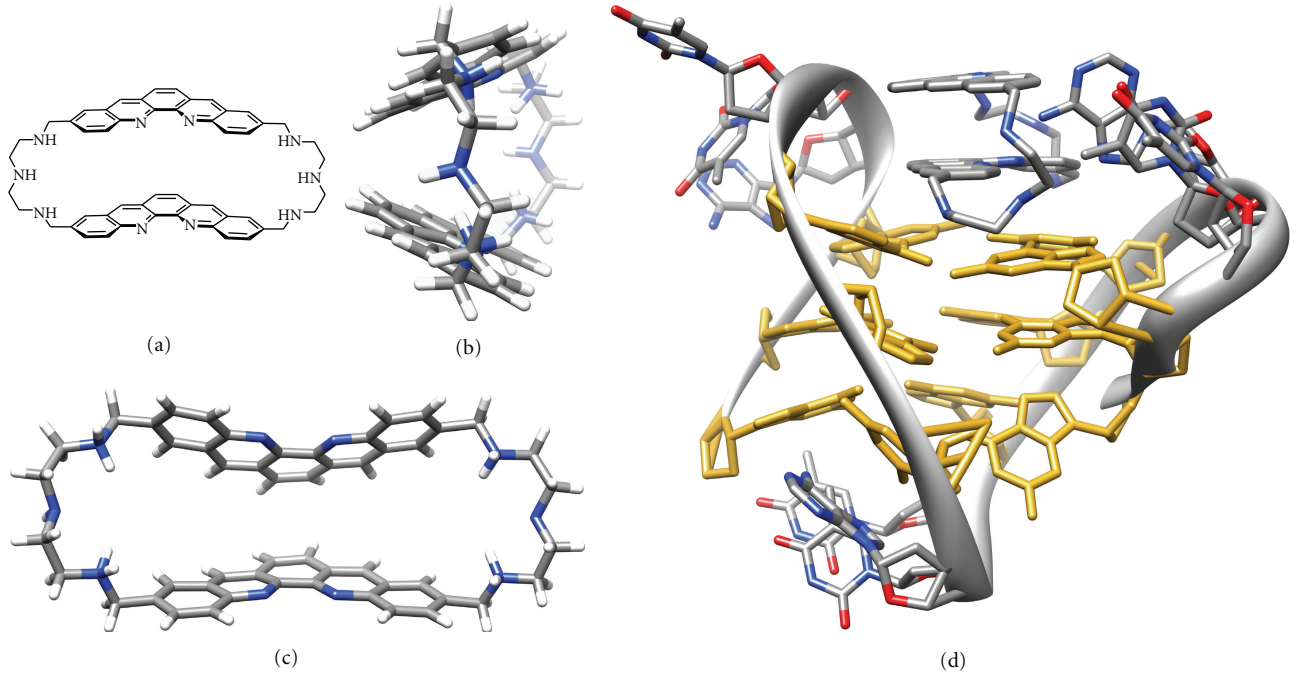

FIGURE 14: Structure of **BOQ$_1$** (a), side (b), and front views (c) of the lowest-energy conformation during the molecular dynamic simulation (see [39]) and modelled interaction between **BOQ$_1$** and the human telomeric quadruplex ((d), see [205]); guanine residues appear in gold; the carbon, nitrogen, oxygen, and hydrogen atoms appear in grey, blue, red, and white, respectively.

as a function of the nature of the quadruplex structure itself. This intra-quadruplex selectivity, motivated by the putative presence of quadruplexes at various genomic localizations (*vide supra*), is one of the major issues that will have to be addressed in the near future. The results previously obtained with CBIs and presented herein, although limited to a few examples, are promising. On this solid basis, an extensive study of binding of CBIs to G-quadruplex has been undertaken which is further reported in the companion paper ("*One Ring to Bind Them All*"—Part II, by A. Granzhan et al.), a research article in the present issue.

5. Conclusion

Macrocyclic scaffolds are particularly attractive for designing selective G-quadruplex ligands essentially for the two following reasons: on one hand, they show a poor affinity for the "standard" B-DNA conformation, due to their sterically difficult intercalation between the base pairs of the double helix; on the other hand, in contrast, they fit nicely with the external G-quartets of quadruplexes that constitute accessible planar sites of large aromatic area. Although synthetic accesses to macrocycles are often difficult, this chemical class is nevertheless a fascinating tool that can be chemically engineered to generate new biological properties. The few macrocyclic families depicted herein have only begun to mine this incredible potential and we hope that the present article will be helpful to understand what the crucial guidelines are to control their efficiencies and selectivities for recognizing quadruplexes.

Acknowledgments

The authors would like to thank sincerely their coworkers for the synthetic work and stimulating scientific discussions related to G-quadruplex DNA and ligands; a particular acknowledgment will be dedicated to A. De Cian, M. Kaiser, and L. Lacroix. The authors are also grateful to all of the collaborators who contributed to the works and to all of their colleagues worldwide whose works are described herein. A special acknowledgment is dedicated to J. R. R. Tolkien for the title inspiration and to J. Martin for careful reading of the manuscript.

References

[1] J. D. Watson and F. H. C. Crick, "Molecular structure of nucleic acids: a structure for deoxyribose nucleic acid," *Nature*, vol. 171, no. 4356, pp. 737–738, 1953.

[2] M. H. F. Wilkins, A. R. Stokes, and H. R. Wilson, "Molecular structure of nucleic acids: molecular structure of deoxypentose nucleic acids," *Nature*, vol. 171, no. 4356, pp. 738–740, 1953.

[3] R. E. Franklin and R. G. Gosling, "Molecular configuration in sodium thymonucleate," *Nature*, vol. 171, no. 4356, pp. 740–741, 1953.

[4] I. C. M. Kwan, X. Mo, and G. Wu, "Probing hydrogen bonding and ion-carbonyl interactions by solid-state 17O NMR spectroscopy: G-ribbon and G-quartet," *Journal of the American Chemical Society*, vol. 129, no. 8, pp. 2398–2407, 2007.

[5] S. Burge, G. N. Parkinson, P. Hazel, A. K. Todd, and S. Neidle, "Quadruplex DNA: sequence, topology and structure,"

Nucleic Acids Research, vol. 34, no. 19, pp. 5402–5415, 2006.

[6] A. T. Phan, V. Kuryavyi, and D. J. Patel, "DNA architecture: from G to Z," *Current Opinion in Structural Biology*, vol. 16, no. 3, pp. 288–298, 2006.

[7] D. J. Patel, A. T. Phan, and V. Kuryavyi, "Human telomere, oncogenic promoter and 5′-UTR G-quadruplexes: diverse higher order DNA and RNA targets for cancer therapeutics," *Nucleic Acids Research*, vol. 35, no. 22, pp. 7429–7455, 2007.

[8] J. Dai, M. Carver, and D. Yang, "Polymorphism of human telomeric quadruplex structures," *Biochimie*, vol. 90, no. 8, pp. 1172–1183, 2008.

[9] J. T. Davis, "G-quartets 40 years later: from 5′-GMP to molecular biology and supramolecular chemistry," *Angewandte Chemie International Edition*, vol. 43, no. 6, pp. 668–698, 2004.

[10] T. de Lange, "Shelterin: the protein complex that shapes and safeguards human telomeres," *Genes and Development*, vol. 19, no. 18, pp. 2100–2110, 2005.

[11] S. Neidle, "Human telomeric G-quadruplex: the current status of telomeric G-quadruplexes as therapeutic targets in human cancer," *FEBS Journal*, vol. 277, no. 5, pp. 1118–1125, 2010.

[12] A. De Cian, L. Lacroix, C. Douarre, et al., "Targeting telomeres and telomerase," *Biochimie*, vol. 90, no. 1, pp. 131–155, 2008.

[13] L. Oganesian and J. Karlseder, "Telomeric armor: the layers of end protection," *Journal of Cell Science*, vol. 122, no. 22, pp. 4013–4025, 2009.

[14] L. H. Hurley, "DNA and its associated processes as targets for cancer therapy," *Nature Reviews Cancer*, vol. 2, no. 3, pp. 188–200, 2002.

[15] S. Neidle and G. Parkinson, "Telomere maintenance as a target for anticancer drug discovery," *Nature Reviews Drug Discovery*, vol. 1, no. 5, pp. 383–393, 2002.

[16] J.-L. Mergny, J.-F. Riou, P. Mailliet, M.-P. Teulade-Fichou, and E. Gilson, "Natural and pharmacological regulation of telomerase," *Nucleic Acids Research*, vol. 30, no. 4, pp. 839–865, 2002.

[17] E. M. Rezler, D. J. Bearss, and L. H. Hurley, "Telomere inhibition and telomere disruption as processes for drug targeting," *Annual Review of Pharmacology and Toxicology*, vol. 43, pp. 359–379, 2003.

[18] S. Neidle and D. E. Thurston, "Chemical approaches to the discovery and development of cancer therapies," *Nature Reviews Cancer*, vol. 5, no. 4, pp. 285–296, 2005.

[19] L. Oganesian and T. M. Bryan, "Physiological relevance of telomeric G-quadruplex formation: a potential drug target," *BioEssays*, vol. 29, no. 2, pp. 155–165, 2007.

[20] N. Maizels, "Dynamic roles for G4 DNA in the biology of eukaryotic cells," *Nature Structural and Molecular Biology*, vol. 13, no. 12, pp. 1055–1059, 2006.

[21] M. Fry, "Tetraplex DNA and its interacting proteins," *Frontiers in Bioscience*, vol. 12, pp. 4336–4351, 2007.

[22] L. Kelland, "Targeting the limitless replicative potential of cancer: the telomerase/telomere pathway," *Clinical Cancer Research*, vol. 13, no. 17, pp. 4960–4963, 2007.

[23] B. Pagano and C. Giancola, "Energetics of quadruplex-drug recognition in anticancer therapy," *Current Cancer Drug Targets*, vol. 7, no. 6, pp. 520–540, 2007.

[24] S. Balasubramanian and S. Neidle, "G-quadruplex nucleic acids as therapeutic targets," *Current Opinion in Chemical Biology*, vol. 13, no. 3, pp. 345–353, 2009.

[25] A. De Cian, G. Cristofari, P. Reichenbach, et al., "Reevaluation of telomerase inhibition by quadruplex ligands and their mechanisms of action," *Proceedings of the National Academy of Sciences of the United States of America*, vol. 104, no. 44, pp. 17347–17352, 2007.

[26] Y. Qin and L. H. Hurley, "Structures, folding patterns, and functions of intramolecular DNA G-quadruplexes found in eukaryotic promoter regions," *Biochimie*, vol. 90, no. 8, pp. 1149–1171, 2008.

[27] P. S. Shirude, B. Okumus, L. Ying, T. Ha, and S. Balasubramanian, "Single-molecule conformational analysis of G-quadruplex formation in the promoter DNA duplex of the proto-oncogene C-kit," *Journal of the American Chemical Society*, vol. 129, no. 24, pp. 7484–7485, 2007.

[28] J. Eddy and N. Maizels, "Conserved elements with potential to form polymorphic G-quadruplex structures in the first intron of human genes," *Nucleic Acids Research*, vol. 36, no. 4, pp. 1321–1333, 2008.

[29] D. Monchaud and M.-P. Teulade-Fichou, "A hitchhiker's guide to G-quadruplex ligands," *Organic and Biomolecular Chemistry*, vol. 6, no. 4, pp. 627–636, 2008.

[30] A. Arola and R. Vilar, "Stabilisation of G-quadruplex DNA by small molecules," *Current Topics in Medicinal Chemistry*, vol. 8, no. 15, pp. 1405–1415, 2008.

[31] M. Franceschin, "G-quadruplex DNA structures and organic chemistry: more than one connection," *European Journal of Organic Chemistry*, no. 14, pp. 2225–2238, 2009.

[32] S. Neidle, "The structures of quadruplex nucleic acids and their drug complexes," *Current Opinion in Structural Biology*, vol. 19, no. 3, pp. 239–250, 2009.

[33] K. Shin-ya, K. Wierzba, K. Matsuo, et al., "Telomestatin, a novel telomerase inhibitor from *Streptomyces anulatus*," *Journal of the American Chemical Society*, vol. 123, no. 6, pp. 1262–1263, 2001.

[34] F. X. Han, R. T. Wheelhouse, and L. H. Hurley, "Interactions of TMPyP4 and TMPyP2 with quadruplex DNA. Structural basis for the differential effects on telomerase inhibition," *Journal of the American Chemical Society*, vol. 121, no. 15, pp. 3561–3570, 1999.

[35] D.-F. Shi, R. T. Wheelhouse, D. Sun, and L. H. Hurley, "Quadruplex-interactive agents as telomerase inhibitors: synthesis of porphyrins and structure-activity relationship for the inhibition of telomerase," *Journal of Medicinal Chemistry*, vol. 44, no. 26, pp. 4509–4523, 2001.

[36] J.-L. Mergny and L. Lacroix, "UV melting of G-quadruplexes," *Current Protocols in Nucleic Acid Chemistry*, supplement 37, pp. 17.1.1–17.1.15, 2009.

[37] A. De Cian, L. Guittat, M. Kaiser, et al., "Fluorescence-based melting assays for studying quadruplex ligands," *Methods*, vol. 42, no. 2, pp. 183–195, 2007.

[38] J. Fajkus, "Detection of telomerase activity by the TRAP assay and its variants and alternatives," *Clinica Chimica Acta*, vol. 371, no. 1-2, pp. 25–31, 2006.

[39] E. F. Pettersen, T. D. Goddard, C. C. Huang, et al., "UCSF Chimera—a visualization system for exploratory research and analysis," *Journal of Computational Chemistry*, vol. 25, no. 13, pp. 1605–1612, 2004.

[40] W. Liu, D. Sun, and L. H. Hurley, "Binding of G-quadruplex-interactive agents to distinct G-quadruplexes induces different biological effects in MiaPaCa cells," *Nucleosides, Nucleotides and Nucleic Acids*, vol. 24, no. 10–12, pp. 1801–1815, 2005.

[41] M. Sumi, T. Tauchi, G. Sashida, et al., "A G-quadruplex-interactive agent, telomestatin (SOT-095), induces telomere

shortening with apoptosis and enhances chemosensitivity in acute myeloid leukemia," *International Journal of Oncology*, vol. 24, no. 6, pp. 1481–1487, 2004.

[42] T. Tauchi, K. Shin-ya, G. Sashida, et al., "Telomerase inhibition with a novel G-quadruplex-interactive agent, telomestatin: in vitro and in vivo studies in acute leukemia," *Oncogene*, vol. 25, no. 42, pp. 5719–5725, 2006.

[43] H. Tahara, K. Shin-ya, H. Seimiya, H. Yamada, T. Tsuruo, and T. Ide, "G-Quadruplex stabilization by telomestatin induces TRF2 protein dissociation from telomeres and anaphase bridge formation accompanied by loss of the 3′ telomeric overhang in cancer cells," *Oncogene*, vol. 25, no. 13, pp. 1955–1966, 2006.

[44] D. Gomez, T. Wenner, B. Brassart, et al., "Telomestatin-induced telomere uncapping is modulated by POT1 through G-overhang extension in HT1080 human tumor cells," *Journal of Biological Chemistry*, vol. 281, no. 50, pp. 38721–38729, 2006.

[45] M.-Y. Kim, M. Gleason-Guzman, E. Izbicka, D. Nishioka, and L. H. Hurley, "The different biological effects of Telomestatin and TMPyP4 can be attributed to their selectivity for interaction with intramolecular or intermolecular G-quadruplex structures," *Cancer Research*, vol. 63, no. 12, pp. 3247–3256, 2003.

[46] D. Gomez, M.-F. O'Donohue, T. Wenner, et al., "The G-quadruplex ligand telomestatin inhibits POT1 binding to telomeric sequences in vitro and induces GFP-POT1 dissociation from telomeres in human cells," *Cancer Research*, vol. 66, no. 14, pp. 6908–6912, 2006.

[47] M. A. Shammas, R. J. Shmookler Reis, C. Li, et al., "Telomerase inhibition and cell growth arrest after telomestatin treatment in multiple myeloma," *Clinical Cancer Research*, vol. 10, no. 2, pp. 770–776, 2004.

[48] N. Binz, T. Shalaby, P. Rivera, K. Shin-ya, and M. A. Grotzer, "Telomerase inhibition, telomere shortening, cell growth suppression and induction of apoptosis by telomestatin in childhood neuroblastoma cells," *European Journal of Cancer*, vol. 41, no. 18, pp. 2873–2881, 2005.

[49] N. Arnoult, K. Shin-ya, and J. A. Londoño-Vallejo, "Studying telomere replication by Q-CO-FISH: the effect of telomestatin, a potent G-quadruplex ligand," *Cytogenetic and Genome Research*, vol. 122, no. 3-4, pp. 229–236, 2009.

[50] D. Sun, K. Guo, J. J. Rusche, and L. H. Hurley, "Facilitation of a structural transition in the polypurine/polypyrimidine tract within the proximal promoter region of the human VEGF gene by the presence of potassium and G-quadruplex-interactive agents," *Nucleic Acids Research*, vol. 33, no. 18, pp. 6070–6080, 2005.

[51] S. L. Palumbo, S. W. Ebbinghaus, and L. H. Hurley, "Formation of a unique end-to-end stacked pair of G-quadruplexes in the hTERT core promoter with implications for inhibition of telomerase by G-quadruplex-interactive ligands," *Journal of the American Chemical Society*, vol. 131, no. 31, pp. 10878–10891, 2009.

[52] J. Seenisamy, S. Bashyam, V. Gokhale, et al., "Design and synthesis of an expanded porphyrin that has selectivity for the c-MYC G-quadruplex structure," *Journal of the American Chemical Society*, vol. 127, no. 9, pp. 2944–2959, 2005.

[53] T. S. Dexheimer, D. Sun, and L. H. Hurley, "Deconvoluting the structural and drug-recognition complexity of the G-quadruplex-forming region upstream of the bcl-2 P1 promoter," *Journal of the American Chemical Society*, vol. 128, no. 16, pp. 5404–5415, 2006.

[54] K. Guo, A. Pourpak, K. Beetz-Rogers, V. Gokhale, D. Sun, and L. H. Hurley, "Formation of pseudosymmetrical G-quadruplex and i-motif structures in the proximal promoter region of the RET oncogene," *Journal of the American Chemical Society*, vol. 129, no. 33, pp. 10220–10228, 2007.

[55] Y. Wu, K. Shin-ya, and R. M. Brosh Jr., "FANCJ helicase defective in Fanconia anemia and breast cancer unwinds G-quadruplex DNA to defend genomic stability," *Molecular and Cellular Biology*, vol. 28, no. 12, pp. 4116–4128, 2008.

[56] N. Temime-Smaali, L. Guittat, A. Sidibe, K. Shin-ya, C. Trentesaux, and J.-F. Riou, "The G-quadruplex ligand telomestatin impairs binding of topoisomerase IIIα to G-quadruplex-forming oligonucleotides and uncaps telomeres in ALT cells," *PLoS ONE*, vol. 4, no. 9, article e6919, 2009.

[57] M.-Y. Kim, H. Vankayalapati, K. Shin-ya, K. Wierzba, and L. H. Hurley, "Telomestatin, a potent telomerase inhibitor that interacts quite specifically with the human telomeric intramolecular G-quadruplex," *Journal of the American Chemical Society*, vol. 124, no. 10, pp. 2098–2099, 2002.

[58] S. Agrawal, R. P. Ojha, and S. Maiti, "Energetics of the human tel-22 quadruplex—telomestatin interaction: a molecular dynamics study," *Journal of Physical Chemistry B*, vol. 112, no. 22, pp. 6828–6836, 2008.

[59] E. M. Rezler, J. Seenisamy, S. Bashyam, et al., "Telomestatin and diseleno sapphyrin bind selectively to two different forms of the human telomeric G-quadruplex structure," *Journal of the American Chemical Society*, vol. 127, no. 26, pp. 9439–9447, 2005.

[60] T. I. Gaynutdinov, R. D. Neumann, and I. G. Panyutin, "Structural polymorphism of intramolecular quadruplex of human telomeric DNA: effect of cations, quadruplex-binding drugs and flanking sequences," *Nucleic Acids Research*, vol. 36, no. 12, pp. 4079–4087, 2008.

[61] J. Deeley and G. Pattenden, "Synthesis and establishment of stereochemistry of the unusual polyoxazole-thiazole based cyclopeptide YM-216391 isolated from Streptomyces nobilis," *Chemical Communications*, no. 6, pp. 797–799, 2005.

[62] J. M. Atkins and E. Vedejs, "A two-stage iterative process for the synthesis of poly-oxazoles," *Organic Letters*, vol. 7, no. 15, pp. 3351–3354, 2005.

[63] C. M. Marson and M. Saadi, "Synthesis of the penta-oxazole core of telomestatin in a convergent approach to poly-oxazole macrocycles," *Organic and Biomolecular Chemistry*, vol. 4, no. 21, pp. 3892–3893, 2006.

[64] S. K. Chattopadhyay and S. Biswas, "Convergent synthesis of a 24-membered macrocyclic hexaoxazole derivative related to the novel telomerase inhibitor telomestatin," *Tetrahedron Letters*, vol. 47, no. 45, pp. 7897–7900, 2006.

[65] D. Hernandez, E. Riego, A. Francesch, C. Cuevas, F. Albericio, and M. Alvarez, "Preparation of penta-azole containing cyclopeptides: challenges in macrocyclization," *Tetrahedron*, vol. 63, no. 39, pp. 9862–9870, 2007.

[66] T. Doi, M. Yoshida, K. Shin-ya, and T. Takahashi, "Total synthesis of (*R*)-telomestatin," *Organic Letters*, vol. 8, no. 18, pp. 4165–4167, 2006.

[67] G. S. Minhas, D. S. Pilch, J. E. Kerrigan, E. J. LaVoie, and J. E. Rice, "Synthesis and G-quadruplex stabilizing properties of a series of oxazole-containing macrocycles," *Bioorganic and Medicinal Chemistry Letters*, vol. 16, no. 15, pp. 3891–3895, 2006.

[68] C. M. Barbieri, A. R. Srinivasan, S. G. Rzuczek, J. E. Rice, E. J. LaVoie, and D. S. Pilch, "Defining the mode, energetics and specificity with which a macrocyclic hexaoxazole binds

to human telomeric G-quadruplex DNA," *Nucleic Acids Research*, vol. 35, no. 10, pp. 3272–3286, 2007.

[69] M. Tera, Y. Sohtome, H. Ishizuka, et al., "Design and synthesis of telomestatin derivatives and their inhibitory activity of telomerase," *Heterocycles*, vol. 69, no. 1, pp. 505–514, 2006.

[70] Y.-C. Tsai, H. Qi, C.-P. Lin, et al., "A G-quadruplex stabilizer induces M-phase cell cycle arrest," *Journal of Biological Chemistry*, vol. 284, no. 34, pp. 22535–22543, 2009.

[71] M. Satyanarayana, S. G. Rzuczek, E. J. LaVoie, et al., "Ring-closing metathesis for the synthesis of a highly G-quadruplex selective macrocyclic hexaoxazole having enhanced cytotoxic potency," *Bioorganic and Medicinal Chemistry Letters*, vol. 18, no. 13, pp. 3802–3804, 2008.

[72] D. S. Pilch, C. M. Barbieri, S. G. Rzuczek, E. J. LaVoie, and J. E. Rice, "Targeting human telomeric G-quadruplex DNA with oxazole-containing macrocyclic compounds," *Biochimie*, vol. 90, no. 8, pp. 1233–1249, 2008.

[73] S. G. Rzuczek, D. S. Pilch, E. J. LaVoie, and J. E. Rice, "Lysinyl macrocyclic hexaoxazoles: synthesis and selective G-quadruplex stabilizing properties," *Bioorganic and Medicinal Chemistry Letters*, vol. 18, no. 3, pp. 913–917, 2008.

[74] Calculator Plugins were used for pK_a calculation, Marvin 5.0.1, 2008, ChemAxon, http://www.chemaxon.com/.

[75] M. Tera, H. Ishizuka, M. Takagi, M. Suganuma, K. Shin-ya, and K. Nagasawa, "Macrocyclic hexaoxazoles as sequence- and mode-selective G-quadruplex binders," *Angewandte Chemie International Edition*, vol. 47, no. 30, pp. 5557–5560, 2008.

[76] K. Iida, M. Tera, T. Hirokawa, K. Shin-ya, and K. Nagasawa, "G-quadruplex recognition by macrocyclic hexaoxazole (6OTD) dimer: greater selectivity than monomer," *Chemical Communications*, no. 42, pp. 6481–6483, 2009.

[77] M. Tera, K. Iida, H. Ishizuka, et al., "Synthesis of a potent G-quadruplex-binding macrocyclic heptaoxazole," *ChemBioChem*, vol. 10, no. 3, pp. 431–435, 2009.

[78] K. Jantos, R. Rodriguez, S. Ladame, P. S. Shirude, and S. Balasubramanian, "Oxazole-based peptide macrocycles: a new class of G-quadruplex binding ligands," *Journal of the American Chemical Society*, vol. 128, no. 42, pp. 13662–13663, 2006.

[79] T. K. Chakraborty, A. Arora, S. Roy, N. Kumar, and S. Maiti, "Furan based cyclic oligopeptides selectively target G-quadruplex," *Journal of Medicinal Chemistry*, vol. 50, no. 23, pp. 5539–5542, 2007.

[80] P. S. Shirude, E. R. Gillies, S. Ladame, et al., "Macrocyclic and helical oligoamides as a new class of G-quadruplex ligands," *Journal of the American Chemical Society*, vol. 129, no. 39, pp. 11890–11891, 2007.

[81] P. V. Jena, P. S. Shirude, B. Okumus, et al., "G-quadruplex DNA bound by a synthetic ligand is highly dynamic," *Journal of the American Chemical Society*, vol. 131, no. 35, pp. 12522–12523, 2009.

[82] R. J. Fiel, J. C. Howard, E. H. Mark, and N. Datta Gupta, "Interaction of DNA with a porphyrin ligand: evidence for intercalation," *Nucleic Acids Research*, vol. 6, no. 9, pp. 3093–3118, 1979.

[83] R. J. Fiel and B. R. Munson, "Binding of meso-tetra (4-N-methylpyridyl) porphine to DNA," *Nucleic Acids Research*, vol. 8, no. 12, pp. 2835–2842, 1980.

[84] R. F. Pasternack, E. J. Gibbs, and J. J. Villafranca, "Interactions of porphyrins with nucleic acids," *Biochemistry*, vol. 22, no. 10, pp. 2406–2414, 1983.

[85] E. Izbicka, R. T. Wheelhouse, E. Raymond, et al., "Effects of cationic porphyrins as G-quadruplex interactive agents in human tumor cells," *Cancer Research*, vol. 59, no. 3, pp. 639–644, 1999.

[86] A. De Cian, L. Guittat, K. Shin-ya, J. F. Riou, and J. L. Mergny, "Affinity and selectivity of G4 ligands measured by FRET," *Nucleic Acids Symposium Series*, no. 49, pp. 235–236, 2005.

[87] J. Ren and J. B. Chaires, "Sequence and structural selectivity of nucleic acid binding ligands," *Biochemistry*, vol. 38, no. 49, pp. 16067–16075, 1999.

[88] D. Monchaud, C. Allain, and M.-P. Teulade-Fichou, "Development of a fluorescent intercalator displacement assay (G4-FID) for establishing quadruplex-DNA affinity and selectivity of putative ligands," *Bioorganic and Medicinal Chemistry Letters*, vol. 16, no. 18, pp. 4842–4845, 2006.

[89] A. Granzhan, H. Ihmels, and K. Jäger, "Diazonia- and tetraazoniapolycyclic cations as motif for quadruplex-DNA ligands," *Chemical Communications*, no. 10, pp. 1249–1251, 2009.

[90] E. W. White, F. Tanious, M. A. Ismail, et al., "Structure-specific recognition of quadruplex DNA by organic cations: influence of shape, substituents and charge," *Biophysical Chemistry*, vol. 126, no. 1–3, pp. 140–153, 2007.

[91] P. Wang, L. Ren, H. He, F. Liang, X. Zhou, and Z. Tan, "A phenol quaternary ammonium porphyrin as a potent telomerase inhibitor by selective interaction with quadruplex DNA," *ChemBioChem*, vol. 7, no. 8, pp. 1155–1159, 2006.

[92] T. A. Brooks and L. H. Hurley, "The role of supercoiling in transcriptional control of MYC and its importance in molecular therapeutics," *Nature Reviews Cancer*, vol. 9, no. 12, pp. 849–861, 2009.

[93] A. Rangan, O. Y. Fedoroff, and L. H. Hurley, "Induction of duplex to G-quadruplex transition in the c-myc promoter region by a small molecule," *Journal of Biological Chemistry*, vol. 276, no. 7, pp. 4640–4646, 2001.

[94] A. Siddiqui-Jain, C. L. Grand, D. J. Bearss, and L. H. Hurley, "Direct evidence for a G-quadruplex in a promoter region and its targeting with a small molecule to repress c-MYC transcription," *Proceedings of the National Academy of Sciences of the United States of America*, vol. 99, no. 18, pp. 11593–11598, 2002.

[95] C. L. Grand, H. Han, R. M. Muñoz, et al., "The cationic porphyrin TMPyP4 down-regulates c-MYC and human telomerase reverse transcriptase expression and inhibits tumor growth in vivo," *Molecular Cancer Therapeutics*, vol. 1, no. 8, pp. 565–573, 2002.

[96] J. Seenisamy, E. M. Rezler, T. J. Powell, et al., "The dynamic character of the G-quadruplex element in the c-MYC promoter and modification by TMPyP4," *Journal of the American Chemical Society*, vol. 126, no. 28, pp. 8702–8709, 2004.

[97] C. L. Grand, T. J. Powell, R. B. Nagle, et al., "Mutations in the G-quadruplex silencer element and their relationship to c-MYC overexpression, NM23 repression, and therapeutic rescue," *Proceedings of the National Academy of Sciences of the United States of America*, vol. 101, no. 16, pp. 6140–6145, 2004.

[98] D. Yang and L. Hurley, "Structure of the biologically relevant g-quadruplex in the c-MYC promoter," *Nucleosides, Nucleotides and Nucleic Acids*, vol. 25, no. 8, pp. 951–968, 2006.

[99] M. W. Freyer, R. Buscaglia, K. Kaplan, D. Cashman, L. H. Hurley, and E. A. Lewis, "Biophysical studies of the c-MYC NHE III1 promoter: model quadruplex interactions with

a cationic porphyrin," *Biophysical Journal*, vol. 92, no. 6, pp. 2007–2015, 2007.

[100] D. J. Cashman, R. Buscaglia, M. W. Freyer, J. Dettler, L. H. Hurley, and E. A. Lewis, "Molecular modeling and biophysical analysis of the c-MYC NHE-III1 silencer element," *Journal of Molecular Modeling*, vol. 14, no. 2, pp. 93–101, 2008.

[101] R. De Armond, S. Wood, D. Sun, L. H. Hurley, and S. W. Ebbinghaus, "Evidence for the presence of a guanine quadruplex forming region within a polypurine tract of the hypoxia inducible factor 1α promoter," *Biochemistry*, vol. 44, no. 49, pp. 16341–16350, 2005.

[102] D. Sun, W.-J. Liu, K. Guo, et al., "The proximal promoter region of the human vascular endothelial growth factor gene has a G-quadruplex structure that can be targeted by G-quadruplex-interactive agents," *Molecular Cancer Therapeutics*, vol. 7, no. 4, pp. 880–889, 2008.

[103] K. Guo, V. Gokhale, L. H. Hurley, and D. Sun, "Intramolecularly folded G-quadruplex and i-motif structures in the proximal promoter of the vascular endothelial growth factor gene," *Nucleic Acids Research*, vol. 36, no. 14, pp. 4598–4608, 2008.

[104] J. Dai, D. Chen, R. A. Jones, L. H. Hurley, and D. Yang, "NMR solution structure of the major G-quadruplex structure formed in the human BCL2 promoter region," *Nucleic Acids Research*, vol. 34, no. 18, pp. 5133–5144, 2006.

[105] M. del Toro, P. Bucek, A. Avino, et al., "Targeting the G-quadruplex-forming region near the P1 promoter in the human BCL-2 gene with the cationic porphyrin TMPyP4 and with the complementary C-rich strand," *Biochimie*, vol. 91, no. 7, pp. 894–902, 2009.

[106] M. Paramasivam, A. Membrino, S. Cogoi, H. Fukuda, H. Nakagama, and L. E. Xodo, "Protein hnRNP A1 and its derivative Up1 unfold quadruplex DNA in the human KRAS promoter: implications for transcription," *Nucleic Acids Research*, vol. 37, no. 9, pp. 2841–2853, 2009.

[107] Y. Qin, E. M. Rezler, V. Gokhale, D. Sun, and L. H. Hurley, "Characterization of the G-quadruplexes in the duplex nuclease hypersensitive element of the *PDGF-A* promoter and modulation of *PDGF-A* promoter activity by TMPyP4," *Nucleic Acids Research*, vol. 35, no. 22, pp. 7698–7713, 2007.

[108] M. Gunaratnam, S. Swank, S. M. Haider, et al., "Targeting human gastrointestinal stromal tumor cells with a quadruplex-binding small molecule," *Journal of Medicinal Chemistry*, vol. 52, no. 12, pp. 3774–3783, 2009.

[109] Y. Mikami-Terao, M. Akiyama, Y. Yuza, et al., "Antitumor activity of TMPyP4 interacting G-quadruplex in retinoblastoma cell lines," *Experimental Eye Research*, vol. 89, no. 2, pp. 200–208, 2009.

[110] Y. Mikami-Terao, M. Akiyama, Y. Yuza, T. Yanagisawa, O. Yamada, and H. Yamada, "Antitumor activity of G-quadruplex-interactive agent TMPyP4 in K562 leukemic cells," *Cancer Letters*, vol. 261, no. 2, pp. 226–234, 2008.

[111] A. Verma, K. Halder, R. Halder, et al., "Genome-wide computational and expression analyses reveal G-quadruplex DNA motifs as conserved cis-regulatory elements in human and related species," *Journal of Medicinal Chemistry*, vol. 51, no. 18, pp. 5641–5649, 2008.

[112] M. Wieland and J. S. Hartig, "Turning inhibitors into activators: a hammerhead ribozyme controlled by a guanine quadruplex," *Angewandte Chemie International Edition*, vol. 45, no. 35, pp. 5875–5878, 2006.

[113] Y. Xu, Y. Hirao, Y. Nishimura, and H. Sugiyama, "I-motif and quadruplex-based device that can control a protein release or bind and release small molecule to influence biological processes," *Bioorganic and Medicinal Chemistry*, vol. 15, no. 3, pp. 1275–1279, 2007.

[114] A. K. Pomerantz, W. E. Moerner, and E. T. Kool, "Visualization of long human telomere mimics by single-molecule fluorescence imaging," *Journal of Physical Chemistry B*, vol. 112, no. 42, pp. 13184–13187, 2008.

[115] Z. Chen, K.-W. Zheng, Y.-H. Hao, and Z. Tan, "Reduced or diminished stabilization of the telomere G-quadruplex and inhibition of telomerase by small chemical ligands under molecular crowding condition," *Journal of the American Chemical Society*, vol. 131, no. 30, pp. 10430–10438, 2009.

[116] P. Weisman-Shomer, E. Cohen, I. Hershco, et al., "The cationic porphyrin TMPyP4 destabilizes the tetraplex form of the fragile X syndrome expanded sequence $d(CGG)_n$," *Nucleic Acids Research*, vol. 31, no. 14, pp. 3963–3970, 2003.

[117] A. Joachimi, G. Mayer, and J. S. Hartig, "A new anticoagulant-antidote pair: control of thrombin activity by aptamers and porphyrins," *Journal of the American Chemical Society*, vol. 129, no. 11, pp. 3036–3037, 2007.

[118] N. Ofer, P. Weisman-Shomer, J. Shklover, and M. Fry, "The quadruplex $r(CGG)_n$ destabilizing cationic porphyrin TMPyP4 cooperates with hnRNPs to increase the translation efficiency of fragile X premutation mRNA," *Nucleic Acids Research*, vol. 37, no. 8, pp. 2712–2722, 2009.

[119] C. Wei, G. Jia, J. Yuan, Z. Feng, and C. Li, "A spectroscopic study on the interactions of porphyrin with G-quadruplex DNAs," *Biochemistry*, vol. 45, no. 21, pp. 6681–6691, 2006.

[120] A. T. Phan, V. Kuryavyi, H. Y. Gaw, and D. J. Patel, "Small-molecule interaction with a five-guanine-tract G-quadruplex structure from the human MYC promoter," *Nature Chemical Biology*, vol. 1, no. 3, pp. 167–173, 2005.

[121] G. N. Parkinson, R. Ghosh, and S. Neidle, "Structural basis for binding of porphyrin to human telomeres," *Biochemistry*, vol. 46, no. 9, pp. 2390–2397, 2007.

[122] M. Cavallari, A. Garbesi, and R. Di Felice, "Porphyrin intercalation in G4-DNA quadruplexes by molecular dynamics simulations," *Journal of Physical Chemistry B*, vol. 113, no. 40, pp. 13152–13160, 2009.

[123] Y. Ishikawa and S. Fujii, "Molecular docking study of binding of TMPyP4 to a bimolecular human telomeric G-quadruplex," *Nucleic Acids Symposium Series*, vol. 52, no. 1, pp. 173–179, 2008.

[124] G. Jia, Z. Feng, C. Wei, J. Zhou, X. Wang, and C. Li, "Dynamic insight into the interaction between porphyrin and G-quadruplex DNAs: time-resolved fluorescence anisotropy study," *Journal of Physical Chemistry B*, vol. 113, no. 50, pp. 16237–16245, 2009.

[125] C. Wei, G. Jia, J. Zhou, G. Han, and C. Li, "Evidence for the binding mode of porphyrins to G-quadruplex DNA," *Physical Chemistry Chemical Physics*, vol. 11, no. 20, pp. 4025–4032, 2009.

[126] C. Wei, L. Wang, G. Jia, J. Zhou, G. Han, and C. Li, "The binding mode of porphyrins with cation side arms to $(TG_4T)4$ G-quadruplex: spectroscopic evidence," *Biophysical Chemistry*, vol. 143, no. 1-2, pp. 79–84, 2009.

[127] H.-J. Zhang, X.-F. Wang, P. Wang, X.-C. Ai, and J.-P. Zhang, "Spectroscopic study on the binding of a cationic porphyrin to DNA G-quadruplex under different K^+ concentrations," *Photochemical and Photobiological Sciences*, vol. 7, no. 8, pp. 948–955, 2008.

[128] H. Zhang, X. Xiao, P. Wang, et al., "Conformational conversion of DNA G-quadruplex induced by a cationic porphyrin," *Spectrochimica Acta A*, vol. 74, no. 1, pp. 243–247, 2009.

[129] I. Lubitz, N. Borovok, and A. Kotlyar, "Interaction of monomolecular G4-DNA nanowires with TMPyP: evidence for intercalation," *Biochemistry*, vol. 46, no. 45, pp. 12925–12929, 2007.

[130] A. Arora and S. Maiti, "Stability and molecular recognition of quadruplexes with different loop length in the absence and presence of molecular crowding agents," *Journal of Physical Chemistry B*, vol. 113, no. 25, pp. 8784–8792, 2009.

[131] I. Haq, J. O. Trent, B. Z. Chowdhry, and T. C. Jenkins, "Intercalative G-tetraplex stabilization of telomeric DNA by a cationic porphyrin," *Journal of the American Chemical Society*, vol. 121, no. 9, pp. 1768–1779, 1999.

[132] L. Martino, B. Pagano, I. Fotticchia, S. Neidle, and C. Giancola, "Shedding light on the interaction between TMPyP4 and human telomeric quadruplexes," *Journal of Physical Chemistry B*, vol. 113, no. 44, pp. 14779–14786, 2009.

[133] A. Arora and S. Maiti, "Effect of loop orientation on quadruplex—TMPyP4 interaction," *Journal of Physical Chemistry B*, vol. 112, no. 27, pp. 8151–8159, 2008.

[134] H. Li, Y. Liu, S. Lin, and G. Yuan, "Spectroscopy probing of the formation, recognition, and conversion of a G-quadruplex in the promoter region of the *bcl-2* oncogene," *Chemistry: A European Journal*, vol. 15, no. 10, pp. 2445–2452, 2009.

[135] R. D. Gray, J. Li, and J. B. Chaires, "Energetics and kinetics of a conformational switch in G-quadruplex DNA," *Journal of Physical Chemistry B*, vol. 113, no. 9, pp. 2676–2683, 2009.

[136] M. del Toro, R. Gargallo, R. Eritja, and J. Jaumot, "Study of the interaction between the G-quadruplex-forming thrombin-binding aptamer and the porphyrin 5,10,15,20-tetrakis-(*N*-methyl-4-pyridyl)-21,23H-porphyrin tetratosylate," *Analytical Biochemistry*, vol. 379, no. 1, pp. 8–15, 2008.

[137] C. Vialas, G. Pratviel, and B. Meunier, "Oxidative damage generated by an oxo-metalloporphyrin onto the human telomeric sequence," *Biochemistry*, vol. 39, no. 31, pp. 9514–9522, 2000.

[138] A. Maraval, S. Franco, C. Vialas, G. Pratviel, M. A. Blasco, and B. Meunier, "Porphyrin-aminoquinoline conjugates as telomerase inhibitors," *Organic and Biomolecular Chemistry*, vol. 1, no. 6, pp. 921–927, 2003.

[139] I. M. Dixon, F. Lopez, J.-P. Estève, et al., "Porphyrin derivatives for telomere binding and telomerase inhibition," *ChemBioChem*, vol. 6, no. 1, pp. 123–132, 2005.

[140] L. R. Keating and V. A. Szalai, "Parallel-stranded guanine quadruplex interactions with a copper cationic porphyrin," *Biochemistry*, vol. 43, no. 50, pp. 15891–15900, 2004.

[141] S. E. Evans, M. A. Mendez, K. B. Turner, et al., "End-stacking of copper cationic porphyrins on parallel-stranded guanine quadruplexes," *Journal of Biological Inorganic Chemistry*, vol. 12, no. 8, pp. 1235–1249, 2007.

[142] J. Pan and S. Zhang, "Interaction between cationic zinc porphyrin and lead ion induced telomeric guanine quadruplexes: evidence for end-stacking," *Journal of Biological Inorganic Chemistry*, vol. 14, no. 3, pp. 401–407, 2009.

[143] I. M. Dixon, F. Lopez, A. M. Tejera, et al., "A G-quadruplex ligand with 10000-fold selectivity over duplex DNA," *Journal of the American Chemical Society*, vol. 129, no. 6, pp. 1502–1503, 2007.

[144] B. Nguyen, F. A. Tanious, and W. D. Wilson, "Biosensor-surface plasmon resonance: quantitative analysis of small molecule-nucleic acid interactions," *Methods*, vol. 42, no. 2, pp. 150–161, 2007.

[145] D. P. N. Gonçalves, S. Ladame, S. Balasubramanian, and J. K. M. Sanders, "Synthesis and G-quadruplex binding studies of new 4-N-methylpyridinium porphyrins," *Organic and Biomolecular Chemistry*, vol. 4, no. 17, pp. 3337–3342, 2006.

[146] R. McGuire Jr. and D. R. McMillin, "Steric effects direct the binding of porphyrins to tetramolecular quadruplex DNA," *Chemical Communications*, no. 47, pp. 7393–7395, 2009.

[147] N. P. E. Barry, N. H. Abd Karim, R. Vilar, and B. Therrien, "Interactions of ruthenium coordination cubes with DNA," *Dalton Transactions*, no. 48, pp. 10717–10719, 2009.

[148] R. Kieltyka, P. Englebienne, J. Fakhoury, C. Autexier, N. Moitessier, and H. F. Sleiman, "A platinum supramolecular square as an effective G-quadruplex binder and telomerase inhibitor," *Journal of the American Chemical Society*, vol. 130, no. 31, pp. 10040–10041, 2008.

[149] T. Lu and L. H. Hurley, "Synthesis of 5,10,15,20-tetra(N-methyl-6-quinolyl)-21,23-dithiaporphyrin chloride as cationic core-modified porphyrin," *Chinese Chemical Letters*, vol. 15, no. 11, pp. 1261–1264, 2004.

[150] S. R. Wang, D. Zhang, F. L. Luo, et al., "Some cationic porphyrins: synthesis, stabilization of G-qua druplexes, and down-regulation of c-myc in Hep G2 cells," *Journal of Porphyrins and Phthalocyanines*, vol. 13, no. 8-9, pp. 865–875, 2009.

[151] T. Murashima, D. Sakiyama, D. Miyoshi, et al., "Cationic porphyrin induced a telomeric DNA to G-quadruplex form in water," *Bioinorganic Chemistry and Applications*, vol. 2008, Article ID 294756, 5 pages, 2008.

[152] C.-C. Kang, C.-T. Chen, C.-C. Cho, Y.-C. Lin, C.-C. Chang, and T.-C. Chang, "A dual selective antitumor agent and fluorescence probe: the binary BMVC-porphyrin photosensitizer," *ChemMedChem*, vol. 3, no. 5, pp. 725–728, 2008.

[153] B. Fu, J. Huang, L. Ren, et al., "Cationic corrole derivatives: a new family of G-quadruplex inducing and stabilizing ligands," *Chemical Communications*, no. 31, pp. 3264–3266, 2007.

[154] B. Fu, D. Zhang, X. Weng, et al., "Cationic metal-corrole complexes: design, synthesis, and properties of guanine-quadruplex stabilizers," *Chemistry: A European Journal*, vol. 14, no. 30, pp. 9431–9441, 2008.

[155] D. P. N. Gonçalves, R. Rodriguez, S. Balasubramanian, and J. K. M. Sanders, "Tetramethylpyridiniumporphyrazines—a new class of G-quadruplex inducing and stabilising ligands," *Chemical Communications*, no. 45, pp. 4685–4687, 2006.

[156] A. Henn, A. Joachimi, D. P. Gonçalves, et al., "Inhibition of dicing of guanosine-rich shRNAs by quadruplex-binding compounds," *ChemBioChem*, vol. 9, no. 16, pp. 2722–2729, 2008.

[157] L. Ren, A. Zhang, J. Huang, et al., "Quaternary ammonium zinc phthalocyanine: inhibiting telomerase by stabilizing G quadruplexes and inducing G-quadruplex structure transition and formation," *ChemBioChem*, vol. 8, no. 7, pp. 775–780, 2007.

[158] L. Zhang, J. Huang, L. Ren, et al., "Synthesis and evaluation of cationic phthalocyanine derivatives as potential inhibitors of telomerase," *Bioorganic and Medicinal Chemistry*, vol. 16, no. 1, pp. 303–312, 2008.

[159] J. Alzeer, B. R. Vummidi, P. J. C. Roth, and N. W. Luedtke, "Guanidinium-modified phthalocyanines as high-affinity G-quadruplex fluorescent probes and transcriptional regulators," *Angewandte Chemie International Edition*, vol. 48, no. 49, pp. 9362–9365, 2009.

[160] A. Membrino, M. Paramasivam, S. Cogoi, J. Alzeer, N. W. Luedtke, and L. E. Xodo, "Cellular uptake and binding of guanidine-modified phthalocyanines to KRAS/HRAS

G-quadruplexes," *Chemical Communications*, vol. 46, no. 4, pp. 625–627, 2010.

[161] Y. Li, C. R. Geyer, and D. Sen, "Recognition of anionic porphyrins by DNA aptamers," *Biochemistry*, vol. 35, no. 21, pp. 6911–6922, 1996.

[162] Y. Li and D. Sen, "A catalytic DNA for porphyrin metallation," *Nature Structural Biology*, vol. 3, no. 9, pp. 743–747, 1996.

[163] P. Travascio, Y. Li, and D. Sen, "DNA-enhanced peroxidase activity of a DNA aptamer-hemin complex," *Chemistry and Biology*, vol. 5, no. 9, pp. 505–517, 1998.

[164] P. Travascio, A. J. Bennet, D. Y. Wang, and D. Sen, "A ribozyme and a catalytic DNA with peroxidase activity: active sites versus cofactor-binding sites," *Chemistry and Biology*, vol. 6, no. 11, pp. 779–787, 1999.

[165] P. Travascio, P. K. Witting, A. G. Mauk, and D. Sen, "The peroxidase activity of a hemin-DNA oligonucleotide complex: free radical damage to specific guanine bases of the DNA," *Journal of the American Chemical Society*, vol. 123, no. 7, pp. 1337–1348, 2001.

[166] Y. Xiao, V. Pavlov, R. Gill, T. Bourenko, and I. Willner, "Lighting up biochemiluminescence by the surface self-assembly of DNA—hemin complexes," *ChemBioChem*, vol. 5, no. 3, pp. 374–379, 2004.

[167] V. Pavlov, Y. Xiao, R. Gill, A. Dishon, M. Kotler, and I. Willner, "Amplified chemiluminescence surface detection of DNA and telomerase activity using catalytic nucleic acid labels," *Analytical Chemistry*, vol. 76, no. 7, pp. 2152–2156, 2004.

[168] Y. Xiao, V. Pavlov, T. Niazov, A. Dishon, M. Kotler, and I. Willner, "Catalytic beacons for the detection of DNA and telomerase activity," *Journal of the American Chemical Society*, vol. 126, no. 24, pp. 7430–7431, 2004.

[169] B.-C. Yin, B.-C. Ye, W. Tan, W. Hui, and C.-C. Xie, "An allosteric dual-DNAzyme unimolecular probe for colorimetric detection of copper(II)," *Journal of the American Chemical Society*, vol. 131, no. 41, pp. 14624–14625, 2009.

[170] B. Li, Y. Du, T. Li, and S. Dong, "Investigation of 3, 3′,5, 5′-tetramethylbenzidine as colorimetric substrate for a peroxidatic DNAzyme," *Analytica Chimica Acta*, vol. 651, no. 2, pp. 234–240, 2009.

[171] Y. Weizmann, M. K. Beissenhirtz, Z. Cheglakov, R. Nowarski, M. Kotler, and I. Willner, "A virus spotlighted by an autonomous DNA machine," *Angewandte Chemie International Edition*, vol. 45, no. 44, pp. 7384–7388, 2006.

[172] M. Deng, D. Zhang, Y. Zhou, and X. Zhou, "Highly effective colorimetric and visual detection of nucleic acids using an asymmetrically split peroxidase DNAzyme," *Journal of the American Chemical Society*, vol. 130, no. 39, pp. 13095–13102, 2008.

[173] Y. Weizmann, Z. Cheglakov, and I. Willner, "A fok l/DNA machine that duplicates its analyte gene sequence," *Journal of the American Chemical Society*, vol. 130, no. 51, pp. 17224–17225, 2008.

[174] S. Nakayama and H. O. Sintim, "Colorimetric split G-quadruplex probes for nucleic acid sensing: improving reconstituted DNAzyme's catalytic efficiency via probe remodeling," *Journal of the American Chemical Society*, vol. 131, no. 29, pp. 10320–10333, 2009.

[175] T. Li, L. Shi, E. Wang, and S. Dong, "Multifunctional G-quadruplex aptamers and their application to protein detection," *Chemistry: A European Journal*, vol. 15, no. 4, pp. 1036–1042, 2009.

[176] D. Li, B. Shlyahovsky, J. Elbaz, and I. Willner, "Amplified analysis of low-molecular-weight substrates or proteins by the self-assembly of DNAzyme-aptamer conjugates," *Journal of the American Chemical Society*, vol. 129, no. 18, pp. 5804–5805, 2007.

[177] T. Li, E. Wang, and S. Dong, "G-quadruplex-based DNAzyme for facile colorimetric detection of thrombin," *Chemical Communications*, no. 31, pp. 3654–3656, 2008.

[178] T. Li, S. Dong, and E. Wang, "Label-free colorimetric detection of aqueous mercury ion (Hg^{2+}) using Hg^{2+}-modulated G-quadruplex-based dnazymes," *Analytical Chemistry*, vol. 81, no. 6, pp. 2144–2149, 2009.

[179] D.-M. Kong, J. Wu, N. Wang, W. Yang, and H.-X. Shen, "Peroxidase activity-structure relationship of the intermolecular four-stranded G-quadruplex-hemin complexes and their application in Hg^{2+} ion detection," *Talanta*, vol. 80, no. 2, pp. 459–465, 2009.

[180] J. Elbaz, B. Shlyahovsky, and I. Willner, "A DNAzyme cascade for the amplified detection of Pb^{2+} ions or L-histidine," *Chemical Communications*, no. 13, pp. 1569–1571, 2008.

[181] T. Li, E. Wang, and S. Dong, "G-quadruplex-based DNAzyme as a sensing platform for ultrasensitive colorimetric potassium detection," *Chemical Communications*, no. 5, pp. 580–582, 2009.

[182] T. Li, E. Wang, and S. Dong, "Potassium-lead-switched G-quadruplexes: a new class of DNA logic gates," *Journal of the American Chemical Society*, vol. 131, no. 42, pp. 15082–15083, 2009.

[183] B. Shlyahovsky, Y. Li, O. Lioubashevski, J. Elbaz, and I. Willner, "Logic gates and antisense DNA devices operating on a translator nucleic acid scaffold," *ACS Nano*, vol. 3, no. 7, pp. 1831–1843, 2009.

[184] D.-M. Kong, J. Wu, Y.-E. Ma, and H.-X. Shen, "A new method for the study of G-quadruplex ligands," *Analyst*, vol. 133, no. 9, pp. 1158–1160, 2008.

[185] X. Cheng, X. Liu, T. Bing, Z. Cao, and D. Shangguan, "General peroxidase activity of G-quadruplex-hemin complexes and its application in ligand screening," *Biochemistry*, vol. 48, no. 33, pp. 7817–7823, 2009.

[186] H. Arthanari, S. Basu, T. L. Kawano, and P. H. Bolton, "Fluorescent dyes specific for quadruplex DNA," *Nucleic Acids Research*, vol. 26, no. 16, pp. 3724–3728, 1998.

[187] F. Rosu, V. Gabelica, C. Houssier, P. Colson, and E. De Pauw, "Triplex and quadruplex DNA structures studied by electrospray mass spectrometry," *Rapid Communications in Mass Spectrometry*, vol. 16, no. 18, pp. 1729–1736, 2002.

[188] S. Paramasivan and P. H. Bolton, "Mix and measure fluorescence screening for selective quadruplex binders," *Nucleic Acids Research*, vol. 36, no. 17, article e106, 2008.

[189] P. Ragazzon and J. B. Chaires, "Use of competition dialysis in the discovery of G-quadruplex selective ligands," *Methods*, vol. 43, no. 4, pp. 313–323, 2007.

[190] S. G. Hershman, Q. Chen, J. Y. Lee, et al., "Genomic distribution and functional analyses of potential G-quadruplex-forming sequences in Saccharomyces cerevisiae," *Nucleic Acids Research*, vol. 36, no. 1, pp. 144–156, 2008.

[191] J. E. Johnson, J. S. Smith, M. L. Kozak, and F. B. Johnson, "In vivo veritas: using yeast to probe the biological functions of G-quadruplexes," *Biochimie*, vol. 90, no. 8, pp. 1250–1263, 2008.

[192] A. K. Todd, M. Johnston, and S. Neidle, "Highly prevalent putative quadruplex sequence motifs in human DNA," *Nucleic Acids Research*, vol. 33, no. 9, pp. 2901–2907, 2005.

[193] J. L. Huppert and S. Balasubramanian, "Prevalence of quadruplexes in the human genome," *Nucleic Acids Research*, vol. 33, no. 9, pp. 2908–2916, 2005.

[194] J. L. Huppert and S. Balasubramanian, "G-quadruplexes in promoters throughout the human genome," *Nucleic Acids Research*, vol. 35, no. 2, pp. 406–413, 2007.

[195] J. S. Smith and F. B. Johnson, "Isolation of G-quadruplex DNA using NMM-sepharose affinity chromatography," in *G-Quadruplex DNA: Methods and Protocols*, P. Baumann, Ed., vol. 608 of *Methods in Molecular Biology*, chapter 13, pp. 207–221, 2010.

[196] M.-P. Teulade-Fichou and J.-P. Vigneron, "Interactions of macrocyclic compounds with nucleic acids," in *Small Molecule DNA and RNA Binders: From Synthesis to Nucleic Acid Complexes*, M. Demeunynck, C. Bailly, and W. D. Wilson, Eds., vol. 1, chapter 11, pp. 278–314, 2003.

[197] A. David, N. Bleimling, C. Beuck, J.-M. Lehn, E. Weinhold, and M.-P. Teulade-Fichou, "DNA mismatch-specific base flipping by a Bisacridine macrocycle," *ChemBioChem*, vol. 4, no. 12, pp. 1326–1331, 2003.

[198] M. Bahr, V. Gabelica, A. Granzhan, M.-P. Teulade-Fichou, and E. Weinhold, "Selective recognition of pyrimidine-pyrimidine DNA mismatches by distance-constrained macrocyclic bis-intercalators," *Nucleic Acids Research*, vol. 36, no. 15, pp. 5000–5012, 2008.

[199] A. Granzhan and M.-P. Teulade-Fichou, "A fluorescent bisanthracene macrocycle discriminates between matched and mismatch-containing DNA," *Chemistry: A European Journal*, vol. 15, no. 6, pp. 1314–1318, 2009.

[200] A. Granzhan, E. Largy, N. Saettel, and M.-P. Teulade-Fichou, "Macrocyclic DNA-mismatch-binding ligands: structural determinants of selectivity," *Chemistry: A European Journal*, vol. 16, no. 3, pp. 878–889, 2010.

[201] M. Jourdan, J. Garcia, J. Lhomme, M.-P. Teulade-Fichou, J.-P. Vigneron, and J.-M. Lehn, "Threading bis-intercalation of a macrocyclic bisacridine at abasic sites in DNA: nuclear magnetic resonance and molecular modeling study," *Biochemistry*, vol. 38, no. 43, pp. 14205–14213, 1999.

[202] S. Amrane, A. De Cian, F. Rosu, et al., "Identification of trinucleotide repeat ligands with a FRET melting assay," *ChemBioChem*, vol. 9, no. 8, pp. 1229–1234, 2008.

[203] M.-P. Teulade-Fichou, C. Carrasco, L. Guittat, et al., "Selective recognition of G-quadruplex telomeric DNA by a bis(quinacridine) macrocycle," *Journal of the American Chemical Society*, vol. 125, no. 16, pp. 4732–4740, 2003.

[204] C. Allain, D. Monchaud, and M.-P. Teulade-Fichou, "FRET templated by G-quadruplex DNA: a specific ternary interaction using an original pair of donor/acceptor partners," *Journal of the American Chemical Society*, vol. 128, no. 36, pp. 11890–11893, 2006.

[205] V. Gabelica, E. S. Baker, M.-P. Teulade-Fichou, E. De Pauw, and M. T. Bowers, "Stabilization and structure of telomeric and c-myc region intramolecular G-quadruplexes: the role of central cations and small planar ligands," *Journal of the American Chemical Society*, vol. 129, no. 4, pp. 895–904, 2007.

[206] P. Alberti, J. Ren, M. P. Teulade-Fichou, et al., "Interaction of an acridine dimer with DNA quadruplex structures," *Journal of Biomolecular Structure and Dynamics*, vol. 19, no. 3, pp. 505–513, 2001.

[207] P. Belmont, J. Bosson, T. Godet, and M. Tiano, "Acridine and acridone derivatives, anticancer properties and synthetic methods: where are we now?" *Anti-Cancer Agents in Medicinal Chemistry*, vol. 7, no. 2, pp. 139–169, 2007.

[208] M. Demeunynck, "Antitumour acridines," *Expert Opinion on Therapeutic Patents*, vol. 14, no. 1, pp. 55–70, 2004.

[209] W. A. Denny, "Acridine derivatives as chemotherapeutic agents," *Current Medicinal Chemistry*, vol. 9, no. 18, pp. 1655–1665, 2002.

[210] J.-L. Mergny, L. Lacroix, M.-P. Teulade-Fichou, et al., "Telomerase inhibitors based on quadruplex ligands selected by a fluorescence assay," *Proceedings of the National Academy of Sciences of the United States of America*, vol. 98, no. 6, pp. 3062–3067, 2001.

[211] C. Hounsou, L. Guittat, D. Monchaud, et al., "G-quadruplex recognition by quinacridines: a SAR, NMR, and biological study," *ChemMedChem*, vol. 2, no. 5, pp. 655–666, 2007.

[212] D. Monchaud, C. Allain, H. Bertrand, et al., "Ligands playing musical chairs with G-quadruplex DNA: a rapid and simple displacement assay for identifying selective G-quadruplex binders," *Biochimie*, vol. 90, no. 8, pp. 1207–1223, 2008.

[213] O. Baudoin, F. Gonnet, M.-P. Teulade-Fichou, J.-P. Vigneron, J.-C. Tabet, and J.-M. Lehn, "Molecular recognition of nucleotide pairs by a cyclo-bis-intercaland-type receptor molecule: a spectrophotometric and electrospray mass spectrometry study," *Chemistry: A European Journal*, vol. 5, no. 9, pp. 2762–2771, 1999.

[214] D. M. Crothers, "Calculation of binding isotherms for heterogenous polymers," *Biopolymers*, vol. 6, no. 4, pp. 575–584, 1968.

[215] J. D. McGhee and P. H. von Hippel, "Theoretical aspects of DNA protein interactions: cooperative and non cooperative binding of large ligands to a one dimensional homogeneous lattice," *Journal of Molecular Biology*, vol. 86, no. 2, pp. 469–489, 1974.

[216] M. Kaiser, A. De Cian, M. Sainlos, C. Renner, J.-L. Mergny, and M.-P. Teulade-Fichou, "Neomycin-capped aromatic platforms: quadruplex DNA recognition and telomerase inhibition," *Organic and Biomolecular Chemistry*, vol. 4, no. 6, pp. 1049–1057, 2006.

[217] A. De Cian, P. Grellier, E. Mouray, et al., "Plasmodium telomeric sequences: structure, stability and quadruplex targeting by small compounds," *ChemBioChem*, vol. 9, no. 16, pp. 2730–2739, 2008.

[218] A. Bugaut, K. Jantos, J.-L. Wietor, R. Rodriguez, J. K. M. Sanders, and S. Balasubramanian, "Exploring the differential recognition of DNA G-quadruplex targets by small molecules using dynamic combinatorial chemistry," *Angewandte Chemie International Edition*, vol. 47, no. 14, pp. 2677–2680, 2008.

[219] J. E. Redman, J. M. Granadino-Roldan, J. A. Schouten, et al., "Recognition and discrimination of DNA quadruplexes by acridine-peptide conjugates," *Organic and Biomolecular Chemistry*, vol. 7, no. 1, pp. 76–84, 2009.

SAGE-Hindawi Access to Research
Journal of Nucleic Acids
Volume 2010, Article ID 460561, 11 pages
doi:10.4061/2010/460561

Research Article

"*One Ring to Bind Them All*"—Part II: Identification of Promising G-Quadruplex Ligands by Screening of Cyclophane-Type Macrocycles

Anton Granzhan,[1] David Monchaud,[1,2] Nicolas Saettel,[1] Aurore Guédin,[3] Jean-Louis Mergny,[4] and Marie-Paule Teulade-Fichou[1]

[1] *Section Recherche, Institut Curie, CNRS UMR176, Centre Universitaire Paris XI, Bat. 110, 91405 Orsay, France*
[2] *Institut de Chimie Moléculaire, CNRS UMR5260, Université de Bourgogne, 21000 Dijon, France*
[3] *INSERM, U565, Acides Nucléiques : Dynamique, Ciblage et Fonctions Biologiques & CNRS, UMR5153, Laboratoire des Régulations et Dynamique du Génome, Muséum National d'histoire Naturelle USM 503, 43, Rue Cuvier, 75005 Paris, France*
[4] *INSERM U869, Institut Européen de Chimie et Biologie, Université de Bordeaux, 33607 Pessac cedex, France*

Correspondence should be addressed to Marie-Paule Teulade-Fichou, mp.teulade-fichou@curie.fr

Received 29 January 2010; Accepted 10 February 2010

Academic Editor: R. Eritja

A collection of 26 polyammonium cyclophane-type macrocycles with a large structural diversity has been screened for G-quadruplex recognition. A two-step selection procedure based on the FRET-melting assay was carried out enabling identification of macrocycles of high affinity ($\Delta T_{1/2}$ up to 30°C) and high selectivity for the human telomeric G-quadruplex. The four selected hits possess sophisticated architectures, more particularly the presence of a pendant side-arm as well as the existence of a particular topological arrangement appear to be strong determinants of quadruplex binding. These compounds are thus likely to create multiple contacts with the target that may be at the origin of their high selectivity, thereby suggesting that this class of macrocycles offers unique advantages for targeting G-quadruplex-DNA.

1. Introduction

The macrocyclic scaffold has proven to be highly valuable for the design of efficient and selective G-quadruplex ligands (see the review article in the present issue, "*One Ring to Bind Them All*"—Part I, by Monchaud et al.) [1–4]. Along these lines, two families of macrocyclic ligands have been particularly and thoroughly studied for their ability to specifically interact with quadruplex-DNA, namely, the families of telomestatin- [5] and porphyrin (TMPyP4)-related compounds [6–8]. Recently, a third family has emerged, namely the polyammonium cyclophane-type macrocycles, generally referred to as "CBI macrocycles" (for Cyclo-Bis-Intercalators), that adopt a non-planar conformation and therefore are structurally highly different from the two aforementioned classes. The efficiency of this family of ligands with regard to quadruplex DNA recognition is particularly illustrated by the compound BOQ_1 (Figure 1(a)) [9–11] as discussed in "*One Ring to Bind Them All*"—Part I. This compound is comprised of two large aromatic quinacridine units [12–14] able to interact with DNA bases through π-π interactions, and linked together *via* two short polyamine side chains, which ensure a global tetracationic charge at physiological pH affording both high water solubility and strong electrostatic attraction to DNA.

We have previously reported that BOQ_1 exhibits a high affinity for the human telomeric G-quadruplex DNA, along with a poor ability to associate with double-stranded DNA [9–11]. Consequently, this compound not only rivals the performances of telomestatin and TMPyP4 in terms of quadruplex-affinity (Figure 1(c)) [16], but elicits a quadruplex- over duplex-DNA selectivity comparable to that of telomestatin and highly superior to that of TMPyP4. One key to explain the very good quadruplex-binding properties

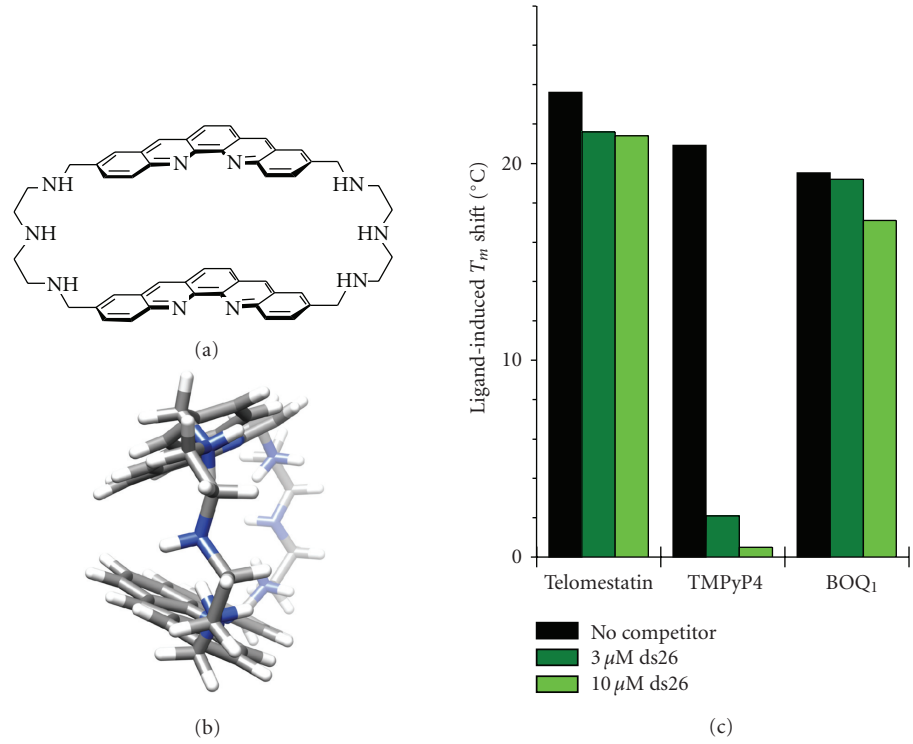

FIGURE 1: (a) Structure of BOQ_1. (b) Side-view of the lowest-energy conformation of BOQ_1 during the molecular dynamic simulation. (c) FRET-melting results obtained with telomestatin, TMPyP4, and BOQ_1 (1 μM), for experiments carried out with 0.2 μM F21T in lithium cacodylate buffer (10 mM, pH 7.2) with NaCl (100 mM), in the absence (black bars) or in the presence of 3 (dark green bars) or 10 μM (light green bars) of double-stranded competitor (ds26). (It is worth noting that the FRET-melting values obtained herein for BOQ_1 differ from that of the initial publication (see [9]). This discrepancy originates in the different experimental conditions used, given that FRET-melting is performed herein as an HTS unlike the initial report (single-cell experiment); the disparities between the two methods are extensively detailed in [15] (among which can be cited the final volume (25 versus 600 μL), the buffer conditions (10 mM lithium cacodylate + 100 mM NaCl versus 10 mM sodium cacodylate, 100 mM LiCl), etc.).)

of CBIs stands in their peculiar structural organization, which represents a non-planar conformation with a significant degree of molecular flexibility [11], thus clearly distinct from the planar rigid macrocycles telomestatin and TMPyP4. Indeed, previous works (NMR, X-rays and molecular modelling studies, *vide infra*) have shown that the CBI scaffold exists in a semiclosed conformation (Figure 1(b)) that results both from internal hydrophobic interactions between the two aromatic moieties and from a constrained distance between them imposed by the linkers [17]. This particular spatial organization is an essential determinant that governs the interaction of CBIs with secondary structures of DNA. In the case of quadruplex-DNA, BOQ_1 was initially thought to interact in an open-state conformation [9], but subsequent modelling studies [11] as well as recent molecular dynamics studies [18], suggested that the CBI scaffold never adopts the fully open conformation. In fact the semi-closed conformation of BOQ_1 has been shown to be not only the most stable conformation after *in silico* geometry optimization (Figure 1(b)) but also to be the favoured one when interacting with quadruplex structures (see "*One Ring to bind them all*"—Part I) [11]. It is thus hypothesized that this particular structure is at the origin of the efficient G-quadruplex recognition performed by BOQ_1, which is supposed to occur *via* a mixed binding mode combining quartet and loop interactions. Finally, given that the length of the polyammonium linker does not enable intercalation of both aromatic residues between contiguous base pairs in duplex-DNA due to the neighbour-exclusion principle [19, 20], the macrocyclic scaffold of BOQ_1 impedes binding to duplex-DNA, and consequently is responsible for the good selectivity for quadruplex- versus duplex-DNA.

The promising results obtained with BOQ_1 in terms of quadruplex recognition and selectivity prompted us to screen a collection of 26 CBI-type macrocycles previously synthesized [17, 18, 21, 22]. The members of this series (represented schematically in Figure 2, in extenso in Figure 3) differ by the nature of the aromatic units, the topology of the macrocyclic framework that contains either two different aromatic units or the same units, but with different connectivities; the nature and the derivatization of the linking chains; and finally the number of the constitutive "intercalator" units (two for CBI, three for CTI (Cyclo-Tris-Intercalators), Figure 2). In detail, the macrocycles are comprised of either polyaromatic cycles (naphthalene, anthracene, and biphenyl moieties), or heterocycles (such as acridine, quinacridine, phenanthroline, phenazine and bipyridine moieties) or even an organometallic unit (ferrocene), along with the possibility

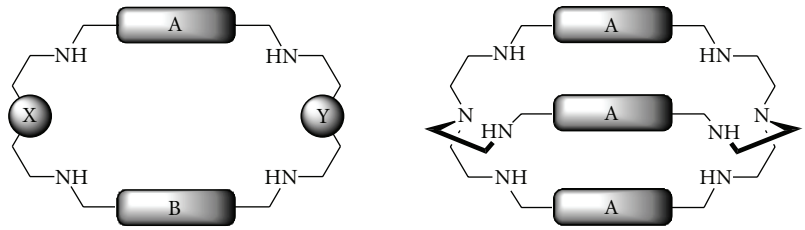

Figure 2: General representation of CBI (a) and CTI (b) macrocycles studied in this work. A, B: (hetero)aromatic residues; X, Y: O, NH, S, or pendant side arms.

of various connectivities that can be present in a given series. Moreover, oxygen or sulphur atoms were introduced in the linking chains in place of the secondary amino groups present in BOQ_1 (X = Y = NH, O or S, Figure 2), and in some cases the linkers bear tertiary amino groups due to substitution with pendant arms (X = Y = NR). All these structural variations allow to divide the present collection of macrocycles into four categories (Figure 3): (a) *homodimeric* macrocycles, containing two identical aromatic units (A = B); (b) *heterodimeric* macrocycles, containing two different aromatic units (A≠B); (c) pendant-arm macrocycles containing a bis-naphthalene scaffold (A = B = 2,6-naphthylene) with one (*monobrachial*) or two (*bibrachial*) side-chains with additional functional groups; and (d) *homotrimeric* macrocycles (cryptand–type) containing three identical aromatic units. With this series in hand, we systematically studied the influence of the various structural components of the macrocyclic scaffold on both the quadruplex-affinity and selectivity.

2. Results and Discussion

To evaluate the 26 compounds shown in Figure 3, we used the FRET-melting assay, which has been recently developed to a high-throughput screening format and provides reliable information concerning quadruplex-affinity and -selectivity in a straightforward manner [15]. This method is based on monitoring the ligand-induced stabilization of a fluorescently labelled quadruplex-forming structure (F21T, *FAM*-$G_3[T_2AG_3T]_3$-*Tamra*). The stabilization, measured *via* a *fluorescence resonance energy transfer* (FRET) between the two fluorescent partners (6-carboxyfluorescein, *FAM*, and 6-carboxytetramehtylrhodamine, *Tamra*), is expressed as an increase in melting temperature of F21T ($\Delta T_{1/2}$) in the presence of the ligand. This method also enables to gain insight into the quadruplex- over duplex-DNA selectivity if the melting experiments are carried out in the presence of various amounts of a 26-bp double-stranded DNA competitor (ds26, the self-complementary [5′-$CA_2TCG_2ATCGA_2T_2CGATC_2GAT_2G$-3′], up to 50 equiv.) Last but not least, FRET-melting enables also a direct comparison with recently reported ligands, given that this technique is now widely used by the quadruplex DNA community and often, as it is the case herein, as a test for the primary selection of ligands.

3. Selection of the High-Affinity Ligands

In the first round of experiments, we searched for the ligands with high affinity for the human telomeric quadruplex-DNA. FRET-melting experiments were thus carried out in the standard conditions previously calibrated for selection of high-affinity ligands [15], that is, with 0.2 μM F21T and 1 μM ligand. This first round of selection was performed both in sodium (10 mM lithium cacodylate, 100 mM NaCl) and potassium conditions (10 mM lithium cacodylate, 10 mM KCl, 90 mM LiCl) of identical ionic strength. This systematic comparison was necessary since the telomeric quadruplex is known to fold into different conformations depending on the cation present in the medium, displaying different loop arrangements that might result in differences in ligand binding [23–25]. The two conformations currently admitted to correspond to the predominant species in solution and in each are represented in Figure 1 of "*One Ring to Bind Them All*"—Part I. The results of the FRET-melting experiments with the 26 macrocycles are presented as a bar graph in Figure 4.

This series of experiment enabled us to classify the compounds in two categories, namely the high-affinity ligands ($\Delta T_{1/2} > 10°C$) and the ligands of moderate to low affinity ($\Delta T_{1/2} < 10°C$). The selection criteria, that is, the affinity threshold of 10°C, was motivated by the experience acquired over the past years when developing the FRET-melting assay.

As depicted in Figure 4, ten compounds (corresponding to blue structures in Figure 3) did not reach the affinity threshold (2,7-BisNP-S, 1,5-BisNP, 9,10-BisAN, 1,8-BisAN, 1,8/9,10-BisAN, 4,4′-BisBPy, 2,8-BisPZ, 4,7-BisPN, 2,7-NP/1,1′-FC, and 2,8-TrisPZ). Among the ligands which induce a stabilization by over 10°C, 8 ligands (corresponding to black structures in Figure 3) display a high quadruplex-affinity ($10°C < \Delta T_{1/2} < 20°C$: 2,7-BisNP, 2,7-BisNP-N, 1,5/2,6-BisNP, 3,3′-BisBP, 4,5-BisA, 2,7-NP/9,10-AN, 2,7-NP/2,7-A and 3,3′-TrisBP), and 8 ligands (corresponding to red structures in Figure 3) elicit a very high affinity ($\Delta T_{1/2} > 20°C$: 2,6-BisNP, 2,9-BisPN, BisNP-1NH2, BisNP-1PY, BisNP-2PY, BisNP-1FC, BisNP-2FC, and 2,7-TrisNP). It is worth noting that a $\Delta T_{1/2}$ value of 30–35°C as observed for BisNP-2PY represents the upper practical limit of the assay (corresponding to a $T_m \geq 80$–85°C for the ligand-DNA complex).

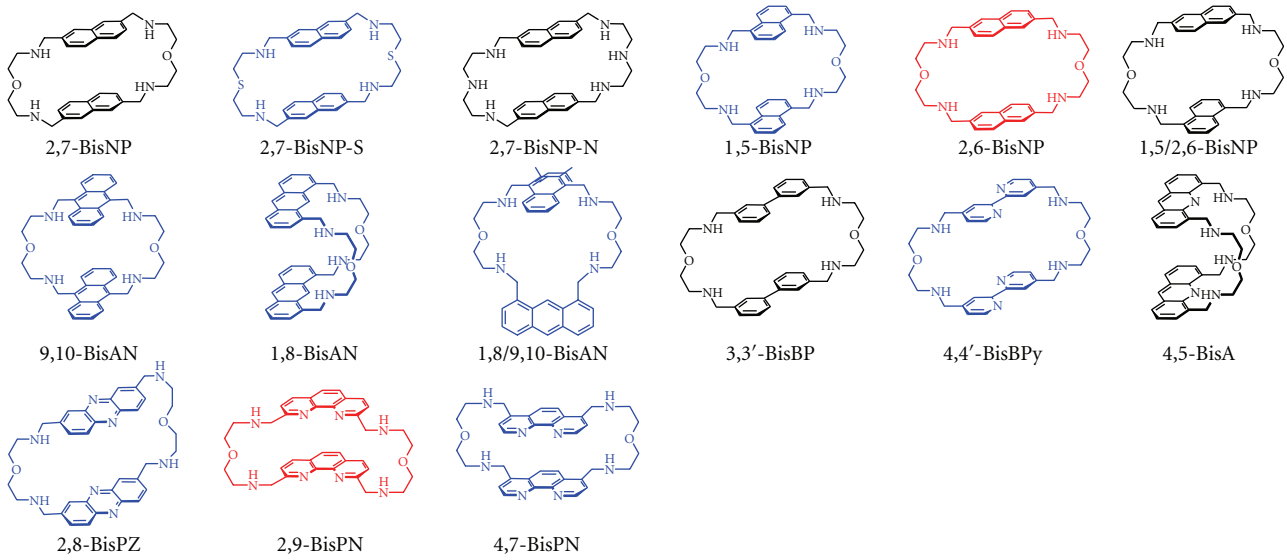

(a) Homodimeric macrocycles

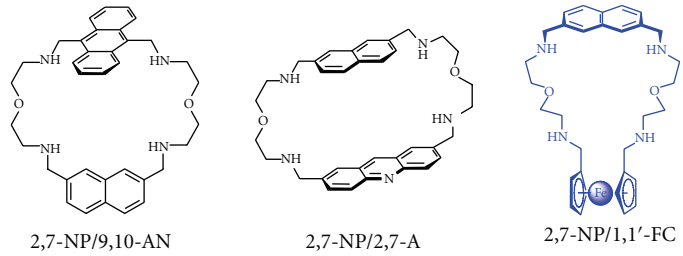

(b) Heterodimeric macrocycles

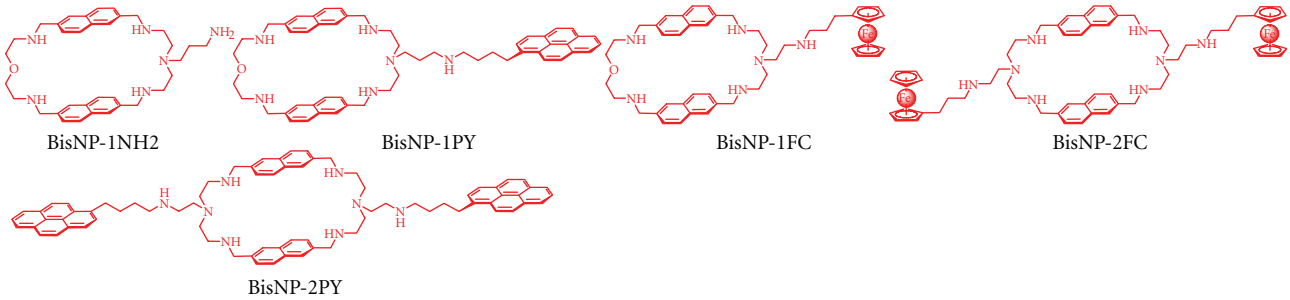

(c) Homodimeric pendant-arm macrocycles

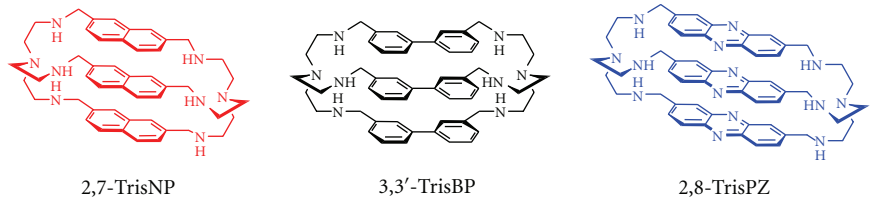

(d) Homotrimeric macrocycles

Figure 3: Structures of the 26 studied CBIs; see text below for the explanations of the color codes related to affinity and selectivity of the ligands.

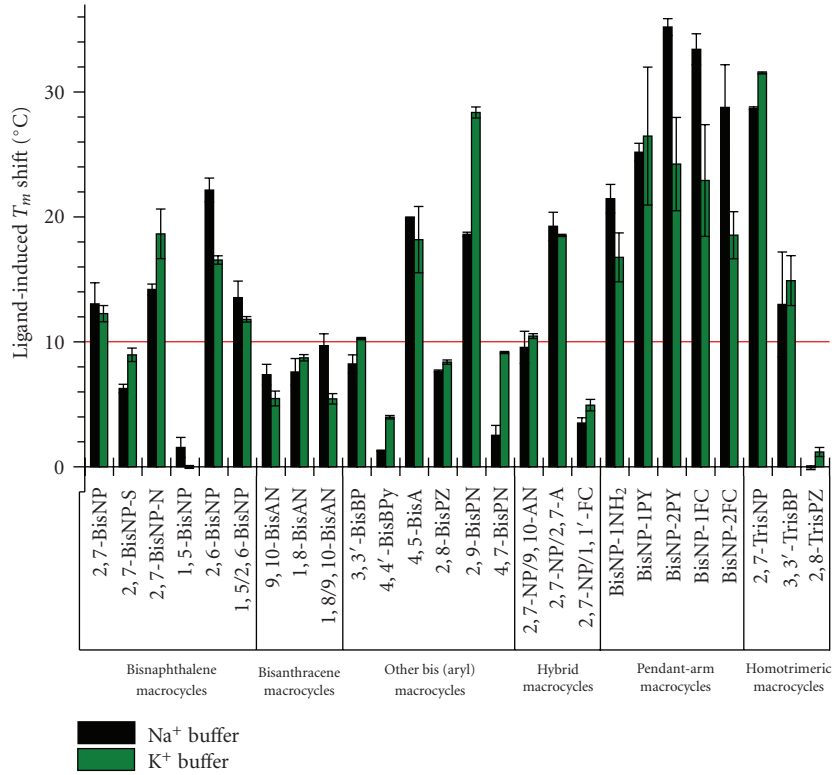

FIGURE 4: Stabilisation of F21T oligonucleotide ($\Delta T_{1/2}$, °C) induced by CBI macrocycles (1 μM) in Na^+- (black bars) or K^+-rich conditions (green bars); see main text for experimental details.

A close examination of these results enables us to identify the parameters that influence the efficiency of the quadruplex-recognition by the macrocyclic scaffold, namely, (a) the nature and (b) the connectivity of the intercalator units, (c) the nature of the linker, (d) the global charge of the ligand and (e) the number of intercalator units.

(a) *The nature of the intercalator unit*: (i) rigid fused aromatic units lead to better results than the unfused flexible ones. Indeed, the two CBIs containing biphenyl or bipyridine units 3,3′-BisBP and 4,4′-BisBPy induce a lower stabilization ($\Delta T_{1/2}$ Na/K = 8.2/10.4 and 1.3/4.0°C, resp.) than the corresponding naphthalene analogue 2,7-BisNP ($\Delta T_{1/2}$ Na/K = 9.1/12.2°C). (ii) The size of the aromatic units appears less important than their relative arrangement, since the four ligands comprising an anthracene unit (i.e., the largest intercalator used herein), namely, 1,8-, 9,10-, 1,8/9,10-BisAN and the anthracene-naphthalene hybrid 2,7-NP/9,10-AN, give results either below (the three former) or just reaching (the latter) the affinity threshold, whereas most naphthalene derivatives strongly stabilize the quadruplex-DNA. (iii)- Finally, the presence of two flat aromatic units in the typical CBI arrangement is an absolute requirement, as shown by the poor quadruplex-stabilizing properties of the unsymmetrical macrocycle 2,7-NP/1,1′-FC containing a bulky ferrocene unit ($\Delta T_{1/2} < 5$°C).

(b) *The connectivity of the intercalator units*: the connectivity of the two aromatic units determines the conformation and the internal molecular dynamics of the macrocycle. Consequently, it must have a profound influence on the DNA binding ability. This is fully confirmed herein by the striking differences observed within a given series: for example, in the naphthalene series, the 1,5-BisNP does not induce notable stabilization ($\Delta T_{1/2} < 2$°C) while 2,6-BisNP and 2,7-BisNP are above the affinity threshold ($\Delta T_{1/2}$ Na/K = 19.6/18.3 and 9.1/12.2°C, resp.). Similar conclusions can be drawn for the phenanthroline series, since 2,9-BisPN is much more efficient than its analogue 4,7-BisPN ($\Delta T_{1/2}$ = 13.8/16.8 and 2.5/9.1°C, resp.).

(c) *The nature of the linker*: interestingly, the replacement of the central oxygen atom by a sulfur atom (2,7-BisNP versus 2,7-BisNP-S) significantly reduces the stabilisation ($\Delta T_{1/2}$ Na/K = 9.1/12.2 and 6.3/9.0°C, resp.), an observation that can be attributed to the larger steric hindrance of the sulfur atom. On the other hand, the replacement of the central oxygen atom by a nitrogen atom improves the stabilization (2,7-BisNP versus 2,7-BisNP-N, $\Delta T_{1/2}$ Na/K = 9.1/12.2 and 13.3/16.3°C, resp.), suggesting a possible involvement of the NH group in H-bond interactions with the quadruplex target.

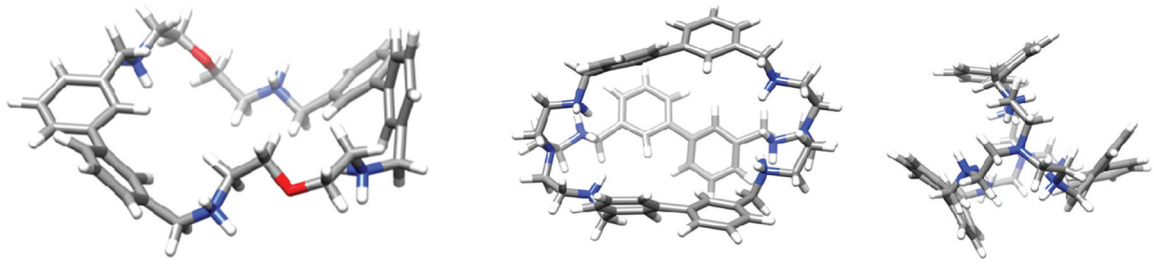

(a) (b)

Figure 5: Lowest energy conformations of (a) 3, 3′-BisBP and (b) 3, 3′-TrisBP (front and side-view) during a molecular dynamic simulation in a water box [29].

(d) *The global charge of the ligand*: previous studies have shown that only the benzylic nitrogens of the linkers are protonated at the experimental pH (7.2) both in the CBI and CTI series [26–28]. Thus, it can be assumed that the global cationic charge of the whole series varies from 4 (for CBIs) to 5 (for monosubstituted CBIs) up to 6+ (for disubstituted CBIs and CTIs). The data collected (Figure 4) show that there is no obvious dependence on the global charge of the ligand given that CBI compounds (4+) globally induce better stabilizations than CTI compounds (6+) and that the monosubstituted CBIs (5+) are more efficient than their disubstituted analogues (6+). We can conclude that the quadruplex-recognition is not dominated only by electrostatic parameters, although this interaction may contribute strongly to the stabilisation effect.

(e) *The number of intercalative units:* the number of intercalative units appears to play a crucial role since, in the biphenyl series, the bismacrocycle 3,3′-BisBP is less efficient than the corresponding trismacrocyclic compound 3, 3′-TrisBP ($\Delta T_{1/2}$Na/K= 8.2/10.4°C and 13.0/14.9°C). Although this difference could be explained by the higher cationic charge of the trimer (6+ for the CTI*versus* 4+ for the CBI), the poor activity of the trisphenazine (2,8-TrisPZ) that is also hexacationic argues against a dominant electrostatic effect (see also (d)). Thus the large difference between the two compounds is more likely attributable to the higher rigidity of the CTI as compared to that of the corresponding CBI. To support this hypothesis, molecular dynamic simulation in a water box has been performed with the two compounds: the results presented in Figure 5 show that 3, 3′-BisBP has an extremely high degree of flexibility and adopts a largely open conformation whilst 3, 3′-TrisBP is strongly conformationally restrained [29].

Altogether the results of this primary screen confirm that the association between the macrocycles and the quadruplex-DNA is strongly dependent on both the rigidity and the topology of the macrocyclic framework. Finally, as depicted in Figure 6, the behaviour of the majority of compounds shows a poor dependency on the cation present in the medium, thereby confirming that the quadruplex-recognition is primarily governed by tetrad-recognition.

4. Selection of Highly Selective Ligands

The first selection based on the amplitude of the F21T stabilisation induced by the ligand resulted in the selection of 16 compounds. For entering the second round of experiments, we further decided to arbitrary remove two candidates (3, 3′-BisBP and 2,7-NP/9,10-AN), since they do not reach the affinity threshold ($\Delta T_{1/2}$ = 10°C) in the two cationic conditions (Figure 4). The 14 remaining compounds were thus subjected to the second selection step that consists in reproducing the melting experiment of F21T in the presence of the nonlabelled duplex-DNA competitor ds26. As shown in previous works, the presence of the duplex-DNA competitor diminishes the quadruplex-binding of nonselective compounds (thus resulting in decreased $\Delta T_{1/2}$ values) and poorly affects the binding of selective compounds (thus resulting in unchanged $\Delta T_{1/2}$ values). The competitive FRET-melting assay enables thus a rapid evaluation of quadruplex- over duplex-DNA selectivity, a criterion that is of utmost importance for further developments of quadruplex ligands in cell-based assays.

Competitive FRET-melting experiments were carried out in the conditions used in the first experiment [15], that is, with 0.2 μM F21T, 1 μM ligand without ds26 or with two different concentrations of ds26 (3 and 10 μM, i.e., 15- and 50-molar excess relative to F21T). These experiments have been performed with the 14 selected macrocycles both in Na^+ and K^+ conditions; the results ($\Delta T_{1/2}$ values) are summarized as bar graphs shown in Figure 7.

In this second selection, 8 compounds (whose name is squared in red in Figure 7, see also Table 1) appear to keep on stabilizing efficiently the quadruplex-DNA ($\Delta T_{1/2}$ > 10°C, red dashed line in Figure 7(a), lower red dashed line in Figure 7(b)) in presence of 10 μM of duplex-DNA (i.e., 2,9-BisPN, 2,7-NP/2,7-A, BisNP-1PY, BisNP-2PY, BisNP-1FC, BisNP-2FC, 2,7-TrisNP, and 3, 3′-TrisBP); on the other hand, 6 compounds (2,7-BisNP, 2,7-BisNP-N, 2,6-BisNP, 1,5/2,6-BisNP, 4,5-BisA and BisNP-1NH2) are found less selective since their $\Delta T_{1/2}$ value was reduced to < 10°C in presence of 10 μM of ds26.

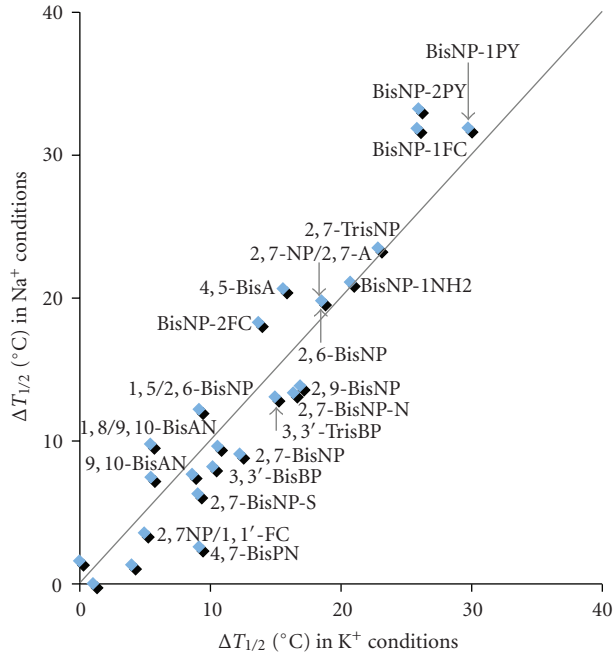

FIGURE 6: Plot of stabilization ($\Delta T_{1/2}$) measured in K^+- versus Na^+-rich conditions for the CBI macrocycles.

To further examine the properties of the eight ligands selected after the second selection step, we quantified the quadruplex- *versus* duplex-DNA selectivity by the ^{FRET}S value [30], which is defined as $^{FRET}S = \Delta T_{1/2}$ (10 μM ds26)/$\Delta T_{1/2}$ (no ds26); consequently, $^{FRET}S \rightarrow 1$ for highly selective ligands. This ratio has the advantage to paramter the $\Delta T_{1/2}$ value in presence of ds26 competitor as a function the $\Delta T_{1/2}$ value without ds26. Moderate (down to 0.36/0.48, Table 1) to excellent ^{FRET}S values (up to 1.01/0.98, Table 1) were determined for the eight selected compounds. This values ranking enables us to discard the two ligands showing the lowest selectivity (i.e., $^{FRET}S < 0.5$), namely BisNP-2PY and 2,7-TrisNP, thereby leaving six promising candidates (2,9-BisPN, 2,7-NP/2,7-A, BisNP-1PY, BisNP-1FC, and BisNP-2FC, 3, 3′-TrisBP) for entering the final round of selection (*vide infra*).

It is worth mentioning here that the selectivity ranking is not globally affected by the nature of the cation (Na^+ versus K^+, Figures 7(a) and 7(b), resp., Table 1); however, the values are significantly higher in presence of K^+, thereby indicating a higher resistance of the ligands to the competition of the duplex-DNA in these conditions. For this reason and also for the sake of clarity, we used only results obtained in K^+ (Figure 7(b)) for rationalizing the data: a close examination of the results enables us to identify three structural parameters that influence the selectivity of the quadruplex-recognition by the macrocycles, namely, (a) the presence of pendant arms, (b) the existence of a specific three-dimensional conformation, and (c) the rigidity of the macrocyclic framework.

(a) *The presence of pendant side-arm(s)*: this parameter contributes strongly to the quadruplex-selectivity, as demonstrated by the much higher $\Delta T_{1/2}$ values obtained in presence of 10 μM ds26 for the monobrachial and bibrachial compounds ($\Delta T_{1/2}$ = 21.5, 17.2, 12.6 and 11.5°C for BisNP-1PY, BisNP-1FC, BisNP-2PY, and BisNP-2FC, resp.) as compared with their nonsubstituted analogue 2,6-BisNP ($\Delta T_{1/2}$ = 5.6°C). Remarkably, pendant side-arms terminated by a functional group (pyrene (PY) or ferrocene (FC)) lead to ligands that exhibit higher quadruplex-affinity and -selectivity than their amino-terminated counterpart (i.e., BisNP-1NH_2, Figure 7 and Table 1; e.g., in presence of 10 μM ds26, $\Delta T_{1/2}$ = 29.7 versus 20.7°C and ^{FRET}S = 0.72 *versus* 0.38 for BisNP-1PY and BisNP-1NH_2, resp.). This clearly indicates that these functional groups are responsible for additional interactions with quadruplex-DNA, eventually with loops and/or grooves, which may result in the multiple anchorage of the ligand in its binding site. Finally, the better performances of monobrachial compounds as compared to bibrachial ones, both in terms of affinity (in presence of 10 μM ds26, $\Delta T_{1/2}$ = 29.7/25.8°C for BisNP-1PY/BisNP-1FC versus 25.9/13.6°C for BisNP-2PY/BisNP-2FC) and selectivity (^{FRET}S = 0.72/0.66 for BisNP-1PY/BisNP-1FC versus 0.48/0.84 for BisNP-2PY/BisNP-2FC) suggest that one pendant side-arm is enough to create optimized interactions with the quadruplex-DNA. The second pendant side-arm may impair the quadruplex-binding due to steric hindrance and also may participate to create nonspecific interactions since it increases the global charge of the molecule.

(b) *The existence of a specific 3D conformation*: in the naphthalene (NP) series, the replacement of an NP

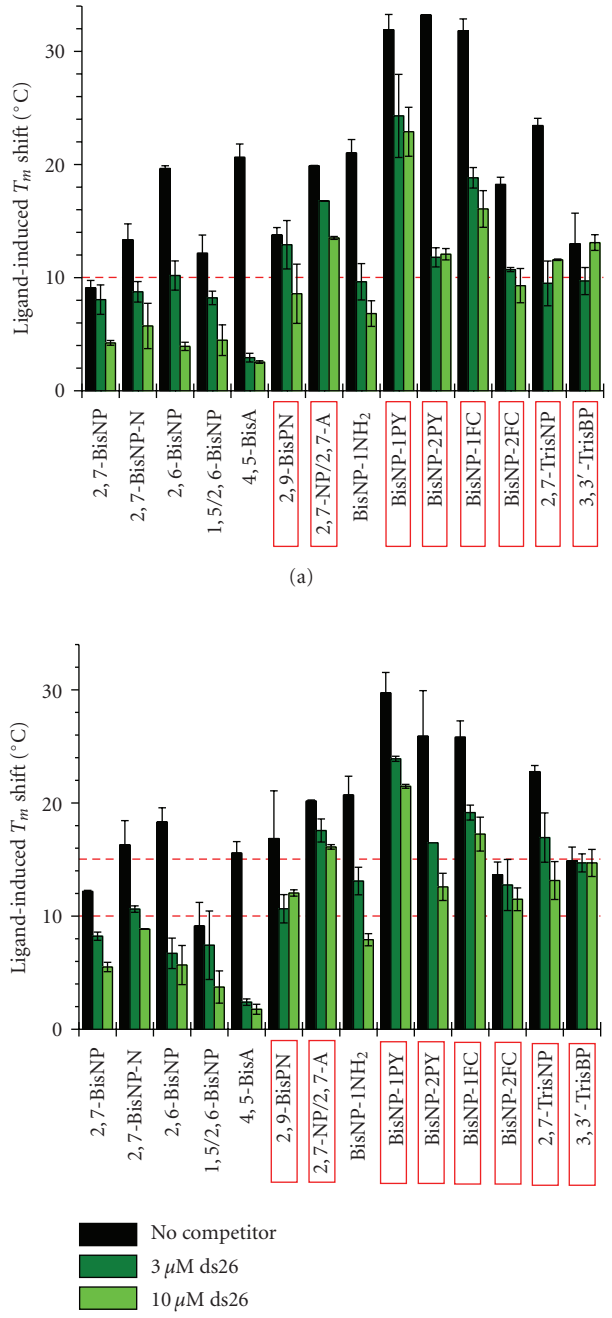

Figure 7: Stabilisation of F21T oligonucleotide ($\Delta T_{1/2}$, °C) induced by CBI and CTI macrocycles (1 μM) in (a) Na^+- and (b) K^+-rich conditions, for experiments carried out in the absence (black bars) or in the presence of 3 (dark green bars) or 10 μM (light green bars) of the duplex competitor (ds26).

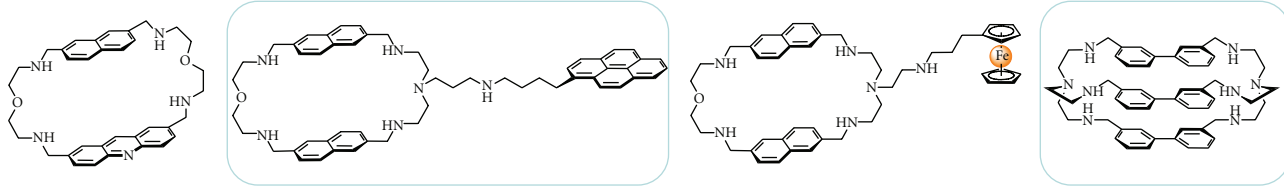

2,7-NP/2,7-A BisNP-1PY BisNP-1FC 3,3'-TrisBP

Figure 8: Structures of the four most promising members of the macrocyclic series.

Table 1: Competitive FRET-melting results of the 8 ligands selected after the second selection step.

	in Na^+-conditions				in K^+-conditions			
	$\Delta T_{1/2}$ (°C)			^{FRET}S	$\Delta T_{1/2}$ (°C)			^{FRET}S
	no competitior	+3 μM ds26	+10 μM ds26	10 μM ds26	no competitior	+3 μM ds26	+10 μM ds26	10 μM ds26
2,9-BisPN	13.7	12.9	8.6	0.62	16.8	10.6	12.0	0.71
2,7-NP/2,7-A	19.9	16.8	13.5	0.68	20.1	17.6	16.1	0.79
BisNP-1PY	31.9	24.3	22.9	0.71	29.7	23.9	21.5	0.72
BisNP-2PY	33.2	11.8	12.0	0.36	25.9	16.5	12.6	0.48
BisNP-1FC	31.8	18.8	16.1	0.50	25.8	19.1	17.2	0.66
BisNP-2FC	18.2	10.7	9.3	0.51	13.6	12.7	11.5	0.84
2,7-TrisNP	23.4	9.5	11.6	0.49	22.8	16.9	13.1	0.57
3, 3′-TrisBP	13.0	9.7	13.1	1.01	14.9	14.7	14.7	0.98

unit in 2,7-BisNP by an acridine unit (i.e., 2,7-NP/2,7-A) increases the internal stacking interactions between the aromatic units, which in turn results in a more stable semi-closed conformation; given that 2,7-NP/2,7-A displays a better binding properties than 2,7-BisNP, both in terms of affinity (in presence of 10 μM ds26, $\Delta T_{1/2}$ = 20.1 versus 12.2°C) and selectivity (^{FRET}S = 0.79 versus 0.45), we can conclude that a particular topology could be highly favorable for increasing the efficiency of the ligand/quadruplex-DNA interactions. The same trend is observed when the NP units are replaced by the surface-extended phenanthroline (PN) units; the resulting compound, 2,9-BisPN, displays improved performances as compared to 2,7-BisNP (in presence of 10 μM ds26, $\Delta T_{1/2}$ = 16.8°C, and ^{FRET}S = 0.71). These two cases indicate that subtle modifications of the aromatic units that compose the CBI scaffold significantly increase the selectivity; these modifications may contribute to determine a particular topology of the CBI, thus disfavoring the association with duplex-DNA. Interestingly, the crystal structure of 2,9-BisPN has recently described [31] evidence of a "horse-shoe" conformation that may be prone to fit into the quadruplex-DNA bonding site. The importance of the 3D topology suggested here is in line with the role of the connectivity observed during the primary screen (*vide supra*).

(c) Finally, in the NP series, the formal introduction of a third NP branch in 2,7-BisNP scaffold significantly improves the binding properties of the resulting compounds (i.e., 2,7-TrisNP, in presence of 10 μM ds26, $\Delta T_{1/2}$ = 22.7, and ^{FRET}S = 0.57); we can thus conclude that, given that 2,7-TrisNP is structurally more constrained than 2,7-BisNP, the rigidity of the ligand is a valuable parameter to control when searching to improve the quality of the recognition of the DNA target. The same trend is observed in the bipyridine (BP) series, since 3, 3′-TrisBP displays a higher quadruplex-affinity than 3, 3′-BisBP ($\Delta T_{1/2}$ = 14.9 versus 10.2°C); interestingly, 3, 3′-TrisBP shows a quite exceptional selectivity (with ^{FRET}S >0.98), although its stabilizing effect is modest as compared to 2,7-TrisNP. These two examples demonstrate the interest of the CTI design for improving the quadruplex-selectivity, supporting the observation that the rigidity of the CBI is not only favorable for the quadruplex-binding but also for decreasing the duplex-binding. Last but not least, these results also indicate that electrostatic interactions are not critically determinant for the binding of CTI to both quadruplex- and duplex-DNA.

Thus, the two-step selection process described herein (step 1: affinity, step 2: selectivity) enables the rapid identification of six candidates (2,9-BisPN, 2,7-NP/2,7-A, BisNP-1PY, BisNP-1FC, BisNP-2FC, and 3, 3′-TrisBP) with remarkable quadruplex-interacting properties, that is, high affinity and selectivity. To further increase the selection pressure and select hits for subsequent developments, we decided to focus our attention on compounds that display $\Delta T_{1/2} \geq$ 15°C in presence of 10 μM ds26 (upper red dashed line in Figure 7(b)). Four compounds fulfill this requirement, namely, 2,7-NP/2,7-A, BisNP-1PY, BisNP-1FC, and 3, 3′-TrisBP (Figures 7 and 8, it is worth noting that this selection has been extended to 3, 3′-TrisBP, since its $\Delta T_{1/2}$ in presence of 10 μM ds26 (14.7°C) is an average value resulting from experiments with $\Delta T_{1/2} \geq$ 15°C). Amongst these four compounds, two were thus elected as the most promising compounds over the 26 macrocycles screened: (i) BisNP-1PY, since this CBI combines the best affinity and selectivity on the basis of the three values used for the selection procedure (in K^+ conditions: $\Delta T_{1/2}$ = 29.7 and 21.5°C in absence and presence of 10 μM ds26, resp. ^{FRET}S = 0.72; in Na^+ conditions: $\Delta T_{1/2}$ = 31.9 and 22.9°C in absence and presence of 10 μM ds26, resp., ^{FRET}S = 0.71), and (ii)- 3, 3′-TrisBP, since, while displaying a decent affinity, this CTI reaches an unprecedented level of quadruplex- over duplex-DNA selectivity (^{FRET}S = 1.01 and 0.98 in Na^+ and K^+ conditions, resp.).

5. Conclusion

The CBIs were initially designed to trap flat aromatic substrates between their aromatic units [22, 26, 32]; however, it turned out very rapidly that these compounds

display remarkable binding preference for single-stranded and locally unpaired DNA (abasic [33], mismatched sites) [17, 18, 21, 34] and various secondary structures (hairpins [35], trinucleotide repeats [36], G-quadruplex) [9–11, 37]. We show here that this class of macrocycles offers unique advantages for targeting G-quadruplex-DNA.

The two-step selection procedure followed herein as well as the structural diversity of the collection studied enabled us to identify several structural features that govern the efficiency of the quadruplex-recognition by the CBI ligands. Among these, the presence of a pendant side-arm and the existence of a particular topological arrangement appear to be strong determinants. The selected hits possess sophisticated architectures and are thus likely to create multiple contacts with the quadruplex-DNA structure. This should result from a complex interplay of π-stacking interactions, H-bonding, and electrostatic forces both with the accessible G-tetrad of the quadruplex-DNA and with the quadruplex-elements that surround the G-tetrad (loops and/or grooves). These secondary interactions may be at the origin of the high selectivity observed.

In conclusion, we have performed the first step toward the identification of two molecules that are highly promising ligands of the human telomeric quadruplex in vitro and opened the way towards new molecular designs of high efficiency. We are thus now performing further studies with these ligands to investigate their peculiar binding mode and in vivo properties.

Acknowledgments

The authors would like to thank sincerely their coworkers, C. Guetta, A. De Cian, E. Largy, and L. Lacroix, for technical assistance and stimulating scientific discussions related to G-quadruplex DNA and ligands. A special acknowledgment is due to J. R. R. Tolkien for the title inspiration.

References

[1] D. Monchaud and M.-P. Teulade-Fichou, "A hitchhiker's guide to G-quadruplex ligands," *Organic and Biomolecular Chemistry*, vol. 6, no. 4, pp. 627–636, 2008.

[2] A. Arola and R. Vilar, "Stabilisation of G-quadruplex DNA by small molecules," *Current Topics in Medicinal Chemistry*, vol. 8, no. 15, pp. 1405–1415, 2008.

[3] M. Franceschin, "G-quadruplex DNA structures and organic chemistry: more than one connection," *European Journal of Organic Chemistry*, no. 14, pp. 2225–2238, 2009.

[4] S. Neidle, "The structures of quadruplex nucleic acids and their drug complexes," *Current Opinion in Structural Biology*, vol. 19, no. 3, pp. 239–250, 2009.

[5] K. Shin-ya, K. Wierzba, K. Matsuo, et al., "Telomestatin, a novel telomerase inhibitor from Streptomyces anulatus," *Journal of the American Chemical Society*, vol. 123, no. 6, pp. 1262–1263, 2001.

[6] F. X. Han, R. T. Wheelhouse, and L. H. Hurley, "Interactions of TMPyP4 and TMPyP2 with quadruplex DNA. Structural basis for the differential effects on telomerase inhibition," *Journal of the American Chemical Society*, vol. 121, no. 15, pp. 3561–3570, 1999.

[7] E. Izbicka, R. T. Wheelhouse, E. Raymond, et al., "Effects of cationic porphyrins as G-quadruplex interactive agents in human tumor cells," *Cancer Research*, vol. 59, no. 3, pp. 639–644, 1999.

[8] D.-F. Shi, R. T. Wheelhouse, D. Sun, and L. H. Hurley, "Quadruplex-interactive agents as telomerase inhibitors: synthesis of porphyrins and structure-activity relationship for the inhibition of telomerase," *Journal of Medicinal Chemistry*, vol. 44, no. 26, pp. 4509–4523, 2001.

[9] M.-P. Teulade-Fichou, C. Carrasco, L. Guittat, et al., "Selective recognition of G-quadruplex telomeric DNA by a bis(quinacridine) macrocycle," *Journal of the American Chemical Society*, vol. 125, no. 16, pp. 4732–4740, 2003.

[10] C. Allain, D. Monchaud, and M.-P. Teulade-Fichou, "FRET templated by G-quadruplex DNA: a specific ternary interaction using an original pair of donor/acceptor partners," *Journal of the American Chemical Society*, vol. 128, no. 36, pp. 11890–11893, 2006.

[11] V. Gabelica, E. S. Baker, M.-P. Teulade-Fichou, E. De Pauw, and M. T. Bowers, "Stabilization and structure of telomeric and c-myc region intramolecular G-quadruplexes: the role of central cations and small planar ligands," *Journal of the American Chemical Society*, vol. 129, no. 4, pp. 895–904, 2007.

[12] J.-L. Mergny, L. Lacroix, M.-P. Teulade-Fichou, et al., "Telomerase inhibitors based on quadruplex ligands selected by a fluorescence assay," *Proceedings of the National Academy of Sciences of the United States of America*, vol. 98, no. 6, pp. 3062–3067, 2001.

[13] C. Hounsou, L. Guittat, D. Monchaud, et al., "G-quadruplex recognition by quinacridines: a SAR, NMR, and biological study," *ChemMedChem*, vol. 2, no. 5, pp. 655–666, 2007.

[14] D. Monchaud, C. Allain, H. Bertrand, et al., "Ligands playing musical chairs with G-quadruplex DNA: a rapid and simple displacement assay for identifying selective G-quadruplex binders," *Biochimie*, vol. 90, no. 8, pp. 1207–1223, 2008.

[15] A. De Cian, L. Guittat, M. Kaiser, et al., "Fluorescence-based melting assays for studying quadruplex ligands," *Methods*, vol. 42, no. 2, pp. 183–195, 2007.

[16] A. De Cian, L. Guittat, K. Shin-ya, J. F. Riou, and J. L. Mergny, "Affinity and selectivity of G4 ligands measured by FRET," *Nucleic Acids Symposium Series*, no. 49, pp. 235–236, 2005.

[17] M. Bahr, V. Gabelica, A. Granzhan, M.-P. Teulade-Fichou, and E. Weinhold, "Selective recognition of pyrimidine-pyrimidine DNA mismatches by distance-constrained macrocyclic bis-intercalators," *Nucleic Acids Research*, vol. 36, no. 15, pp. 5000–5012, 2008.

[18] A. Granzhan, E. Largy, N. Saettel, and M.-P. Teulade-Fichou, "Macrocyclic DNA-mismatch-binding ligands: structural determinants of selectivity," *Chemistry—A European Journal*, vol. 16, no. 3, pp. 878–889, 2010.

[19] D. M. Crothers, "Calculation of binding isotherms for heterogenous polymers," *Biopolymers*, vol. 6, no. 4, pp. 575–584, 1968.

[20] J. D. McGhee and P. H. Von Hippel, "Theoretical aspects of DNA protein interactions: cooperative and non cooperative binding of large ligands to a one dimensional homogeneous lattice," *Journal of Molecular Biology*, vol. 86, no. 2, pp. 469–489, 1974.

[21] A. Granzhan and M.-P. Teulade-Fichou, "A fluorescent bisanthracene macrocycle discriminates between matched and mismatch-containing DNA," *Chemistry—A European Journal*, vol. 15, no. 6, pp. 1314–1318, 2009.

[22] A. Granzhan and M.-P. Teulade-Fichou, "Synthesis of mono- and bibrachial naphthalene-based macrocycles with pyrene or

ferrocene units for anion detection," *Tetrahedron*, vol. 65, no. 7, pp. 1349–1360, 2009.

[23] S. Burge, G. N. Parkinson, P. Hazel, A. K. Todd, and S. Neidle, "Quadruplex DNA: sequence, topology and structure," *Nucleic Acids Research*, vol. 34, no. 19, pp. 5402–5415, 2006.

[24] D. J. Patel, A. T. Phan, and V. Kuryavyi, "Human telomere, oncogenic promoter and 5′-UTR G-quadruplexes: diverse higher order DNA and RNA targets for cancer therapeutics," *Nucleic Acids Research*, vol. 35, no. 22, pp. 7429–7455, 2007.

[25] J. Dai, M. Carver, and D. Yang, "Polymorphism of human telomeric quadruplex structures," *Biochimie*, vol. 90, no. 8, pp. 1172–1183, 2008.

[26] M. Dhaenens, J.-M. Lehn, and J.-P. Vigneron, "Molecular recognition of nucleosides, nucleotides and anionic planar substrates by a water-soluble bis-intercaland-type receptor molecule," *Journal of the Chemical Society, Perkin Transactions 2*, no. 7, pp. 1379–1381, 1993.

[27] M. P. Teulade-Fichou, J.-P. Vigneron, and J.-M. Lehn, "Molecular recognition of nucleosides and nucleotides by a water-soluble cyclo-bis-intercaland receptor based on acridine subunits," *Journal of Supramolecular Chemistry*, vol. 5, no. 2, pp. 139–147, 1995.

[28] M.-P. Teulade-Fichou, J.-P. Vigneron, and J.-M. Lehn, "Detection of organic anions in water through complexation enhanced fluorescence of a macrobicyclic tris-acridine cryptand," *Journal of the Chemical Society. Perkin Transactions 2*, vol. 10, pp. 2169–2175, 1996.

[29] E. F. Pettersen, T. D. Goddard, C. C. Huang, et al., "UCSF Chimera—a visualization system for exploratory research and analysis," *Journal of Computational Chemistry*, vol. 25, no. 13, pp. 1605–1612, 2004.

[30] A. De Cian, P. Grellier, E. Mouray, et al., "Plasmodium telomeric sequences: structure, stability and quadruplex targeting by small compounds," *ChemBioChem*, vol. 9, no. 16, pp. 2730–2739, 2008.

[31] C. Cruz, R. Delgado, M. G. B. Drew, and V. Félix, "Evaluation of the binding ability of a novel dioxatetraazamacrocyclic receptor that contains two phenanthroline units: selective uptake of carboxylate anions," *Journal of Organic Chemistry*, vol. 72, no. 11, pp. 4023–4034, 2007.

[32] O. Baudoin, F. Gonnet, M.-P. Teulade-Fichou, J.-P. Vigneron, J.-C. Tabet, and J.-M. Lehn, "Molecular recognition of nucleotide pairs by a cyclo-bis-intercaland-type receptor molecule: a spectrophotometric and electrospray mass spectrometry study," *Chemistry—A European Journal*, vol. 5, no. 9, pp. 2762–2771, 1999.

[33] M. Jourdan, J. Garcia, J. Lhomme, M.-P. Teulade-Fichou, J.-P. Vigneron, and J.-M. Lehn, "Threading bis-intercalation of a macrocyclic bisacridine at abasic sites in DNA: nuclear magnetic resonance and molecular modeling study," *Biochemistry*, vol. 38, no. 43, pp. 14205–14213, 1999.

[34] A. David, N. Bleimling, C. Beuck, J.-M. Lehn, E. Weinhold, and M.-P. Teulade-Fichou, "DNA mismatch-specific base flipping by a bisacridine macrocycle," *ChemBioChem*, vol. 4, no. 12, pp. 1326–1331, 2003.

[35] A. Slama-Schwok, F. Peronnet, E. Hantz-Brachet, et al., "A macrocyclic bis-acridine shifts the equilibrium from duplexes towards DNA hairpins," *Nucleic Acids Research*, vol. 25, no. 13, pp. 2574–2581, 1997.

[36] S. Amrane, A. De Cian, F. Rosu, et al., "Identification of trinucleotide repeat ligands with a FRET melting assay," *ChemBioChem*, vol. 9, no. 8, pp. 1229–1234, 2008.

[37] P. Alberti, J. Ren, M.-P. Teulade-Fichou, et al., "Interaction of an acridine dimer with DNA quadruplex structures," *Journal of Biomolecular Structure and Dynamics*, vol. 19, no. 3, pp. 505–513, 2001.

SAGE-Hindawi Access to Research
Journal of Nucleic Acids
Volume 2010, Article ID 247137, 7 pages
doi:10.4061/2010/247137

Research Article

Selective Binding of Distamycin A Derivative to G-Quadruplex Structure $[d(TGGGGT)]_4$

Bruno Pagano,[1] Iolanda Fotticchia,[2] Stefano De Tito,[3] Carlo A. Mattia,[1] Luciano Mayol,[3] Ettore Novellino,[4] Antonio Randazzo,[3] and Concetta Giancola[2]

[1] *Dipartimento di Scienze Farmaceutiche, Università di Salerno, Via Ponte don Melillo, 84084 Fisciano, Italy*
[2] *Dipartimento di Chimica "P. Corradini", Università di Napoli Federico II, Via Cintia, 80126 Napoli, Italy*
[3] *Dipartimento di Chimica delle Sostanze Naturali, Università di Napoli Federico II, Via D. Montesano 49, 80131 Napoli, Italy*
[4] *Dipartimento di Chimica Farmaceutica e Tossicologica, Università di Napoli Federico II, Via D. Montesano 49, 80131 Napoli, Italy*

Correspondence should be addressed to Antonio Randazzo, antonio.randazzo@unina.it and Concetta Giancola, giancola@unina.it

Received 21 January 2010; Accepted 7 March 2010

Academic Editor: Jean Louis Mergny

Guanine-rich nucleic acid sequences can adopt G-quadruplex structures stabilized by layers of four Hoogsteen-paired guanine residues. Quadruplex-prone sequences are found in many regions of human genome and in the telomeres of all eukaryotic organisms. Since small molecules that target G-quadruplexes have been found to be effective telomerase inhibitors, the identification of new specific ligands for G-quadruplexes is emerging as a promising approach to develop new anticancer drugs. Distamycin A is known to bind to AT-rich sequences of duplex DNA, but it has recently been shown to interact also with G-quadruplexes. Here, isothermal titration calorimetry (ITC) and NMR techniques have been employed to characterize the interaction between a dicationic derivative of distamycin A (compound **1**) and the $[d(TGGGGT)]_4$ quadruplex. Additionally, to compare the binding behaviour of netropsin and compound **1** to the same target, a calometric study of the interaction between netropsin and $[d(TGGGGT)]_4$ has been performed. Experiments show that netropsin and compound **1** are able to bind to $[d(TGGGGT)]_4$ with good affinity and comparable thermodynamic profiles. In both cases the interactions are entropically driven processes with a small favourable enthalpic contribution. Interestingly, the structural modifications of compound **1** decrease the affinity of the ligand toward the duplex, enhancing the selectivity.

1. Introduction

It is well known that G-rich sequences can adopt unusual DNA secondary structures with biological significance, the G-quadruplexes. These structures are four-stranded helical complexes, composed of stacks of G-tetrads, a cyclic array of four guanine bases which are connected by Hoogsteen hydrogen bonding. The phosphodiester backbones of the four quadruplex-forming strands could be in parallel or antiparallel relative orientation, generating grooves of different width and several loops arrangement. Generally, the formation of G-quadruplexes requires the presence of metal cations that selectively bind to guanine O6 carbonyl groups in the central cavity generated by the stacked layers of G-tetrads [1].

Sequences with propensity to form G-quadruplexes have been identified in biologically significant genomic regions such as telomeres or oncogene promoter regions [2, 3], which have emerged as potential targets for anticancer drug development. Very importantly, DNA G-quadruplex structures that form in the promoter region of oncogenes have recently showed to play a role in the control of gene expression and the modulation of such expression could be achieved by targeting these structures [4].

Telomeric sequences, which are found at the ends of eukaryotic chromosomes, consist of G-rich repeats on the single-stranded 3′ end. Oligonucleotides corresponding to the G-rich 3′ strand of telomeric DNA of a variety of organisms have been shown to fold into G-quadruplex DNA structures [5]. The truncated sequence of *Tetrahymena* telomeric DNA, d(TGGGGT), forms a tetramolecular quadruplex in presence of cations, with a parallel-stranded, right-handed helical structure containing four equivalent grooves [6].

The biological importance of telomeric G-quadruplex structures arises from the evidence that high telomerase activity (not present in somatic cells) has been implicated in about 85% of tumours [7]. The telomerase elongates the G-rich strand of telomeric DNA, leading the cancer cells to infinite lifetime. For that reason, the inhibition of telomerase has become an interesting strategy for the anticancer therapy [8]. Since the formation of G-quadruplexes by telomeric DNA inhibits the activity of telomerase, small molecules that stabilize the G-quadruplex structures could potentially be effective chemotherapeutic agents [9].

In this scenario, the identification of new ligands that are specific for G-quadruplex structures is emerging as a promising approach to develop new anticancer drugs. Despite the fact that the structures of G-quadruplexes differ considerably from the double helix, the design of selective quadruplex ligands is very difficult, because the structure of G-quadruplexes varies in several different ways, including number and orientation of strands, grooves width, and loops topology [1]. Nevertheless, a number of G-quadruplex binding agents has been proposed so far and some of these have been demonstrated to be effective telomerase inhibitors [10].

Most of the reported G-quadruplex ligands interact with the outer G-tetrads of the structures through π-π stacking interactions [11]. The only groove binder experimentally proven to date has been investigated in our laboratories; it is the distamycin A that interacts in a groove-binding mode with the quadruplex $[d(TGGGGT)]_4$ [12]. This finding, along with the observation that derivatives of distamycin could be effective inhibitors of the human telomerase [13], has stimulated other investigations. In a previous study, we investigated the importance of the crescent shape extension by varying the pyrrole units number in distamycin A [14, 15]. We focused our attention on the interaction of two carbamoyl analogues of distamycin A, containing four and five pyrrole units, respectively. Experiments revealed that the presence of one additional pyrrole unit affects the affinity as well as the stoichiometry of the binding whereas the addition of two pyrrole units leads to a total loss of interaction between the derivative and the $[d(TGGGGT)]_4$.

In this work, we evaluate the effect of a second cationic group, placed at the end of the molecule, on the interaction with DNA molecules. In particular, we report a calorimetric and NMR study of the interaction between the $[d(TGGGGT)]_4$ quadruplex and a new distamycin A derivative (compound **1**, Figure 1), where the initial formamide group is replaced by a charged N-formimidoil moiety.

In addition, since compound **1** can also be considered as an analogue of netropsin because it presents one pyrrole unit more than netropsin (three instead of two), but two cationic ends like it (even if different groups), we compare the binding of compound **1** to $[d(TGGGGT)]_4$ with the binding of netropsin to the same target.

Finally, to investigate the selectivity of compound **1** for the G-quadruplex relative to duplex, we also performed a study of the interaction between the drug and the self-complementary DNA duplex $d(CGCGAATTCGCG)_2$. This symmetric dodecamer was chosen because (a) it contains the central AATT core, which is considered the specific binding site for distamycin and netropsin; (b) the interaction with netropsin is well characterized in literature, from both structural and thermodynamic point of view [16–19].

2. Materials and Methods

2.1. Materials. The d(TGGGGT) and d(CGCGAATTCGCG) oligonucleotide sequences used for this study were purchased from the Primm Company (Milan, Italy).

Quadruplex and duplex samples were prepared by dissolving the lyophilised compound in a buffer solution containing 20 mM phosphate with 70 mM KCl, 0.1 mM EDTA at pH 7.0. The resulting solutions were annealed by heating at 95°C for 5 minutes. The solutions were then slowly cooled to room temperature and equilibrated for 1 day at 4°C. The concentration of oligonucleotides was determined by UV adsorption measurements at 90°C using molar extinction coefficient values $\varepsilon_{(260\,nm)}$ of 57800 and 110700 $M^{-1}\,cm^{-1}$ for d(TGGGGT) and d(CGCGAATTCGCG), respectively. The molar extinction coefficients were calculated by the nearest neighbour model [20].

Compound **1** has been synthesized as reported in the literature [21], while netropsin has been purchased from Sigma-Aldrich (St. Louis, MO). Drug solutions have been prepared in the same buffer used for the oligonucleotides, and the concentration has been estimated by UV spectroscopy using the calculated extinction coefficient value $\varepsilon_{(297\,nm)}$ of 30000 $M^{-1}\,cm^{-1}$ for compound **1** and the reported extinction coefficient value $\varepsilon_{(296\,nm)}$ of 21500 $M^{-1}\,cm^{-1}$ for netropsin [22].

2.2. Nuclear Magnetic Resonance Experiments. $[d(TGGGGT)]_4$ and $d(CGCGAATTCGCG)_2$ NMR samples were prepared at a concentration of 2 mM and 1 mM respectively, in 0.2 ml (H_2O/D_2O 9 : 1) buffer solution having 10 mM KH_2PO_4/K_2HPO_4, 70 mM KCl, 0.1 mM EDTA, and pH 7.0. NMR spectra were recorded with Varian ^{Unity}INOVA 700 MHz spectrometer. ^1H chemical shifts were referenced relative to external sodium 2,2-dimethyl-2-silapentane-5-sulfonate (DSS). 1D proton spectra of samples were recorded using pulsed-field gradient DPFGSE for H_2O suppression [23, 24].

2.3. Isothermal Titration Calorimetry Experiments. ITC experiments were carried out at 298 K using a high-sensitivity CSC-5300 Nano-ITC microcalorimeter from Calorimetry Science Corporation (Lindon, Utah) with a cell volume of 1 ml. Before each ITC experiment, the pH of each solution was checked, the reference cell was filled with deionised water, and the DNA solutions were degassed for 5 minutes to eliminate air bubbles. Care was taken to start the first addition after baseline stability had been achieved. In each titration, volumes of 5–10 μL of a solution containing compound **1** or netropsin at a concentration of 600–700 μM were injected into a solution of quadruplex or duplex DNA (30 μM) in the same buffer, using a computer-controlled 250 μL microsyringe. In order to allow the system to reach

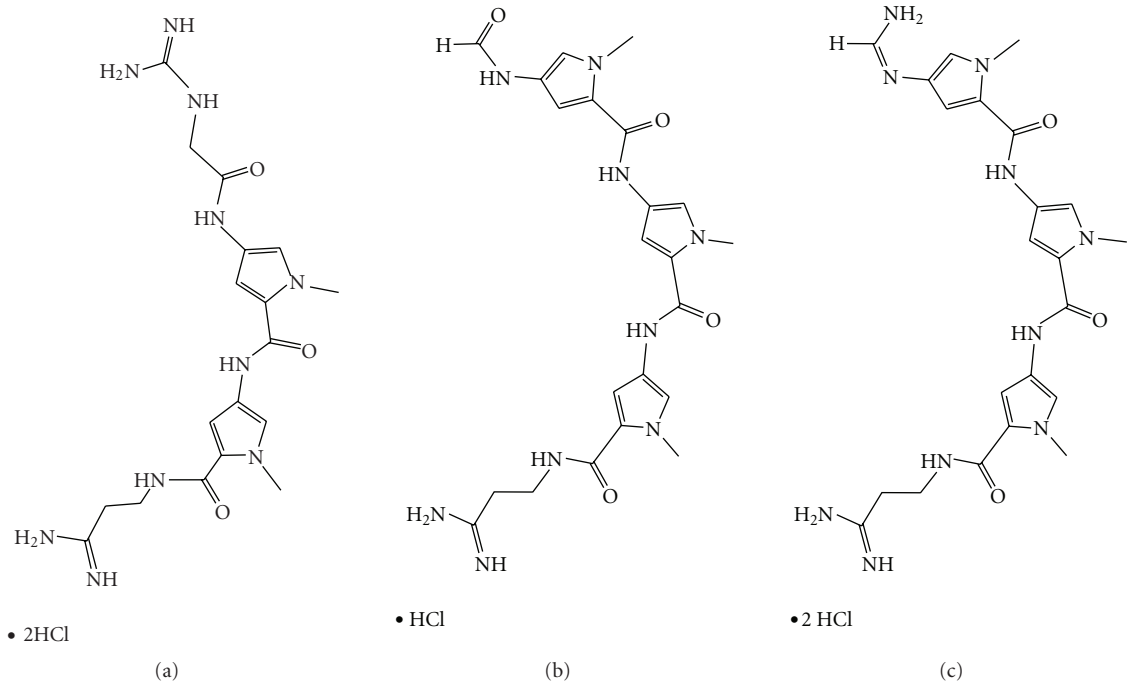

Figure 1: (a) Chemical structures of netropsin, (b) distamycin A, and (c) compound **1**.

the equilibrium, we applied a spacing of 300 or 400 s between each ligand injection. Heat produced by ligands dilution was evaluated by performing a control experiment, titrating each ligand into the buffer alone. The interaction heat for each injection was calculated after correction for the heat of ligand dilution. The corrected heat values were plotted as a function of the molar ratio, to give the corresponding binding isotherms. The resulting isotherms were fitted to a single set of identical sites model employing a nonlinear least-squares minimisation algorithm to a theoretical titration curve, using the program Bindwork from Calorimetry Science Inc. ΔH° (reaction enthalpy change in kJ mol^{-1}), K_b (binding constant in M^{-1}), and n (number of binding sites) were the fitting parameters. The Gibbs energy and the entropic contribution were calculated using the relationships $\Delta_b G^\circ = -RT \ln K_b$, ($R = 8.314\,\text{J mol}^{-1}\,\text{K}^{-1}$, $T = 298\,\text{K}$) and $-T\Delta_b S^\circ = \Delta_b G^\circ - \Delta_b H^\circ$.

3. Results

3.1. NMR Experiments. The addition of compound **1** to the quadruplex $[d(TGGGGT)]_4$ (Figure 2) caused gradual changes in the chemical shift and a broadening of DNA proton resonances in the ^{1}H-NMR spectra. The titration was virtually completed at ligand : DNA ratio of 2 : 1. The four strands resulted to be magnetically equivalent throughout the titration, since no splitting of resonances was observed at any stage. Furthermore, a single set of signals was present for derivative **1** protons throughout the whole NMR titration, which only grew in intensity and did not show any significant change in chemical shift values by increasing ligand concentration.

We also studied the interaction of compound **1** with the DNA duplex $d(CGCGAATTCGCG)_2$ containing the central AATT core, which is considered the specific binding site for distamycin and netropsin, to evaluate a possible selectivity of this analogue. The ^{1}H-NMR spectrum (700 MHz, $T = 25^\circ$C) of $d(CGCGAATTCGCG)_2$ turned out to be consistent with the assignment already published by Hare et al. (taking in due account the different temperature at which it has been assigned) [25]. The NMR titration of $d(CGCGAATTCGCG)_2$ with **1** is reported in Figure 3. In this case, most of the DNA resonances turned out to be not affected by the addition of ligand, but some resonances of residues C1, A5, A6, T7, T8, C9.

3.2. ITC Experiments. Examples of the raw ITC and integrated heat data for the titration of $[d(TGGGGT)]_4$ quadruplex with netropsin and compound **1** are shown in Figure 4. The ITC data for drugs binding to $[d(TGGGGT)]_4$ indicate, in both cases, the formation of a 2 : 1 (drug:quadruplex) complex with good affinity. The raw data for the titration of drugs with $[d(TGGGGT)]_4$ (insets in Figure 4) indicate an exothermic interaction, based on the positive values observed for the peaks. With each injection of ligand, less and less heat release was observed until constant values were obtained, reflecting, in both cases, a saturable process. The thermodynamic results obtained from fitting the ITC data for netropsin and compound **1** binding to $[d(TGGGGT)]_4$ are given in Table 1. The values of the binding constants and the Gibbs energy changes ($-34\,\text{kJ mol}^{-1}$ and $-36\,\text{kJ mol}^{-1}$ for netropsin and compound **1**, resp.) indicate that, from a thermodynamic point of view, the interactions with the quadruplex molecule are favoured at 25°C.

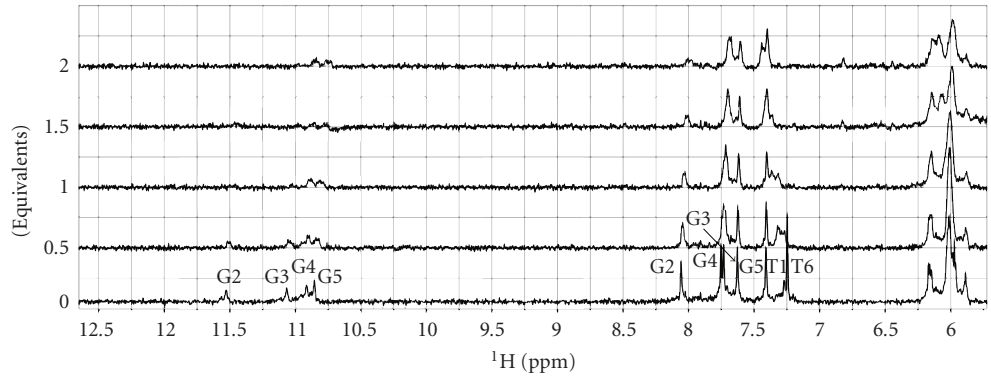

Figure 2: NMR titration of $[d(TGGGGT)]_4$ with derivative **1** (700 MHz, $T = 25°C$). 2 mM (8 mM single strand concentration), in 0.2 ml (H_2O/D_2O 9 : 1) buffer solution having 10 mM KH_2PO_4, 70 mM KCl, 0.2 mM EDTA, and pH 7.0. Equivalents of the drug are reported on the left of each spectrum.

Table 1: Thermodynamic parameters for the interaction of compound **1** and netropsin with $[d(TGGGGT)]_4$ determined by ITC at 25°C and pH 7.0.

Ligand	n	$K_b(\times 10^6\ M^{-1})$	$\Delta_b H°$ (kJ mol^{-1})	$T\Delta_b S°$ (kJ mol^{-1})	$\Delta_b G°$ (kJ mol^{-1})
Compound **1**	2.0 ± 0.1	1.9 ± 0.2	−11.0 ± 2.0	25 ± 2	−36 ± 2
Netropsin	2.0 ± 0.1	1.2 ± 0.1	−10.6 ± 1.0	23 ± 2	−34 ± 2

The values of $\Delta H°$ and $T\Delta S°$ show that in both cases the interactions are associated with a favourable binding enthalpy (−10.6 kJ mol^{-1} and −11.0 kJ mol^{-1} for netropsin and compound **1**, resp.), however, the binding processes are always entropically driven (23 kJ mol^{-1} and 25 kJ mol^{-1} for netropsin and compound **1**, resp.).

Finally, we also performed experiments on the interaction of compound **1** with the DNA duplex $d(CGCGAATTCGCG)_2$ containing the central AATT core, which is considered the specific binding site for distamycin and netropsin, to evaluate if the structural modifications of compound **1** influence the binding. An example of the raw ITC data for the titration of the $d(CGCGAATTCGCG)_2$ duplex with compound **1** is shown in Figure 5. Resolvable binding isotherm was never obtained for the interaction of compound **1** with duplex using any combination of reactant concentrations, suggesting low affinity of the molecule for the investigated duplex.

4. Discussion

Distamycin and netropsin have been recognized for decades as nonintercalative DNA binding ligands that show specificity for the minor groove of dA · dT base pairs [22, 26]. The binding of the drugs to duplex DNA involves an electrostatic component from the cationic ends, hydrogen bonds from the amide NH groups, and van der Waals interactions with the wall of the groove. Some years ago, NMR studies indicated that, depending on DNA sequence, some binding sites can accommodate two distamycin molecules side-by-side in an antiparallel orientation [27]. In this 2 : 1 complex each ligand molecule preserves all the molecular recognition elements of groove binders. In contrast to distamycin, the dication netropsin binds only as a single molecule per binding site, suggesting that the side-by-side arrangement of two molecules is inhibited by charge repulsions. Both drugs have been shown little or no affinity for single-stranded DNA or RNA or for double-stranded RNA or DNA-RNA hybrids as well as they do not bind to the A helix or the left-handed Z-DNA [26, 28].

Surprisingly, distamycin A has recently been shown to interact also with four-stranded parallel DNA quadruplexes [12, 29, 30]. Particularly, we have proved, by using NMR and ITC methodology, that distamycin is able to interact with the quadruplex $[d(TGGGGT)]_4$. We showed that four ligand molecules bind as antiparallel dimers to the quadruplex in two opposite grooves, establishing hydrogen bonds with the guanine bases and strong coulombic interactions between the positively charged amidinium moiety of the ligand and the backbone phosphate groups of the quadruplex [12]. On the other hand, netropsin turned out to possess a lower affinity (NMR data) towards the quadruplex $[d(TGGGGT)]_4$ [29], even if, till now, this has never been confirmed by ITC. Interestingly, it seems that netropsin is not able to bind the quadruplex in dimeric form, most probably due to the doubly charged nature of molecule that prevents a side-by-side arrangement into the grooves.

In order to evaluate the binding properties of derivative **1**, and to perform a direct comparison with the binding behaviour of distamycin A and netropsin, $[d(TGGGGT)]_4$ has been titrated with **1** at the same experimental conditions (buffer, temperature, DNA concentration) used for distamycin A [29]. As far as distamycin A is concerned, below 2 : 1 ligand : quadruplex stoichiometry, the addition of distamycin A to $[d(TGGGGT)]_4$ caused gradual changing in chemical shift of the signal of the quadruplex, whereas

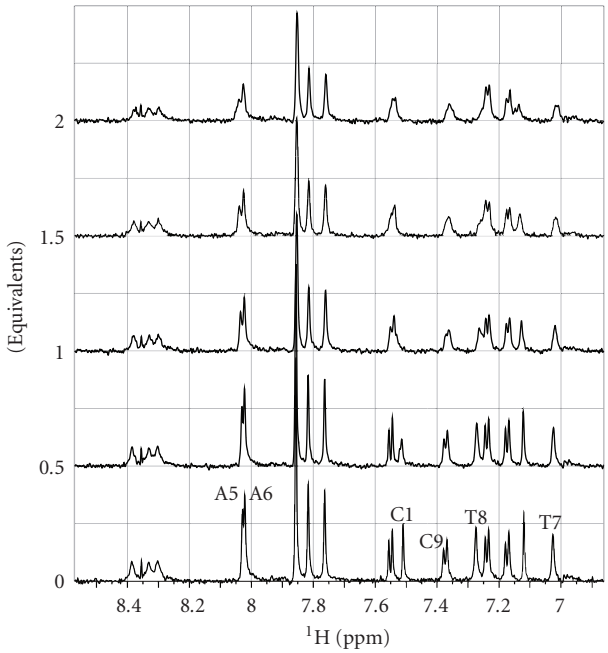

FIGURE 3: Expanded region of the ^{1}H-NMR titration of d(CGCGAATTCGCG)$_2$ with derivative **1** (700 MHz, T = 25°C). 1 mM (4 mM single strand concentration), in 0.2 ml (H_2O/D_2O 9 : 1) buffer solution having 10 mM KH_2PO_4, 70 mM KCl, 0.2 mM EDTA, and pH 7.0. Equivalents of the drug are reported on the left of each spectrum. Residues that are slightly affected by the binding are indicated.

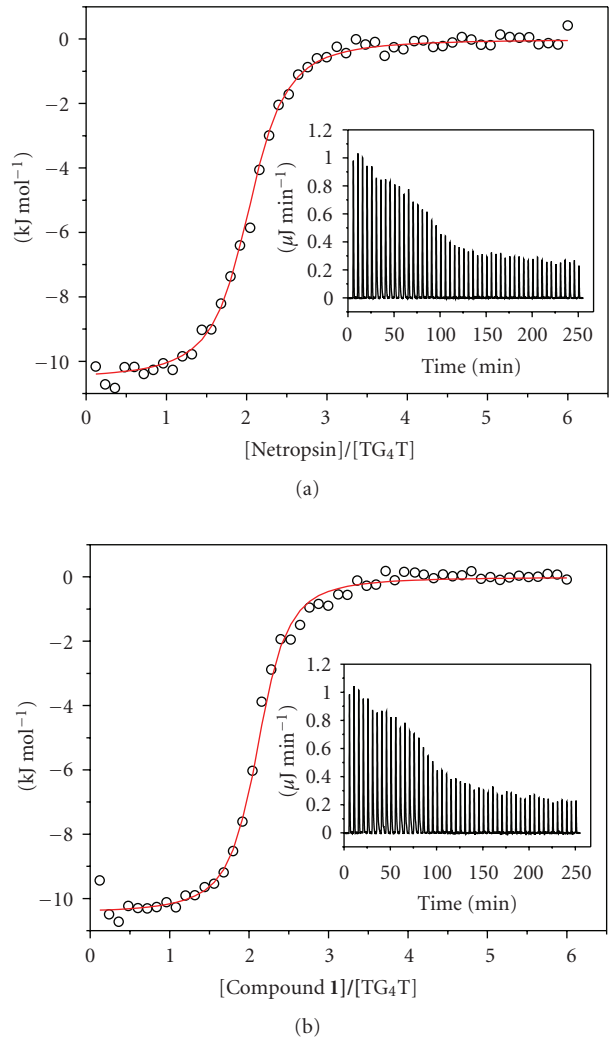

FIGURE 4: Raw ITC data (insets) and binding isotherms for titration of [d(TGGGGT)]$_4$ with netropsin (a) and with compound **1** (b).

further addition of drug caused the appearance of a new set of proton signals, whose intensities rose by increasing the amount of drug with the concomitant falling off of the original signals which completely disappeared at a ratio of 4 : 1 drug-DNA. Differently, the NMR titration profile of **1** (Figure 2) turned out to be very different from that observed in the case of distamycin A and clearly suggests that derivative **1** binds the quadruplex in a fast process on the NMR time scale, very similarly to the NMR titration profile observed for netropsin [29].

In order to preliminarily evaluate the binding site of derivative **1**, a comparison of resonances of some protons of the uncomplexed DNA and the complexed one has been done. In particular, we report the $\Delta\delta$ values (chemical shifts of the complex minus free DNA) of aromatic, methyl, and imino protons in Figure 6. Interestingly, all analyzed DNA resonances shifted. Nevertheless, the signal of the protons of T1 residue shifted the least, whereas the ones of residue T6 the more. In any case, a general shift of the aromatic and imino signals could be observed also for the G2, G3, G4, and G5. This means that, basically, derivative **1** is able to recognize most of the molecule surface.

On the other hand, the addition of **1** to d(CGCGAATTCGCG)$_2$ affected only slightly some DNA resonances. In particular, at 2 : 1 (drug/DNA) molar ratio the aromatic protons of residue C1, A5, A6, T7, T8, C9 residues underwent to a shift of only 0.03, 0.01, 0.01, 0.02, 0.03, and 0.01 ppm, respectively, indicating a very poor affinity towards the dodecamer.

ITC is an useful methodology for a complete understanding of drug-DNA interactions, and it has been applied many times to determine the thermodynamic properties of drug-quadruplex interactions [31]. Indeed, ITC is the only technique that directly measures the binding enthalpy change for the formation of a complex, allowing the free energy change to be dissected into the enthalpic and entropic contribution to the association process. This reveals the nature of the forces that drive the binding and can provide insight into the nature of the intermolecular contacts formed and even into changes in solvation [19]. The understanding of those factors can be helpful in both screening among various drugs and optimizing the drug-target interactions, to direct the design of new drugs.

ITC experiments reveal that both compound **1** and netropsin bind to the investigated quadruplex. The thermodynamic profiles of the two drug-quadruplex interactions are qualitatively similar and in both cases the stoichiometry observed is 2 : 1 (drug : quadruplex). Interestingly, the thermodynamic parameters determined by ITC (Table 1)

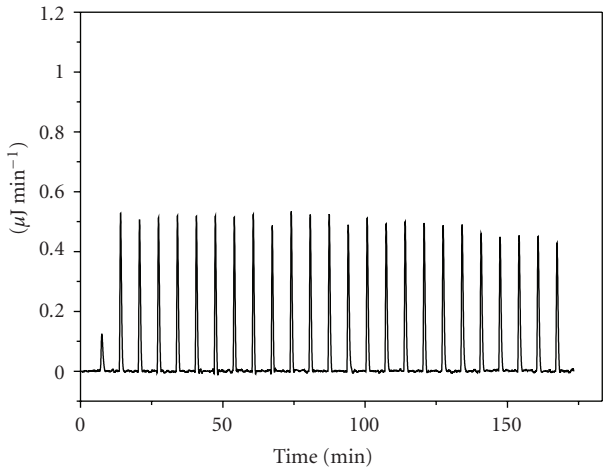

Figure 5: Raw ITC data for titration of $d(CGCGAATTCGCG)_2$ duplex with compound **1**. With each injection of ligand, constant heat release was observed due only to ligand dilution.

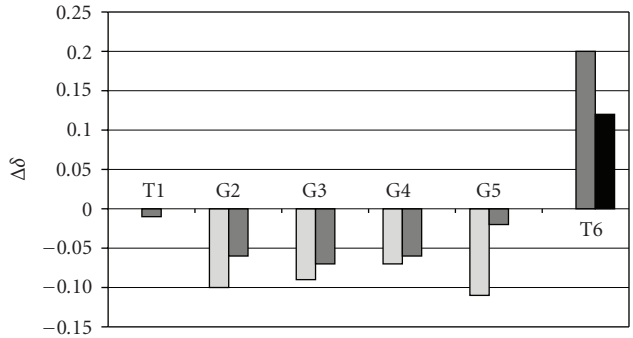

Figure 6: Difference in chemical shifts ($\Delta\delta$) of DNA upon binding of **1** (complex **1**: DNA minus DNA alone) with $[d(TGGGGT)]_4$. $\Delta\delta$ values are reported for imino (light gray), aromatic (dark gray), and methyl (black) protons.

indicate that the association reactions of both ligands with $[d(TGGGGT)]_4$ are entropically driven processes, even if the direct ITC measurements of the binding enthalpy change indicate that also the enthalpic contribution favours the associations. In the case of the interaction of distamycin with $[d(TGGGGT)]_4$, similar results were obtained (entropically driven process with a small favourable enthalpic contribution), except for stoichiometry and magnitude of binding constant.

As reported in the literature many times, a groove binding is generally characterized by a large favourable increase of entropy and a small favourable or unfavourable enthalpy change [32]. This could be mainly due to the fact that the association reaction is driven in large part by a hydrophobic effect and the favorable entropy is derived from the release of bound water molecules from the DNA and drug upon complex formation as well as release of counterions upon binding of cationic ligands. Interestingly, the entropically driven interactions of the compound **1** and of netropsin suggest a groove-binding mechanism also in these cases, as observed for distamycin A. Additionally, in contrast to many other groove binders, netropsin binding to duplex DNA is accompanied on average by a favourable enthalpy change. This is the result of both electrostatic interactions and hydrogen bonds formation between netropsin molecule and DNA. A favourable enthalpy change is observed by ITC for netropsin binding to $[d(TGGGGT)]_4$ as well as for compound **1**, suggesting once again a similar groove binding mode.

As stated before, the stoichiometry obtained for the association of the investigated ligands to $[d(TGGGGT)]_4$ is 2 : 1 (drug : quadruplex), while for distamycin a stoichiometry of 4 : 1 was found. This finding is consistent with the observation that the distamycin molecules are able to bind as dimers, while netropsin (and probably also compound **1**) is not able to dimerise because of charge repulsions. Notably, in the distamycin-$[d(TGGGGT)]_4$ complex, each distamycin dimer expands its bounded groove (similarly to that observed with duplex DNA), with concomitant reduction of the size of the adjacent ones, preventing a further interaction with other ligand molecules. In the binding of netropsin to duplex DNA the minor groove is widened by 0.5–2.0 Å by the entry of the drug [16]. We can speculate that the binding of the two netropsin molecules to $[d(TGGGGT)]_4$ could similarly expand the bounded grooves, reducing the size of the adjacent ones and preventing more interactions.

The experiments on the interaction of compound **1** with the DNA duplex $d(CGCGAATTCGCG)_2$ show that compound **1** has a poor affinity for the investigated duplex, while it is well known that both distamycin and netropsin have a high binding constant (between 10^6 and 10^8 M^{-1}) for that target containing the specific binding site. This finding demonstrates that the structural modifications of compound **1** decrease the affinity of the ligand toward the duplex, enhancing the selectivity.

5. Conclusions

The combination of calorimetric and NMR methodologies has enabled us to demonstrate that netropsin and compound **1** are able to bind to $[d(TGGGGT)]_4$ with good affinity, forming, in both cases, a 2 : 1 (drug : quadruplex) complex.

Very interestingly, this study shows that the structural modifications of compound **1** do not influence, compared to netropsin, the interaction with the quadruplex, but such modifications decrease the affinity of the ligand toward the duplex, enhancing the selectivity.

Acknowledgments

This work is supported by the Italian Institute of Technology (IIT), Italian M.U.R.S.T. (P.R.I.N. 2007), Regione Campania (L.41, L.5), and by the COST Action MP0802. The authors are grateful to "Centro di Servizio Interdipartimentale di Analisi Strumentale", C.S.I.A.S., for supplying NMR facilities.

References

[1] S. Burge, G. N. Parkinson, P. Hazel, A. K. Todd, and S. Neidle, "Quadruplex DNA: sequence, topology and structure," *Nucleic Acids Research*, vol. 34, no. 19, pp. 5402–5415, 2006.

[2] J. L. Huppert and S. Balasubramanian, "Prevalence of quadruplexes in the human genome," *Nucleic Acids Research*, vol. 33, no. 9, pp. 2908–2916, 2005.

[3] J. E. Johnson, J. S. Smith, M. L. Kozak, and F. B. Johnson, "In vivo veritas: using yeast to probe the biological functions of G-quadruplexes," *Biochimie*, vol. 90, no. 8, pp. 1250–1263, 2008.

[4] Y. Qin and L. H. Hurley, "Structures, folding patterns, and functions of intramolecular DNA G-quadruplexes found in eukaryotic promoter regions," *Biochimie*, vol. 90, no. 8, pp. 1149–1171, 2008.

[5] S. Neidle and G. N. Parkinson, "The structure of telomeric DNA," *Current Opinion in Structural Biology*, vol. 13, no. 3, pp. 275–283, 2003.

[6] G. Laughlan, A. I. H. Murchie, D. G. Norman, et al., "The high-resolution crystal structure of a parallel-stranded guanine tetraplex," *Science*, vol. 265, no. 5171, pp. 520–524, 1994.

[7] N. W. Kim, M. A. Piatyszek, K. R. Prowse, et al., "Specific association of human telomerase activity with immortal cells and cancer," *Science*, vol. 266, pp. 2011–2015, 1994.

[8] J. W. Shay and W. E. Wright, "Telomerase therapeutics for cancer: challenges and new directions," *Nature Reviews Drug Discovery*, vol. 5, no. 7, pp. 577–584, 2006.

[9] B. Pagano and C. Giancola, "Energetics of quadruplex-drug recognition in anticancer therapy," *Current Cancer Drug Targets*, vol. 7, no. 6, pp. 520–540, 2007.

[10] J.-F. Riou, "G-quadruplex interacting agents targetting the telomeric G-overhang are more than simple telomerase inhibitors," *Current Medicinal Chemistry*, vol. 4, no. 5, pp. 439–443, 2004.

[11] S. Neidle, "The structures of quadruplex nucleic acids and their drug complexes," *Current Opinion in Structural Biology*, vol. 19, no. 3, pp. 239–250, 2009.

[12] L. Martino, A. Virno, B. Pagano, et al., "Structural and thermodynamic studies of the interaction of distamycin A with the parallel quadruplex structure $[d(TGGGGT)]_4$," *Journal of the American Chemical Society*, vol. 129, no. 51, pp. 16048–16056, 2007.

[13] N. Zaffaroni, S. Lualdi, R. Villa, et al., "Inhibition of telomerase activity by a distamycin derivative: effects on cell proliferation and induction of apoptosis in human cancer cells," *European Journal of Cancer*, vol. 38, no. 13, pp. 1792–1801, 2002.

[14] B. Pagano, A. Virno, C. A. Mattia, L. Mayol, A. Randazzo, and C. Giancola, "Targeting DNA quadruplexes with distamycin A and its derivatives: an ITC and NMR study," *Biochimie*, vol. 90, no. 8, pp. 1224–1232, 2008.

[15] B. Pagano, C. A. Mattia, A. Virno, A. Randazzo, L. Mayol, and C. Giancola, "Thermodynamic analysis of quadruplex DNA-drug interaction," *Nucleosides, Nucleotides and Nucleic Acids*, vol. 26, no. 6-7, pp. 761–765, 2007.

[16] M. L. Kopka, C. Yoon, D. Goodsell, P. Pjura, and R. E. Dickerson, "The molecular origin of DNA-drug specificity in netropsin and distamycin," *Proceedings of the National Academy of Sciences of the United States of America*, vol. 82, no. 5, pp. 1376–1380, 1985.

[17] M. L. Kopka, C. Yoon, D. Goodsell, P. Pjura, and R. E. Dickerson, "Binding of an antitumor drug to DNA netropsin and C-G-C-G-A-A-T-T-^{Br}C-G-C-G," *Journal of Molecular Biology*, vol. 183, no. 4, pp. 553–563, 1985.

[18] L. A. Marky and K. J. Breslauer, "Origins of netropsin binding affinity and specificity: correlations of thermodynamic and structural data," *Proceedings of the National Academy of Sciences of the United States of America*, vol. 84, no. 13, pp. 4359–4363, 1987.

[19] I. Haq, "Thermodynamics of drug-DNA interactions," *Archives of Biochemistry and Biophysics*, vol. 403, no. 1, pp. 1–15, 2002.

[20] C. R. Cantor, M. M. Warshaw, and H. Shapiro, "Oligonucleotide interactions. 3. Circular dichroism studies of the conformation of deoxyoligonucleotides," *Biopolymers*, vol. 9, no. 9, pp. 1059–1077, 1970.

[21] G. Di Pietro, G. Giannini, E. M. Iafrate, et al., "*N*-formimidoyl analogues of distamycin," *Journal of the Chemical Society, Perkin Transactions 1*, no. 12, pp. 1333–1335, 1996.

[22] D. Rentzeperis, L. A. Marky, T. J. Dwyer, B. H. Geierstanger, J. G. Pelton, and D. E. Wemmer, "Interaction of minor groove ligands to an AAATT/AATTT site: correlation of thermodynamic characterization and solution structure," *Biochemistry*, vol. 34, no. 9, pp. 2937–2945, 1995.

[23] T. L. Hwang and A. J. Shaka, "Water suppression that works. Excitation sculpting using arbitrary wave-forms and pulsed-field gradients," *Journal of Magnetic Resonance A*, vol. 112, pp. 275–279, 1995.

[24] C. Dalvit, "Efficient multiple-solvent suppression for the study of the interactions of organic solvents with biomolecules," *Journal of Biomolecular NMR*, vol. 11, no. 4, pp. 437–444, 1998.

[25] D. R. Hare, D. E. Wemmer, S.-H. Chou, G. Drobny, and B. R. Reid, "Assignment of the non-exchangeable proton resonances of d(C-G-C-G-A-A-T-T-C-G-C-G) using two-dimensional nuclear magnetic resonance methods," *Journal of Molecular Biology*, vol. 171, no. 3, pp. 319–336, 1983.

[26] R. M. Wartell, J. E. Larson, and R. D. Wells, "Netropsin. A specific probe for AT regions of duplex deoxyribonucleic acid," *The Journal of Biological Chemistry*, vol. 249, no. 21, pp. 6719–6731, 1974.

[27] J. G. Pelton and D. E. Wemmer, "Binding modes of distamycin A with $d(CGCAAATTTGCG)_2$ determined by two-dimensional NMR," *Journal of the American Chemical Society*, vol. 112, no. 4, pp. 1393–1399, 1990.

[28] C. Zimmer, "Effects of the antibiotics netropsin and distamycin A on the structure and function of nucleic acids," *Progress in Nucleic Acid Research and Molecular Biology*, vol. 15, pp. 285–318, 1975.

[29] A. Randazzo, A. Galeone, and L. Mayol, "^{1}H-NMR study of the interaction of distamycin A and netropsin with the parallel stranded tetraplex $[d(TGGGGT)]_4$," *Chemical Communications*, vol. 11, pp. 1030–1031, 2001.

[30] M. J. Cocco, L. A. Hanakahi, M. D. Huber, and N. Maizels, "Specific interactions of distamycin with G-quadruplex DNA," *Nucleic Acids Research*, vol. 31, no. 11, pp. 2944–2951, 2003.

[31] B. Pagano, C. A. Mattia, and C. Giancola, "Applications of isothermal titration calorimetry in biophysical studies of G-quadruplexes," *International Journal of Molecular Sciences*, vol. 10, no. 7, pp. 2935–2957, 2009.

[32] J. B. Chaires, "A thermodynamic signature for drug-DNA binding mode," *Archives of Biochemistry and Biophysics*, vol. 453, no. 1, pp. 24–29, 2006.

SAGE-Hindawi Access to Research
Journal of Nucleic Acids
Volume 2010, Article ID 121259, 7 pages
doi:10.4061/2010/121259

Research Article

Cation Involvement in Telomestatin Binding to G-Quadruplex DNA

Frédéric Rosu,[1,2] Valérie Gabelica,[1,2] Nicolas Smargiasso,[1,2] Gabriel Mazzucchelli,[1,2] Kazuo Shin-Ya,[3] and Edwin De Pauw[1,2]

[1] *Mass Spectrometry Laboratory, Department of Chemistry, University of Liège, 4000 Liège, Belgium*
[2] *GIGA-Systems Biology and Chemical Biology, University of Liège, 4000 Liège, Belgium*
[3] *Biomedicinal Information Research Center, Biological Systems Control Team, National Institute of Advanced Industrial Science and Technology, Tokyo 135-0064, Japan*

Correspondence should be addressed to Valérie Gabelica, v.gabelica@ulg.ac.be

Received 1 February 2010; Accepted 13 April 2010

Academic Editor: Daniela Montesarchio

The binding mode of telomestatin to G-quadruplex DNA has been investigated using electrospray mass spectrometry, by detecting the intact complexes formed in ammonium acetate. The mass measurements show the incorporation of one extra ammonium ion in the telomestatin complexes. Experiments on telomestatin alone also show that the telomestatin alone is able to coordinate cations in a similar way as a crown ether. Finally, density functional theory calculations suggest that in the G-quadruplex-telomestatin complex, potassium or ammonium cations are located between the telomestatin and a G-quartet. This study underlines that monovalent cation coordination capabilities should be integrated in the rational design of G-quadruplex binding ligands.

1. Introduction

The formation of G-quadruplex folds by telomeric DNA is thought to play a role in telomere regulation. It has been shown that G-quadruplex ligands binding specifically to the telomeric G-quadruplex structure effectively alter telomere capping and cause the senescence or apoptosis of cancer cells [1–5]. A variety of ligands have now been described as G-quadruplex binders, but a key issue in ligand design is often the specificity for G-quadruplexes over duplex sequences [4, 6–8]. Identifying binding modes that make a ligand a specific and highly active G-quadruplex binder is crucial for the rational design of novel molecules.

Telomestatin (Figure 1) is one of the most emblematic G-quadruplex ligands. The molecule was first extracted from Streptomyces anulatus 3533-SV4 [9]. It is highly specific for G-quadruplexes, with no significant binding to duplexes [10–12]. Telomestatin was found to effectively inhibit the DNA binding of telomere-associated proteins such as telomerase [13], POT1 and TRF2 [14], and even Topo III in ALT cell lines [15]. It therefore induces telomere shortening and apoptosis [16–19] not only via telomerase inhibition but also via telomere uncapping, and therefore has potential activity against many cancer cell types.

Telomestatin binds to G-quadruplexes, among which is the human telomeric G-quadruplex, by external stacking [12]. One G-quadruplex unit can therefore accommodate two telomestatin ligands, one on each end. A recent modeling study showed that telomestatin has a tendency to capture a potassium ion, either from the G-quadruplex itself or from the solution [20]. Here we show that mass spectrometry provides experimental evidence for the accommodation of one extra cation when a telomestatin molecule is bound to a G-quadruplex. This will be illustrated for three typical G-quadruplexes: the tetramolecular $[TG_4T]_4$ quadruplex, the 4-repeat telomeric sequence $(T_2AG_3)_4$, and the Pu22myc promoter sequence $GAG_3TG_4AG_3TG_4A_2G$. The typical folds adopted by each of these three G-quadruplexes in ammonium acetate were studied previously [21–23] and are summarized in Figure 1.

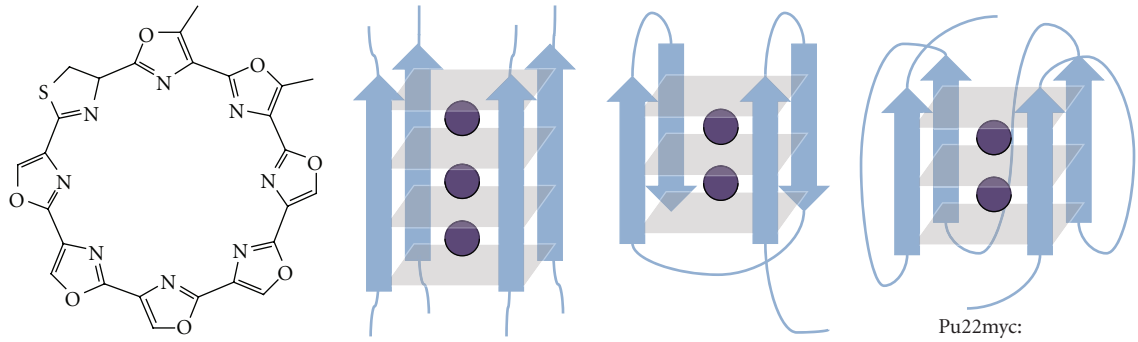

FIGURE 1: Chemical structure of telomestatin and folding pattern of the three G-quadruplexes studied here. $[TG_4T]_4$ adopts a parallel fold and can incorporate three ammonium ions between its four G-quartets [21], the 4-repeat telomeric sequence $(T_2AG_3)_4$ adopts an intramolecular antiparallel fold in ammonium acetate and incorporates up to two ammonium ions [22], and the Pu22myc promoter sequence $GAG_3TG_4AG_3TG_4A_2G$ adopts a predominantly parallel fold in ammonium acetate and incorporates two ammonium ions [23].

2. Experimental Section

2.1. Materials. All oligonucleotides were purchased from Eurogentec (Seraing, Belgium), solubilized in water doubly distilled in house, and the 400 μM stock solutions were stored at −20°C. The solvents used include methanol (absolute, HPLC grade, Biosolve, Valkenswaard, The Netherlands), bi-distilled water, and aqueous ammonium acetate (5 M stock solution from Fluka, diluted with bi-distilled water). KCl for the evaluation of the complexation of telomestatin alone was puriss, p.a., ≥99.5% (T) (Fluka). G-quadruplexes were formed by annealing (heating the oligonucleotides for 5 minutes at 85°C, followed by slow cooling to room temperature) in 150 mM ammonium acetate. The G-quadruplex-forming oligonucleotides were dTG_4T (annealed at 200 μM single strand to form 50 μM tetramolecular G-quadruplex); the telomeric sequence $(T_2AG_3)_4$ and the Pu22myc promoter sequence $GAG_3TG_4AG_3TG_4A_2G$ (annealed at 50 μM single strand to form intramolecular G-quadruplexes). Telomestatin was isolated and purified as described elsewhere [9, 24] to obtain a 1 mM stock solution in DMSO. For the electrospray mass spectrometry analysis of the complexes, the final injected solutions were 5 μM in G-quadruplex and 5 to 10 μM in telomestatin (only 10 μM results are shown), in 80/20 (v/v) aqueous ammonium acetate (150 mM)/methanol.

2.2. Mass Spectrometry. Electrospray mass spectrometry experiments were performed on a Q-TOF Ultima Global (Waters, Manchester, UK). The spectra of the intact G-quadruplexes and their noncovalent complexes with telomestatin were recorded in the negative ion mode (capillary voltage = −2.2 V, source and desolvation temperatures = 70°C, cone = 100 V, RF Lens1 Energy = 45 V, source pirani pressure = 3.94 mbar, collision energy = 10 V), smoothed (mean function, 3 × 20 channels) and subtracted (polynomial order 99, 0.1% below curve). The spectra of telomestatin in the absence of G-quadruplex were recorded in the positive ion mode (capillary voltage = +2.8 V, source and desolvation temperatures = 80 and 100°C, resp., cone = 100 V, RF Lens1 Energy = 50 V, source pirani pressure = 3.33 mbar and collision energy = 7 V) and were not subjected to smoothing or background subtraction.

2.3. Calculations. For the [telomestatin + cation] binary complexes, the ammonium, potassium, and sodium cations were manually docked within the telomestatin ring, and the resulting structures were optimized using density functional theory (DFT) with the hybrid functional B3LYP and the 6-31G(d,p) basis set. For the ternary complexes between [telomestatin + cation + one G-quartet], the telomestatin was manually docked on top of an optimized structure of a G-quartet coordinated with the cation (ammonium, potassium, sodium). The ternary complexes were then optimized using DFT B3LYP at the 6-31G(d,p) level. All electronic structure calculations were performed using the Gaussian 03 rev. D.02 software suite [25]. Comparison with a larger basis set (6-311 + G(d,p)) was performed for one of the complexes (G-tetrad + K + telomestatin), and the results were similar in terms of both energies (0.8 kcal/mol) and geometries (RMSD 0.16 Å). 6-31G(d,p) basis set was therefore used for all calculations. Other hybrid functional BHandHLYP and new meta-GGA hybrid MPWB1K [26] have also been tested for comparison with B3LYP.

3. Results and Discussion

When operated in soft source conditions, electrospray mass spectrometry allows detecting intact noncovalent complexes [27–30]. In the analysis of quadruplex-ligand complexes, it therefore allows determining the number of strands, the number of ligands, and the number of cations in each complex. Electrospray mass spectrometry of nucleic acid noncovalent complexes is typically performed in ammonium acetate solution in order to obtain clean spectra [31]. Ammonium ions present in the counter-ion shell around phosphates are lost during the final stages of desolvation in the electrospray source, even in soft conditions

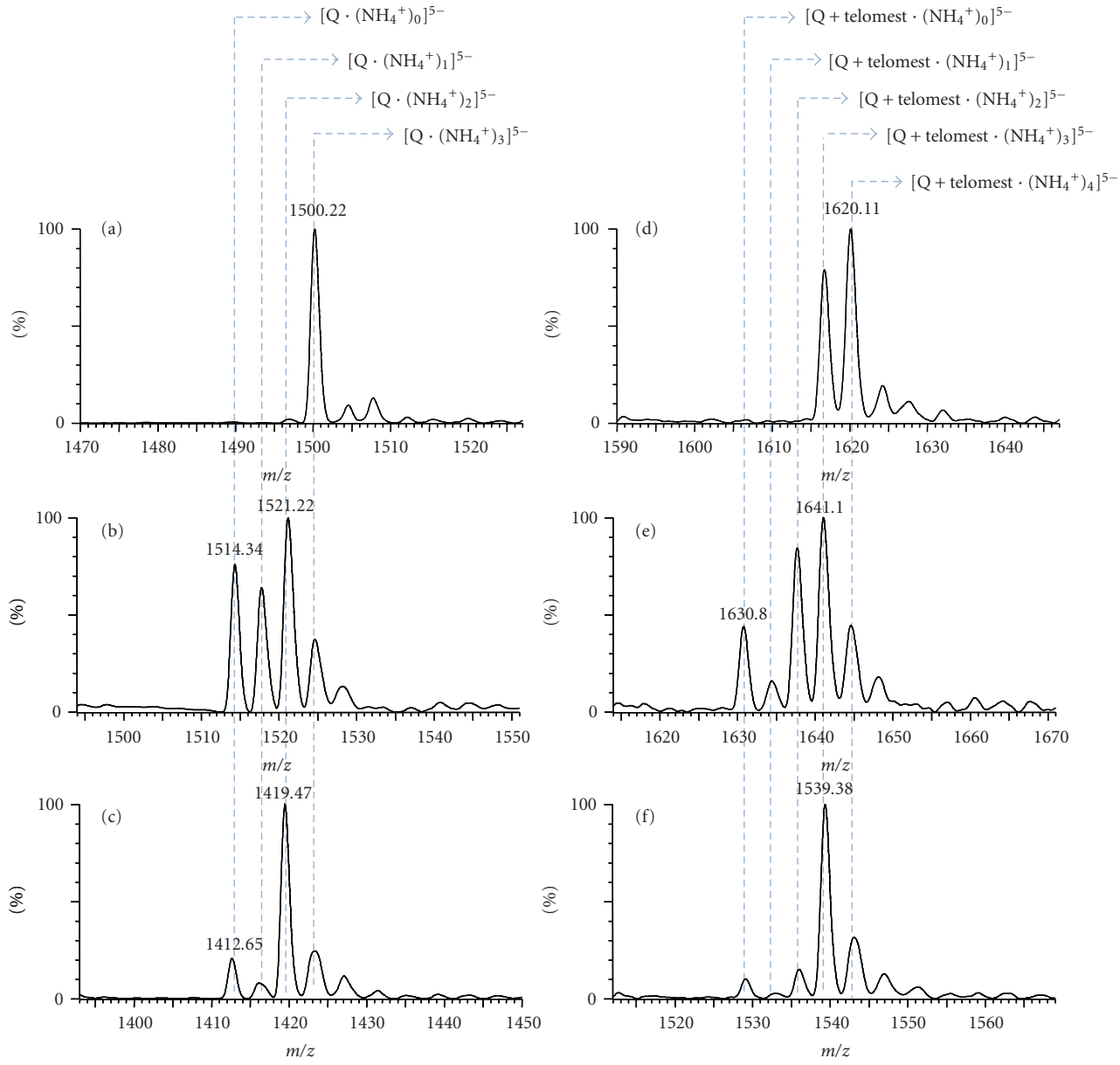

Figure 2: Negative ion mode electrospray mass spectra of mixtures of 10 μM telomestatin and 5 μM of G-quadruplexes. Zooms on the peaks of free G-quadruplex (a) $[TG_4T]_4$, (b) telomeric sequence $(T_2AG_3)_4$, and (c) Pu22myc promoter sequence $GAG_3TG_4AG_3TG_4A_2G$, and on the complexes between (d) one telomestatin and $[TG_4T]_4$, (e) one telomestatin and $(T_2AG_3)_4$, and (f) one telomestatin and $GAG_3TG_4AG_3TG_4A_2G$. The spectra were recorded from and 80/20 aqueous ammonium acetate (150 mM)/methanol solution, using soft source conditions to preserve the specifically bound ammonium ions.

(low acceleration voltages). In contrast, ammonium ions bound sufficiently tightly to the G-quadruplex, such as the ammonium ions trapped between the G-quartets, will persist at higher acceleration voltages in the source than the nonspecifically bound ones [21].

Figure 2 shows the electrospray mass spectra of three typical G-quadruplexes: (a) $[TG_4T]_4$, (b) the telomeric sequence $(T_2AG_3)_4$, and (c) the Pu22myc promoter sequence $GAG_3TG_4AG_3TG_4A_2G$ and on their 1 : 1 complexes with telomestatin (d–f, resp.). The injected mixtures are 5 μM in each G-quadruplex 10 μM in telomestatin, in 80/20 aqueous ammonium acetate (150 mM)/methanol, and the spectra were recorded using soft source conditions to preserve the specifically bound ammonium ions. The free $[TG_4T]_4$ G-quadruplex (Figure 2(a)) contains three ammonium ions: the 5− charge state is found at m/z = 1500.22, corresponding to $[Q \cdot (NH_4^+)_3]^{5-}$. The major peaks of the telomeric (Figure 2(b)) and Pu22myc (Figure 2(c)) G-quadruplexes at charge state 5− are corresponding to the intramolecular G-quadruplex with two ammonium ions, at (m/z) = 1521.22 and 1419.47, respectively. For the charge state z = 5, with the average mass of telomestatin being m = 582.5 Da, the

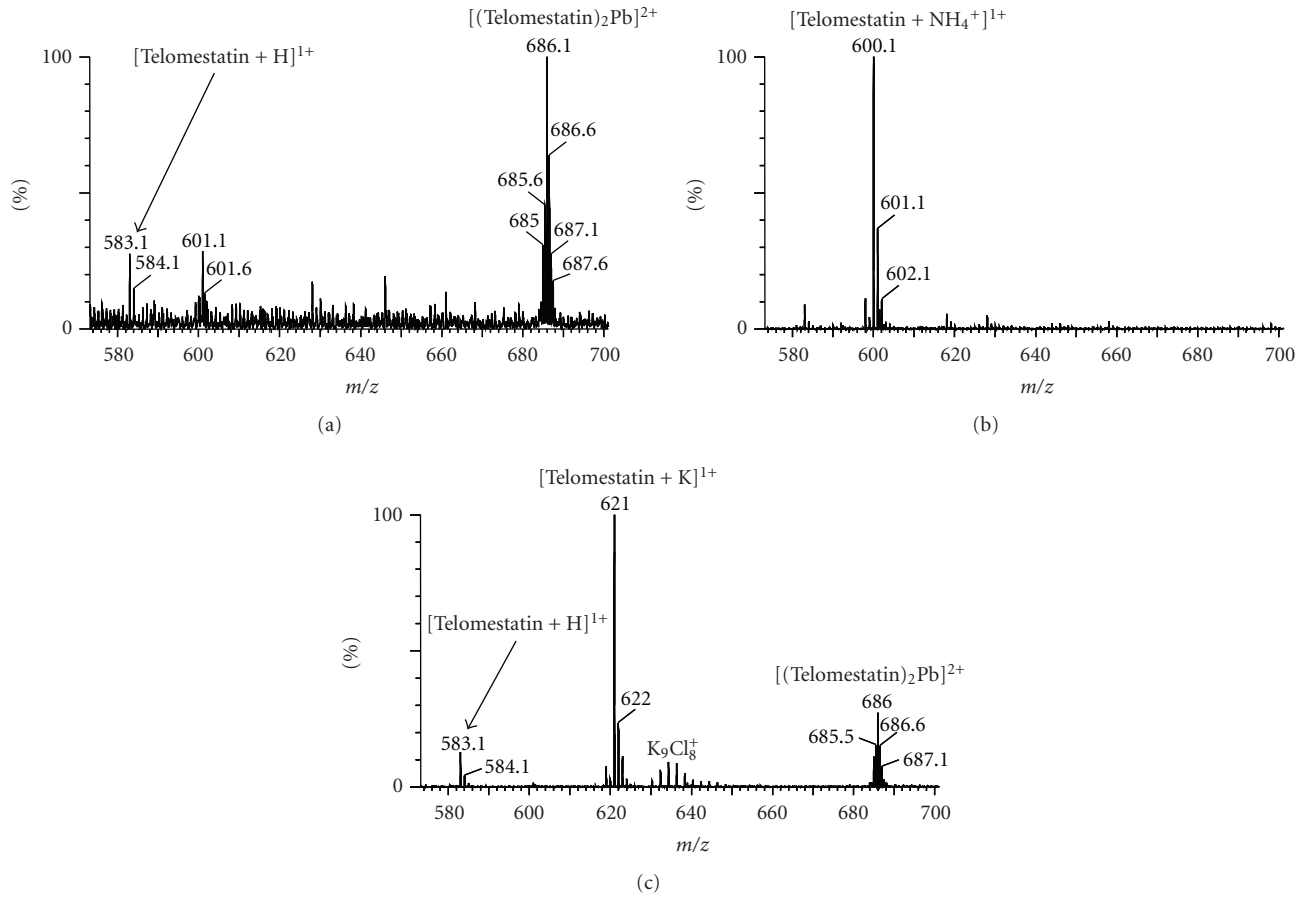

Figure 3: Positive ion mode electrospray mass spectra of 15 μM telomestatin (a) in 80/20 water/methanol, (b) in 80/20 water methanol and 5 μM ammonium acetate, and (c) in 80/20 water methanol and 5 μM potassium chloride.

$\Delta(m/z)$ between the G-quadruplex and its complex with one telomestatin, with no change in the amount of ammonium ions incorporated, is expected to be equal to 582.5/5 = 116.5. In contrast, the observed $\Delta(m/z)$ between the major peak of the quadruplex and the major peak of its complex with one ligand is equal to 119.9 (compare Figure 2(a) with Figure 2(d), and Figure 2(b) with Figure 2(e), Figure 2(c) with Figure 2(f)). This corresponds to the addition of one telomestatin molecule, one extra ammonium ion, and the subtraction of one proton for the charge balance (119.9 = (585.5 + 18−1)/5). The complex with one telomestatin ligand therefore systematically contains one more ammonium ion than the corresponding unbound G-quadruplex. This extra ammonium ion is lost when the acceleration voltage is increased.

In our previous report on the MS detection of telomestatin binding to telomeric DNA [11], we have missed this "extra ammonium" for two reasons. Firstly, for the 3.5-repeat telomeric sequence studied previously it is difficult to preserve two inner ammoniums even in soft conditions. Secondly, soft conditions could not be used because a long duplex had to be detected simultaneously with the G-strand, and the electrospray source conditions were chosen as a compromise.

Electrospray mass spectrometry is also powerful to analyze caged supramolecular complexes such as crown ethers bound to cations [32–35]. To probe whether telomestatin is able to coordinate a cation already in the absence of G-quadruplex, we used ESI-MS in the positive ion mode on telomestatin solutions. Figure 3(a) shows the spectrum obtained with telomestatin dilution in bi-distilled water. The signal-to-noise ratio of all peaks is weak, indicating low protonation and cationization efficiencies. Surprisingly, we found that the major peak was a doubly charged ion at m/z = 686.1 (base peak), whose isotopic distribution matches with that of a complex between two telomestatin ligands and one lead ion adduct. The fragment ion spectrum shows the loss of one telomestatin, and the isotopic distribution of the resulting [Telomestatin + Pb] complex confirms the presence of lead. Traces of lead come from the purification of telomestatin from Streptomyces anulatus 3533-SV4 [24]. Another weak doubly charged peak is tentatively assigned to a complex between two telomestatin and two H_3O^+ ions, and the fragment ion spectrum shows only the singly protonated telomestatin.

We then doped the solution with either ammonium acetate or with potassium chloride, in substoichiometric amounts, to probe if telomestatin was able to coordinate

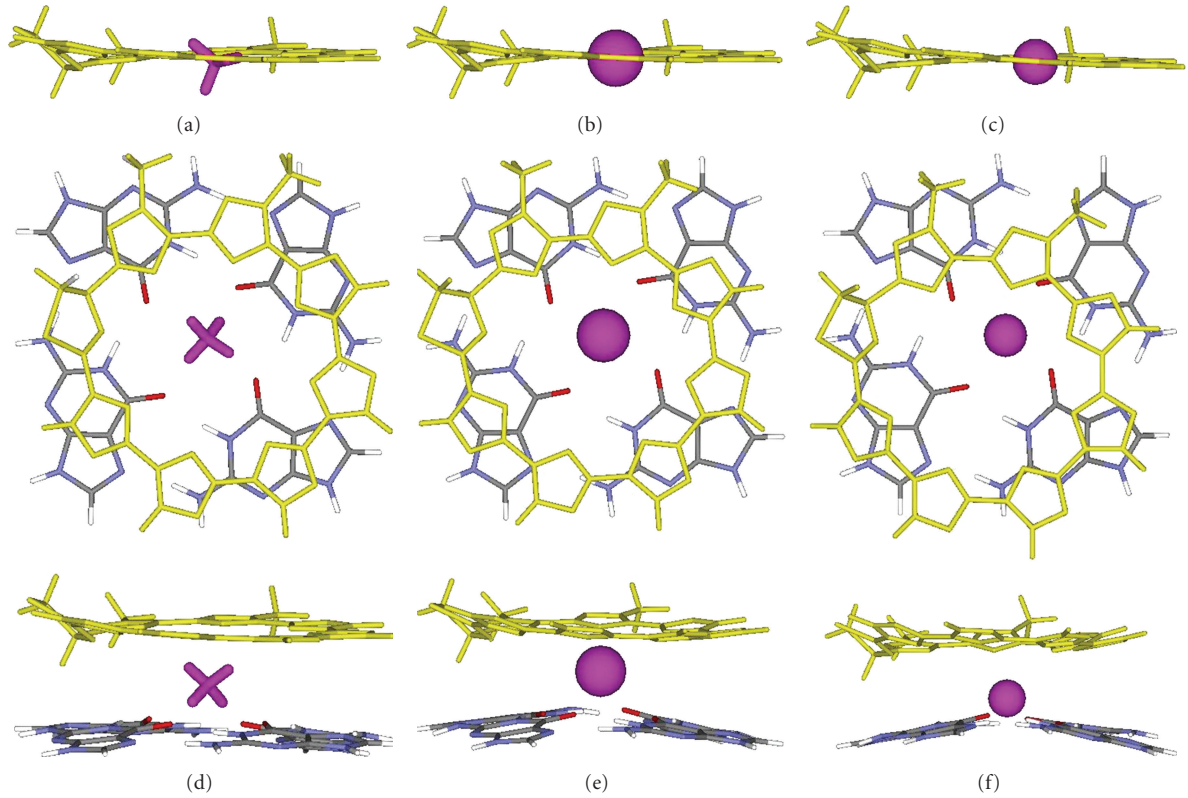

Figure 4: Optimized geometries (DFT B3LYP, 6-31G(d,p)) of the telomestatin—cation complexes (side view) for (a) NH_4^+, (b) K^+, and (c) Na^+, and optimized geometries of the telomestatin—cation—G-quartet complexes (top view and side view) for (d) NH_4^+, (e) K^+, and (f) Na^+. Telomestatin is shown in yellow, the cation is shown in purple, and the G-quartet is colored by elements.

monovalent cations such as those typically coordinated to G-quartets. In the presence of ammonium ions, the lead complex totally disappears and the complex [telomestatin + NH_4^+] is detected at $m/z = 600$. In the presence of potassium ions, the complex [telomestatin + K^+] is detected at $m/z = 621$, but the lead complex has not disappeared completely.

All experimental results suggest that telomestatin has significant affinity for monovalent cations like the ammonium ion, and this could influence its binding mode to the G-quadruplex DNA. We performed DFT calculations in order to ascertain the possible coordination geometries of the monovalent cations to telomestatin. The geometries of the [telomestatin + cation] binary complexes are shown in Figures 4(a)–4(c), and the geometries of the ternary complexes between [telomestatin + cation + one G-quartet] are shown in Figures 4(d)–4(f). In the isolated [telomestatin + cation] complexes, all cations are coordinated in the plane of the telomestatin. In the ternary complexes with the G-quartet, the cation clearly moves towards the G-quartet. The structures of the complexes with K^+ and NH_4^+ are similar, with the cation coordinated midway between the telomestatin and the G-quartet. Sodium, on the other hand, sits closer to the G-quartet than to the telomestatin.

The mode of cation coordination to the telomestatin—G-quartet system is similar to the coordination mode already described for successive G-quartets [36]. In terms of coordination geometries, potassium tends to sit between G-quartets while sodium tends to fit in the middle of one G-quartet because it is smaller. K^+ and NH_4^+ have similar ionic radii [37, 38] and therefore behave similarly, and the same trend is observed for our telomestatin-G-quartet complex. The optimized geometries are similar for all functionals tested (B3LYP, BHandHLYP, MPBW1K) (see Figure S1 in Supplementary Material available online at doi: 10.4061/2010/121259), with the cation in the plane of telomestatin in the absence of G-quartet, and between telomestatin and the G-quartet in the ternary complex. However, the functionals have a greater influence on the computed interaction energies. The root mean square distances (RMSDs) for two-by-two comparisons of hybrid functional, and the interaction energies of NH_4^+, K^+ and Na^+ with telomestatin alone, telomestatin + one G-quartet are given in supplementary Tables S1 and S2, respectively.

4. Conclusion

We have therefore shown that telomestatin readily coordinates monovalent cations such as K^+ and NH_4^+, and that telomestatin retains this cation while binding to G-quadruplexes. The observed stoichiometry and the calculations are consistent with a cation trapped midway between the telomestatin and the G-quartet. Telomestatin therefore acts like an analog of a G-quartet. This study underlines that monovalent cation coordination capabilities should be

integrated in the rational design of G-quadruplex binding ligands.

Acknowledgments

The authors wish it to be known that, in their opinion, the first two authors should be regarded as joint first authors. This work was supported by the Fonds de la Recherche Scientifique (FNRS) (FRFC 2.4.623.05 to Edwin De Pauw, CC.1.5.286.09.F to Valérie Gabelica, research associate position to Valérie Gabelica, postdoctoral fellowship to Frédéric Rosu, and logistician fellowship to Nicolas Smargiasso), and by the University of Liége (starting Grant FRSD-08/10 to V.G.).

References

[1] E. M. Rezler, D. J. Bearss, and L. H. Hurley, "Telomere inhibition and telomere disruption as processes for drug targeting," *Annual Review of Pharmacology and Toxicology*, vol. 43, pp. 359–379, 2003.

[2] D. J. Bearss, L. H. Hurley, and D. D. Von Hoff, "Telomere maintenance mechanisms as a target for drug development," *Oncogene*, vol. 19, no. 56, pp. 6632–6641, 2000.

[3] S. M. Bailey and J. P. Murnane, "Telomeres, chromosome instability and cancer," *Nucleic Acids Research*, vol. 34, no. 8, pp. 2408–2417, 2006.

[4] S. Neidle, "The structures of quadruplex nucleic acids and their drug complexes," *Current Opinion in Structural Biology*, vol. 19, no. 3, pp. 239–250, 2009.

[5] P. Alberti, L. Lacroix, L. Guittat, C. Hélène, and J. L. Mergny, "Nucleic acids as targets for antitelomerase agents," *Mini Reviews in Medicinal Chemistry*, vol. 3, no. 1, pp. 23–36, 2003.

[6] D. Monchaud and M.-P. Teulade-Fichou, "A hitchhiker's guide to G-quadruplex ligands," *Organic and Biomolecular Chemistry*, vol. 6, no. 4, pp. 627–636, 2008.

[7] J.-F. Riou, D. Gomez, H. Morjani, and C. Trentesaux, "Quadruplex ligand recognition: biological aspects," in *Quadruplex Nucleic Acids*, S. Neidle and S. Balasubramanian, Eds., pp. 154–179, The Royal Soceity of Chemistry, Cambridge, UK, 2006.

[8] M. S. Searle and G. D. Balkwill, "DNA quadruplex-ligand recognition: structure and dynamics," in *Quadruplex Nucleic Acids*, S. Neidle and S. Balasubramanian, Eds., pp. 131–153, The Royal Soceity of Chemistry, Cambridge, UK, 2006.

[9] K. Shin-Ya, K. Wierzba, and K. Matsuo et al., "Telomestatin, a novel telomerase inhibitor from Streptomyces anulatus," *Journal of the American Chemical Society*, vol. 123, no. 6, pp. 1262–1263, 2001.

[10] A. De Cian, L. Guittat, K. Shin-Ya, J. F. Riou, and J. L. Mergny, "Affinity and selectivity of G4 ligands measured by FRET," *Nucleic Acids Symposium Series*, no. 49, pp. 235–236, 2005.

[11] F. Rosu, V. Gabelica, K. Shin-Ya, and E. De Pauw, "Telomestatin-induced stabilization of the human telomeric DNA quadruplex monitored by electrospray mass spectrometry," *Chemical Communications*, vol. 9, no. 21, pp. 2702–2703, 2003.

[12] M.-Y. Kim, H. Vankayalapati, K. Shin-Ya, K. Wierzba, and L. H. Hurley, "Telomestatin, a potent telomerase inhibitor that interacts quite specifically with the human telomeric intramolecular G-quadruplex," *Journal of the American Chemical Society*, vol. 124, no. 10, pp. 2098–2099, 2002.

[13] T. Tauchi, K. Shin-Ya, and G. Sashida et al., "Activity of a novel G-quadruplex-interactive telomerase inhibitor, telomestatin (SOT-095), against human leukemia cells: involvement of ATM-dependent DNA damage response pathways," *Oncogene*, vol. 22, no. 34, pp. 5338–5347, 2003.

[14] D. Gomez, T. Wenner, and B. Brassart et al., "Telomestatin-induced telomere uncapping is modulated by POT1 through G-overhang extension in HT1080 human tumor cells," *Journal of Biological Chemistry*, vol. 281, no. 50, pp. 38721–38729, 2006.

[15] N. Temime-Smaali, L. Guittat, A. Sidibe, K. Shin-Ya, C. Trentesaux, and J.-F. Riou, "The G-quadruplex ligand telomestatin impairs binding of topoisomerase IIIα to G-quadruplex-forming oligonucleotides and uncaps telomeres in ALT cells," *PLoS ONE*, vol. 4, no. 9, article e6919, 2009.

[16] T. Tauchi, K. Shin-Ya, and G. Sashida et al., "Telomerase inhibition with a novel G-quadruplex-interactive agent, telomestatin: in vitro and in vivo studies in acute leukemia," *Oncogene*, vol. 25, no. 42, pp. 5719–5725, 2006.

[17] N. Binz, T. Shalaby, P. Rivera, K. Shin-Ya, and M. A. Grotzer, "Telomerase inhibition, telomere shortening, cell growth suppression and induction of apoptosis by telomestatin in childhood neuroblastoma cells," *European Journal of Cancer*, vol. 41, no. 18, pp. 2873–2881, 2005.

[18] M. Sumi, T. Tauchi, and G. Sashida et al., "A G-quadruplex-interactive agent, telomestatin (SOT-095), induces telomere shortening with apoptosis and enhances chemosensitivity in acute myeloid leukemia," *International Journal of Oncology*, vol. 24, no. 6, pp. 1481–1487, 2004.

[19] M. A. Shammas, R. J. Shmookler Reis, and C. Li et al., "Telomerase inhibition and cell growth arrest after telomestatin treatment in multiple myeloma," *Clinical Cancer Research*, vol. 10, no. 2, pp. 770–776, 2004.

[20] S. Agrawal, R. P. Ojha, and S. Maiti, "Energetics of the human Tel-22 quadruplex—telomestatin interaction: a molecular dynamics study," *Journal of Physical Chemistry B*, vol. 112, no. 22, pp. 6828–6836, 2008.

[21] F. Rosu, V. Gabelica, C. Houssier, P. Colson, and E. De Pauw, "Triplex and quadruplex DNA structures studied by electrospray mass spectrometry," *Rapid Communications in Mass Spectrometry*, vol. 16, no. 18, pp. 1729–1736, 2002.

[22] E. S. Baker, S. L. Bernstein, V. Gabelica, E. De Pauw, and M. T. Bowers, "G-quadruplexes in telomeric repeats are conserved in a solvent-free environment," *International Journal of Mass Spectrometry*, vol. 253, no. 3, pp. 225–237, 2006.

[23] V. Gabelica, E. S. Baker, M.-P. Teulade-Fichou, E. De Pauw, and M. T. Bowers, "Stabilization and structure of telomeric and c-myc region intramolecular G-quadruplexes: the role of central cations and small planar ligands," *Journal of the American Chemical Society*, vol. 129, no. 4, pp. 895–904, 2007.

[24] H. Seto, K. Shin-Ya, and K. Wierzba, "Substance GM-95, process for producing the same and utilization thereof," WO 00/24747, October 1999.

[25] *Gaussian 03, Revision D.02*, Gaussian, Wallingford, Conn, USA, 2004.

[26] Y. Zhao and D. G. Truhlar, "How well can new-generation density functional methods describe stacking interactions in biological systems?" *Physical Chemistry Chemical Physics*, vol. 7, no. 14, pp. 2701–2705, 2005.

[27] K. Breuker, "New mass spectrometric methods for the quantification of protein-ligand binding in solution," *Angewandte Chemie - International Edition*, vol. 43, no. 1, pp. 22–25, 2003.

[28] M. M. Siegel, "Early discovery drug screening using mass spectrometry," *Current Topics in Medicinal Chemistry*, vol. 2, no. 1, pp. 13–33, 2002.

[29] B. N. Pramanik, P. L. Bartner, U. A. Mirza, Y.-H. Liu, and A. K. Ganguly, "Electrospray ionization mass spectrometry for the study of non-covalent complexes: an emerging technology," *Journal of Mass Spectrometry*, vol. 33, no. 10, pp. 911–920, 1998.

[30] J. A. Loo, "Studying noncovalent protein complexes by electrospray ionization mass spectrometry," *Mass Spectrometry Reviews*, vol. 16, no. 1, pp. 1–23, 1997.

[31] F. Rosu, E. De Pauw, and V. Gabelica, "Electrospray mass spectrometry to study drug-nucleic acids interactions," *Biochimie*, vol. 90, no. 7, pp. 1074–1087, 2008.

[32] C. A. Schalley, "Molecular recognition and supramolecular chemistry in the gas phase," *Mass Spectrometry Reviews*, vol. 20, no. 5, pp. 253–309, 2001.

[33] E. Leize, A. Jaffrezic, and A. Van Dorsselaer, "Correlation between solvation energies and electrospray mass spectrometric response factors. Study by electrospray mass spectrometry of supramolecular complexes in thermodynamic equilibrium in solution," *Journal of Mass Spectrometry*, vol. 31, no. 5, pp. 537–544, 1996.

[34] S. M. Blair, J. S. Brodbelt, A. P. Marchand, K. A. Kumar, and H.-S. Chong, "Evaluation of binding selectivities of caged crown ligands toward heavy metals by electrospray ionization/quadrupole ion trap mass spectrometry," *Analytical Chemistry*, vol. 72, no. 11, pp. 2433–2445, 2000.

[35] E. C. Kempen, J. S. Brodbelt, R. A. Bartsch, Y. Jang, and J. S. Kim, "Investigation of alkali metal cation selectivities of lariat ethers by electrospray ionization mass spectrometry," *Analytical Chemistry*, vol. 71, no. 24, pp. 5493–5500, 1999.

[36] J. Gu and J. Leszczynski, "Origin of Na^+/K^+ selectivity of the guanine tetraplexes in water: the theoretical rationale," *Journal of Physical Chemistry A*, vol. 106, no. 3, pp. 529–532, 2002.

[37] N. V. Hud, P. Schultze, V. Sklenář, and J. Feigon, "Binding sites and dynamics of ammonium ions in a telomere repeat DNA quadruplex," *Journal of Molecular Biology*, vol. 285, no. 1, pp. 233–243, 1999.

[38] P. Schultze, N. V. Hud, F. W. Smith, and J. Feigon, "The effect of sodium, potassium and ammonium ions on the conformation of the dimeric quadruplex formed by the Oxytricha nova telomere repeat oligonucleotide d(G4T4G4)," *Nucleic Acids Research*, vol. 27, no. 15, pp. 3018–3028, 1999.

SAGE-Hindawi Access to Research
Journal of Nucleic Acids
Volume 2010, Article ID 217627, 9 pages
doi:10.4061/2010/217627

Research Article

Synthesis of Macrocyclic Hexaoxazole (6OTD) Dimers, Containing Guanidine and Amine Functionalized Side Chains, and an Evaluation of Their Telomeric G4 Stabilizing Properties

Keisuke Iida,[1] Masayuki Tera,[1] Takatsugu Hirokawa,[2] Kazuo Shin-ya,[3] and Kazuo Nagasawa[1]

[1] *Department of Biotechnology and Life Science Faculty of Technology, Tokyo University of Agriculture and Technology (TUAT), Koganei, Tokyo 184-8588, Japan*
[2] *Computational Biology Research Center, National Institute of Advanced Industrial Science and Technology, Koto-ku, Tokyo 135-0064, Japan*
[3] *Biological Information Research Center, National Institute of Advanced Industrial Science and Technology, Koto-ku, Tokyo 135-0064, Japan*

Correspondence should be addressed to Kazuo Nagasawa, knaga@cc.tuat.ac.jp

Received 15 February 2010; Accepted 1 March 2010

Academic Editor: R. Eritja

Structure-activity relationship studies were carried out on macrocyclic hexaoxazole (6OTD) dimers, whose core structure stabilizes telomeric G-quadruplexes (G4). Two new 6OTD dimers having side chain amine and guanidine functional groups were synthesized and evaluated for their stabilizing ability against a telomeric G4 DNA sequence. The results show that the 6OTD dimers interact with the DNA to form 1:1 complexes and stabilize the antiparallel G4 structure of DNA in the presence of potassium cation. The guanidine functionalized dimer displays a potent stabilizing ability of the G4 structure, as determined by using a FRET melting assay ($\Delta T_m = 14\,^{\circ}\mathrm{C}$).

1. Introduction

G-quadruplexes (G4), secondary DNA structures consisting of G-quartet planers in G-rich regions, play significant biological roles for example, control of transcription and telomeric lengths [1–19]. One typical G4 forming DNA sequence is a telomere, which exists at the ends of chromosomes consisting of $(TTAGGG)_n$ repeating single-stranded sequences [1–12]. Telomeres protect chromosomes from end to end fusion events, which result in replication of the chromosome (the Hayflick limit) [20]. The telomere repeats are elongated by the reverse transcriptase telomerase, which is overexpressed in most tumor cells. In contrast, telomerase activity is not observed in normal somatic cells [21]. Since the activity of this enzyme is inhibited by the G4 structure of telomeres owing to steric hindrance, small molecules that selectively bind and stabilize the telomeric G4 should be potential anticancer agents. As a result, a number of G4 ligands, inspired by artificial DNA intercalators as well as natural products, have been developed during the past decade [22].

Telomestatin (TMS) is a natural product isolated from *Streptomyces anulatus* 3533-SV4, which displays one of the most potent telomeric G4 binding activity (Figure 1) [23–28]. Interaction analysis has shown that two molecules of TMS induce conversion of telomeric G4 into an antiparallel type by way of an end stacking mode [25–28]. We have recently developed macrocyclic hexaoxazole compounds 6OTD, containing a variety of side chain functional groups, that serve as a novel TMS derivative [29–32]. In addition, by considering the proposed binding mode of TMS with telomeric G4, we have carried out further structural development of dimeric 6OTD derivatives (Figure 1) [33]. The results of molecular dynamics calculations guided the selection of 6OTD dimer **1** that contains an appropriate length of a linker between the monomeric units of 6OTD. Studies showed that dimer **1** binds to telomeric G4 more tightly than do other 6OTD dimers with linkers of shorter or

longer lengths. One possible structural development strategy to enhance the stabilizing ability of **1** against the G4 would be to install cationic functional groups on the side chain [30]. Below, we describe synthesis of new 6OTD dimers **2** and **3** that derivatize **1** but possess cationic amine and guanidine functional groups on their side chains. In addition, the ability of these substances to stabilize telomeric G4 along with their interaction mode was investigated.

2. Materials and Methods

2.1. General. Flash chromatography was performed on Silica gel 60 (spherical, particle size 0.040 ~ 0.100 μm; Kanto). Optical rotations were measured on a JASCO P-2200 polarimeter, using the sodium D line. ^{1}H and ^{13}C NMR spectra were recorded on JEOL JNM-ECX 300, 400, and 500. The spectra are referenced internally according to residual solvent signals of $CDCl_3$ (^{1}H NMR; δ = 7.26 ppm, ^{13}C NMR δ = 77.0; ppm) and DMSO $d-6$ (^{1}H NMR; δ = 2.50 ppm, ^{13}C NMR; δ = 39.5 ppm). Data for ^{1}H NMR are recorded as follows: chemical shift (δ, ppm), multiplicity (s, singlet; d, doublet; m, multiplet; br, broad), integration, and coupling constant (Hz). Data for ^{13}C NMR are reported in terms of chemical shift (δ, ppm). Mass spectra were recorded on a JEOL JMS-T100X spectrometer with ESI-MASS mode using methanol as solvent. All oligonucleotides purified were obtained from Sigma Genosys and dissolved in double-distilled water to be used without further purification. Fluorescence resonance energy transfer (FRET) melting assay was made with an excitation wavelength of 470–505 nm and a detection wavelength of 523–543 nm using the DNA Engine Opticon 2 Real-Time Cycler PCR detection system (BioRad). CD spectra were recorded on a JASCO-810 spectropolarimeter (Jasco, Easton, MD) using a quartz cell of 1 mm optical path length and an instrument scanning speed of 500 nm/min with a response time of 1 s, and over a wavelength range of 220–320 nm. CD spectra are representative of ten averaged scans taken at 25°C.

2.2. Synthesis

*Synthesis of **5**.* To a solution of trioxazole **4** (2.1 g, 3.6 mmol) in MeOH-THF (1 : 1, 60 mL) was added $Pd(OH)_2/C$ (420 mg), and the reaction mixture was stirred at room temperature under hydrogen gas (balloon). After 3 h, the catalyst was removed by filtration through a pad of Celite, and the filtrates were concentrated in vacuo to give amine **5**, which was used without further purification.

*Synthesis of **7**.* To a solution of trioxazole **6** (2.1 g, 3.6 mmol) in THF-H_2O (3 : 1, 80 mL) was added LiOH (230 mg, 5.4 mmol) at 0°C. After stirring at room temperature for 1 h,to the resulting mixture was added 1 N HCl, to give carboxylic acid **7**, which was used without further purification.

*Synthesis of **8**.* To a solution of amine **5** (abovementioned) in THF-H_2O (1 : 1) was added the carboxylic acid **7** (above-mentioned), *N*-methylmorpholine (1.2 mL, 11 mmol), and 4-(4, 6-dimethoxy-1, 3, 5-triazin-2-yl)-4-methylmorpholinium chloride (DMT-MM) (3.0 g, 11 mmol), and the mixture was stirred at room temperature for 15 h. To the reaction mixture was added H_2O and precipitate was formed. This precipitate was collected with filtration using filter paper, to give **8** as a white solid (3.3 g, 3.2 mmol 89% 2 steps, mp = 200–203°C). Spectral data for **8**: $[\alpha]^{25}_D = -2.7$ (c 1.1, $CHCl_3$–MeOH (1 : 1)); ^{1}H NMR (300 MHz, $CDCl_3$) δ 8.43 (s, 1H), 8.35–8.27 (m, 5H), 7.53 (d, J = 8.9 Hz, 1H), 7.34 (m, 5H), 5.98–5.81 (m, 1H), 5.57–5.44 (m, 2H), 5.30 (d, J = 18 Hz, 1H), 5.21 (d, J = 11 Hz, 1H), 5.15–4.97 (m, 2H), 4.82 (br, 1H), 4.58 (d, J = 5.5 Hz, 3H), 3.95 (s, 3H), 3.30–3.01 (m, 4H), 2.25–1.80 (m, 4H), 1.70–1.30 (m, 17H); ^{13}C NMR (125 MHz, DMSO $d-6$) δ 165.7, 165.2, 160.9, 159.8, 156.1, 155.8, 155.7, 155.6, 155.0, 154.4, 145.7, 142.8, 141.0, 140.9, 140.7, 137.3, 136.6, 133.4, 133.3, 130.1, 130.0, 128.9, 128.8, 128.3, 127.7, 117.3, 77.3, 65.1, 64.9, 64.7, 52.0, 48.9, 46.8, 31.8, 31.3, 29.2, 28.9, 28.2, 28.1, 22.8, 22.6; HRMS (ESI, M + Na) calcd for $C_{48}H_{52}N_{10}O_{15}Na$ 1031.3511, found 1031.3479.

*Synthesis of **9**.* To a solution of bis-trioxazole **8** (510 mg, 0.50 mmol) in DMF-THF (1 : 5, 30 mL) was added morpholine (440 μL, 5.0 mmol) and $Pd(PPh_3)_4$ (29 mg, 0.025 mmol), and the mixture was stirred at room temperature for 1 h. To the reaction mixture was added ether and precipitate was formed. This precipitate was collected with filtration using filter paper. The solid was purified by column chromatography on silica gel ($CHCl_3$-MeOH = 9 : 1) to give **9** (460 mg, 0.50 mmol 99%). Spectral data for **9**: $[\alpha]^{25}_D = 28$ (c 1.0, $CHCl_3$-MeOH (1 : 1)); ^{1}H NMR (300 MHz, $CDCl_3$) δ 8.43 (s, 1H), 8.35–8.25 (m, 5H), 7.53 (d, J = 8.9 Hz, 1H), 7.33 (m, 5H), 5.56–5.43 (m, 1H), 5.08 (br, 2H), 4.80 (br, 1H), 4.56 (br, 1H), 4.14–4.05 (m, 1H), 3.95 (s, 3H), 3.26–3.04 (m, 4H), 2.25–1.75 (m, 4H), 1.73–1.30 (m, 17H); ^{13}C NMR (125 MHz, DMSO $d-6$) δ 169.3, 165.2, 160.9, 159.8, 156.1, 155.9, 155.7, 155.6, 154.9, 154.4, 145.7, 142.7, 141.0, 140.9, 140.6, 140.5, 137.3, 136.6, 133.3, 130.0, 129.9, 128.8, 128.5, 128.3, 127.7, 77.3, 65.1, 52.0, 49.4, 46.7, 35.3, 31.3, 29.2, 28.2, 28.1, 22.8, 22.6; HRMS (ESI, M + Na) calcd for $C_{44}H_{48}N_{10}O_{13}Na$ 947.3300, found 947.3308.

*Synthesis of **10**.* To a solution of bis-trioxazole **9** (2.2 g, 2.4 mmol) in THF-H_2O (3 : 1, 200 mL) was added lithium hydroxide (300 mg, 7.2 mmol), and the mixture was stirred at room temperature for 2 h. To the reaction mixture was added 1N HCl, and the resulting mixture was concentrated in vacuo. To the residual solution in DMF-CH_2Cl_2 (1 : 2, 800 mL) was added DMAP (1.5 g, 12 mmol), diisopropylethylamine (2.0 mL, 12 mmol), and DPPA (2.6 mL, 12 mmol), and the resulting mixture was stirred for 22 h at 90°C. To the reaction mixture was added H_2O and the organic layer was extracted with ethyl acetate. The extracts were washed with brine, dried over $MgSO_4$, filtered, and concentrated in vacuo. The residue was purified by column chromatography on silica gel (ethyl acetate 100%) to give **10** as a white solid (1.7 g, 1.9 mmol 79%, mp = 220–225°C

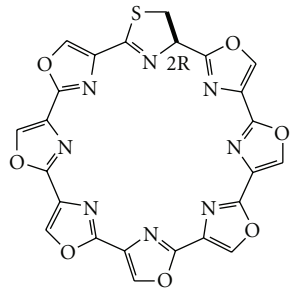

Telomestatin (TMS)

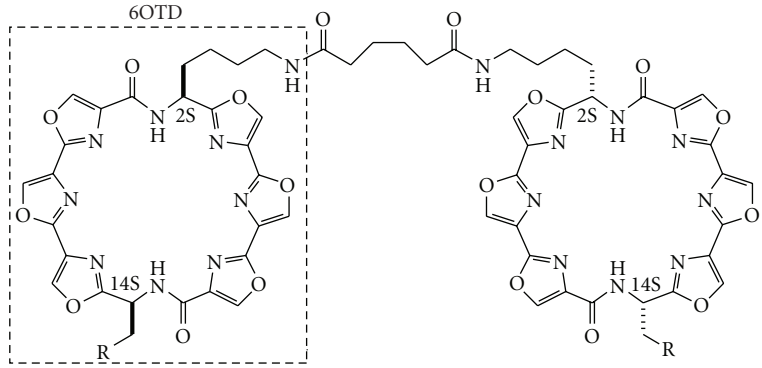

6OTD dimers (**1**) : R = OAc
(**2**) : R = $(CH_2)_3NH_2$
(**3**) : R = $(CH_2)_3NHC(NH)NH_2$

Figure 1: Structures of telomestatin and 6OTD dimers.

dec). Spectral data for **10**: $[\alpha]^{25}{}_D = -12$ (*c* 0.4, $CHCl_3$-MeOH (1 : 1)); ^{H}H NMR (400 MHz, $CDCl_3$) δ 8.54 (d, J = 7.3 Hz, 2H), 8.25–8.16 (m, 6H), 7.36–7.27 (m, 5H), 5.47–5.37 (m, 2H), 5.05 (br, 2H), 4.89 (br, 1H), 4.59 (br, 1H), 3.22–2.98 (m, 4H), 2.30–1.89 (m, 4H), 1.62–1.18 (m, 17H); ^{13}C NMR (100 MHz, $CDCl_3$) δ 164.8, 164.7, 161.2, 159.9, 159.8, 156.3, 156.0, 155.9, 154.6, 141.0, 140.9, 139.1, 138.4, 136.9, 136.8, 136.6, 130.9, 129.6, 128.4, 128.1, 128.0, 79.0, 66.5, 47.8, 47.7, 40.7, 40.3, 34.6, 29.5, 29.2, 28.4, 21.9, 21.8; HRMS (ESI, M + Na) calcd for $C_{43}H_{44}N_{10}O_{12}Na$ 915.3038, found 915.2999.

*Synthesis of **11***. To a solution of macrocyclic bis-amide **10** (200 mg, 220 μmol) in MeOH (50 mL) was added $Pd(OH)_2$/C (80 mg) and the reaction mixture was stirred at room temperature under hydrogen (balloon). After 5 h, the reaction mixture was filtered through a pad of Celite, and the filtrates were concentrated in vacuo. To the residual solution in DMF-MeCN (1 : 1, 4.0 mL) was added diisopropylethylamine (190 μL, 1.1 mmol) and adipoyl chloride (16 μL, 110 μmol), and the mixture was stirred at room temperature for 11 h. The reaction mixture was concentrated in vacuo, and the residue was acidified with 0.1 N HCl and extracted with $CHCl_3$. The organic layer was dried over $MgSO_4$, filtrated, and concentrated in vacuo. The residue was purified by column chromatography on silica gel ($CHCl_3$–AcOEt–MeOH = 3 : 2 : 1) to give **11** (51 mg, 31 μmol, 28%). Spectral data for **11**: $[\alpha]^{25}{}_D = -11$ (*c* 0.95, $CHCl_3$-MeOH (1 : 1)); ^{1}H NMR (500 MHz, $CDCl_3$) δ 8.67–8.48 (m, 4H), 8.27–8.15 (m, 12H), 6.38 (br, 2H), 5.47–5.38 (m, 4H), 4.84 (br, 2H), 3.30–2.98 (m, 8H), 2.15–1.90 (m, 12H), 1.65–1.10 (m, 38H); ^{13}C NMR (125 MHz, $CDCl_3$) δ 173.0, 164.9, 164.8, 159.8, 159.7, 156.2, 156.1, 156.0, 154.7, 154.6, 141.0, 140.9, 139.5, 139.3, 138.7, 138.6, 136.9, 136.8, 130.8, 129.5, 129.3, 78.9, 47.8, 47.7, 40.3, 38.9, 36.0, 34.5, 34.3, 29.7, 29.5, 28.8, 28.4, 25.1, 21.9, 21.7; HRMS (ESI, M + Na) calcd for $C_{76}H_{82}N_{20}O_{22}Na$ 1649.5810, found 1649.5811.

*Synthesis of **2***. A solution of **11** (50 mg, 31 μmol) in CH_2Cl_2-TFA (95 : 5, 25 mL) was stirred at room temperature for 2 h. The reaction mixture was concentrated in vacuo to give **2** as a white solid (50 mg, 30 μmol, 98%, mp = 225–230°C dec). Spectral data for **2**: $[\alpha]^{25}{}_D = 72$ (*c* 0.3, $CHCl_3$-MeOH (1 : 1)); ^{1}H NMR (500 MHz, DMSO $d-6$) δ 9.15–9.08 (m, 8H), 8.95–8.89 (m, 4H), 8.38 (d, J = 6.9 Hz, 2H), 8.30 (d, J = 6.9 Hz, 1H), 7.80–7.53 (m, 6H), 5.50–5.35 (m, 4H), 2.98–2.89 (m, 4H), 2.78–2.89 (m, 4H), 2.15–1.85 (m, 12H), 1.55–1.00 (m, 20H); ^{13}C NMR (125 MHz, DMSO d – 6) δ 171.7, 164.5, 164.3, 158.8, 158.7, 155.6, 154.5, 142.5, 141.9, 141.8, 141.1, 136.0, 129.8, 129.7, 128.5, 128.4, 47.4, 47.3, 38.6, 38.1, 35.1,

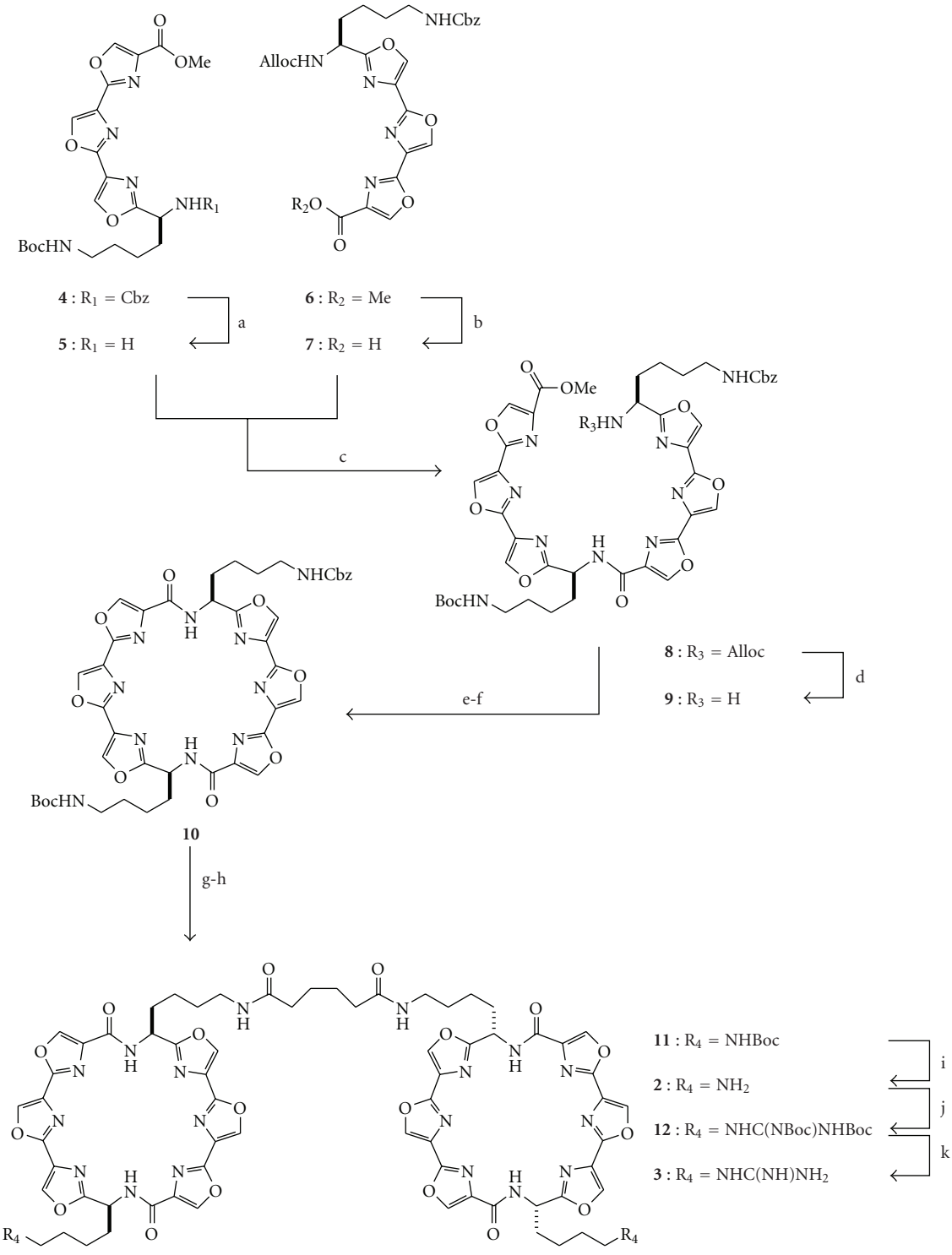

Scheme 1: Synthesis of 6OTD dimers. (a) $Pd(OH)_2/C$, H_2, THF-MeOH; (b) $LiOH \cdot H_2O$, THF-H_2O; (c) DMT-MM, *N*-methylmorpholine, THF-H_2O, 89% over 2 steps from **4** and **6**; (d) $Pd(PPh_3)_4$, morpholine, DMF-THF 99%; (e) $LiOH \cdot H_2O$, THF-H_2O; (f) *N*,*N*-diisopropylethylamine, DMAP, DPPA, DMF-CH_2Cl_2, 78% over 2 steps from **9**; (g) $Pd(OH)_2/C$, H_2, MeOH; h) *N*,*N*-diisopropylethylamine, adipoyl chloride, 28% over 2 steps from **10**; (i) TFA, CH_2Cl_2 98%; (j) Et_3N, $HgCl_2$, 1,3-bis(tert-butoxycarbonyl)-2-methyl-2-thiopseudourea; (k) TFA, CH_2Cl_2, 42%; Boc = tert-butoxycarbonyl, Cbz = benzyloxycarbonyl, DMT-MM = 4-(4,6-dimethoxy-1,3,5-triazin-2-yl)-4-methylmorpholinium chloride, DMAP = 4-dimethylaminopyridine, DPPA = diphenylphosphoryl azide, TFA = trifluoroacetic acid.

33.1, 28.7, 26.7, 24.9, 21.3, 20.8; HRMS (ESI, M + H) calcd for $C_{66}H_{67}N_{20}O_{18}$ 1427.4942, found 1427.4961.

*Synthesis of **12**.* To a solution of **2** (50 mg, 30 μmol) in MeOH (5.0 mL) was added Amberlyst A-26(OH) ion-exchange

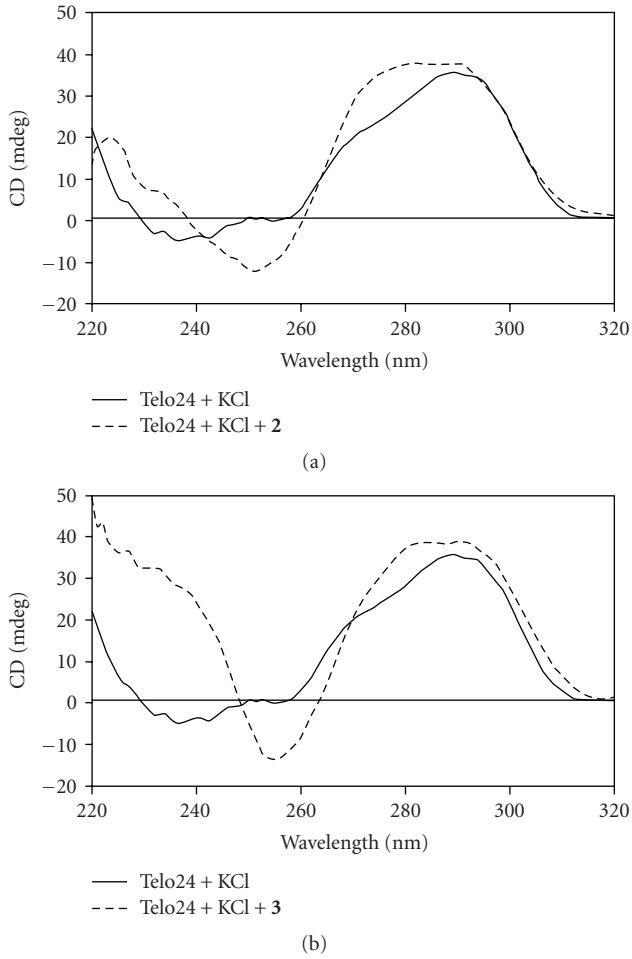

FIGURE 2: CD spectra of telo24 (10 $\mu\Delta$M) in Tris-HCl buffer (50 mM, pH 7.0) with KCl (100 mM) and/or ligands (50 μM). (a) solid line: telo24 + KCl; dashed line: telo24 + KCl + **2**. (b) solid line: telo24 + KCl; dashed line: telo24 + KCl + **3**.

resin, and the mixture was stirred for 30 minutes. The resulting mixture was filtered through a cotton with MeOH, and the filtrates were concentrated in vacuo. To a residual solution of **2** in DMF (5.0 mL) was added diisopropylethylamine (52 μL, 0.31 mmol), $HgCl_2$ (50 mg, 0.18 mmol), and 1,3-Bis(*tert*butoxycarbonyl)-2-methyl-2-thiopseudourea (66 mg, 0.18 mmol), and the mixture was stirred for 1 h at room temperature. To the reaction mixture was added H_2O, and the organic layer was extracted with ethyl acetate. The extracts were dried over $MgSO_4$, filtered, and concentrated in vacuo. The residue was chromatographed on silica gel ($CHCl_3$-ethyl acetate-MeOH = 3 : 2 : 1) to give **12** as a white solid (30 mg, 16 μmol, 52%). Spectral data for **12**: $[\alpha]^{25}{}_D$ = 3.8 (*c* 1.4, $CHCl_3$-MeOH (1 : 1)); ^{1}H NMR (500 MHz, $CDCl_3$) δ 11.5 (br, 2H), 8.57–8.48 (m, 4H), 8.30–8.17 (m, 14H), 6.17 (br, 2H), 5.45–5.36 (m, 4H), 3.41–3.32 (m 4H), 3.28–3.10 (m, 4H), 2.20–1.88 (m, 12H), 1.65–1.20 (m, 56H); ^{13}C NMR (125 MHz, $CDCl_3$) δ 172.9, 164.8, 164.7, 163.5, 159.9, 159.7, 156.1, 156.0, 154.7, 154.6, 153.2, 141.0, 140.9, 139.3, 139.2, 138.6, 138.5, 136.9, 136.8, 130.8, 129.6, 129.5, 82.9, 79.1, 47.7, 47.6, 40.5, 39.1, 36.0, 34.7, 28.7, 28.6, 28.2, 28.0, 25.0, 22.1, 22.0; HRMS (ESI, M + Na) calcd for $C_{88}H_{102}N_{24}O_{26}Na$ 1933.7295, found 1933.7332.

*Synthesis of **3**.* A solution of **12** (29 mg, 31 μmol) in CH_2Cl_2-TFA (3 : 1, 2.0 mL) was stirred at room temperature for 2 h. To the reaction mixture was added ether and precipitate was formed. This precipitate was collected with filtration using filter paper, to give **3** as a white solid (20 mg, 12 μmol, 80%, mp = 220–225°C dec). Spectral data for **3**: $[\alpha]^{25}{}_D$ = −18 (*c* 0.75, $CHCl_3$-MeOH (1 : 1)); ^{1}H NMR (400 MHz, DMSO *d* − 6) δ 9.14–9.08 (m, 8H), 8.94–8.90 (m, 4H), 8.37 (d, *J* = 7.3 Hz, 1H), 8.32 (d, *J* = 7.3 Hz, 1H), 7.75–7.69 (m, 2H), 7.51–7.45 (m, 2H), 5.48–5.37 (m, 4H), 3.08–2.90 (m, 8H), 2.15–1.84 (m, 12H), 1.50–1.00 (m, 20H); ^{13}C NMR (125 MHz, DMSO *d* − 6) δ171.7, 164.5, 164.4, 158.8, 158.7, 156.7, 155.7, 155.6, 154.5, 142.5, 141.8, 141.1, 136.0, 129.8, 129.7, 128.5, 128.4, 47.4, 40.5, 38.1, 35.1, 33.4, 33.3, 28.7, 28.2, 24.9, 21.3, 21.0; HRMS (ESI, M + H) calcd for $C_{68}H_{71}N_{24}O_{18}$ 1511.5378, found 1511.5368.

2.3. FRET Melting Assay. FRET melting assays were performed as reported methods [34, 35]. The dual fluorescently labeled oligonucleotides Flu-telo21 5′-FAM-[GGG(TTAGGG)3]-TAMRA-3′ and Flu-ds26 5′-FAM-[(TA)2GC(TA)2T6(TA)2GC(TA)2]-TAMRA-3′ were used in this protocol. The donor fluorophore was 6-carboxy-fluorescein, FAM, and the acceptor fluorophore was 6-carboxytetramethylrhodamine, TAMRA. The oligonucleotides were initially dissolved as a 100 μM stock solution in MilliQ water; further dilutions were carried out in 60 mM potassium cacodylate buffer (pH 7.4). Dual-labeled DNA was annealed at a concentration of 400 nM by heating at 94°C for 5 minutes followed by cooling to room temperature. We added the different concentrations of ligands into different samples, using a total reaction volume of 40 μL, with 200 nM of labelled oligonucleotide. Then we lay them at 25°C. Following experiments should keep the temperature procedure in real-time PCR and procedure was finished as following: 25°C for 5 minutes, then a stepwise increase of 1°C every minute from 25°C to reach 99°C. During the procedures, we measured the FAM after each stepwise.

2.4. CD Spectroscopy. The 10 μM oligonucleotide of telo24: ([TTAGGG]$_4$) was dissolved in Tris-HCl buffer (50 mM, pH 7.0) and the solution was heated to 90°C for 5 minutes, then slowly cooled to 25°C. G4 ligands were diluted from 10 mM stock solutions to give a concentration of 1 mM with water and added into the oligonucleotide samples at 50 μM (the 10 mM stock solutions of **2** and **3** were made in DMSO).

2.5. ESI-MASS Spectrometry. ESI-MASS spectra were recorded in a negative-ion mode with JEOL JMS-T100X spectrometer. The direct-infusion flow rate was 5.0 μL min^{-1}. All experiments were performed in 20 mM

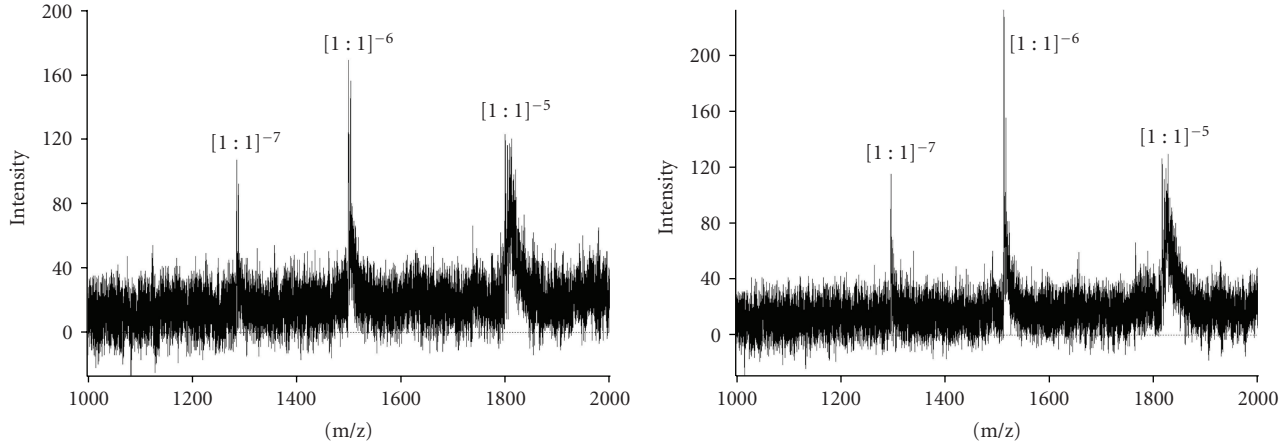

Figure 3: ESI-MASS spectra of 10 μM telo24 with a 40 μM ligands **2** (a) and **3** (b).

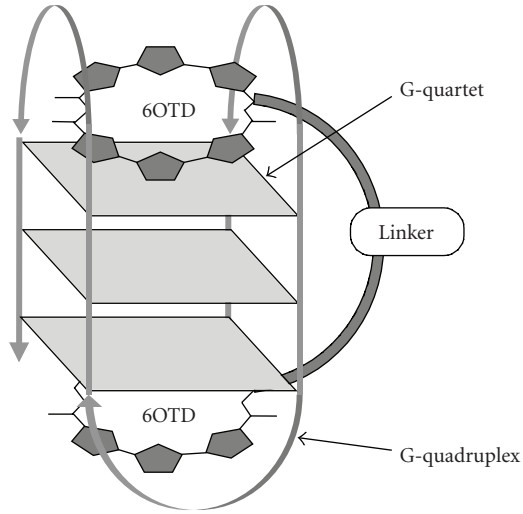

Figure 4: Plausible binding mode of the 6OTD dimers with telo24 [33].

NH_4OAc containing 10 μM of telo24 and 40 μM of **2** and **3**. Methanol (15%) was added just before injection.

3. Results and Discussion

3.1. Synthesis of 6OTD Dimers 2 and 3. The 6OTD dimers **2** and **3** were synthesized by using the sequences as shown in Scheme 1. Trioxazoles **4** and **6** were synthesized starting with L-serine and L-lysine, respectively by using the previously reported procedure [29, 30, 36–38]. The Cbz group of **4** was removed by treatment with hydrogen in the presence of $Pd(OH)_2/C$ to give amine **5**. Hydrolysis of the ester group in **6** with lithium hydroxide followed by coupling of the resulting acid with amine **5** using DMT-MM [39] gave the bis-trioxazole amide **8**. Cleavage of the allyloxycarbonyl group in **8** and hydrolysis of the ester group produced an amino acid, which was subjected to macrocyclization under high dilution conditions (5 mM) to give 6OTD **10**. The Cbz group in **10** was removed with hydrogen in the presence of $Pd(OH)_2/C$ to give corresponding amine. The procedure for synthesis of dimer **11** involved coupling of the amine with adipoyl chloride. Bis-amine **2** was obtained by removal of the Boc group of **11** with TFA. Preparation of the guanidine derivative **3** was carried out by guanidination of the amine moiety in **2** by using 1,3-bis(*tert*-butoxycarbonyl)-2-methyl-2-thiopseudourea followed by deprotection of Boc group with TFA.

3.2. Binding Properties of 2 and 3 toward Telomeric G4. With the desired 6OTD dimers **2** and **3** in hand, their mode of interaction with the telomeric DNA (telo24) was investigated. Firstly, conformational changes of telo24, induced by these substances were evaluated using circular dichroism (CD) spectroscopy. Upon treatment of telo24 with 6OTD dimers **2** and **3** (50 μM) in the presence of potassium chloride (100 mM), the mixed-type structure induced by potassium cation (solid line in Figure 2) is transformed to a typical antiparallel-type G4 structure (dashed line in Figure 2) [28, 40][1]. The binding stoichiometries of the complexes formed between the telo24 and ligands and **3** (molar ratio = 1 : 4) were determined by using ESI-MASS spectrometric analysis [41, 42]. In both cases, only mass peaks that correspond to 1 : 1 complexes of both **2** and **3** with telo24 were observed (at the 7-, 6- or in the 5-charge states). Since these interaction modes are the same as that of 6OTD dimer **1**, the newly synthesized 6OTD dimers **2** and **3**

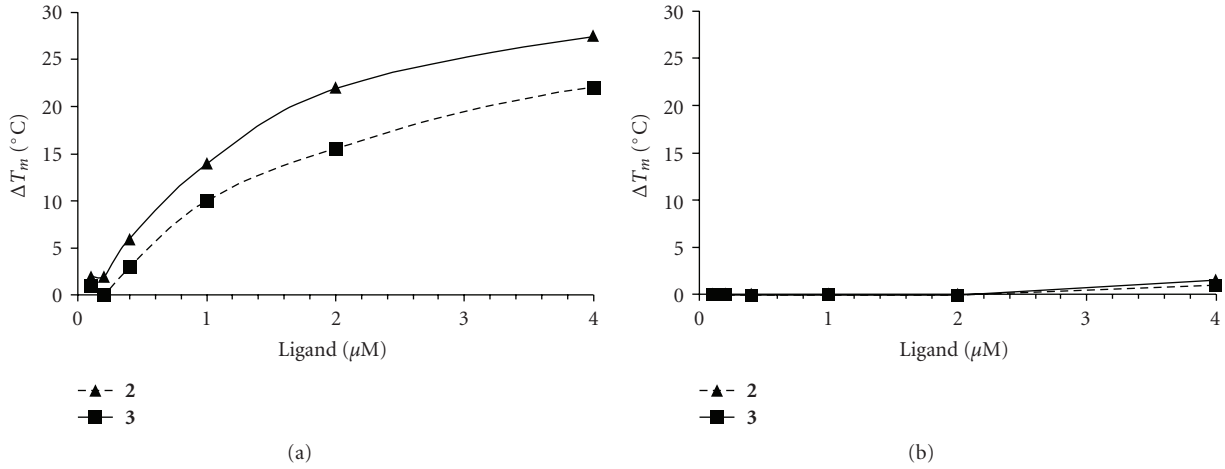

Figure 5: ΔT_m values of 0.2 μM Flu-telo21 (a) and Flu-ds26 (b) in the presence of ligands **2** (solid line) and **3** (dashed line).

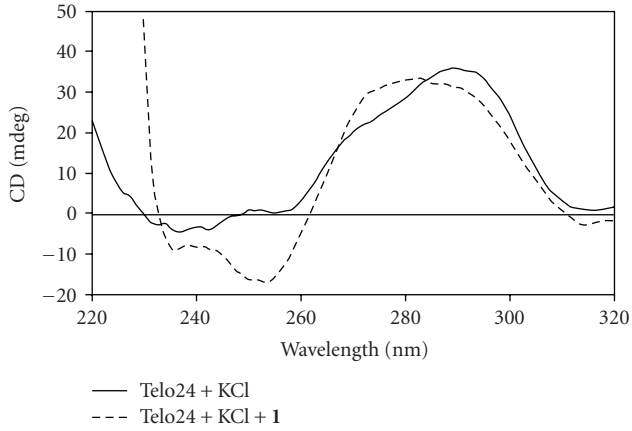

Figure 6

Table 1: ΔT_m values by FRET melting assay.

G4 ligands	**2**	**3**
	ΔT_m at 1 μM G4 ligands (ΔT_m/ °C)	
Flu-telo21	10	14
Flu-ds26	0	0

appear to interact with telo24 through an end stacking mode using two 6OTD moieties in a manner similar to that of TMS and/or 6OTD dimer **1** (Figures 4 and 6) [33][2,3].

The ability to stabilize the G4 structure of telo24 by 6OTD dimers **2** and **3** was evaluated by employing a fluorescence resonance energy transfer -(FRET-) based assay [34, 35]. The ΔT_m values of labeled oligonucleotide flu-telo21 with **2** and **3** at a concentration of 1 μM, which corresponds to 5 equivalents, are 10 and 14°C, respectively (Figure 5(a) and Table 1). Since under the same conditions the ΔT_m value for **1** was 12°C, among the substances explored to date guanidine **3** is a potent stabilizer of the G4 structure[4]. This stabilization effect is likely caused by the attractive interaction between positively charged guanidinium residue and anionic phosphates backbone of the telomeric G4. Interactions of the ligands with the duplex form of flu-ds26 were also investigated by using the same protocol (Figure 5(b) and Table 1). The observation that no differences in the ΔT_m values exist in the presence or absence of dimers **2** and suggests that these ligands are selective for the telomere DNA sequence.

4. Conclusions

In summary, the efforts described above have led to the design and syntheses of **2** and **3**, two novel macrocyclic hexaoxazole dimeric derivatives of 6OTD that have amine and guanidine groups in their respective side chains. These compounds, together with 6OTD dimer acetate **1**, were found to induce a change of the telomeric DNA sequence of telo24 into an antiparallel structure through the formation of 1 : 1 complexes with the DNA. The guanidine functionalized 6OTD dimer **3** was determined to have the greatest ability to stabilize the telomere DNA sequence. Also, both dimers selectively bind to the telomeric DNA sequence and not double-stranded DNA. Further studies, aimed at the structural development of 6OTD dimers with different linkers, are currently underway.

Acknowledgments

This work was supported in part by the Novartis Foundation (Japan) for the Promotion of Science, a Grant-in-Aid for Exploratory Research (21655060), and a Grant under the Industrial Technology Research Grant Program (01A04006b) from the New Energy and Industrial Technology Development Organization (NEDO) of Japan. Keisuke Iida and Masayuki Tera are grateful for a JSPS Research Fellowship for Young Scientists and a grant under the education program "Human Resource Development Program for Scientific Powerhouse" provided through Tokyo University of Agriculture & Technology.

Endnotes

1. Telomeric antiparallel intramolecular G-quadruplexes have characteristic CD spectra consisting of a positive peak at 290 nm and a negative peak at 260 nm [28, 40].

2. A similar conformational change was observed for 6OTD dimer **1** by using CD spectroscopic analysis of a solution of 10 μM of telo24 in the presence of potassium chloride (100 mM) and Tris-HCl buffer (50 mM, pH 7.0) as shown in Figure 6 (solid line: telo24 + KCl, dashed line: telo24 + KCl + dimer **1**).

3. The 6OTD dimer **1** also interacts with telo24 by forming 1 : 1 complex based on ESI-MASS analysis [33].

4. Under the same measurement conditions, the ΔT_m values in the presence of 1 μM **1** are 12°C (Flu-telo21) and 0°C (Flu-ds26), respectively.

References

[1] D. J. Patel, A. T. Phan, and V. Kuryavyi, "Human telomere, oncogenic promoter and 5′-UTR G-quadruplexes: diverse higher order DNA and RNA targets for cancer therapeutics," *Nucleic Acids Research*, vol. 35, no. 22, pp. 7429–7455, 2007.

[2] S. Neidle and G. N. Parkinson, "Quadruplex DNA crystal structures and drug design," *Biochimie*, vol. 90, no. 8, pp. 1184–1196, 2008.

[3] A. T. Phan, "Human telomeric G-quadruplex: structures of DNA and RNA sequences," *FEBS Journal*, vol. 277, no. 5, pp. 1107–1117, 2010.

[4] Y. Wang and D. J. Patel, "Solution structure of the human telomeric repeat d[AG3(T2AG3)3] G-tetraplex," *Structure*, vol. 1, no. 4, pp. 263–282, 1993.

[5] Y. Xu, Y. Noguchi, and H. Sugiyama, "The new models of the human telomere d[AGGG(TTAGGG)3] in K^+ solution," *Bioorganic and Medicinal Chemistry*, vol. 14, no. 16, pp. 5584–5591, 2006.

[6] J. Dai, C. Punchihewa, A. Ambrus, D. Chen, R. A. Jones, and D. Yang, "Structure of the intramolecular human telomeric G-quadruplex in potassium solution: a novel adenine triple formation," *Nucleic Acids Research*, vol. 35, no. 7, pp. 2440–2450, 2007.

[7] A. T. Phan, V. Kuryavyi, K. N. Luu, and D. J. Patel, "Structure of two intramolecular G-quadruplexes formed by natural human telomere sequences in K^+ solution," *Nucleic Acids Research*, vol. 35, no. 19, pp. 6517–6525, 2007.

[8] G. N. Parkinson, M. P. H. Lee, and S. Neidle, "Crystal structure of parallel quadruplexes from human telomeric DNA," *Nature*, vol. 417, no. 6891, pp. 876–880, 2002.

[9] T. Simonsson, P. Pecinka, and M. Kubista, "DNA tetraplex formation in the control region of c-myc," *Nucleic Acids Research*, vol. 26, no. 5, pp. 1167–1172, 1998.

[10] S. Rankin, A. P. Reszka, J. Huppert, et al., "Putative DNA quadruplex formation within the human c-kit oncogene," *Journal of the American Chemical Society*, vol. 127, no. 30, pp. 10584–10589, 2005.

[11] J. Dai, T. S. Dexheimer, D. Chen, et al., "An intramolecular G-quadruplex structure with mixed parallel/antiparallel G-strands formed in the human BCL-2 promoter region in solution," *Journal of the American Chemical Society*, vol. 128, no. 4, pp. 1096–1098, 2006.

[12] S. Cogoi and L. E. Xodo, "G-quadruplex formation within the promoter of the KRAS proto-oncogene and its effect on transcription," *Nucleic Acids Research*, vol. 34, no. 9, pp. 2536–2549, 2006.

[13] S. Neidle, "Human telomeric G-quadruplex: the current status of telomeric G-quadruplexes as therapeutic targets in human cancer," *FEBS Journal*, vol. 277, no. 5, pp. 1118–1125, 2010.

[14] T.-M. Ou, Y.-J. Lu, J.-H. Tan, Z.-S. Huang, K.-Y. Wong, and L.-Q. Gu, "G-quadruplexes: targets in anticancer drug design," *ChemMedChem*, vol. 3, no. 5, pp. 690–713, 2008.

[15] J. F. Riou, L. Guittat, P. Mailliet, et al., "Cell senescence and telomere shortening induced by a new series of specific G-quadruplex DNA ligands," *Proceedings of the National Academy of Sciences of the United States of America*, vol. 99, no. 5, pp. 2672–2677, 2002.

[16] M. Bejugam, S. Sewitz, P. S. Shirude, R. Rodriguez, R. Shahid, and S. Balasubramanian, "Trisubstituted isoalloxazines as a new class of G-quadruplex binding ligands: small molecule regulation of c-kit oncogene expression," *Journal of the American Chemical Society*, vol. 129, no. 43, pp. 12926–12927, 2007.

[17] A. Siddiqui-Jain, C. L. Grand, D. J. Bearss, and L. H. Hurley, "Direct evidence for a G-quadruplex in a promoter region and its targeting with a small molecule to repress c-MYC transcription," *Proceedings of the National Academy of Sciences of the United States of America*, vol. 99, no. 18, pp. 11593–11598, 2002.

[18] S. L. Palumbo, R. M. Memmott, D. J. Uribe, Y. Krotova-Khan, L. H. Hurley, and S. W. Ebbinghaus, "A novel G-quadruplex-forming GGA repeat region in the c-myb promoter is a critical regulator of promoter activity," *Nucleic Acids Research*, vol. 36, no. 6, pp. 1755–1769, 2008.

[19] S. Cogoi and L. E. Xodo, "G-quadruplex formation within the promoter of the KRAS proto-oncogene and its effect on transcription," *Nucleic Acids Research*, vol. 34, no. 9, pp. 2536–2549, 2006.

[20] L. Hayflick and P. S. Moorhead, "The serial cultivation of human diploid cell strains," *Experimental Cell Research*, vol. 25, no. 3, pp. 585–621, 1961.

[21] M. A. Blasco, "Telomere length, stem cells and aging," *Nature Chemical Biology*, vol. 3, no. 10, pp. 640–649, 2007.

[22] A. Arora, N. Kumar, T. Agarwal, and S. Maiti, "Retraction: human telomeric G-quadruplex: targeting with small molecules," *FEBS Journal*, vol. 277, no. 5, p. 1345, 2010.

[23] K. Shin-ya, K. Wierzba, K. Matsuo, et al., "Telomestatin, a novel telomerase inhibitor from Streptomyces anulatus," *Journal of the American Chemical Society*, vol. 123, no. 6, pp. 1262–1263, 2001.

[24] T. Doi, M. Yoshida, K. Shin-ya, and T. Takahashi, "Total synthesis of (R)-telomestatin," *Organic Letters*, vol. 8, no. 18, pp. 4165–4167, 2006.

[25] P. S. Shirude, E. R. Gillies, S. Ladame, et al., "Macrocyclic and helical oligoamides as a new class of G-quadruplex ligands," *Journal of the American Chemical Society*, vol. 129, no. 39, pp. 11890–11891, 2007.

[26] M.-Y. Kim, H. Vankayalapati, K. Shin-ya, K. Wierzba, and L. H. Hurley, "Telomestatin, a potent telomerase inhibitor that interacts quite specifically with the human telomeric intramolecular G-quadruplex," *Journal of the American Chemical Society*, vol. 124, no. 10, pp. 2098–2099, 2002.

[27] F. Rosu, V. Gabelica, K. Shin-ya, and E. D. Pauw, "Telomestatin-induced stabilization of the human telomeric DNA quadruplex monitored by electrospray mass

spectrometry," *Chemical Communications*, vol. 9, no. 21, pp. 2702–2703, 2003.

[28] E. M. Rezler, J. Seenisamy, S. Bashyam, et al., "Telomestatin and diseleno sapphyrin bind selectively to two different forms of the human telomeric G-quadruplex structure," *Journal of the American Chemical Society*, vol. 127, no. 26, pp. 9439–9447, 2005.

[29] M. Tera, Y. Sohtome, H. Ishizuka, et al., "Design and synthesis of telomestatin derivatives and their inhibitory activity of telomerase," *Heterocycles*, vol. 69, no. 1, pp. 505–514, 2006.

[30] M. Tera, H. Ishizuka, M. Takagi, M. Suganuma, K. Shin-ya, and K. Nagasawa, "Macrocyclic hexaoxazoles as sequence- and mode-selective G-quadruplex binders," *Angewandte Chemie: International Edition*, vol. 47, no. 30, pp. 5557–5560, 2008.

[31] M. Tera, K. Iida, H. Ishizuka, et al., "Synthesis of a potent G-quadruplex-binding macrocyclic heptaoxazole," *ChemBioChem*, vol. 10, no. 3, pp. 431–435, 2009.

[32] G. S. Minhas, D. S. Pilch, J. E. Kerrigan, E. J. LaVoie, and J. E. Rice, "Synthesis and G-quadruplex stabilizing properties of a series of oxazole-containing macrocycles," *Bioorganic and Medicinal Chemistry Letters*, vol. 16, no. 15, pp. 3891–3895, 2006.

[33] K. Iida, M. Tera, T. Hirokawa, K. Shin-ya, and K. Nagasawa, "G-quadruplex recognition by macrocyclic hexaoxazole (6OTD) dimer: greater selectivity than monomer," *Chemical Communications*, no. 42, pp. 6481–6483, 2009.

[34] A. De Cian, L. Guittat, M. Kaiser, et al., "Fluorescence-based melting assays for studying quadruplex ligands," *Methods*, vol. 42, no. 2, pp. 183–195, 2007.

[35] J.-L. Mergny and J.-C. Maurizot, "Fluorescence resonance energy transfer as a probe for G-quartet formation by a telomeric repeat," *ChemBioChem*, vol. 2, no. 2, pp. 124–132, 2001.

[36] J. Deeley, A. Bertram, and G. Pattenden, "Novel polyoxazole-based cyclopeptides from Streptomyces sp. Total synthesis of the cyclopeptide YM-216391 and synthetic studies towards telomestatin," *Organic and Biomolecular Chemistry*, vol. 6, no. 11, pp. 1994–2010, 2008.

[37] D. Hernandez, G. Vilar, E. Riego, et al., "Synthesis of IB-01211, a cyclic peptide containing 2,4-concatenated thia- and oxazoles, via Hantzsch macrocyclization," *Organic Letters*, vol. 9, no. 5, pp. 809–811, 2007.

[38] D. Hernandez, M. Altuna, C. Cuevas, R. Aligu, F. Albericio, and M. Alvarez, "Synthesis and antitumor activity of mechercharmycin A analogues," *Journal of Medicinal Chemistry*, vol. 51, no. 18, pp. 5722–5730, 2008.

[39] M. Kunishima, C. Kawachi, F. Iwasaki, K. Terao, and S. Tani, "Synthesis and characterization of 4-(4,6-dimethoxy-1,3,5-triazin-2-yl)- 4-methylmorpholinium chloride," *Tetrahedron Letters*, vol. 40, no. 29, pp. 5327–5330, 1999.

[40] P. Balagurumoorthy and S. K. Brahmachari, "Structure and stability of human telomeric sequence," *Journal of Biological Chemistry*, vol. 269, no. 34, pp. 21858–21869, 1994.

[41] F. Rosu, V. Gabelica, C. Houssier, P. Colson, and E. D. Pauw, "Triplex and quadruplex DNA structures studied by electrospray mass spectrometry," *Rapid Communications in Mass Spectrometry*, vol. 16, no. 18, pp. 1729–1736, 2002.

[42] H. Li, Y. Liu, S. Lin, and G. Yuan, "Spectroscopy probing of the formation, recognition, and conversion of a G-quadruplex in the promoter region of the bcl-2 oncogene," *Chemistry European Journal*, vol. 15, no. 10, pp. 2445–2452, 2009.

SAGE-Hindawi Access to Research
Journal of Nucleic Acids
Volume 2010, Article ID 489060, 10 pages
doi:10.4061/2010/489060

Research Article

Synthesis and G-Quadruplex-Binding Properties of Defined Acridine Oligomers

Rubén Ferreira,[1] Anna Aviñó,[1] Ricardo Pérez-Tomás,[2] Raimundo Gargallo,[3] and Ramon Eritja[1]

[1] *Institute for Research in Biomedicine, IQAC-CSIC, CIBER-BBN Networking Centre on Bioengineering, Biomaterials and Nanomedicine, Edifici Helix, Baldiri Reixac 15, 08028 Barcelona, Spain*
[2] *Cancer Cell Biology Research Group, Department of Pathology and Experimental Therapeutics, Faculty of Medicine, University of Barcelona Campus Bellvitge, Feixa Llarga, L'Hospitalet de Llobregat, 08907 Barcelona, Spain*
[3] *Department of Analytical Chemistry, University of Barcelona, Diagonal 647, 08028 Barcelona, Spain*

Correspondence should be addressed to Ramon Eritja, recgma@cid.csic.es

Received 14 January 2010; Revised 22 March 2010; Accepted 13 April 2010

Academic Editor: Daniela Montesarchio

The synthesis of oligomers containing two or three acridine units linked through 2-aminoethylglycine using solid-phase methodology is described. Subsequent studies on cell viability showed that these compounds are not cytotoxic. Binding to several DNA structures was studied by competitive dialysis, which showed a clear affinity for DNA sequences that form G-quadruplexes and parallel triplexes. The fluorescence spectra of acridine oligomers were affected strongly upon binding to DNA. These spectral changes were used to calculate the binding constants (K). Log K were found to be in the order of 4–6.

1. Introduction

Small organic molecules with specific interactions with DNA have become antitumor, antiviral, and antibiotic drugs [1, 2]. Duplex DNA-binding drugs interact in two main ways, through groove binding and through intercalation. Medicinal chemistry has made a considerable effort in searching for and testing of a large number of drugs with increased selectivity to a range of DNA sequences or structures. More recently, some of this interest has moved to the search of new ligands for G-quadruplexes [3]. This structure motif is formed by the planar association of four guanines in a cyclic Hoogsteen hydrogen bonding tetrad.

Guanine-rich sequences form G-quadruplex structures and have been found in telomeres [4] and in transcriptional regulatory regions of critical oncogenes such as *c-myc* and *c-kit* [5, 6]. Ligands that selectively bind and stabilize these structures have become anticancer drugs of interest [7].

The G-quadruplex stabilization occurs in most cases by π-π stacking and electrostatic interaction. G-quadruplex ligands are normally planar aromatic molecules that are prone to stacking with G-tetrads. Some of them are also positively charged or have hydrophilic groups to favor electrostatic interaction [8].

Although there is a long way to go in the development of potent drugs that target G-quadruplexes, some promising lead compounds have been achieved [9]. Several ligand structures have been studied, such as anthraquinones, cationic porphyrins, perylene derivatives, and a large number of compounds [9]. Among the acridine compounds, 3,6,9-trisubstituted acridines have inhibitory activity in the nanomolar range and they have entered preclinical studies [8, 10, 11].

In previous studies we described the preparation of sequence specific oligomers of DNA-intercalating drugs using protocols based on solid-phase synthesis in an attempt to facilitate the preparation of compounds with improved DNA-binding selectivity [12, 13]. It has been proposed that bis- and tris-intercalating drugs show promising activity and selectivity [14, 15]. Here we described solid-phase synthesis protocols for the preparation of several acridine oligomers linked through 2-aminoethylglycine units as well as their DNA-binding properties. Although the acridine derivatives described in this study are not cytotoxic, they show a clear

Table 1: Sequences of oligonucleotides.

No.	Name	Sequence (5′–3′)
1	T20	TTT TTT TTT TTT TTT TTT TT
2	24bclc	CCC GCC CCC TTC CTC CCG CGC CCG
3	Dickerson	CGC GAA TTC GCG
4	Ds26	CAA TCG GAT CGA ATT CGA TCC GAT TG
5	GA triplex	GAA AGA GAG GAG GCC TTT TTG GAG GAG AGA AAG + CCT CCT CTC TTT C
6	TC triplex	CCT CCT CTC TTT CCC TTT TTC TTT CTC TCC TCC + GAA AGA GAG GAG G
7	TG4T	TGG GGT
8	TBA	GGT TGG TGT GGT TGG
9	HT24	TAG GGT TAG GGT TAG GGT TAG GGT
10	24bcl	CGG GCG CGG GAG GAA GGG GGC GGG
11	cmyc	GGG GAG GGT GGG GAG GGT GGG GAA GGT GGG G

affinity for several DNA G-quadruplex structures, especially those sequences found in the promoter regions of *c-myc* [16] and *bcl*-2 [17, 18] oncogenes.

2. Materials and Methods

2.1. Chemicals. The phosphoramidites and ancillary reagents used during oligonucleotide synthesis were obtained from Applied Biosystems (USA) and Link Technologies Ltd. (Scotland). The rest of the chemicals were purchased from commercial sources. The Slide-A-Lyzer Mini Dialysis Units 3500 MWCO were purchased from Pierce. Acridine-9-carboxylic acid was obtained from Aldrich. 2-(Acridine-9-carboxamide)acetic acid was prepared by reaction of acridine-9-carboxylic acid with glycine methyl ester and subsequent saponification of the methyl ester as described [10]. Boc-(2-aminoethyl)glycine(Fmoc) (Boc-Aeg(Fmoc)-OH) was obtained from Iris Biotech and Fmoc-glycine (Fmoc-Gly-OH) was obtained from Bachem. Boc-6-aminohexyl hemisuccinate was prepared by reaction of Boc-6-aminohexanol with succinic anhydride.

2.2. Oligonucleotide Synthesis. Oligonucleotide sequences (Table 1) were prepared on an automatic Applied Biosystems 3400 DNA synthesizer on 1 μmoL (CPG resin) scale using commercially available 2-cyanoethyl phosphoromidites. After the assembly of the sequences, oligonucleotide-supports were deprotected using 32% aqueous ammonia at 55°C for 16 h. Ammonia solutions were concentrated to dryness and the residue was desalted by a NAP-10 (*Sephadex G-25*) column.

2.3. Solid-Phase Synthesis of Acridine Oligomers. Acridine dimers and trimers (**1–4**, Figure 1) were prepared with the 2-aminoethylglycine scaffold, which allows the growth of a polyamide skeleton on solid-phase and the following incorporation of acridine unit.

The assembly of 2-aminoethylglycine derivatives was carried out on methylbenzhydrylamine (MBHA) polystyrene-1%-divinylbenzene solid support applying an Fmoc/Boc hybrid strategy using Boc-Aeg(Fmoc)-OH, Fmoc-Gly-OH, and acridine-9-carboxylic acid as building blocks (Figure 2).

Fmoc-Sarcosine-OH (5 eq) was coupled to the resin using standard coupling conditions (5 eq. PyBOP and 10 eq. DIEA, 1 h), then the Fmoc group was removed (20% of piperidine in DMF, 30 min), and Boc-6-aminohexyl hemisuccinate (Boc–NH–$(CH_2)_6$–$OCOCH_2CH_2COOH$) was coupled (5 eq R-COOH, 5 eq. PyBOP and 10 eq. DIEA, 1 h) to the support. The residual unreacted amino groups were acetylated with 5 eq. of acetic anhydride and 5 eq. of DIEA.

Next, the Boc group was removed (40% trifluoroacetic acid in dichloromethane) and the 2-aminoethylglycine skeleton was synthesized by repetitive couplings of Boc-Aeg(Fmoc)-OH until reaching the desired dimer or trimer compound. The last Boc group of the sequence was removed and the resulting amino group was acetylated (5 eq. acetic anhydride and 5 eq. DIEA).

Once the aminoethylglycine backbone was built, the Fmoc-protecting groups of the side chains were removed (20% of piperidine in DMF, 30 min), and Fmoc-Gly-OH followed by 9-acridine carboxyl acid was coupled to the support. The progress of the coupling reactions was followed by ninhydrine test and by UV monitoring of the 9-methylene-9H-fluorene released during deprotection, which allowed optimization of the coupling conditions.

The acridine dimer **1** and trimer **3** were obtained by treatment of the appropriate solid supports with HF anhydrous at 0°C. Finally the acridine dimer **2** and trimer **4** were obtained by treatment of dimer **1** and trimer **3** respectively with 32% aqueous ammonia (1 h, 55°C).

Good yields and purities were obtained for the products (around 85% for **1** and **2,** 75% for **3** and **4**). HPLC and MALDI-TOF spectra are shown in Supplementary Material available onlie at doi: 10.4061/2010/489060.

The compounds were analyzed by MALDI-TOF, **1** $[M+Na^+]$ = 1080.3 (expected 1054.2), **2** [M] = 885.2 (expected 884.0), **3** [M] = 1418.9 (expected 1416.5), and **4** [M] = 1247.4 (expected 1246.4). MALDI-TOF spectra were obtained using a *Perseptive* Voyager DETMRP mass spectrometer, equipped with nitrogen laser at 337 nm using a 3 ns pulse. The matrix used contained 2,5-dihydroxybenzoic acid (DHB, 10 mg/mL in water).

Analytical HPLC was performed using XBridge OST C_{18} (*Waters*), 2.5 μm, 4.6 × 50 mm column using a 10-minute

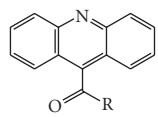

R = OH, acridine-9-carboxylic acid
R = $NHCH_2COOH$, 2-(acridine-9-carboxamide) acetic acid

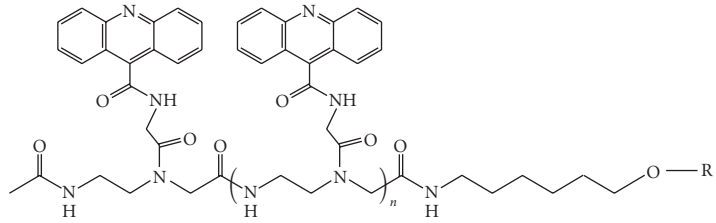

Dimer **1** R = $CO–CH_2CH_2CONH(CH_3)CH_2CONH_2$, $n = 1$
Dimer **2** R = H, $n = 1$
Trimer **3** R = $CO–CH_2CH_2CONH(CH_3)CH_2CONH_2$, $n = 2$
Trimer **4** R = H, $n = 2$

Figure 1: Structure of the acridine derivatives prepared.

linear gradient from 9% to 45% B, flow rate 1 mL/min; solution A was 5% ACN in 0,1 M aqueous TEAA, and B 70% ACN in 0.1M aqueous TEAA. HPLC chromatograms and MS spectra can be found in Supplementary Material.

Fluorescence spectra were recorded using a Jasco FP-6200 spectrofluorometer equipped with a Peltier temperature controller, $\lambda_{em} = 435$ nm ($\lambda_{exc} = 252$ nm).

UV spectra were recorded using a Jasco spectrophotometer V-650, $\lambda_{max} = 252$ nm, 360 nm.

2.4. Cell Viability Assays. The *in vitro* cytotoxicity of the compounds (Figure 1) was evaluated by colorimetric assays with tetrazole salts (MTT) on Jurkat clone E6-1 (human leukemia), GLC-4 clone (human lung carcinoma) cell lines, and one mouse fibroblast cell line (NIHT-3T3).

GLC4 and Jurkat cell lines were cultured in RPMI and NIH3T3 in DMEM and supplemented with 10% fetal calf serum, 10000 u/mL penicillin, 10 μg/mL streptomycin and 200 mM L-glutamine. Cells were grown in a humidified atmosphere of air containing 5% CO_2 at 37°. Cells were plated in triplicate wells ($1.5 \cdot 10^4$ cells well) in 100 μL of growth medium in 96-well plates and proliferate for 24 h and then treated with increasing concentrations of acridine oligomers. After 72 h of incubation, 10 μM of MTT (5 mg/mL in Phosphate buffer saline 10%) was added for an additional 4 h. The absorbance at 570 nm was measured on a multiwell plate reader after addition of 100 μl of isopropanol : 1N HCl (24 : 1). Cell viability was expressed as a percentage of control and IC_{50} was determined as the concentration of drug that produced a 50% reduction of absorbance at 570 nm.

2.5. Competitive Dialysis Assays. 100 μL of a 50 μM oligonucleotide (Table 1) in potassium phosphate buffer (185 mM NaCl, 185 mM KCl, 2 mM NaH_2PO4, 1 mM Na_2EDTA, 6 mM Na_2HPO_4 at pH 7) was introduced into a separated dialysis unit. A blank sample containing only buffer without oligonucleotide was also prepared. All 12 dialysis units were then placed in the beaker containing the 1 μM solution of the appropriate acridine derivative. The samples were allowed to equilibrate with continuous stirring at room temperature overnight. After the equilibration period, DNA samples were removed to an Eppendorf tube. SDS is usually added to denature the DNA sample and release the acridine oligomer, but in our case the presence of K^+ ions induced the formation of a white precipitate, which interfered with the measurement of the fluorescence spectra of the samples.

In order to measure the compound retained in the dialysis unit, samples were treated with snake-venom phosphodiesterase to degrade the DNA and release the acridine oligomer. 350 μL of potassium phosphate buffer (without EDTA), buffer at pH 8.5, 50 μL of 100 mM $MgCl_2$, and 1 μm of snake venom phosphodiesterase solution were added for an additional overnight incubation at 37°C. Finally, the fluorescence of each sample was measured (λ_{ex} and λ_{em} were set to 252 and 435 nm, resp.).

2.6. Fluorescence Assays. The study of the interaction equilibrium of acridine derivatives and oligonucleotides consists of recording the fluorescence spectra of a 0.2 μM solution of the acridine derivative after the addition of increasing amounts of oligonucleotide (from 0 to 10 μM) in potassium phosphate buffer (185 mM NaCl, 185 mM KCl, sodium phosphate, 1 mM EDTA, pH 7). These experiments were carried out by adding small volumes of an oligonucleotide stock solution to the 0.2 μM solution of the acridine derivative. After 24 h the emission spectra of the resulting solutions were recorded from 300 to 500 nm at 252 nm excitation wavelength at 25°C.

The macroscopic binding constant (K) corresponding to the reaction

$$\text{DNA} + \text{ligand} \rightleftarrows \text{Interaction complex} \quad (1)$$

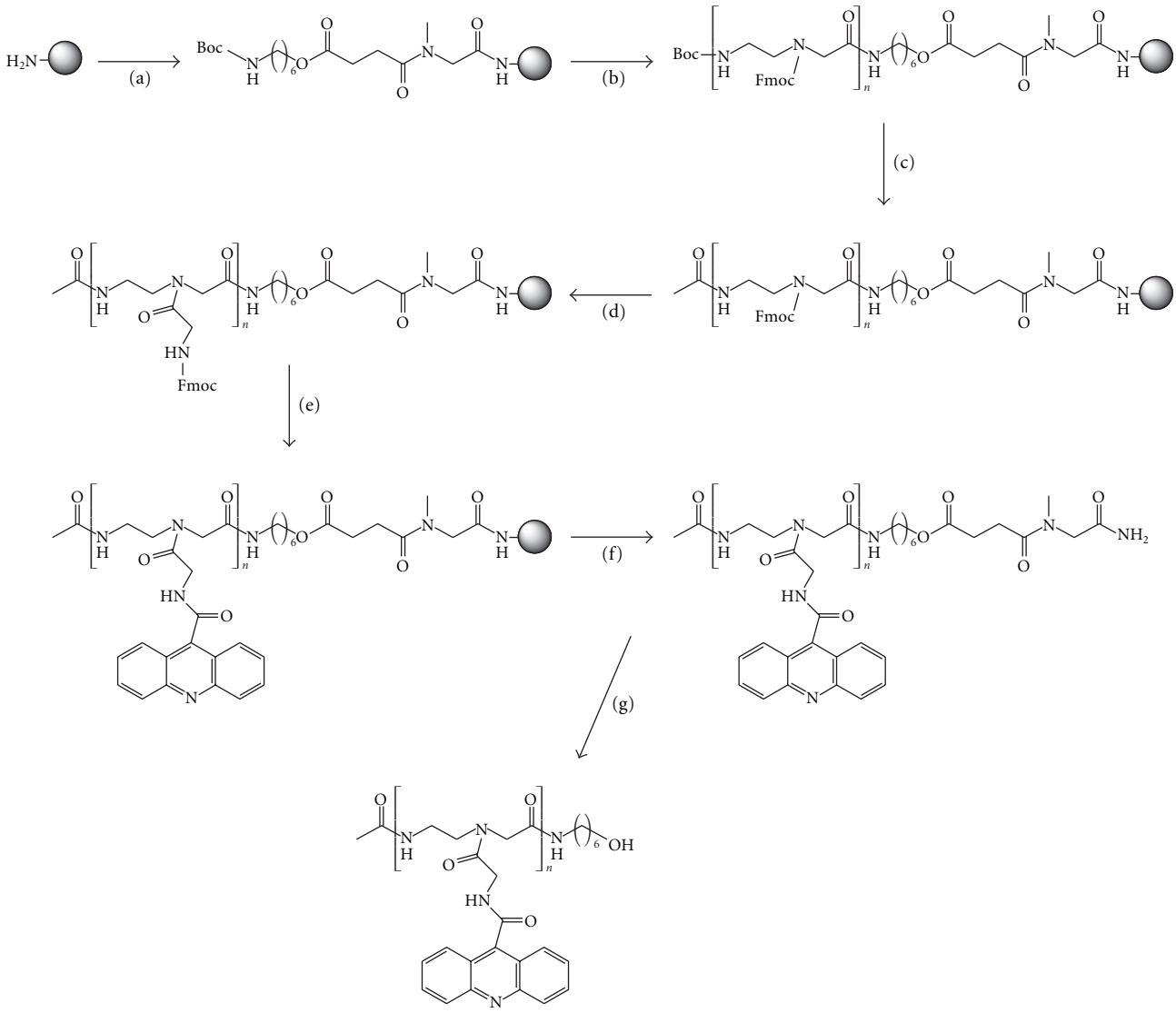

Figure 2: Solid-phase synthesis of dimer and trimer acridine derivatives. (a) (i) Fmoc-Sar-OH, PyBOP, DIEA; (ii) 20% piperidine, DMF; (iii) Boc–NH–$(CH_2)_6$–OCH_2CH_2COOH, PyBOP, DIEA; (b) (i) 40% TFA, DCM; (ii) Fmoc-Aeg(Boc)-OH, PyBOP, DIEA; (iii) Repeat steps (i) and (ii) n times; (c) (i) 40% TFA, DCM; (ii) Ac_2O, DIEA, DMF; (d) (i) 20% piperidine, DMF; (ii) Fmoc-Gly-OH, PyBOP, DIEA; (e) (i) 20% piperidine, DMF; (ii) acridine-9-carboxylic acid, PyBOP, DIEA; (f) anhydrous HF (0°); (g) 32% aqueous NH_3.

was calculated from the multivariate analysis of fluorescence data recorded in the range 300–390 nm using the hard-modeling program Equispec [19]. This program performs a nonlinear least squares optimization of K and of the pure fluorescence spectra corresponding to each of the species considered (DNA, ligand, and interaction complex). A 1 : 1 stoichiometry DNA : ligand for the interaction complex was assumed. The logarithms of the binding constants calculated are given as their weighted means with twice their standard errors (units of the least significant digit). Results are shown in Table 2.

2.7. Circular Dichroism. An increasing amount of **1** (from 0 to 8 μM) in potassium phosphate buffer (185 mM NaCl, 185 mM KCl, sodium phosphate, 1 mM EDTA, pH 7) was added to a 1 μM solution of the oligonucleotide. The CD spectra were recorded after 24 h on a Jasco J-810 spectropolarimeter attached to a Julabo F/25HD circulating water bath in 1 cm path-length quartz cylindrical cells, using a 50 nm/min scan rate, a spectral band width of 1 nm, and a time constant of 4 s. All the spectra were corrected with the buffer blank, normalized to facilitate comparisons and noise-reduced using Matlab software. CD spectra are shown as supplementary data.

3. Results and Discussion

3.1. Synthesis of Acridine Oligomers. The synthesis of acridine dimer and trimers has been described previously [13] using a Boc-(2-aminoethyl)glycine derivative carrying the

Table 2: Logarithm of the binding constants (log K) calculated from data recorded throughout fluorescence titrations using Equispec program assuming a 1 : 1 stoichiometry DNA : ligand for the interaction complex (details in materials and methods). Compounds 1–4 correspond to the acridine dimers and trimers prepared in this study. HT24, 24bcl, cmyc, and Dickerson correspond to oligonucleotide sequences shown in Table 1.

	1	**2**	**3**	**4**
HT24	4.9 ± 0.4	4.6 ± 0.5	5.3 ± 0.3	n.d.
24bcl	6.8 ± 0.5	5.1 ± 0.1	5.3 ± 0.2	n.d.
cmyc	5.5 ± 0.3	4.9 ± 0.2	4.8 ± 0.5	5.3 ± 0.2
Dickerson	n.d.	n.d.	n.d.	n.d.

n.d. not determined.

2-(acridine-9-carboxamide)acetyl residue. The synthesis of this monomer was long and yields were low.

An alternative method developed is to first assemble the Boc-(2-aminoethyl)glycine backbone on solid-phase, and then the intercalating agent is added. This strategy is more convenient for rapid synthesis, as it is unnecessary to construct each intercalating monomer.

Thus, acridine oligomers were assembled using the methylbenzhydrylamine (MBHA) resin by applying an Fmoc/Boc hybrid strategy and using Boc-(2-aminoethyl)-(Fmoc)glycine [Boc-Aeg(Fmoc)-OH] as building block (Figure 2). The Boc group was used to protect the aminoethyl group of each unit, which thus facilitated elongation of the backbone. Fmoc was the semipermanent protecting group for the amino group of glycine through which the intercalating compound was introduced. The succinyl linker was selected to connect the solid support and the oligomer. This linker is used in oligonucleotide synthesis and it is labile to ammonia. Unfortunately, the linker is not compatible with Fmoc chemistry. It has been described that an intramolecular side reaction can lead to premature loss of the oligomers during the base treatment used to remove the Fmoc group [20]. Thus, N-methylglycine (sarcosine) was incorporated between the amino-support and the succinyl linker. The presence of the N-methyl group prevents the potential side reaction [20]. 6-Aminohexanol was used to connect the succinyl linker and the oligomer backbone, as described for the synthesis of peptide nucleic acid (PNA) oligomers [21].

The (2-aminoethyl)glycine backbone was assembled by consecutive additions of Boc-Aeg(Fmoc)-OH to obtain the dimer and trimer sequence. Acetylation of the N-terminal position was carried out using acetic anhydride and a base.

Next, the removal of the Fmoc group allowed the addition of a Fmoc-glycine unit as a spacer, which was followed by the addition of acridine-9-carboxylic acid. The acridine dimer and trimer were synthesized in this way (Figure 2).

After assembly of the oligomers, the resulting supports were treated with ammonia. The desired oligomers were not released from the support even after prolonged time and high temperatures. We therefore treated the supports with anhydrous HF to yield the acridine oligomers **1** and **3**, which contain the sarcosyl succinyl linker. At this point HPLC spectra showed a major peak that had the expected molecular weight for the oligomers **1** and **3** carrying the sarcosyl succinyl linker (see supplementary data). This observation indicates that the simultaneous incorporation of all acridines proceeded with excellent yields. Ammonia treatment of acridines **1** and **3** in solution now yielded the desired acridine dimer **2** and trimer **4** in excellent yields and purity (see supplementary data). Compounds **1–4** were fully characterized and their properties were analyzed.

The pKa of the acridine ring of acridine-9-carboxylic acid and 2-(acridine-9-carboxamide)acetic acid was measured by UV titration. pKa of acridine-9-carboxylic acid was 5.5 ± 0.1 and 2-(acridine-9-carboxamide)acetic acid 4.1 ± 0.2. We therefore estimated that the acridine rings of compounds **1–4** are mainly unprotonated at pH 7.0.

3.2. Cell Viability Assay. The *in vitro* cytotoxicity of the compounds was evaluated by colorimetric assays with tetrazole salts (MTT). This assay is based on the capacity of living cells to incorporate and reduce MTT. This reaction can be followed by the change of absorbance of the reduced and oxidized forms. This reaction is done by the action of the mitochondrial enzyme succinatehydrogenase, which is active only in living cells. The intensity of color is directly correlated with the number of living cells in the sample. No cytotoxicity activity was observed in compounds **1–4** at concentrations up to 50 μM.

3.3. Competitive Dialysis Studies. In order to evaluate the selectivity of the compounds for DNA structures, a competitive dialysis experiment was performed using 11 oligonucleotides (Table 1) representing several nucleic acid structures [22]. The more acridine accumulated in the dialysis unit indicates a higher binding affinity to the oligonucleotide present in the dialysis unit. As model for single stranded structures we used T_{20} and the C-rich complementary strand of *bcl-2* (24bclc). This last oligonucleotide folds in an *i*-form quadruplex structure at acidic pH but has no structure in the conditions used in the dialysis (pH 7) [18]. As duplexes we used the self-complementary sequences *Dickerson-Drew* dodecamer (Dickerson) and a 26 mer (ds26). A parallel triplex (TC triplex) and an antiparallel triplex (GA triplex) were also prepared by mixing a hairpin Watson-Crick sequence and the corresponding triplex-forming sequence. Finally, the following G-quadruplex sequences were prepared: the tetramolecular parallel G-quadruplex TG_4T [23], the antiparallel thrombin-binding aptamer (TBA) [24], the human telomere sequence (HT24) [25], and the promoter sequences of *c-myc* (cmyc) [16] and *bcl*-2 (24bcl) [17, 18].

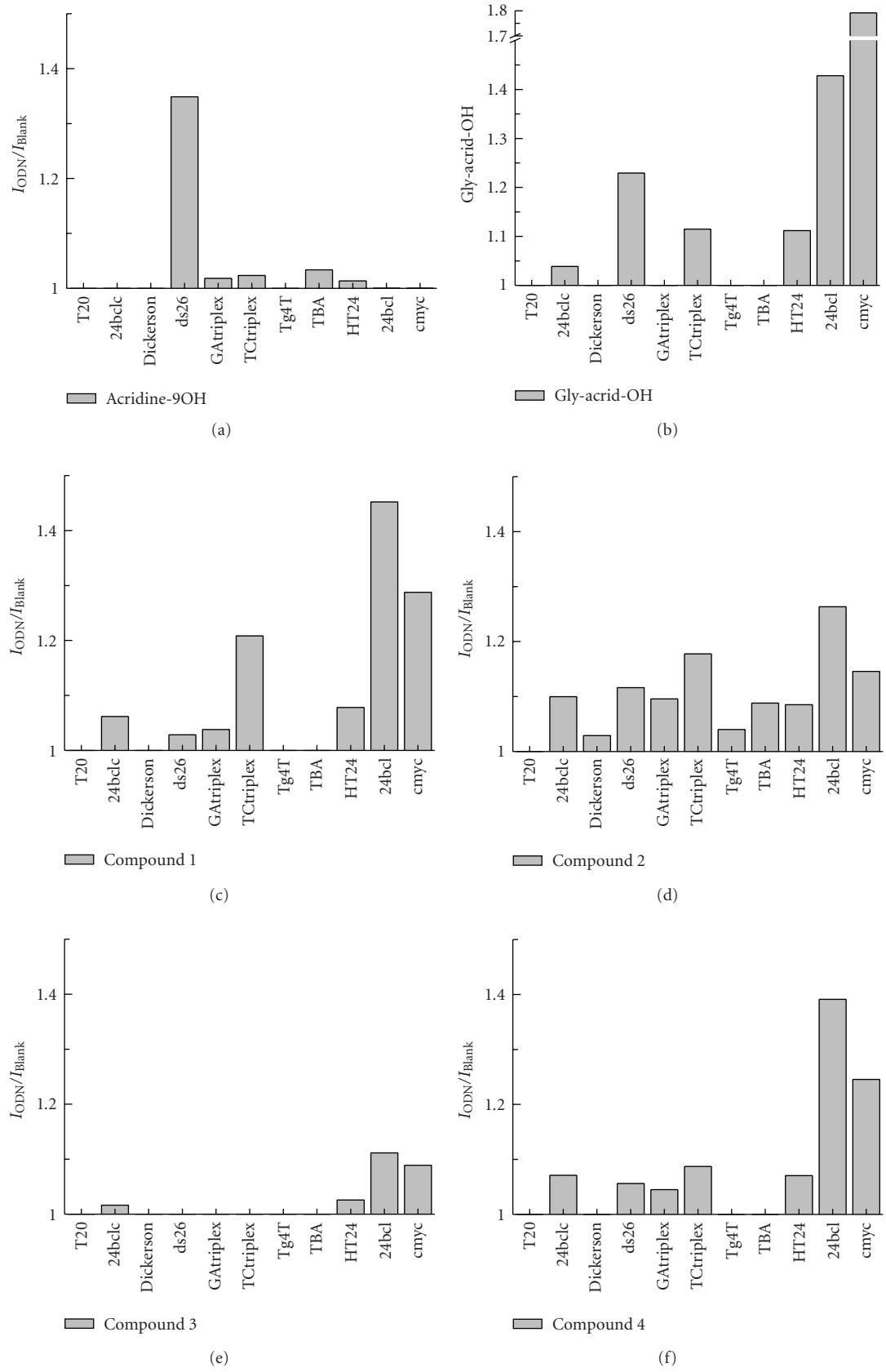

Figure 3: Results obtained by the competitive dialysis assay. The amount of ligand bound to each DNA structure is shown as a bar graph. The fluorescence of each sample was measured using an excitation wavelength of 252 nm and an emission wavelength of 435 nm, respectively.

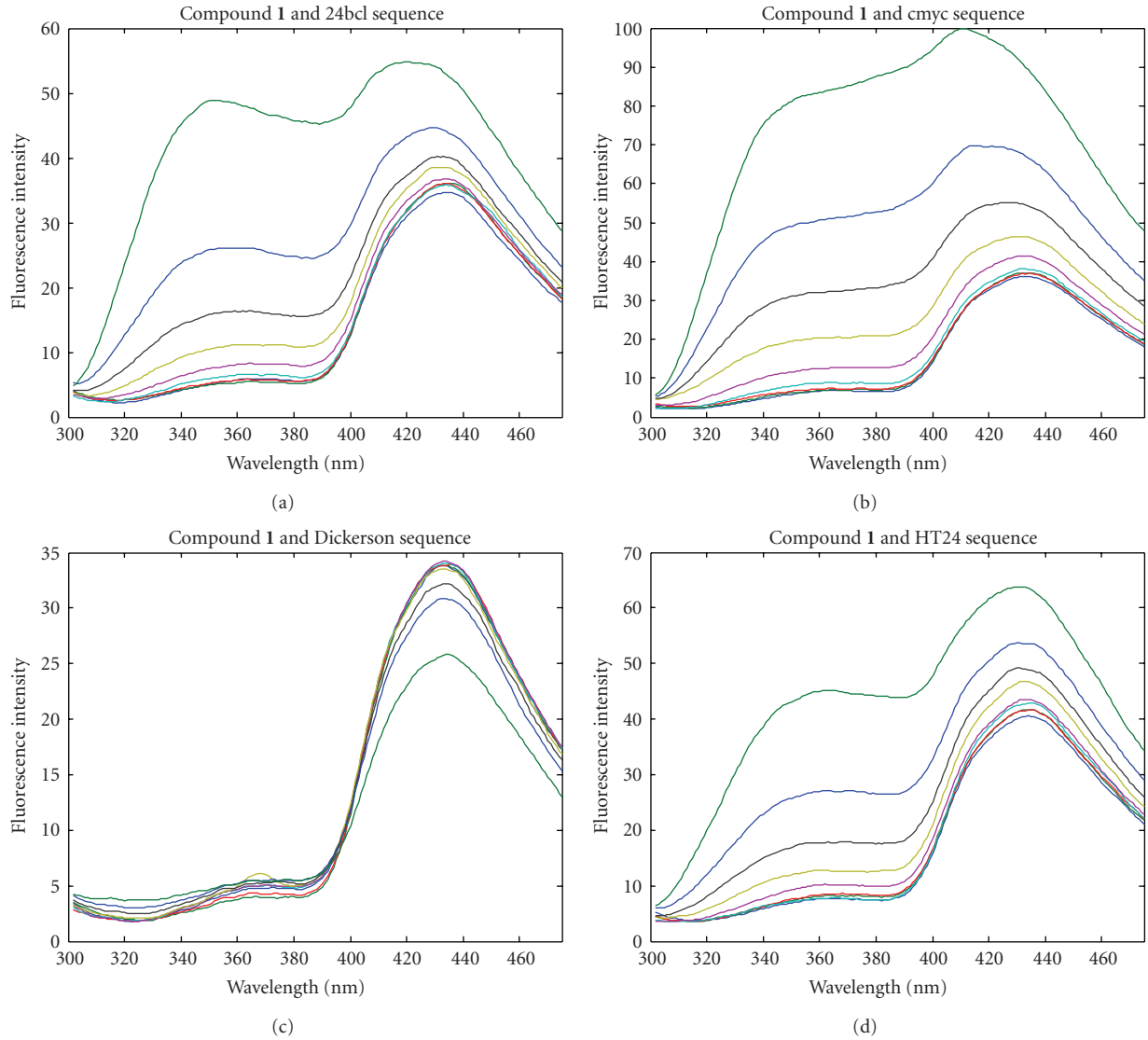

Figure 4: Fluorescence titration spectra. Fluorescence spectra of a 0.2 μM solution of the acridine derivative after the addition of increasing amounts of oligonucleotide (from 0 to 10 μM) in potassium phosphate buffer. Excitation wavelength is 252 nm.

We used the protocol described by Ren and Chaires [26] with a few modifications. The buffer solution was similar to that described in [26] but K^+ was included (185 mM) to ensure the formation of the most stable G-quadruplex structures. At the end of the dialysis experiment, the amount of acridine derivative bound to the DNA was analyzed by fluorescence measurement of the acridine compound. After dialysis, we observed that the spectra of the acridine derivatives of some samples (especially those from G-quadruplexes) differed greatly from the fluorescence spectra of the initial compounds. This difference is attributed to the interaction of the acridine derivatives with the G-quadruplex. In order to release the acridine oligomer, the addition of SDS is recommended [26, 27]. Using SDS, the presence of K^+ ions resulted in the formation of a white precipitate with SDS which did not allow the measurements of the fluorescence spectra [27]. In order to solve this problem, the oligonucleotide was digested with snake venom phosphodiesterase at the end of the dialysis experiment. Thus, the fluorescence spectra of the acridine derivatives were recorded with high accuracy without the interference of DNA and without the use of SDS.

We measured the binding preferences of compounds **1–4** and the acridine monomers acridine-9-carboxylic acid and 2-(acridine-9-carboxamide)acetic acid (Figure 1). Acridine-9-carboxylic acid showed affinity only for duplex ds26 (Figure 3). Unexpectedly, the addition of the glycine residue, used as spacer, induced a change in the affinity. 2-(Acridine-9-carboxamide)acetic acid showed the highest affinity for the G-quadruplex sequences cmyc and 24bcl and less affinity for duplex ds26.

Dimer **1** (dimer with the sarcosylsuccinyl linker) has a similar profile as 2-(acridine-9-carboxamide)acetic acid. In this case, the G-quadruplex 24bcl is preferred to the cmyc

sequence. Some affinity for the TC triplex is observed but no affinity for duplex ds26. Surprisingly, dimer **2** (without the sarcosylsuccinyl linker) lost most of the selectivity although some residual higher affinity for G-quadruplex 24bcl was observed.

In contrast, trimer **3** (trimer with the sarcosylsuccinyl linker) presented lower binding affinity than the other compounds. However, trimer **4** (without the sarcosylsuccinyl linker) recovered most of the affinity for 24bcl and cmyc showing a similar profile to that observed for dimer **1**.

3.4. Measurement of G-Quadruplex-Affinity Constants by Fluorescence Spectroscopy. Dialysis experiments suggest that some of the acridine derivatives prepared have special affinity for 24bcl and cmyc G-quadruplexes. In order to confirm this observation, binding constants were estimated using mole-ratio experiments monitored with fluorescence spectroscopy. Hence, increasing amounts of oligonucleotides 24bcl, HT24, cmyc, and Dickerson were added to a solution with a fixed concentration of the acridine derivatives, and the fluorescence spectra were recorded at excitation wavelengths 252 and 360 nm.

At both wavelengths, changes in the fluorescence spectra upon the addition of oligonucleotides were observed. Figure 4 shows the changes in the fluorescence spectra of acridine dimer **1** at excitation wavelengths 252 nm when oligonucleotides 24bcl, HT24, cmyc, and Dickerson were added. A dramatic increase in fluorescence intensity was observed around 360 nm upon addition of G-quadruplex DNA sequences (24bcl, HT24, and cmyc). The greatest changes were seen with 24bcl and cmyc. Similar results were found with compounds **2**, **3**, and **4** as well as 2-(acridine-9-carboxamide)acetic acid (see supplementary data). Interestingly, when the Dickerson dodecamer was added, no changes in the fluorescence spectra were detected. The progressive modification of the fluorescence spectrum of these compounds reflects their interaction with the G-quadruplex.

Fluorescence data obtained at an excitation wavelength of 252 nm were analyzed with the hard-modelling EQUISPEC program in order to calculate the corresponding binding constants (Table 2). The values of the logarithm of the binding constant ($\log K$) obtained lie in the range 4–6, suggesting a weak interaction with DNA. Of all the compounds, dimer **1** showed the highest binding constants, thereby suggesting a stronger interaction with DNA than the other compounds studied. However these values were slightly lower than the binding constants calculated for other similar ligands, such as the acridine monomers BRACO-19 ($\log K = 7.4$) and BSU6048 ($\log K = 6.5$) [28] or a hemicyanine-peptide ligand ($\log K = 7.1$ [29]), when interacting with human telomere quadruplex.

Changes in the fluorescence spectra at an excitation wavelength of 360 nm were also recorded. Fluorescent emission at this wavelength 360 nm was much lower than that recorded at 252 nm; so the fluorescent signal was low. Upon addition of the oligonucleotide to a solution of compounds **1–4**, the formation of a new maximum at 442 nm was observed (see supplementary data). Although the fluorescent intensity was low, we could estimate the binding constant of the stronger interactions of compound **1** with 24bcl (7.2 ± 0.4) and cmyc (5.5 ± 0.2) sequences (see supplementary data). These values are in agreement with those recorded at an excitation wavelength of 252 nm (Table 1).

Finally, CD spectra of the DNA : ligand mixtures showed no significant differences in relation to those of DNA (see supplementary data). This observation suggests that the DNA G-quadruplex structure is not altered significantly upon binding of the acridine derivatives.

4. Conclusions

In summary, here we have described a new optimized protocol for the synthesis of acridine oligomers with a (2-aminoethyl)glycine backbone. In this method, the Boc-(2-aminoethyl)glycine backbone is first assembled on solid-phase, and then the intercalating agent is assembled on the backbone. This strategy is faster and more efficient than the one described previously [13] and yields the desired oligomers with good yields. A succinyl linker was used to connect the oligomers to the solid support. The succinyl linker attached to sarcosine was unexpectedly too stable and oligomers could not be directly released from the support by a single ammonia treatment. Instead a two-step protocol was used obtaining the desired compounds and an intermediate oligomer carrying a long succinyl sarcosine chain at the C-terminal position.

Competitive dialysis experiments have shown differences on the affinity of acridine oligomers to G-quadruplexes. Higher affinities are found in G-quadruplex sequences present on the promoter regions of *c-myc* and *bcl*-2 oncogenes. This affinity is modulated by the number of acridines and the presence of the succinyl sarcosine chain at the C-terminal position, dimer **1** and trimer **4** being the more relevant compounds for G-quadruplex binding. The monomer 2-(acridine-9-carboxamide)acetic acid also shows binding properties of interest and it is the simplest compound to be prepared. Unfortunately, the compounds synthesized in this study did not have antiproliferative activity in spite of their affinity to quadruplex. This observation contrasts with other reported quadruplex-binding acridine derivatives, such as BRACO-19 [11, 30] which shows anticancer activity. The lower affinity to telomere G-quadruplex sequence and the larger size of the acridine derivatives described in the present study may hinder cellular uptake and may explain the absence of antiproliferative activity.

The acridine nucleus is described to interact to G-quadruplex. Depending on the substituents, the acridine nitrogen can be charged when bound to DNA, and with the ring stacked on a G-tetrad, the charge will occupy a position similar to that of the potassium cation that stabilizes the G-quadruplex [28]. The introduction of protonable side chains on the acridine ligand enhances binding by electrostatic interactions [28]. In our case the acridines had no protonable substituents and the acridine nitrogen was not charged when bound to DNA. For this reason, the affinity of oligomeric acridines to G-quadruplexes is due to the multimeric nature of the compounds as well as the addition of a glycine

to acridine-9-carboxylic acid. An interesting possibility for future development is the introduction of protonable sites at the oligomeric acridines, which may increase solubility in water, affinity to target, and cellular uptake. The method described here will contribute to accelerating the preparation of potential active oligomeric compounds.

Abbreviations

ACN:	Acetonitrile
Ac_2O:	acetic anhydride
Aeg:	(2-aminoethyl)glycine
Boc:	*t*-butoxycarbonyl
CPG:	controlled pore glass
DIEA:	diisopropylethylamine
DCM:	dichloromethane
DMEM:	Dulbecco's Modified Eagle's Medium
DMF:	*N*,*N*-dimethylformamide
EDTA:	Ethylenediaminetetraacetic acid
Fmoc:	(9-fluorenyl)methoxycarbonyl
MALDI-TOF:	Matrix-assisted laser desorption ionization time-of-flight
MBHA:	methylbenzhydrylamine
MTT:	Thiazolyl blue tetrazolium bromide
PNA:	peptide nucleic acid
PyBOP:	(benzotriazol-1-yloxy) trispyrrolidino-phosphonium hexafluorophosphate
Sar:	sarcosine
SDS:	sodium dodecasulphate
TEAA:	Triethylammonium acetate
TFA:	trifluoroacetic acid
UV:	Ultraviolet.

Acknowledgments

This study was supported by the Dirección General de Investigación Científica y Técnica (Grant BFU2007-63287) and the Generalitat de Catalunya (2009/SGR/208). R. Ferreira acknowledges a predoctoral fellowship from the Spanish Ministry of Science.

References

[1] R. Palchaudhuri and P. J. Hergenrother, "DNA as a target for anticancer compounds: methods to determine the mode of binding and the mechanism of action," *Current Opinion in Biotechnology*, vol. 18, no. 6, pp. 497–503, 2007.

[2] B. A. D. Neto and A. A. M. Lapis, "Recent developments in the chemistry of deoxyribonucleic acid (DNA) intercalators: principles, design, synthesis, applications and trends," *Molecules*, vol. 14, no. 5, pp. 1725–1746, 2009.

[3] D. J. Patel, A. T. Phan, and V. Kuryavyi, "Human telomere, oncogenic promoter and 5′-UTR G-quadruplexes: diverse higher order DNA and RNA targets for cancer therapeutics," *Nucleic Acids Research*, vol. 35, no. 22, pp. 7429–7455, 2007.

[4] G. N. Parkinson, M. P. H. Lee, and S. Neidle, "Crystal structure of parallel quadruplexes from human telomeric DNA," *Nature*, vol. 417, no. 6891, pp. 876–880, 2002.

[5] J. L. Huppert, "Hunting G-quadruplexes," *Biochimie*, vol. 90, no. 8, pp. 1140–1148, 2008.

[6] L. H. Hurley, "Secondary DNA structures as molecular targets for cancer therapeutics," *Biochemical Society Transactions*, vol. 29, no. 6, pp. 692–696, 2001.

[7] H. Han and L. H. Hurley, "G-quadruplex DNA: a potential target for anti-cancer drug design," *Trends in Pharmacological Sciences*, vol. 21, no. 4, pp. 136–142, 2000.

[8] N. H. Campbell, G. N. Parkinson, A. P. Reszka, and S. Neidle, "Structural basis of DNA quadruplex recognition by an acridine drug," *Journal of the American Chemical Society*, vol. 130, no. 21, pp. 6722–6724, 2008.

[9] D. Monchaud and M.-P. Teulade-Fichou, "A hitchhiker's guide to G-quadruplex ligands," *Organic and Biomolecular Chemistry*, vol. 6, no. 4, pp. 627–636, 2008.

[10] S. M. Haider, G. N. Parkinson, and S. Neidle, "Structure of a G-quadruplex-ligand complex," *Journal of Molecular Biology*, vol. 326, no. 1, pp. 117–125, 2003.

[11] M. J. B. Moore, C. M. Schultes, J. Cuesta, et al., "Trisubstituted acridines as G-quadruplex telomere targeting agents. Effects of extensions of the 3,6- and 9-side chains on quadruplex binding, telomerase activity, and cell proliferation," *Journal of Medicinal Chemistry*, vol. 49, no. 2, pp. 582–599, 2006.

[12] A. Aviñó, I. Navarro, J. Farrera-Sinfreu, et al., "Solid-phase synthesis of oligomers carrying several chromophore units linked by phosphodiester backbones," *Bioorganic and Medicinal Chemistry Letters*, vol. 18, no. 7, pp. 2306–2310, 2008.

[13] J. Farrera-Sinfreu, A. Aviñó, I. Navarro, et al., "Design, synthesis and antiproliferative properties of oligomers with chromophore units linked by amide backbones," *Bioorganic and Medicinal Chemistry Letters*, vol. 18, no. 7, pp. 2440–2444, 2008.

[14] D. P. Arya and B. Willis, "Reaching into the major groove of B-DNA: synthesis and nucleic acid binding of a neomycin-Hoechst 33258 conjugate," *Journal of the American Chemical Society*, vol. 125, no. 41, pp. 12398–12399, 2003.

[15] E. J. Fechter, B. Olenyuk, and P. B. Dervan, "Design of a sequence-specific DNA bisintercalator," *Angewandte Chemie—International Edition*, vol. 43, no. 27, pp. 3591–3594, 2004.

[16] A. Siddiqui-Jain, C. L. Grand, D. J. Bearss, and L. H. Hurley, "Direct evidence for a G-quadruplex in a promoter region and its targeting with a small molecule to repress c-MYC transcription," *Proceedings of the National Academy of Sciences of the United States of America*, vol. 99, no. 18, pp. 11593–11598, 2002.

[17] J. Dai, T. S. Dexheimer, D. Chen, et al., "An intramolecular G-quadruplex structure with mixed parallel/antiparallel G-strands formed in the human BCL-2 promoter region in solution," *Journal of the American Chemical Society*, vol. 128, no. 4, pp. 1096–1098, 2006.

[18] M. del Toro, P. Bucek, A. Aviñó, et al., "Targeting the G-quadruplex-forming region near the P1 promoter in the human BCL-2 gene with the cationic porphyrin TMPyP4 and with the complementary C-rich strand," *Biochimie*, vol. 91, no. 7, pp. 894–902, 2009.

[19] R. M. Dyson, S. Kaderli, G. A. Lawrance, and M. Maeder, "Second order global analysis: the evaluation of series of spectrophotometric titrations for improved determination of equilibrium constants," *Analytica Chimica Acta*, vol. 353, no. 2-3, pp. 381–393, 1997.

[20] K.-P. Stengele and W. Pfleiderer, "Improved synthesis of oligodeoxyribonucleotides," *Tetrahedron Letters*, vol. 31, no. 18, pp. 2549–2552, 1990.

[21] D. W. Will, G. Breipohl, D. Langner, J. Knolle, and E. Uhlmann, "The synthesis of polyamide nucleic acids using

a novel monomethoxytrityl protecting-group strategy," *Tetrahedron*, vol. 51, no. 44, pp. 12069–12082, 1995.

[22] C. Granotier, G. Pennarun, L. Riou, et al., "Preferential binding of a G-quadruplex ligand to human chromosome ends," *Nucleic Acids Research*, vol. 33, no. 13, pp. 4182–4190, 2005.

[23] J. Gros, F. Rosu, S. Amrane, et al., "Guanines are a quartet's best friend: iImpact of base substitutions on the kinetics and stability of tetramolecular quadruplexes," *Nucleic Acids Research*, vol. 35, no. 9, pp. 3064–3075, 2007.

[24] L. C. Bock, L. C. Griffin, J. A. Latham, E. H. Vermaas, and J. J. Toole, "Selection of single-stranded DNA molecules that bind and inhibit human thrombin," *Nature*, vol. 355, no. 6360, pp. 564–566, 1992.

[25] Y. Wang and D. J. Patel, "Solution structure of the human telomeric repeat d[AG3(T2AG3)3] G-tetraplex," *Structure*, vol. 1, no. 4, pp. 263–282, 1993.

[26] J. Ren and J. B. Chaires, "Sequence and structural selectivity of nucleic acid binding ligands," *Biochemistry*, vol. 38, no. 49, pp. 16067–16075, 1999.

[27] P. Ragazzon and J. B. Chaires, "Use of competition dialysis in the discovery of G-quadruplex selective ligands," *Methods*, vol. 43, no. 4, pp. 313–323, 2007.

[28] E. W. White, F. Tanious, M. A. Ismail, et al., "Structure-specific recognition of quadruplex DNA by organic cations: influence of shape, substituents and charge," *Biophysical Chemistry*, vol. 126, no. 1–3, pp. 140–153, 2007.

[29] J. J. Green, S. Ladame, L. Ying, D. Klenerman, and S. Balasubramanian, "Investigating a quadruplex—ligand interaction by unfolding kinetics," *Journal of the American Chemical Society*, vol. 128, no. 30, pp. 9809–9812, 2006.

[30] A. M. Burger, F. Dai, C. M. Schultes, et al., "The G-quadruplex-interactive molecule BRACO-19 inhibits tumor growth, consistent with telomere targeting and interference with telomerase function," *Cancer Research*, vol. 65, no. 4, pp. 1489–1496, 2005.